Doctoral Dissertations   Student Theses and Dissertations

Summer 2015

Development, testing, and analytical modeling of fiber-reinforced polymer bridge deck panels

Hesham R. Tuwair

DEVELOPMENT, TESTING, AND ANALYTICAL MODELING OF FIBER-

REINFORCED POLYMER BRIDGE DECK PANELS

by

HESHAM R. TUWAIR

A DISSERTATION

Presented to the Faculty of the Graduate School of the

MISSOURI UNIVERSITY OF SCIENCE AND TECHNOLOGY

In Partial Fulfillment of the Requirements for the Degree

DOCTOR OF PHILOSOPHY

in

CIVIL ENGINEERING

2015

Approved by:

Jeffery S. Volz, Co-advisor
Mohamed A. ElGawady, Co-advisor
John J. Myers
K. Chandrashekhara
Victor Birman

PUBLICATION DISSERTATION OPTION

This dissertation has been prepared in the style such that the individual sections may be submitted for publication in the *Journal of Bridge Engineering* published by the American Society of Civil Engineers (ASCE) and the *Journal of Composites Part B: Engineering* published by ELSEVIER.

Paper I (pages 28-80) is a manuscript entitled "Evaluation of Sandwich Panels with Various Polyurethane Foam-cores and Ribs." This manuscript was published in the *Journal of Composites Part B: Engineering*.

Paper II (pages 81-134) is the manuscript "Testing and Evaluation of Polyurethane-based GFRP Sandwich Bridge Deck Panels with Polyurethane Foam Core," which was published in the *ASCE Journal of Bridge Engineering*.

Paper III (pages 135-186) is a manuscript entitled "Modeling and Analysis of GFRP Bridge Deck Panels Filled with Polyurethane Foam." This manuscript was submitted for publication in the *Journal of Bridge Engineering*.

Pages 187-237, the manuscript entitled "Durability of Polyurethane Foam Infill for GFRP Bridge Deck Panels Subjected to Various Environmental Exposure" is intended for submission to the *Journal of Composites Part B: Engineering*.

ABSTRACT

A fiber-reinforced, polyurethane foam core was developed, tested, and evaluated as a possible replacement for the costly honeycomb core that is currently used to manufacture fiber-reinforced polymer (FRP) bridge deck panels. Replacing these panels would reduce both initial production costs and construction times while also enhancing structural performance. Experimental, numerical, and analytical investigations were each conducted. Three different polyurethane foam (PU) configurations were used for the inner core during the study's first phase. These configurations consisted of a high-density PU foam (Type 1), a gridwork of thin, interconnecting, glass fiber/resin webs that formed a bidirectional gridwork in-filled with a low-density PU foam (Type 2), and a trapezoidal-shaped, low-density PU foam that utilized E-glass web layers (Type 3). Based on the experimental results of this phase, the Type 3 core was recommended to move forward to the second phase of the study, where a larger-scale version of the Type 3, namely "mid-scale panels," were tested both statically and dynamically. Analytical models and finite element analysis (FEA) were each conducted during a third phase. Analytical models were used to predict critical facesheet wrinkling that had been observed during phase two. A three-dimensional model using ABAQUS was developed to analyze each panel's behavior. A parametric study considering a wide variety of parameters was also conducted to further evaluate the behavior of the prototype panel. The fourth phase of this research investigated the performance of Type 3 panels under exposure to various environmental conditions to duplicate seasonal effects in Midwestern states. The results gathered from these four phases showed that the proposed Type 3 panel is a cost effective alternative to both honeycomb and reinforced concrete bridge decks.

ACKNOWLEDGMENTS

First and foremost, I thank God for making all things possible. I would also like to express my deepest gratitude to my co-advisors, Dr. Jeffery Volz and Dr. Mohamed ElGawady, for their guidance, friendship, and unwavering support throughout this research project. They played a tremendously influential role in helping me achieve one of the greatest accomplishments of my life. This study would not have been as enjoyable as it was without their great help, advising, motivation and encouragement. Words cannot express how grateful I am to have such amazing co-advisors.

All of the specimens tested in this study were manufactured in the Composites Manufacturing Laboratory under the lead of Dr. K. Chandrashekhara. I would like to thank both him and his group for their work.

I would like to thank the members of my advisory committee: Dr. John Myers, Dr. K. Chandrashekhara, and Dr. Victor Birman. Each provided valuable knowledge, great technical experience, and suggestions that continuously improved my knowledge and understanding.

I would also like to acknowledge my fellow graduate students in the civil and mechanical departments: Matthew Hopkins, Mohaned Mohamed, and Omar Abdelkarim. Thanks also goes to civil department staff: Brian Swift, Gary Abbott, Scott Parker, Jason Cox, and John Bullock. They offered a tremendous amount of technical assistance and support.

I could not have survived the duration of this study without my family. I would like to thank my parents for providing me with their love and prayers. I would also like to thank my brothers, sisters, brothers-in-law, and sisters-in-law for their love, support, and encouragement.

In closing, from all of my heart, I would like to express my sincere gratitude to my lovely wife, Haifa, who has enlightened my life with her love. I owe her more than words can express.

TABLE OF CONTENTS

SECTION

LIST OF ILLUSTRATIONS

PAPER II

PAPER III

LIST OF TABLES

NOMENCLATURE

Symbol	Description
A_i	Cross-sectional area of segment i
$A_{tr,i}$	Transformed area of segment i
a	Distance between the support and the loading point
c	Distance from the extreme upper fiber of the panel to the neutral axis
d_i	Distance from the center of segment i to the neutral axis
d	Panel thickness
E_i	Modulus of elasticity for component i
E_{sw}	GFRP web's modulus of elasticity
E_c	Young's modulus of the core material
E_{ct}	Transverse Young's modulus of the core
E_f	Young's modulus of facesheet material
E_e	Effective modulus of elasticity
EI	Bending stiffness
F_i	Compressive or tensile force of segment i
$F_{c,total}$	Total of all of the compressive forces in the compression side
$F_{t,total}$	Total of all of the tensile forces in the tension side
G_c	Transverse shear modulus of the core
GA	Core's shear stiffness
h_c	Core thickness
h_f	Facesheet thickness
I	Panel's moment of inertia
I_{tr}	Transformed section's moment of inertia
$I_{tr,i}$	Moment of inertia of the transformed section for component i
k	Shear correction factor
k_c	Ratio of the second stress invariant on the tensile meridian
L	Span length
m	Flow potential eccentric
M_{xx}	Bending moment along the x axis

M_{cap}	Capacity flexural moment for the sandwich panel
P	Applied load
Q_x	Transverse shear force
v_c	Out-of-plane Poisson's ratio of the core
v_f	Poisson's ratio of the facesheet material
w(x)	Displacement along the x axis
y_i	Distance from the center of gravity of the component to the extreme lower fiber
$\bar{y}$	Distance from the neutral axis of the transformed cross-section to the extreme lower fiber.
ε_i	Strain in segment i,
ε_{wr}	Wrinkling strain for the compressed facesheet
φ	Angle of rotation of the normal to mid-surface of the beam
ψ	Dilation angle
σ_f	Maximum bending stress
σ_{c0}/ σ_{b0}	Initial biaxial/uniaxial ratio
σ_{wr}	wrinkling stress
μ	Viscosity parameter
$\Delta_{midspan}$	Deflection at mid-span
$\Delta_{loading-point}$	Deflection at loading point

1. INTRODUCTION

1.1. BACKGROUND

Traditionally, most highway bridge decks were constructed with steel-reinforced concrete. The life-span of such materials can be greatly reduced by weathering. It is also greatly affected by traffic, de-icing chemicals, and reduced maintenance. Transportation agencies have been trying to identify new, cost-effective, reliable construction materials. Fiber reinforced polymers (FRPs) have exhibited great promise in eliminating corrosion concerns while also achieving a longer lifespan without requiring frequent maintenance. Fiber reinforced polymer sandwich panels have a number of advantages, including a high flexural stiffness, tremendous strength, reduced weight, environmental resistance, and fast construction. These advantages make the FRP sandwich panels an excellent candidate for the replacement of bridge decks that are comprised of traditional materials (e.g., concrete and steel).

An FRP bridge deck weighs approximately one-fifth that of a reinforced concrete bridge deck. The FRP sandwich panel is composed of two thin facings that are bonded to a thick core. These facings are typically comprised of materials that have not only a high strength but also a high Young's modulus. The core is made of a rigid foam that typically has a low to moderate strength and stiffness. The facings are largely responsible for carrying flexural loads while the core provides shear capacity and bending stiffness.

Complicated geometric honeycomb sandwich panels are widely used in bridge applications. Nevertheless, these panels introduce a number of problems. For example, the honeycomb core is difficult to construct, increasing both the initial production costs as well

as the construction time. This type of sandwich panel is also susceptible to core-to-facing delamination.

Accordingly, the industrial market demands not only continuous innovation but also the use of more efficient, economical structural systems and new construction materials.

1.2. OBJECTIVE AND SCOPE OF WORK

The primary *objective* of this research was to develop, test, and evaluate fiber-reinforced, polyurethane (PU) foams that could replace the costly honeycomb structure currently used to manufacture FRP bridge deck panels.

The following scope of work was implemented in an effort to obtain these objectives: (1) review applicable literature; (2) develop and design panel configurations; (3) investigate the behavior of small-scale FRP/PU sandwich panels; (4) examine the structural behavior of mid-scale FRP/PU sandwich panels; (5) compare test results with both first order shear deformation theory and other well-known models; (6) develop a finite element model that could be used to validate experimental results and conduct parametric studies; (7) perform durability testing of the proposed panel; (8) summarize findings and develop conclusions and recommendations; (9) prepare this thesis in order to document the information obtained during this study.

1.3. DISSERTATION OUTLINE

This thesis includes three sections and five appendices. Section 1 includes a brief introduction to the subject area and explains the need for this research. The objective and

scope of the work of the study, as well as a detailed literature review establishing the state-of-the-art on the proposed topic is also presented in this section.

Section 2 contains four journal papers that discuss the evaluation of various section profiles of sandwich panels, testing, evaluation, and modeling of the proposed sandwich panel. Durability studies were also conducted on the proposed sandwich panel.

Section 3 summarizes the work that was accomplished in this dissertation. It also presents the key findings of all experiments and theoretical analyses, which were executed during this research study, as well as a proposal for future research. The appendices include detailed test data and photographs from the research study.

2. LITERATURE REVIEW

Over half of the nation's 607,000 bridges were built before 1940 (Kirk and Mallett 2013). Thus, these bridges have reached the end of their useful service lives. Bridge deck panels are among the most deteriorated elements in these bridges as a result of de-icing salts. A recent study was conducted by Ellis (2011) for the Federal Highway Administration (FHWA) and estimated the annual direct cost of corrosion for highway bridges to be $6.43 to $10.15 billion. This contains $1.07 to $2.93 billion for maintaining the concrete bridge decks. Fiber reinforced polymer materials have received considerable attention as a strong candidate to replace deteriorated concrete and steel structures. These panels are lightweight, easily installed (reducing traffic delay), and resistant to both environmental and chemical attacks. Research conducted on FRP composites for bridge applications has increased substantially since the mid-1990s (Hollaway 2003). Many have reported that the use of FRP composites within an infrastructure is promising. Others, however, expressed concerns about the high initial costs, lack of familiarity, and learning curve for the industry (Busel and Lockwood 2000; Anon 2001; Karbhari 2004; Bank 2005; Harries 2006; Hong and Hastak 2007). Since then, however, the application of FRP sandwich panels in the United States has been identified as an alternative solution for either bridge construction or rehabilitation.

2.1. RELATED RESEARCH ON SANDWICH PANELS

Sandwich panels are typically comprised of two stiff FRP facesheets that are separated by a core material (Figure 2.1.). The separation of the facesheets by the core increases the moment of inertia of the panel with little increase in weight, producing an

efficient structure. The facesheets are rigid while the core is relatively weak and flexible. When combined in a sandwich panel, however, they produce a structure that is stiff, strong and lightweight (Rocca and Nanni 2005).

Sandwich panels should be designed to meet basic structural criteria, such as the facesheets should be stiff enough to withstand the tensile, compressive and shear stresses. In addition, the core should have sufficient strength to withstand the shear stresses induced by the design loads. The adhesive that is used must have sufficient strength to carry shear stress into the core. The core should be thick enough, with a sufficient shear modulus, to prevent overall buckling of the sandwich under load to prevent crimping. The compressive modulus of both the core and the facesheets should be able to prevent wrinkling within the facesheets under a design load.

A sandwich panel can be treated as a traditional I-beam which has two flanges that are connected by a web (Bruhn 1973). Thus, the sandwich panel components act together when the structure is subjected to bending, resisting the external bending moment so that one facesheet is loaded in compression and the other in tension. The core resists transverse forces. At the same time, it supports the facesheets while stabilizing them against buckling and local buckling (Norlin and Reuterlöv 2002).

Facesheet

Core
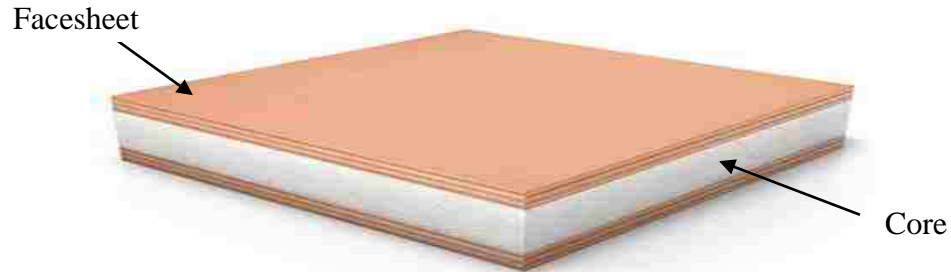
Figure 2.1. Main components of sandwich structures

Many sandwich panels used during the early part of the 20th century were used in the aircraft industry (Allen, 1969). A number of industries, such as automotive, marine, and civil engineering industries soon followed. Allen (1969) and Plantema (1966) summarized the information available up to the end of the 1960s in two text books. Researchers around the world have studied several combinations of core and facesheet materials to achieve improved crashworthiness (Mamalis, et al. 2005). The facesheet's configuration is relatively standard. However, there is a wide variations for the core structure (Figure 2.2.), allowing them to be custom-made for specific applications. Changing the core configuration, the core thickness, and the facesheet thickness allows for section optimization without significantly increasing the weight (Vinson 1999).
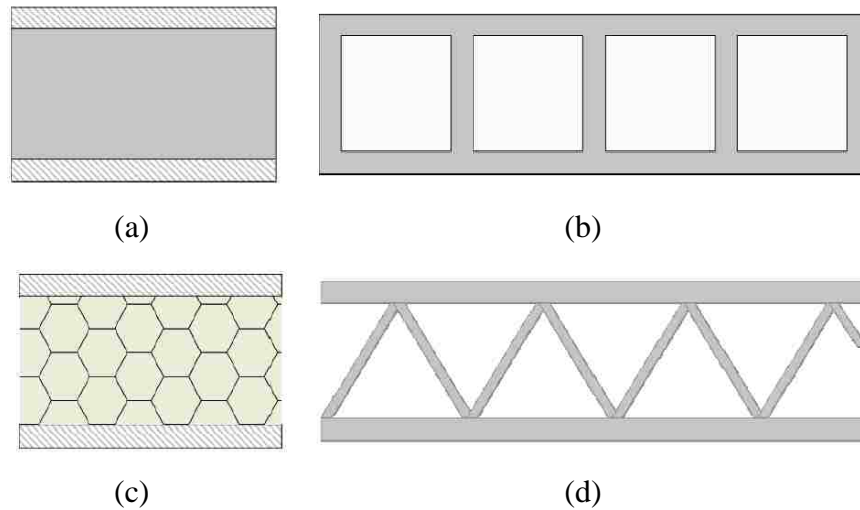
Figure 2.2. Different sandwich panel configurations (a) Foam core sandwich, (b) Web core sandwich, (c) Honeycomb core sandwich, and (d) Truss core sandwich

A honeycomb core is one of the most well known cores used in sandwich panels, excessively implemented in both rehabilitation and new bridge decks (Plunkett 1997; Stone et al. 2001; Henderson 2000; Reising et al. 2001; Zou 2008; Camata and Shing, 2010 Davalos 2001, 2012). Plunkett (1997) was the first one who introduced it for highway bridge decks. It was originally developed for use in the aerospace industry. The honeycomb core consists of sinusoidal wave corrugations and straight components sandwiched between the facings. Previous laboratory and field testing showed that this type of panel is effective in providing high mechanical performance for minimum unit weight (Plunkett 1997; Davalos et al 2001). However, honeycomb cores have several drawbacks. For example, the honeycomb core is difficult to construct as it requires special care to guarantee sufficient bonding. This special care increases the initial production costs. Another concern for this type of core is that it is susceptible to core-to-facing debonding (Camata and Shing 2010). The high cost of the honeycomb cores limits its application, primarily to the

aerospace industry. A number of researchers have used various techniques to overcome these shortcomings. One of the techniques has been to use less expensive material to replace the honeycomb core, such as polyvinyl chloride (PVC) and polyurethane (PURE) foams, in an attempt to reduce the production costs (Zenkert 1997). These foams have a smaller strength-to-weight ratios than do honeycomb cores, resulting in a delay in their use.

These type of foams, however, do offer their own advantages. Foam cores are typically lower in cost than honeycomb cores. They also have improved workability. Foams have an uncomplicated surface preparation that allows for an improved bond between the core and facesheet layers. Additionally, foams prevent water from penetrating into the interior of a panel. Finally, polyurethane foams can be made fire resistant when additives that contain phosphorus are used (Zenkert 1997).

A number of researchers have used various techniques to improve the strength and stiffness of the foam core. Kim et al. (1999) studied both the static and the fatigue behavior of different polyurethane foam core configurations in one-way bending of GFRP sandwich panels. These core configurations consisted of a plain foam core, a foam core with through-thickness GFRP stitches, and a foam core with continuous, internal GFRP webs. Kim et al. (1999) found that the sandwich panel with continuous internal GFRP webs outperformed the other two types in terms of flexural strength. The ultimate strength, however, was reduced to between 20 and 40% when the panels were loaded up to 1 million fatigue cycles.

Potluri et al. (2003) investigated the effect of introducing stitches to the core. They found that both static and fatigue structural behavior can be improved by stitching together the top and bottom facings. Hassan et al. (2003) proposed an alternative system for FRP bridge decks using three-dimensional fibers (known also as through thickness-fiber),

manufactured using either weaving or injection technology. These fibers are used to connect the top and bottom GFRP facings and thus overcome delamination in the facings and debonding between the facings and the core. The proposed design also enhanced strength and stiffness over traditional sandwich composites. Rocca and Nanni (2005) investigated the flexural and fatigue behavior of GFRP sandwich panels that contained a fiber reinforced foam (FRF) core. They found that the residual compressive strength was not significantly reduced after two million fatigue cycles. The authors also observed that the deflection associated with the shear contribution (in the total deflection) can be ignored due to the shear strength provided by the core.

Zi et al. (2008) proposed a new type of GFRP bridge deck that consisted of GFRP with rectangular holes filled with polyurethane foam. They found that, when the rectangular holes were filled with polyurethane foam, the structural response and strength in the transverse direction were improved significantly. The elastic modulus (i.e., stiffness), however, did not increase. Dawood et al. (2010) proposed an innovative 3-D GFRP sandwich panel that was somewhat similar to the panel Hassan et al. (2003) proposed to be used in civil infrastructures and transportation applications. Dawood et al.'s proposed panel was produced by a pultrusion process. The top and bottom facings consisted of a glass fiber of [0/90] fabric that was passed through a vinyl ester resin bath. These through-thickness fibers were inserted throughout the facings and the polyisocyanurate foam core. Findings from this study indicate that, when subjected to fatigue loads, the panels with more through-thickness fibers (stiffer cores) generally exhibited a higher degree of degradation than panels with less through-thickness fibers.

A number of researchers (Hayes 2000; Zhou 2005) at Virginia Tech proposed different panel techniques. These techniques involved the use of cellular pultruded FRP sandwich deck panels that were comprised of both mechanically and adhesively bonded pultruded box shapes. These panels were laboratory tested statically and dynamically under simulated truck tire loading. The failure mode was localized punching shear failure of the deck around the loading patch.

Ji et al. (2010) proposed the use of a GFRP corrugated-core sandwich panel in which an aluminum sheet was used for the inner core. The proposed deck was tested in-situ and analyzed through finite element analysis. They found that both the stiffness and the strength were enhanced.

The choice of using a numerical simulation tool is motivated by not only the high cost of FRP materials but also the ease in which material properties can be changed. Hence, a wide variety of parameters can be altered so that a range of sandwich panel behaviors can be investigated. Exact solutions for FRP sandwich panels can be challenging to identify with theoretical approaches (including approximations and assumptions). Researchers have begun to implement finite element analysis (FEA) approaches to allow for modeling the behavior with greater accuracy. Several researchers (e.g., Aref et al. 2001) used a finite element program within ABAQUS to analyze the dynamic response of FRP bridge sandwich panel systems. Zureick (1997) used a finite element analysis to compare the structural behavior of different FRP deck cross-sections that were simply supported. This study compared four different cross-sections. Zureick (1997) concluded that both the box-shaped and the V-shaped cores behaved much better than did the other sections.

Wan et al. (2005) used ANSYS to develop a 3D model aid for investigating the structural behavior of a GFRP bridge sandwich system. They conducted a parametric study and found that a good balance must exist between the supporting girders' rigidity and the GFRP deck to meet design strength and serviceability demands. Morcous et al. (2010) used four finite element models (one-layer modeling, three-layer modeling, actual configuration modeling, and simplified I-beam modeling) to assess the structural behavior of honeycomb sandwich panels. They found that the simplified I-beam modeling method was the most efficient method when studying the overall performance of honeycomb sandwich panels. They also found that this method was computationally efficient. Although the results from these studies provided a noteworthy understanding of an FRP panel's behavior, most of these results cannot be extrapolated to other products.

2.2. RELATED FIELD APPLICATIONS

Approximately 40 FRP vehicular bridges were built in the USA between 1996 and 2013 (FHWA 2013). Most are in states in which de-icing salts are used. The No-Name Creek Bridge installed in Russell, Kansas in 1996 was the nation's first composite short-span bridge (Ji et al. 2010). This bridge is 23 ft. long and capable of supporting an AASHTO HS20-44 truck (Figure 2.3.). It contains FRP honeycomb sandwich panels (Figure 2.3.), manufactured by Kansas Structural Composites, that are 22 in. deep. The hand lay-up process was used to assemble the panels with glass/polyester fabrics. The entire bridge was constructed in less than two days.

<center>(a)   (b)</center>

Figure 2.3. The no-name creek bridge in Russell, KS (a) Bridge overview and (b) Honeycomb core

The Wickwire Run Bridge, located in Taylor Co., West Virginia, was the first modular FRP pultruded deck installed in the USA (Lopez-Anido et al. 1998); it was installed on a 30 ft. long bridge in 1997. The new bridge replaced an existing steel-girder beam that had a timber decking. The cross-section of this modular deck is comprised of two pultruded profiles: double trapezoids and hexagons (Figure 2.4.). These profiles are locked and bonded to create a deck module. The installation of the FRP deck panels is shown in Figure 2.4. The FRP deck was designed according to AASHTO standard to carry an HS25-44 truck load.

Figure 2.4. The Wickwire Run Bride in Taylor Co., WV

The Salem Avenue Bridge, located in Dayton, Ohio, was also constructed with composite materials (Henderson 2000; Reising et al. 2001). The overall bridge (pictured in Figure 2.5.a) is 679 ft. long with an average span length of 136 ft. Its composition includes FRP deck panels that are supported by steel girders spaced 8.75 ft. on the center. The four different panel configurations that were used to evaluate several different panel technologies within a single project are illustrated in Figures 2.5.b-e. These panels were provided by Composite Deck Solutions, Creative Pultrusions Inc., Hardcore Composites, Inc. and Infrastructure Composites International.

(a)

(b)   (c)   (d)
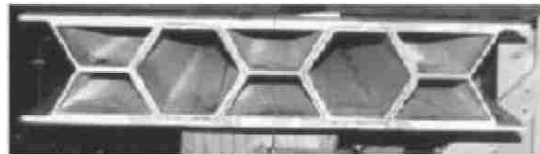
(e)

Figure 2.5. Salem Ave. bridge in Dayton, OH (a) Bridge overview, (b) Honeycomb core, (c) Foam wrapped with fiber cloth, (d) Interlocking pultruded FRP tube, and (e) FRP stay-in-place forms

An FRP bridge deck was installed on the Missouri University of Science and Technology (Missouri S&T) campus in 2000 (Kumar et al. 2001). This bridge is 30 ft. long and 9 ft. wide (see Figure 2.6.a). Pultruded square hollow glass and carbon FRP tubes were used to build the panels (Figure 2.6.b). The CFRP tubes that comprised the top and bottom layers helped increase the bridge's strength. The middle layers were comprised of GFRP

tubes to limit cost. Both an epoxy adhesive and mechanical fasteners were used to bond these tubes together. The bridge was designed to carry an H-20 truck load.

(a)   (b)

Figure 2.6. The smart composite bridge in Missouri S&T campus, Rolla, MO (a) Bridge overview and (b) Pultruded tubes core

Three bridges in St. James, Missouri (on St. Johns Street, Jay Street, and St. Francis Street) were constructed with FRP panels (Stone et al. 2001). The St. Johns bridge is illustrated in Figure 2.7.a. Honeycomb sandwich panels (manufactured by Kansas Structural Composites) were utilized in these bridges (Figure 2.7.b). Each bridge has an average length of 27 ft. and was designed to carry a standard HS20-44 truck load.

<table>
<tr><td align="center">(a)</td><td align="center">(b)</td></tr>
</table>
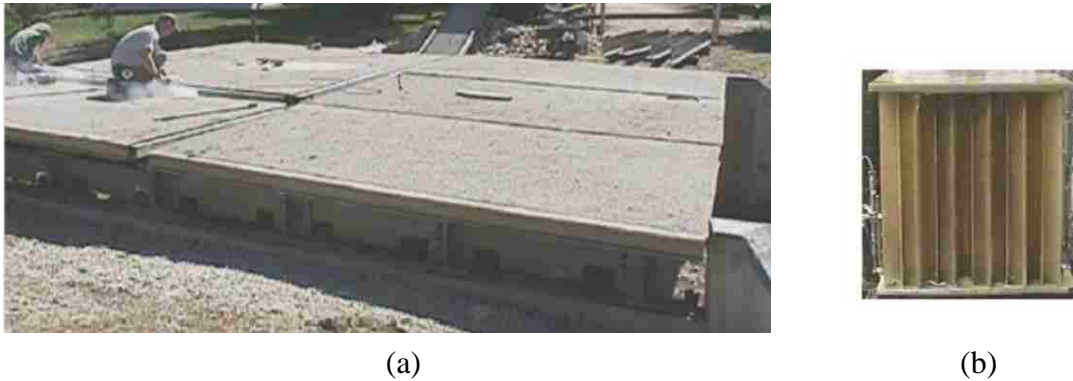
Figure 2.7. The Johns St. bridge in St. James, MO (a) Bridge overview and (b) Honeycomb core

The Colorado Department of Transportation, in cooperation with the Federal Highway Administrations, built a bridge with a glass fiber reinforced polymer (GFRP) deck in O'Fallon Park, Denver (Camata and Shing 2005). Six panels (7.28 ft. wide and 7.5 in. thick) were used to create a total length of 43.75 ft. and a total width of 16.25 ft. The bridge was designed to carry a standard HS25-44 truck. The deck is comprised of a honeycomb sandwich panel that was manufactured by Kansas Structural Composites.

Typically, the connection between the deck panels to the underlying steel girders is made using: adhesive glue at the interface, shear studs, bolted connection, or steel clamps in a simply supported condition (Bakis et al. 2002; Davalos et al. 2013). A study showed that a full composite action could be achieved between the FRP panel and the supporting beams using adhesive glue (Keller and Gurtler 2005). Camata and Shing (2004) used bolts secured by epoxy to anchor the deck to the concrete raisers. Each deck side was anchored by two bolts (Figure 2.8.). Another prototype shear connector was developed by Davalos et al. (2012) to connect an FRP deck-on-steel girder system, as shown in Figure 2.9. This

type of connection was favorable by bridge engineers as it is similar to the shear studs used for concrete decks. Righman et al. (2004) investigated the feasibility of using bolted and clamped connections and found that the installation process is quite labor-intensive, resulting in an increase in the initial costs and construction time. Moon et al. (2002) developed a shear connection for trapezoidal sandwich panels that is similar in the concept of the current proposed panel except that his was manufactured using the pultrusion process.

Figure 2.8. Panel-to-girder connection using bolts (Camata and Shing 2004)

Figure 2.9. Panel-to-girder connection using bolts (Davalos et al. 2012)

Regarding the connections between the FRP panels, they are typically connected to each other by tongue-and-groove ends (see Figure 2.10.) and are then secured to the underlying steel girders using one of the previous devices. Kansas Structural Composites, as an example, used the tongue-and-groove technique (see Figure 2.10.a) to connect the FRP panels that were installed in O'Fallon Park, Denver (Camata and Shing 2004).

(a)

(b)

Figure 2.10. Panel-to-panel connection (a) Camata and Shing (2004) and (b) Davalos et al. (2012)

The successful implementation of these bridges suggests that sustainable, feasible alternatives have been produced for new bridge constructions. These bridges were designed and built without the application of nationally accepted codes and standards. The bridge decks were made of either vinyl ester or polyester resin reinforced with fibers. As a result,

there is still great demand for further research on additional alternative designs in order to expand the database of civil engineering bridge applications, testing and manufacturing standards, and reduce the production costs.

2.3. OVERVIEW OF POLYURETHAN FOAM

Polyurethane foam is commonly used as the core in sandwich panel construction because it is light weight. The polyurethane can be classified as either a flexible or a rigid foam. The flexible foam is most often used in the bedding of car seats and upholstery. The rigid foam is primarily used for thermal insulation (e.g., within automobile dashboards, refrigerators, and building panels). Polyurethane foams are comprised of two structural parts: cell walls and open windows areas (also known as struts and voids, respectively). The composition of struts and voids allows the air to pass through the foam when a load object is applied. The polyurethane foam can absorb high impact loads as a result of the strut's elasticity, which acts as a shock absorber.

The micrograph structure of cellular materials used for both flexible open-cell and flexible closed-cell polyethylene foams (Gibson and Ashby 1988) is illustrated in Figure 2.11. Foams that have membrane cell walls (see Figure 2.11.a) are considered closed cell foams. Foams that do not have such membranes are known as open cell foams (Figure 2.11.b).
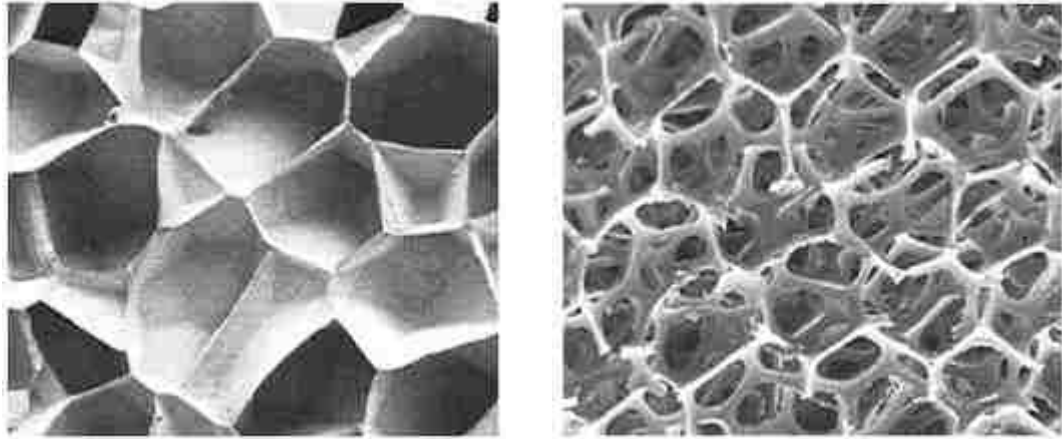
Figure 2.11. Micrographs displaying the structure of cellular materials (a) for closed-cell polyethylene foam; (b) for open-cell polyurethane foam. [Gibson and Ashby, 1988]

The foam's structural properties make the design of such materials quite unique. Excellent thermal insulators for applications like building cladding panels can be achieved by reducing both the cell's size and the volume fraction of solids in closed cell foams. The solid foams have certain properties that cannot be available in many other solids. These properties are comprised of a low compressive strength, a low stiffness, and a high compressibility at a constant load and a high deformation capacity. The solid foams become more beneficial for numerous applications (e.g., cushioning, thermal insulation, and impact absorption) as a result of the unique properties. Polyurethane foams also have a low density, making them an ideal core for lightweight sandwich panels (Gibson and Ashby, 1988).

Several approaches, including experimental, analysis, and the development of constitutive relationships, were used to study the mechanical behavior of foams. A number of researchers (Deshpande and Fleck 2000; Gdoutos et al. 2002; Doyoyo and Wierzbicki

2003) have contributed a great deal of information to this subject. Gibson and Ashby (1997) proposed a simplified model to extract the mechanical properties of foam material (e.g., stiffness, Poisson's ratio, and failure criteria).

The mechanical behavior of solid foams under compressive loading is likely the primary property that distinguishes it from non-cellular solids. A typical compressive stress-strain curve of a foam material is illustrated in Figure 2.12. It can be categorized into three phases. In the first phase, the foam's cells are compressed uniformly where the cells are distributed relatively evenly in both size and location. As a result, the foam has a global response that is linear elastic. Ultimately, some of the cell walls and struts reach their stability limit, forming what may be considered analogous to a yielding point as reported by Gibson and Ashby (1988). In the second phase, the cells begins to fail due to excessive buckling, yielding, or fracturing in the cell wall and struts. Subsequently, the cell walls collapse at an almost constant stress, exhibiting so-called "plateau stress." A densification (hardening) regime occurs in phase three, which was caused by the cell walls stacking together due to wall yielding. As the applied force increases, this results in stiffening and increase in the compressive strength, along with very large corresponding compressive strain.
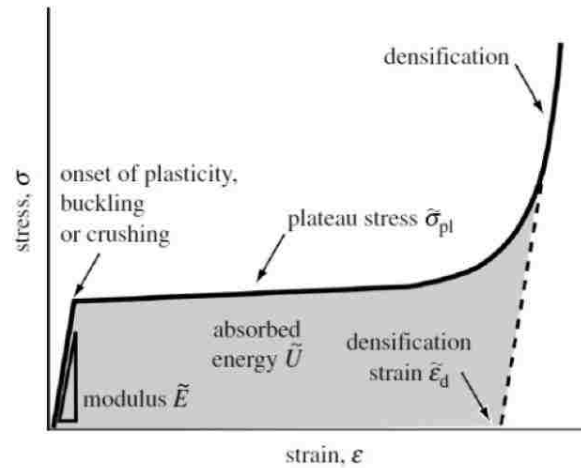
Figure 2.12. Stress strain curve of a cellular material showing the three phases. [Ashby 2005]

A number of researchers have used soft foam as a core within sandwich panels. Triantafillou and Gibson (1987) used a simple mechanics model to predict the possible failure mode of sandwich beams. These beams consisted of aluminum facings that were separated by a rigid polyurethane foam core. The authors successfully captured all possible failure modes. Zhu et al. (1997) investigated a soft core's nonlinear behavior. They determined the effect of nonlinear relation between the material type and its density. Shen et al. (2004) used the high-order sandwich panel theory to predict the bending behavior of soft core sandwich beams. Kim et al. (1999) studied the static and fatigue behavior of different polyurethane foam core configurations of one-way bending of GFRP sandwich panels. These core configurations consisted of a plain foam core, a foam core with through-thickness GFRP stitches, and a foam core with continuous, internal GFRP webs. Kim et al. (1999) found that the sandwich panel with continuous internal GFRP webs outperformed the other two types in terms of flexural strength. The ultimate strength, however, was reduced to between 20 and 40% when the panels were loaded up to 1 million fatigue cycles.

Fam and Sharaf (2010) investigated both the feasibility and the flexural performance of sandwich panels composed of low density polyurethane foam cores. They found that when the ribs between the top and bottom facings were considered, the panel's strength and stiffness increased substantially. The authors found that the shear deformation increased over 50% of the mid-span deflection when the core was comprised of a low density polyurethane foam. Henao et al. (2010) used the through-the-thickness reinforcement of sandwich panels with a polyurethane foam core to investigate a sandwich panel's integrity. They found that the use of tufted fibers significantly improved both the edge-wise compressive and bending strengths. Baba et al. (2011) investigated the dynamic response of composite sandwich beams with polyurethane foam core and debonding between the facing and core using experimental and finite element methods. The authors found that the amount of debonding reduced the natural frequencies as a result of stiffness degradation.

2.4. OVERVIEW OF POLYURETHAN RESIN

Polyurethane is a generic name that is used more for convenience than accuracy. The development of polyurethane-based adhesives began in the late 1930s. Goodyear introduced the first structural use in 1968 (Szycher, 1999). A wide variety of matrix materials are used to manufacture FRP composites. The most commonly used materials, particularly in civil engineering applications, include polyester, vinylester, and epoxy. Recent studies have shown that polyurethane resin is a promising alternative to these traditional resins as it offers the potential for fast cycle times and high toughness. Connolly et al. (2006) proved that polyurethane pultruded sections exhibited superior strength and

toughness when compared to commonly used polyester and vinyl ester resin systems. Polyurethane composites can also be used for moving surfaces applications as they have good wear resistance (Zhao et al. 2011). Additionally, polyurethane resin is environmentally friendly as it does not produce styrene emissions during the manufacturing process.

Polyurethane resin has been used considerably in the past as a composite matrix material, particularly for pultrusion processing (Joshi et al. 2001; Vaughn et al. 2003; Sumerak 2004). Polyurethane composites were successfully manufactured using the pultrusion method. Unfortunately, the pultrusion process is quite costly. For example, the production cost of pultruded deck panels is approximately five times the production cost of hand lay-up deck panels (Alagusundaramoorthy and Reddy 2008). Additionally, the pultrusion process can only be used to manufacture constant cross-section profile composite parts. Therefore, using a manufacturing method other than the pultrusion method would help reduce the first costs while providing flexibility to design non-prismatic cross-section parts. The vacuum assisted resin transfer molding (VARTM) process can be used to manufacture both small and large FRP sandwich panels with a quality that is comparable to that manufactured during the pultrusion process. The polyurethane resin, however, has several disadvantages that prevent it from being used with the VARTM process. These disadvantages include the following:

- high viscosity and short pot-life
- limited thermal stability due to molecular constituents
- sensitivity to moisture in bulk.

These shortcomings have been recently overcome through a major development in novel catalysis chemistry that was developed by Bayer MaterialScience. This development extended the pot-life of the resin so that a relatively constant, low viscosity for a long period of time is maintained (Bareis et al. 2011).

2.5. PROPOSED GFRP SANDWICH PANEL

A number of problems are associated with conventional FRP sandwich panel design. The most common problem in FRP sandwich structures arises when the facings debond from the core material. Another problem occurs when the core is very flexible in shear so that deflections become a function of not only bending but also shear. In certain cases, the contribution of shear deformation to the total deflection can exceed that of bending (Allen and Feng 1998). Polyurethane foam cores are typically much weaker than the equivalent density of honeycomb cores. These weaker, less dense foam cores may allow sudden failure when the facesheets buckle on the compression side (Bitzer 1997).

The conventional sandwich structures are also extremely sensitive to localized external loads (e.g., point loads and line loads). This pronounced sensitivity is related to the inducement of significant local deflections of the loaded face into the core's material, thus causing high local stress concentrations.

In this study, both trapezoidal-shaped web layers and a novel, two-part polyurethane resin are introduced in the proposed panel to overcome the shortcoming of conventional sandwich panels. These two components were added in an attempt to increase composite action in the facesheets, the shear stiffness, and the bending stiffness. They should also delay localized buckling and prevent delamination. Increasing the shear

stiffness helps resist the out-of-plane deflection associated with buckling failure mode while also enhancing the panel's ultimate capacity (Taylor 2009). Finally, this system could reduce initial production costs.

PAPER

I. EVALUATION OF SANDWICH PANELS WITH VARIOUS POLYURETHANE FOAM-CORES AND RIBS

Hesham Tuwair[1]; Matthew Hopkins[2]; Jeffery Volz[3]; Mohamed ElGawady[4]; Mohaned

Mohamed[5]; K.Chandrashekhara[6]; Victor. Birman[7]

ABSTRACT

The objective of this study was to evaluate three potential core alternatives for glass

fiber reinforced polymer (GFRP) foam-core sandwich panels. The proposed system could

reduce the initial production costs and the manufacturing difficulties while improving the

system performance. Three different polyurethane foam configurations were considered

for the inner core, and the most suitable system was recommended for further prototyping.

These configurations consisted of high-density polyurethane foam (Type 1), a bidirectional

gridwork of thin, interconnecting, GFRP webs that is in-filled with low-density

polyurethane foam (Type 2), and trapezoidal-shaped, low-density polyurethane foam

utilizing GFRP web layers (Type 3). The facings of the three cores consisted of three plies

[1] Graduate research assistant, Department of Civil, Architectural, and Environmental Engineering, Missouri University of Science and Technology, USA E-mail: hrthw2@mst.edu

[2] Graduate research assistant, Department of Civil, Architectural, and Environmental Engineering, Missouri University of Science and Technology, USA E-mail: mshbq2@mst.edu

[3] Associate professor, School of Civil Engineering and Environmental Science, The University of Oklahoma, USA E-mail: volz@ou.edu

[4] Associate professor, Department of Civil, Architectural, and Environmental Engineering, Missouri University of Science and Technology, USA E-mail: elgawadym@mst.edu

[5] Graduate research assistant, Department of Mechanical and Aerospace Engineering, Missouri University of Science and Technology, USA E-mail: mmm7vc@mst.edu

[6] Curators' professor, Department of Mechanical and Aerospace Engineering, Missouri University of Science and Technology, USA E-mail: chandra@mst.edu

[7] Professor, Engineering Education Center, Missouri University of Science and Technology, USA E-mail: vbirman@mst.edu

of bidirectional E-glass woven fabric within a compatible polyurethane resin. Several types of small-scale experimental investigations were conducted. The results from this study indicated that the Types 1 and 2 cores were very weak and flexible making their implementation in bridge deck panels less practical. The Type 3 core possessed a higher strength and stiffness than the other two types. Therefore, this type is recommended for the proposed sandwich system to serve as a candidate for further development. Additionally, a finite element model (FEM) was developed using software package ABAQUS for the Type 3 system to further investigate its structural behavior. This model was successfully compared to experimental data indicating its suitability for parametric analysis of panels and their design.

Key words: A. Foams, A. Glass fibres, C. Finite Element Analysis (FEA), C. Analytical modeling

1. Introduction

The majority of highway bridge decks are constructed with steel-reinforced concrete. The life-span of such materials can be significantly reduced by environmental conditions combined with wear from traffic, de-icing chemicals, and insufficient maintenance. As a result, transportation agencies have been endeavored to find new cost-effective, reliable construction materials. Fiber reinforced polymer (FRP) has shown great promise in eliminating corrosion concerns while also achieving a longer lifespan with minimal maintenance [1]. FRP has been used for columns [2-4], beams [5, 6], and panels [7-10]. FRP sandwich panels have many advantages, such as high flexural stiffness,

strength, and environmental resistance, as well as reduced weight and life cycle cost. Using FRP deck panels should also contribute to accelerated bridge construction. These advantages make FRP sandwich panels an excellent candidate for construction of bridge decks.

Sandwich panels are often composed of two thin facings that are bonded to a much thicker core. The facings are typically made of high strength and stiffness material. The core usually consists of a rigid-foam, which has a low to moderate strength and stiffness [11]. However, the core design is industry-related. The facings are largely responsible for carrying flexural loads while the core provides shear capacity and integrity of the structure [12]. Many alternative forms of sandwich panels can be accomplished by combing different facings and core materials combined with varying geometries. As a result, optimum designs can be produced for specific applications [11].

Researchers and manufacturers have developed many FRP bridge deck designs with honeycomb and cellular cores made of E-glass reinforced polyester or vinyl ester resin. These designs have primarily been manufactured using filament winding, hand lay-up, and pultrusion methods [13]. A honeycomb core is one of the famous cores that being used in sandwich panels, implemented in bridge decks [8, 14-20]. The honeycomb core consists of sinusoidal wave corrugations and straight components sandwiched between the facings. Testing showed that this type of panels is effective in providing high mechanical performance for minimum unit weight [14, 19].

Researchers have proposed alternative forms for sandwich panels. Potluri et al. [21] proposed a conventional sandwich panel where the top and bottom facings were separated by a foam core. In their study, they introduced FRP stitches to improve the foam core

performance. The stitches were used also to prevent core-to-facing debonding. It was found that both static and fatigue structural behavior can be improved by stitching together the top and bottom facings. Hassan et al. and Reis and Rizkalla [22, 23] proposed an alternative system for FRP bridge decks. The proposed panel used three-dimensional fibers (stitches through foam cores) to connect the top and bottom GFRP facings. They observed that the delamination concerns were overcome. In addition, the fiber reinforced stitches increased significantly the core shear modulus. Dawood et al. [24] studied the fatigue behavior of sandwich panels with flexible and stiff cores. They found that the panels with flexible cores exhibit less degradation than those with stiffer cores due to the higher induced shear stresses at the same level of applied shear strain. Zureick [25] used finite element analysis to study different cross-sections of simply supported FRP decks. This study compared four different cross-sections, concluding that the box shaped and V shaped cores behaved much better than the other sections. Although the results from these studies provided a noteworthy understanding of FRP sandwich panel's behavior, most of these results cannot be extrapolated to other products.

The connection between the deck panels to the underlying steel girders is typically made using adhesive glue at the interface, shear studs, bolted connection, or steel clamps in a simply supported condition [26-29].

2. Paper scope and objectives

In the present study, small-scale FRP sandwich beams having three different foam core configurations (see Fig. 1) were investigated. The proposed system could reduce the initial production costs and the manufacturing difficulties while improving the system

performance. The facings of the proposed three sandwich beams consist of E-glass woven fabric within a compatible polyurethane resin. Each configuration uses polyurethane foam as an infill material for the inner core. The investigated core configurations include high-density polyurethane foam (Type 1), a gridwork of thin, interconnecting, GFRP webs that is infilled with low-density polyurethane foam (Type 2), and GFRP trapezoidal-shaped infilled with low density polyurethane foam (Type 3). The polyurethane foam was chosen because it provides several advantages. These advantages include:

- Lower material and labor costs.

- Higher impact resistance and damping.

- Compatible material to the polyurethane resin, which aids in the infusion process and bonding with the face sheets.

A polyurethane resin system was used in the proposed sandwich beams as it has good high resistance and superior mechanical properties compared to polyester and vinyl ester [30]. This resin system was also chosen because it can reduce the initial costs of the sandwich beams. The one-step Vacuum Assisted Resin Transfer Molding (VARTM) process was also chosen to manufacture beams as it has a lower production cost than other manufacturing methods. For instance, the production cost of pultruded deck panels is approximately five times the production cost of hand lay-up deck panels [31]. The VARTM process can be used to manufacture both small and large FRP bridge deck panels. Although, polyurethane resin has a low pot life, recent modifications to the resin enabled it to be used with the VARTM process. A thermoset polyurethane resin with a longer pot life developed by Bayer MaterialScience was used in this study to manufacture the sandwich beams. All specimens were manufactured in the Composites Manufacturing

Laboratory, Department of Mechanical and Aerospace Engineering, Missouri University of Science and Technology.

One of the greatest challenges faced by structural sandwich beams/panels is that the inner core has low transverse stiffness and strength. As a result, these panels are vulnerable to in-plane shear, wrinkling instability, and face-to-core deboning [32]. Therefore, the three design criteria considered in this study were chosen to improve the core's mechanical performance. The high-density foam in the first type was used with no webs in the core in an attempt to minimize both weight and cost. The cores in the second and third types consisted of low-density foam to minimize the weight reinforced with GFRP webs. Furthermore, the web elements of Types 2 and 3 potentially will delay both delamination failure and local crushing.

This paper compares the structural characteristics of the three proposed sandwich beam systems. The compressive and tensile strengths were assessed through the flatwise compressive and tensile tests of small sandwich cubes and coupon tests. The flexural strength and bending stiffness of each core system were also evaluated through three and four-point bending tests. The possible modes of failure of the different core configurations were also determined. A finite element model (FEM) was also developed for the Type 3 system and verified using the experimental results. The FEM was used for a better understanding of the structural behavior of this sandwich beam type.

A full-scale of Type 3 system was recently manufactured by the Structural Composites, Inc. [33]. Based on the manufacturer, the resulting costs of the panel system was less than one half the cost of a comparable honeycomb FRP deck construction. Additionally, on a production run for an actual bridge, the manufacture estimates a further

decrease in unit costs of 40% to 50%, bringing the FRP deck alternative in line with initial costs of reinforced concrete decks.

3. Experimental program

This study examined the cross-sections of three different configurations of the closed-cell polyurethane infill-foam beams (see Fig. 1). The facings of the three types consisted of three plies of bidirectional E-Glass woven fabric (WR18/3010) infused with a compatible polyurethane resin. The core of Type 1 was comprised of high-density polyurethane foam that had a mass density of 96 kg/m^3. The Type 2 core consists of thin, interconnecting, glass fiber/resin webs that form a bidirectional FRP gridwork that is infilled with a low-density polyurethane foam of 32 kg/m^3. The Type 3 core was comprised of a trapezoidal-shaped, low-density, polyurethane foam and three-ply web layers (E-BXM1715).

The dry fabric and foam were stacked together in a rigid aluminum mold. High permeability layers placed over the fibers reduced infusion time, and a standard peel ply prevented the resin from adhering to the vacuum bag. Then, the thermoset polyurethane resin was infused through the vacuum-assisted process. The resin was cured for 1 hour at 70 ^{o}C and for 4 hours at 80 ^{o}C in a walk-in oven.

In the following sections detailed descriptions of the tests carried out on material characterization and small-scale sandwich structures are reported. The material characterization included flatwise tensile and compressive tests on the GFRP facings and web layers, and flatwise compressive tests on the two types of polyurethane foam. The

tests on small-scale sandwich structures involved flatwise compressive and tensile tests and three and four-point bending tests.

3.1. Material characterization

3.1.1. Polyurethane foam core

Polyurethane closed-cell foam was used for the three types of cores. The ASTM C365 standard [34] was applied to conduct flatwise compression tests of the foams (Fig. 2a). Three cubes of high-density polyurethane foam and three cubes of low-density polyurethane foam were tested to determine the compressive properties. The coupon dimensions and mechanical properties of the tested specimens are listed in Table 1. Because the foam is quite sensitive to displacement, the tests were conducted in an Instron 4469 testing machine, which can measure the response at small displacements. All specimens were tested under displacement control at a loading rate of 2.54 mm/min.

3.1.2. GFRP facings and web layers

The ASTM D3039 standard [35] was employed to determine the tensile properties of the GFRP laminates extracted from the beams' facings and web cores. All specimens were 254 mm long and 25.40 mm wide. The coupon thicknesses were 2.41 mm and 3.94 mm for the facing and web layers, respectively. End tabs holding the specimen were 63.50 mm long. The tension test was conducted in an MTS-880 testing machine (see Fig. 2b) with a loading rate of 1.27 mm/min. The longitudinal strains were recorded using electrical strain gauges of 350 ohm at the middle of the coupons. Three coupons from the facings and three from the web core were also tested in compression (see Fig. 2c), according to the

ASTM D3410 standard [36]. The coupon dimensions used in compressive tests were 147.32 mm long and 25.40 mm wide; the gauge length was 20.32 mm. The displacement rate of the test was set to 0.127 mm/min. Two strain gauges were attached to the gauge length between the end taps was 147.32 mm long and 25.40 mm.

3.2.   *Small-scale sandwich structures characterization*

3.2.1. *Flatwise compressive tests*

Six specimens were tested: three for Type 1 and three for Type 2. Flatwise compressive strength and elastic modulus for the sandwich core's structural design properties were determined using MTS-880 universal testing machine and following ASTM C365 standard [35] (see Fig. 3a). Since the main purpose of the low-density polyurethane foam of the Type 3 core is its use as a mold for the trapezoidal-shaped FRP layers, the bare foam was tested without any FRP, as demonstrated in the material characterization section. Specimens of Types 1 and 2 had a constant square cross-section of 88.90 mm x 88.90 mm corresponding to a cross-sectional area of 7,903 mm^2 which was smaller than the 10,323 mm^2 area recommended by the ASTM C365 [34]. The composite thickness of Type 1 and 2 was 54.10 mm and 59.18 mm, respectively. Each specimen was centered under the loading plate to ensure a uniform load distribution. The speed of the crosshead displacement was set at a rate of 2.54 mm/mm.

3.2.2. *Flatwise tensile tests*

MTS-880 universal testing machine was used to conduct the flatwise tensile tests (Fig. 3b) according to the ASTM C297 standard [37]. Six specimens were tested (three for

Type 1 and three for Type 2) to determine the flatwise tensile strength of core. This test also provided information on the quality of the core-to-facing bond. Similar to the flatwise compression tests, Types 1 and 2 had a constant square cross-section of 88.90 mm x 88.90 mm corresponding to a cross-sectional area of 7,903 mm^2, which was larger than 645.16 mm^2 recommended by the ASTM C297 [37]. The composite thickness of Type 1 and 2 was 54.10 mm and 59.18 mm, respectively. In order to be gripped in the test frame, each specimen was adhesively bonded to T-shape steel sections with an epoxy adhesive supplied by the 3M Company. The loading rate was set at 1.27 mm/min.

3.2.3. *Flexural tests*

Three-point bending tests were conducted on short beams and four point bending tests on long beams in accordance with ASTM C393 standard [38]. The test setup is illustrated in Fig. 4. A Wyoming test fixture (model no. CU-LF) was used [39]. Thick steel plates and high resistance rubber pads (with a shore A hardness of 60) were inserted at the loading and supporting points to distribute the load uniformly and reduce the stress concentrations. The load was applied using an Instron 4469 testing machine with a load capacity of 50 kN and a displacement rate of 1.27-2.54 mm/min. All specimens were tested under displacement control.

The objective of the three-point bending test is to generate the shear stresses by using relatively short beams and analyze their impact on the total deflection. A total of nine short beams were investigated: four for Type 1, four for Type 2, and one for Type 3. Each specimen was tested over a clear span of 152.40 mm with the load applied at the center of the beam (see Fig. 4a). Four-point bending tests were conducted (Fig. 4b) to investigate

the effect of the three types of cores on flexural behavior of the sandwich beams by increasing the span length. Three specimens of each type were investigated, i.e. a total of nine sandwich beams were examined. They were tested in one-way bending with the span of 609.60 mm, under two equal point loads, applied at 203.20 mm from each support. The specimens were loaded to failure at a displacement rate of 1.27-2.54 mm/min.

Strains in the axial direction of the beams were measured with electrical, high precision strain gauges (produced by Micro Measurements Group) at a resistance of 350 ohm. The bottom deflection at mid-span was recorded using a Linear Potentiometer (LP). A Linear Variable Differential Transducer (LVDT) was mounted on the movable frame of the machine to monitor top deflection at mid-span. The long beams, used for the four-point bending, had gauges attached to the top and bottom of the facesheet surface at the middle of the beam. The short beams, used for the three-point bending, had one gauge attached at the bottom of the facesheet surface (at the middle of the beam). A data acquisition system was used to record the load, displacement, and strain during testing.

4. Assessment of flexural stiffness (EI)

The flexural stiffness (EI) where E is the equivalent modulus of elasticity and I is the equivalent moment of inertia of the sandwich beam was examined because it is typically the driving factor when designing sandwich panels. The flexural stiffness of each beam was calculated using First-order Shear Deformation Theory (FSDT) [40]. These results were used to compare the flexural stiffness of beams with different core types. The FSDT was also used to estimate the shear stiffness of each sandwich beam type by fitting the results collected from three and four-point flexural tests. Note that it is also possible to

estimate the flexural by utilizing the well-known Newmark's equation [41] and the analytical solutions proposed by Faella et al. [42].

In the FSDT analysis, the polyurethane foam and GFRP bidirectional woven fabric facings were modeled as isotropic materials. A perfect bond was assumed to exist between the core and the facings as well as between the core and webs. The bending stiffness was computed accounting for the deflection components that are associated with bending and shear deformations. Given the mid-span deflection values from the three-point loading and four-point loading tests as well as the applied point load (P) and using the following FSDT equations, the shear stiffness GA and flexural stiffness (EI) were determined from ref. [40]:

$$\Delta_{midspan} = \frac{PL^3}{48EI} + \frac{PL}{4kGA} \qquad \text{for three-point loading test} \quad (1)$$

$$\Delta_{midspan} = \frac{23PL^3}{1296EI} + \frac{PL}{6kGA} \qquad \text{for four-point loading test} \quad (2)$$

where L is the span length and k is the shear correction factor (which was assumed to be 5/6).

5. Experimental results

5.1. *Material characterizations*

5.1.1. *Polyurethane foam core*

Figure 5a illustrates the average compressive stress-strain curves of the tested low (soft) and high-density (rigid) polyurethane foam cubes. These curves are linear in the elastic region, with a yield region at an average stress of 0.056 MPa for the low-density foam and 1.04 MPa for the high-density foam. The yield behavior can be explained by the buckling of the foam's internal walls. A long flat plateau was followed. Then, a

densification (hardening) region was created by a gradual stress increase when the cell walls were stacked prior to final densification. No visible signs of failure were observed (see Fig. 5b). Residual displacement of the collapsed foam did, however, occur once the unloading stage was complete.

5.1.2. *GFRP facings and web layers*

Figure 6a illustrates average axial tensile and compressive stress-strain curves for the GFRP facing. In the tensile test, the facing exhibited a linear elastic response up to strain of 0.019 mm/mm at an ultimate stress of 264.7 MPa. In the compressive test, the ultimate compressive strength was 102.73 MPa, or 38.8 % of its ultimate tensile strength. Figure 6b presents average axial tensile and compressive stress-strain curves of the web layers of the Type 3 beam. The curve exhibited nonlinear behavior due to re-orientation of +45/-45 fibers. The ultimate tensile strain was 0.027 mm/mm corresponding to the ultimate stress of 137.9 MPa. In the compression region, the ultimate compressive strength was 102.73 MPa, or 73.5 % of its ultimate tensile strength. These properties were also valid in the transverse direction for both the facings and the web layers due to the symmetric quasi-isotropic architecture of the reinforcing fibers. The observed failure mode for the facing and web layer coupons under tension was a sudden kink rupture and shear rupture, respectively. All tested coupons failed due to micro buckling and kinking of the fibers under compression. A summary of the results collected from the coupon tests is contained in Tables 2 and 3.

5.2.   Small-scale sandwich structures characterization

5.2.1. Flatwise compressive tests

Flatwise compressive tests were conducted on sandwich cubes for the first two types to examine the properties of their cores. Figure 7a displays the compressive stress-strain responses for Types 1 and 2. For Type 1, the curve follows a typical behavior of cellular materials [43]. The first part of the curve was linear in the elastic region, followed by the plateau region where the stress was almost constant under increasing deformation. Then, there was a sharply increasing loading region at a large strain corresponding to solidification. The yield region occurred at an average stress of 1.04 MPa. This yield behavior was attributed to buckling of the foam's internal cell walls. The flat plateau was produced by the development of localized buckling within the cell walls. As the deformation increased, the cell walls stacked on top of each other resulting in the closure of most of the voids. Therefore, the foam became densified and displayed higher strength. A deformed shape of the Type 1 foam is shown in Fig. 7b. For Type 2, the stress-strain curve illustrates that the web core foam initially exhibited a nearly linear behavior up to the maximum stress, which had an average value of 1.18 MPa. It was noticed that the failure mode of this type was buckling of the thin FRP webs and subsequent delamination between the foam and the webs, as shown in Fig. 7c. A summary of the test results for Types 1 and 2 is presented in Table 4.

5.2.2. Flatwise tensile tests

The flatwise tensile properties of the first two types of the sandwich cubes were determined. Figure 8a presents the stress-strain curves for Types 1 and 2. For Type 1, the

response was linearly-elastic up to failure. The failure mode for all of the tested Type 1 specimens was cohesive rupture of the core, which displayed a cup-cone surface (Fig. 8b). The average ultimate tensile strength and the ultimate tensile strain were approximately 0.79 MPa and 0.016 mm/mm, respectively. These results are summarized in Table 5. For Type 2, the curve was linearly elastic up to a strain of 0.0076 mm/mm. Beyond this strain, the response became slightly nonlinear until the specimen ruptured. This nonlinearity was produced by the foam's contribution to tensile resistance. The average ultimate stress and strain were 1.12 MPa and 0.012 mm/mm, respectively. Because of low strength and stiffness of the low-density foam, the initial failure of the foam was Mode I fracture characterized by horizontal cracks. Then, a debonding between the FRP gridwork and the facing occurred, as observed in Fig. 8c.

5.2.3. *Flexural behavior*

Table 6 summarizes the results gathered from the three-point bending tests. Figure 9a presents the load deflection curves at the mid-span for the three core types. For Type 1, all sandwich beams exhibited a linear behavior up to a deflection of approximately 2.79 mm. At larger deflections nonlinearity occurred with stiffness softening up to failure. This behavior can be attributed to the crushable nature of the polyurethane foam. The average of the maximum vertical deflection and the longitudinal bottom strain that were recorded at mid-span were 8.64 mm and 0.006 mm/mm, respectively, at a failure load of 5.16 kN. The recorded strains (see Fig. 9b) at the bottom mid-span exhibited behavior similar to that of the deflection response. As can be observed from the strain curve, the maximum strain value was significantly lower than the ultimate strain of the GFRP facing, which is

attributed to the observed failure mode. All specimens failed due to an inward local bending of the compression facing beneath the loading point, as shown in Fig. 10a, followed by crushing in the top facing and the foam (Fig. 10b). The local bending occurred because the foam's compressive strength and stiffness are insufficient to resist high local stresses.

Type 2 specimens were loaded up to failure. It should be noted from Table 6 that the standard deviation of this type is relatively high. This can be attributed to the distribution of transverse webs as each specimen had a different arrangement due to cutting it from a different location from the large panel. The curve in Fig. 9 suggests a nearly linear response up to failure. The average of the maximum deflection and longitudinal strain recorded at mid-span were 1.12 mm and 0.0023 mm/mm, respectively, at an average failure load of 6.27 kN. The initial failure mode was buckling of the FRP webs coupled with compressive failure in the foam, as depicted in Fig. 10c. Due to post buckling deformations of the webs, the webs subsequently fractured, and the top facing wrinkled inward.

For Type 3 specimens, due to a limited amount of trapezoidal polyurethane foam available, only one specimen was tested. Figure 9a illustrates the tested beam's load-deflection response. In a manner similar to the other two types, the Type 3 specimen also exhibited a linear behavior up to failure as reflected in the strain gauge reading in Fig. 9b. The average of the maximum deflection recorded at mid-span was approximately 6.10 mm at failure load of 21.12 kN. The sandwich beam initially failed by delamination between the web layers and the foam at one corner. The ultimate failure mode included wrinkling of the top facing. This wrinkling was followed by crushing of the web layers under the loading point (see Fig. 10d). It should be noted that the stiffness of the Type 3 curve was slightly lower than of the Type 2, a result that was not anticipated. Overall, these tests

revealed that local failures, rather than global shear failures dominated flexural response. The results provided load versus displacement responses which were needed to estimate the flexural stiffness of each sandwich type.

Table 7 summarizes the results collected from the four-point bending tests. These results were presented in terms of the ultimate load, deflection, and strain in both the upper and lower facings at the ultimate load, and the observed failure modes. Figure 11a presents a load-deflection curve for each of the three types tested. The behavior of each type clearly demonstrated the significant effect produced by the type of core used. In general, all beam types behaved linearly until a certain load. The linear behavior was followed with a nonlinear response that was produced by shear deformation of the polyurethane core. Nonlinearity in the strain curves (see Fig. 11b) was not observed because strain measurements were taken at the facing surface, reflecting the facing's linear behavior. The maximum strains measured on both the compression and tension facings were significantly lower than the ultimate strain measured in the compression and the tension coupon specimens (0.019), which is also attributed to each beam because the strength of the facing materials is high, so that it would be impossible to cause compressive or tensile failure at this span length.

The average mid-span recorded deflection for the Type 1 specimens was 21.10 mm at an approximate ultimate load of 7.0 kN. The initial failure mode occurred when the core yielded under the loading points and the top face sheet wrinkled. All Type 1 sandwich beams exhibited either a bending fracture in the top facing or a shear failure in the core followed by debonding (see Figs. 12a and 12b, respectively). The top facing in Type 2 initially failed due to intercellular buckling (Fig. 12c). Shear failure in the core material

(Fig. 12d) was the ultimate failure mode. As shown in the Table 7, the ultimate loads had a high degree of variability. This variability was attributed to the number of longitudinal webs within each specimen; one specimen had three longitudinal webs, and the other two had two. The maximum measured deflection at mid-span for the Type 3 specimens was 14.22 mm at an ultimate load of approximately 19.10 kN (Fig. 11a). The behavior was linear with a subsequent softening nonlinear response prior to reaching the ultimate load capacity. This softening nonlinearity could be attributed to compression failure under the loading points and associated nonlinear response of the foam (Fig. 12e). The ultimate failure was caused by excessive compressive stresses in the webs, which created a hinge mechanism in the top facing under the loading point (Fig. 12f).

5.3.   *Stiffness (EI) calculations*

Flexural stiffness of Types 1 and 2 was estimated using FSDT equations (1) and (2), and the results are listed in Table 8. The flexural stiffness for Type 3 was based on the deflection associated with bending from the four-point loading test only. The shear stiffness, based on the geometry of Type 3, was expected to be very large. Therefore, shear deformations can be assumed a relatively small percentage of the total deflection as proved by Tuwair et al. [44]. As a result, the Euler-Bernoulli beam theory was used for this type and provided reasonable accuracy.

Since each type had a different geometry, the results were normalized to their widths and weights for comparison purposes (Table 9). When the results were compared to each other, the Type 3 specimens supported higher load at failure. In terms of stiffness per unit width, Type 3 beams outperformed Type 1 and Type 2 beams by 2.38 and 1.79

times, respectively. In terms of weight comparisons, the corresponding flexural stiffness ratios were 2.32 for Type 2 beams and 2.38 for Type 1 beams. A comparison was also made between Type 3 sandwich beam and conventional reinforced concreted (RC) beam of similar cross-sectional dimensions. Notably, Type 3 weigh approximately one-fifth of the RC beam that made of normal weigh concrete. In addition, the RC beam with 27.6 MPa compressive strength would be 4.4 stiffer than Type 3 sandwich beam.

The relative contributions of shear to the total deflection was 63%, 34%, and ~1% for Types 1, 2, and 3, respectively. Therefore, in Type 1 without ribs in the core, shear deformation of the polyurethane foam contributed over half of the total deflection. Evidently this highlights the importance of shear deformation to the total deflection in Type 1. In contrary, the web layers in Type 3 core contributed significantly to the shear stiffness of the of the sandwich beam practically eliminating shear deformations.

As a result, the Type 3 beams are recommended in this study because they:

- Possess the highest flexural strength, flexural stiffness, and shear stiffness.
- Demonstrate excellent bond between the core and facings.
- Did not suffer significantly from localized effects at concentrated loads.
- Produce a more gradual failure compared to the other types, which failed instantaneously.

6. Discussions

The flatwise compressive tests revealed that the Type 2 core was significantly stronger and stiffer than the Type 1 core. These results also revealed excessive deformations under concentrated loads, potentially leading to serviceability issues. The

flatwise tensile tests were used to examine the bond quality between the core and the facings. In Type 1, failure occurred in the polyurethane foam itself, as the bond between the foam and the facing was stronger than the foam core. On the other hand, the Type 2 core failed at the bond between the core and the facings. This occurred due to the higher tensile capacity of the used interconnected GFRP gridwork compared to Type 1 where the tensile stresses were resisted by the foam core only.

The results gathered from the three-point bending tests revealed that in all three types tested, the localized failure under concentrated loads was the critical concern. These local failures led to the stiffness reduction identified in all force-displacement curves prior to final failure. The compressive failure of Type 1 was attributed to the foam's low stiffness and strength. The localized buckling of the thin core webs that occurred in Type 2 was the result of the high aspect ratio of these elements. The initial failure by delamination occurred in Type 3 because of the specimen manufacturing defects. Type 3 specimen finally failed when the top facing wrinkled under the loading point. In four-point loading tests all specimens behaved linearly until yielding, intercellular buckling, and compression failure occurred. Nevertheless, the Type 1 specimens were influenced by localized effects more than the Types 2 and 3. Types 2 and 3 failed in shear in the core and compression in the top facing, respectively, while Types 1 and 2 failed instantaneously with a loud sound, while Type 3 failed more gradually. The difference between the top and bottom deflections recorded at mid-span was much smaller for Type 3 than it was for the other two types. This reflects the local stiffness and strength of the web-reinforced sandwich panels. The web layers in Type 3 enhanced the section by providing support to the top facing and, thus, improved local stiffness and strength.

Serviceability limit state is a key criterion in designing sandwich bridge decks because of the relatively low stiffness of polyurethane composites (E-glass fibers and polyurethane resins). As stated in the stiffness (EI) calculations section of this study, the Type 3 beam possessed the highest flexural and shear stiffness. The web layers that were introduced to this type contributed significantly to the increase in the shear stiffness so that minimal shear deformation occurred. When normalized to the beam widths, the Type 3's core contributed substantially to its flexural stiffness increasing it by 238% and 179% in comparison to Types 1 and 2, respectively.

Overall, the Type 3 core is likely the most practical for implementation in bridge decking. Although meeting the serviceability requirements of bridge decking will require a larger cross-section, it will be achievable with reasonable facing and web layers thicknesses, as well as a smaller and more practical panel depth than in the other two construction types. The typical size of a full-scale deck panel is five feet wide by eight feet long. The span (2.44 m) of the panel will be perpendicular to the traffic direction and will be simply supported on the short dimensions (1.52 m). Thus, the system would behave as a flexural system in the perpendicular direction to traffic and as a truss system in the parallel direction. The design of the panel will be based on the standard AASHTO Truck or Tandem [45], whichever controls a particular aspect. In accordance with FHWA guidelines, panel stresses must be limited to 20% of the ultimate strength. Deflection should be limited to 1/800 of the supporting span length according to the guidelines of AASHTO and FHWA.

7. Numerical study

The low stiffness of the foam materials used in the cores coupled with relatively short spans often lead to complex behavior at the load and support points. As a result, FEM was used to simulate the behavior of the candidate beam to better understand mechanics of the proposed design. As indicated above, Type 3 beam is recommended for real bridge deck applications based on the results of the experimental work. FEM has shown very good accuracy simulating the complex behavior at the loading points of this beam, as will be explained below.

7.1.   Description of the numerical model

The 3-D finite element analysis was conducted using commercial software package ABAQUS/CAE, release 6.11 [46]. The finite element model (FEM) of a representative section of the beam was developed (Fig. 13) and used to predict the flexural behavior of the tested sandwich beams. The Type 3 beam was modeled with the same geometry (Fig. 1c) as that of the investigated beams. The polyurethane foam, webs, and facings (Fig. 13) were modeled with 3-D continuum solid elements that had eight-node, integration-reduced, linear brick elements (C3D8R, hourglass control). These elements had three translational degrees of freedom (DOFs) at each node. The FRP composites of the facing and web layers have the same volume fraction of the fibers in warp (longitudinal) and fill (transverse) directions. Moreover, the thickness of these layers being small compared to other beam dimensions, consequently the facing and web layers were modeled as isotropic materials to simplify the analysis. The properties were determined from the material characterization tests (Tables 1-3). The polyurethane foam material was modeled using crushable foam

model that is available in the ABAQUS library. The crushable foam model has the capability to enhance the ability of a foam material to deform in compression because of the cell wall buckling process [46]. The experimental tests of Type 3 revealed that neither delamination nor relative slip occurred between the facing and the core during testing. Therefore, it is acceptable to assume a full contact (perfect bond) at the interface between the sandwich beam components. The specimen considered in the analysis was loaded and supported by 38.10 mm-wide steel plates, which were free to rotate. The load was applied in displacement control at the metal plates to avoid stress concentration. Contact element was implemented between the loading pads and the GFRP panel. A sensitivity analysis was conducted on the effect of the type of the contact element between the loading pads and the GFRP panel. Two different types of contact elements were investigated: tied contact elements and surface contact element. The first type of contact elements does not allow sliding between the beam surface and loading plate; however, the second contact elements enables such sliding controlled by a coefficient of friction of 0.3. The results of the two models were almost identical; however, the running time of the solution was much lower in the case of tied contact elements. Therefore, tied contact elements were selected for the analysis. The displacement was increased monotonically until the beam failed. The model failed when the FRP materials reached their ultimate tensile or ultimate compressive stress.

7.2.   *Numerical results*

Figure 14a shows the deflection contours generated using FEM for Type 3 specimen. Figure 14b illustrates a comparison between the experimentally measured deflection values and the deflection predicted by the FEM at mid-span of the tested beam.

Good agreement was observed between the experimental results and the FEM predictions. Overall, the FE model accurately captured the tested sandwich beam's behavior. The sandwich beam reached the peak load of 19.10 kN at the ultimate deflection of 14.22 mm during the experiment. It reached the ultimate load of 20.37 kN at the maximum deflection of 16.25 mm according to the FEM analysis. The average maximum tensile strain at the mid-span's bottom facing recorded during the experiment was equal to 0.0046 mm/mm. For the FEM, this value was 0.0058 mm/mm, a difference of 20%. The FEM tended to slightly overestimate the predicted deflection at mid-span. These differences occurred because of the manufacturing process that produced some variability in the thickness of both GFRP facings and the web layers. Failure in the FEM analysis occurred when the top facing at the applied point loads reached the ultimate stress. This mode of failure matches the experimental behavior (see Fig. 15).

8. Conclusions

The structural behavior of three different core alternatives for GFRP foam-infill sandwich panels was investigated. The results of our experimental and numerical research demonstrated the engineering and economic feasibility of the proposed design.

All sandwich beams tested in bending exhibited a linear-elastic behavior. This initial response was followed with a stiffness softening prior to failure. The Type 3 construction exhibited better strength as well as flexural and shear stiffness than the other two types investigated in this research. This is due to the remarkable effect of web layers. Also, excellent bond was observed between the polyurethane foam core and the facings in the Type 3 beams.

The Type 3 beams were less vulnerable to localized stress effects under a concentrated load compared to the other two types. On the other hand, Types 1 and 2 were quite susceptible to localized effects under concentrated loads, such as inward local bending and wrinkling of the compression facing under the concentrated loads, which resulted in a lower ultimate strength. Additionally, Types 1 and 2 experienced large deflections associated with significant shear deformation of the core. The Type 3 beam prevented or reduced the facing-core debonding trend that has been observed in conventional sandwich beam construction.

The FEM allowed us to accurately predict the structural behavior of Type 3 beams in bending under monotonic loading, as well as predicting their actual failure modes. Accordingly, this numerical model can be used at the design stage.

Additional work, such as panel-to-panel connections, panel-to-girder joints, roadway crown effect studies , is necessary to facilitate the implementation of the proposed system.

Referenczes

[1]   Kootstookos A, Burchill PJ. The effect of the degree of cure on corrosion resistance of vinyl ester/glass fiber composites. Composites A; 2004. 35:501-8.

[2]   Abdelkarim O, ElGawady MA. 2015. Analysis and finite element modeling of FRP-concrete-steel double-skin tubular columns. J Bridge Engr, ASCE; 2015. B4014005-1: B4014005-12.

[3]   Dawood H, ElGawady MA. 2013. Performance-based seismic design of unbonded precast post-tensioned concrete filled GFRP tube piers. Compos Part B: Engineering; 2013. 44(1):357-367.

[4]   ElGawady MA, Dawood H. Analysis of segmental piers consisted of concrete filled FRP tubes. Engr Structures; 2012. 38:142-152.

[5]   Camata G, Shing PB. Evaluation of GFRP honeycomb beams for the O'Fallon park bridge. J Compos Construct, ASCE; 2005. 8(6):545–55.

[6]   Davalos JF, Salim HA, Qiao P, Lopez-Anido R, Barbero EJ. Analysis and design of pultruded FRP shapes under bending. Compos Part B: Engineering; 1996. (27B): 295-305.

[7]   Rejab MRM, Cantwell WJ. The mechanical behaviour of corrugated-core sandwich panels. Compos: Part B; 2013. 47:267–277.

[8]   Camata G, Shing PB. Static and fatigue load performance of a GFRP honeycomb bridge deck. Comp Part B: Engineering; 2010. 41(4):299–307.

[9]   Fam A, Sharaf A. Flexural performance of sandwich panels comprising polyurethane core and GFRP skins and ribs of various configurations. Comp Struc; 2010. 92:2927–2935.

[10]   Wang L, Liu W, Wan L, Fang H, Hui D. Mechanical performance of foam-filled lattice composite panels in four-point bending: Experimental investigation and analytical modeling. Comp Part B: Engineering; 2014. 67:270-279

[11]   Correia JR, Garrido M, Gonilha JA, Branco FA. GFRP sandwich panels with PU foam and PP honeycomb cores for civil engineering structural applications: Effects of introducing strengthening ribs. Int J of Struc Integrity; 2012. 3:127-147.

[12]   Noor AK, Burton WS, Bert CW. Computational models for sandwich panels and shells. Applied Mechanics Reviews, 1996. 49(3):155-199.

[13]   Zureick A, Engideniz M, Arnette J, Schneider C. (2003). Acceptance test specifications and guidelines for fiber-reinforced polymeric bridge decks. Final

Report, Volume 1, Submitted to the Federal Highway Administration, 2003. Contract No. DTFH 61-00-C-00022.

[14]   Plunkett JD. Fiber-reinforcement polymer honeycomb short span bridge for rapid installation. IDEA project report, 1997.

[15]   Stone D, Nanni A, Myers J. Field and laboratory performance of FRP bridge panels. Compos in Construction, Porto, Portugal, J Figueiras, L. Juvandes and R. Furia, Eds, 2001. 701-706.

[16]   Henderson M. Evaluation of Salem Avenue bridge deck replacement: Issues regarding the composite materials systems used. Final Report. Ohio Department of Transportation, December, 2000.

[17]   Reising R, Shahrooz B, Hunt V, Lenett M, Christopher S, Neumann A, Helmicki A, Miller R, Konduri S, Morton S. Performance of a five-span steel bridge with fiber reinforced polymer composite deck panels. Transportation Research Board Annual Meeting, Washington, D.C., 2001.

[18]   Zou B. Design guidelines for FRP honeycomb sandwich bridge decks. Doctoral Dissertation, West Virginia University. (UMI Number: 3376458), 2008.

[19]   Davalos JF, Qiao P, Xu XF, Robinson J, Barth KE. Modeling and characterization of fiber-reinforced plastic honeycomb sandwich panels for highway bridge applications. Comp Struc; 2001. 52: 441-452.

[20]   Davalos JF, Chen A, Zou B. Performance of a scaled FRP deck-on-steel girder bridge model with partial degree of composite action. Eng Stru; 2012. 40:51-63.

[21]   Potluri P, Kusak E, Reddy TY. Novel stitch-bonded sandwich composite structures. Compos Struc; 2003. 59(2):251-259.

[22]   Hassan T, Reis EM, Rizkalla SH. Innovative 3-D FRP sandwich panels for bridge decks. Proceedings of the Fifth Alexandria International Conference on Structural and Geotechnical Engineering. Alexandria, Egypt. 2003.

[23]   Reis EM, Rizkalla SH. Material characteristics of 3-D FRP sandwich panels. Construction and Building Materials; 2008. 22(6):1009-18.

[24]   Dawood M, Taylor E, Ballew W, Rizkalla S. Static and fatigue bending behavior of pultruded GFRP sandwich panels with through-thickness fiber insertions. Compos. Part B; 2010. 41(5):363–374.

[25]   Zureick A. Fiber-reinforced polymeric bridge decks. Proceedings of the National Seminar on Advanced Composite Material Bridges, FHWA, 1997.

[26]   Bakis CE, Bank LC, Brown VL, Cosenza E, Davalos JF, Lesko JJ, Machida A, Rizkalla SH, Triantafillou TC. Fiber-reinforced polymer composites for construction state-of-the-Art Review. ASCE Journal Of Composites For Construction; 2002; 6(2):73-87.

[27]   Davalos JF, Chen A, Qiaof P. FRP Deck and Steel Girder Bridge Systems: Analysis and Design. Boca Raton, FL: CRC Press, 2013.

[28]   Keller T, Gurtler H. Composite action and adhesive bond between fiber-reinforced polymer bridge decks and main girders. J of Compos for Const; 2005. 9(4), 360-368.

[29]   Righman J, Barth KE, Davalos JF. Development of an efficient connector system for fiber reinforced polymer bridge decks to steel girders. J of Compos for Const; 2004. 8(4):279-288.

[30]   Connolly M, King J, Shidaker T, Duncan A. Processing and characterization of pultruded polyurethane composites. Huntsman Enriching lives through innovation, 2006.

[31]   Alagusundaramoorthy P, Reddy RV. Testing and evaluation of GFRP composite deck panels. Ocean Engineering, 2008; 35: 287–293.

[32]   Zenkert D. The Hand book of Sandwich Construction. Chameleon Press Ltd, London, UK, 442p. 1997.

[33]   Volz J, Chandrashekhara K, Birman V, Hawkins S, Huo Z, Mohamed M, Tuwair H. Polyurethane foam infill for fiber-reinforced polymer (FRP) bridge deck panels. Final Report Prepared for Missouri Department of Transportation. Project TRyy1203, 2014.

[34]   ASTM. A standard test method for flatwise compressive properties of sandwich cores (C365/C365M-11a). Am Soc Test Mater 2011.

[35]   ASTM. A standard test method for tensile properties of polymer matrix composite materials (ASTM D3039/D3039M-08). Am Soc Test Mater 2008.

[36]   ASTM. A standard test method for compressive properties of polymer matrix composite materials with unsupported gage section by shear loading (D3410 / D3410M – 08). Am Soc Test Mater 2008.

[37]   ASTM. A standard test method for tensile strength of flat sandwich construction in flatwise plane (C297-08). Am Soc Test Mater 2008.

[38]   ASTM. A standard test method for flexural properties of sandwich constructions (C393/C393M-11e1). Am Soc Test Mater 2011.

[39]   Wyoming Test Fixtures INC. Long Beam Flexure Test Fixture. <http://www.wyomingtestfixtures.com/Products/d2.html> [22.07.2014].

[40]   Carlsson LA, Kardomateas GA. Structural and Failure Mechanics of Sandwich Composites. Springer, 2011.

[41]   Newmark NM, Siess CP, Viest IM. Tests and analysis of composite beams with incomplete interaction. Proc Soc Exp Stress Anal, 1951;9(1):75–92.

[42]   Faella C, Martinelli E, Nigro E. Steel–concrete composite beams in partial interaction: Closed-form ''exact'' expression of the stiffness matrix and the vector of equivalent nodal forces. Engineering Structures, 2010; 32:2744–2754.

[43]   Gibson LJ, Ashby MF. Cellular Solids: Structure and Properties. Oxford: Pergamon, 1988.

[44]   Tuwair H, Volz J, ElGawady M, Mohamed M, Chandrashekhara K, Birman V. Testing and evaluation of GFRP sandwich bridge deck panels filled with polyurethane foam. The American Society for Composites 29th Technical Conference, 16th US-Japan Conference on Composite Materials, and ASTM D-30 Meeting, San Diego, CA, Sept. 2014.

[45]   AASHTO. LRFD Bridge Design Specifications. Am Soc of State Highway Tran. 6th Edition, 2013 Interim Revisions, Washington, D.C.

[46]   ABAQUS Software and Documentation. V.6.11-1. ©Dassault Systèmes, SIMULIA; 2013.

Table 1. Polyurethane foam properties from compressive tests

Foam Density	Width (mm)	Length (mm)	Thick. (mm)	Elastic Modulus (MPa)			Compressive Strength (MPa)			Compressive Strain (mm/mm)		
				Mean	S.D*	C.V*	Mean	S.D	C.V	Mean	S.D	C.V
Low	64.26	65.79	69.34	2.1	0.15	7.1	0.056	0.0034	6.9	0.025	0.005	21.4
High	88.90	88.90	49.28	37.1	4.63	12.5	1.04	0.0100	1.0	0.037	0.003	7.7

*S.D: Standard Deviation
*C.V: Coefficient of Variation (%)

Table 2. GFRP properties from tensile coupon tests

Coupon Type	Width (mm)	Thick. (mm)	Tensile Modulus (MPa)			Ultimate Strength (MPa)			Ultimate Strain (mm/mm)		
			Mean	S.D	C.V	Mean	S.D	C.V	Mean	S.D	C.V
Facing	25.40	2.89	13,977	131.7	0.94	264.8	15.9	6.1	0.019	0.001	5.88
Web core	25.40	3.94	11,803	938.4	7.95	137.9	6.2	4.51	0.027	0.004	13.82

Table 3. GFRP properties from compressive coupon tests

Coupon Type	Width (mm)	Thick. (mm)	Compressive Modulus (MPa)			Ultimate Strength (MPa)			Ultimate Strain (mm/mm)		
			Mean	S.D	C.V	Mean	S.D	C.V	Mean	S.D	C.V
Facing	25.40	2.89	13,233	1,711	12.9	102.7	16.27	15.80	0.011	0.004	34.66
Web core	25.40	3.94	5,732	860	15.0	101.4	8.41	8.27	0.023	0.004	17.26

Table 4. Summary of flatwise sandwich compressive tests

Panel Type	Results	Width = Length (mm)	Thick. (mm)	Yield Strength (MPa)	Yield Strain (mm/mm)	Compressive Modulus (MPa)
Type 1	Average	88.90	54.10	1.04	0.034	37.1
	S.D			0.011	0.003	4.6
	C.V			1.01	7.76	12.5
Type 2	Average	88.90	59.18	1.18	0.016	75.3
	S.D			0.030	0.004	12.8
	C.V			2.55	24.54	16.9

Table 5. Summary of flatwise sandwich tensile tests

Panel Type	Results	Width = Length (mm)	Thick. (mm)	Ultimate Strength (MPa)	Ultimate Strain (mm/mm)	Tensile Modulus (MPa)
Type 1	Average	88.90	54.10	0.79	0.016	47.23
	S.D			0.024	0.001	0.49
	C.V			3.09	5.91	1.03
Type 2	Average	88.90	59.18	1.12	0.012	96.80
	S.D			0.35	0.001	19.87
	C.V			31.14	10.20	20.53

Table 6. Test results of three-point loading tests

Panel Type	Results	Width [b] (mm)	Depth (mm)	Span (mm)	Pu (kN)	Δu (mm)	εmax (mm/mm)	Failure Mode
Type 1	Average	76.45	54.10		5.16	8.64	0.0060	Indentation + Crushing
	S.D				0.34	0.66	0.0008	
	C.V				6.62	7.68	14.48	
Type 2	Average	76.45	59.18	152.40	6.27	1.12	0.0023	Buckling
	S.D				1.28	0.25	0.001	
	C.V				20.47	23.39	43.56	
Type 3	-	See Fig. 1	60.96		21.12	6.10	0.0054	Wrinkling

Table 7. Test results of four-point loading tests

Panel Type	Results	Pu (kN)	Width [b] (mm)	Depth (mm)	Span (mm)	Δu (mm)	Bottom-Face εmax (mm/mm)	Top-Face εmax (mm/mm)	Failure Mode
Type 1	Average	7.0	102.11	54.10		21.08	0.0037	-0.0038	Bending Fracture or Shear Failure
	S.D	0.14				1.21	0.0003	0.0006	
	C.V	1.94				5.71	6.63	15.87	
Type 2	Average	12.2	105.66	59.18	609.60	13.21	0.0061	-0.0092	Intercellular Buckling + Shear Failure
	S.D	3.0				2.42	0.0018	0.0028	
	C.V (%)	24.76				18.36	30.83	30.75	
Type 3	-	19.1	See Fig. 1	60.96		14.22	0.0046	-0.0045	Compression Failure

Table 8. Calculated stiffness results

Panel Type	Flexural Stiffness (EI) (kN.mm2)			Shear Stiffness (GA) (kN)		
	Mean	S.D	C.V	Mean	S.D	C.V
1	5,056,821	650,934	12.9	91.7	1.3	1.4
2	6,549,876	1,014,418	15.5	391.2	25.1	6.4
3	8,865,849	-	-	$\sim \infty$	-	-

Table 9. Normalized stiffness values

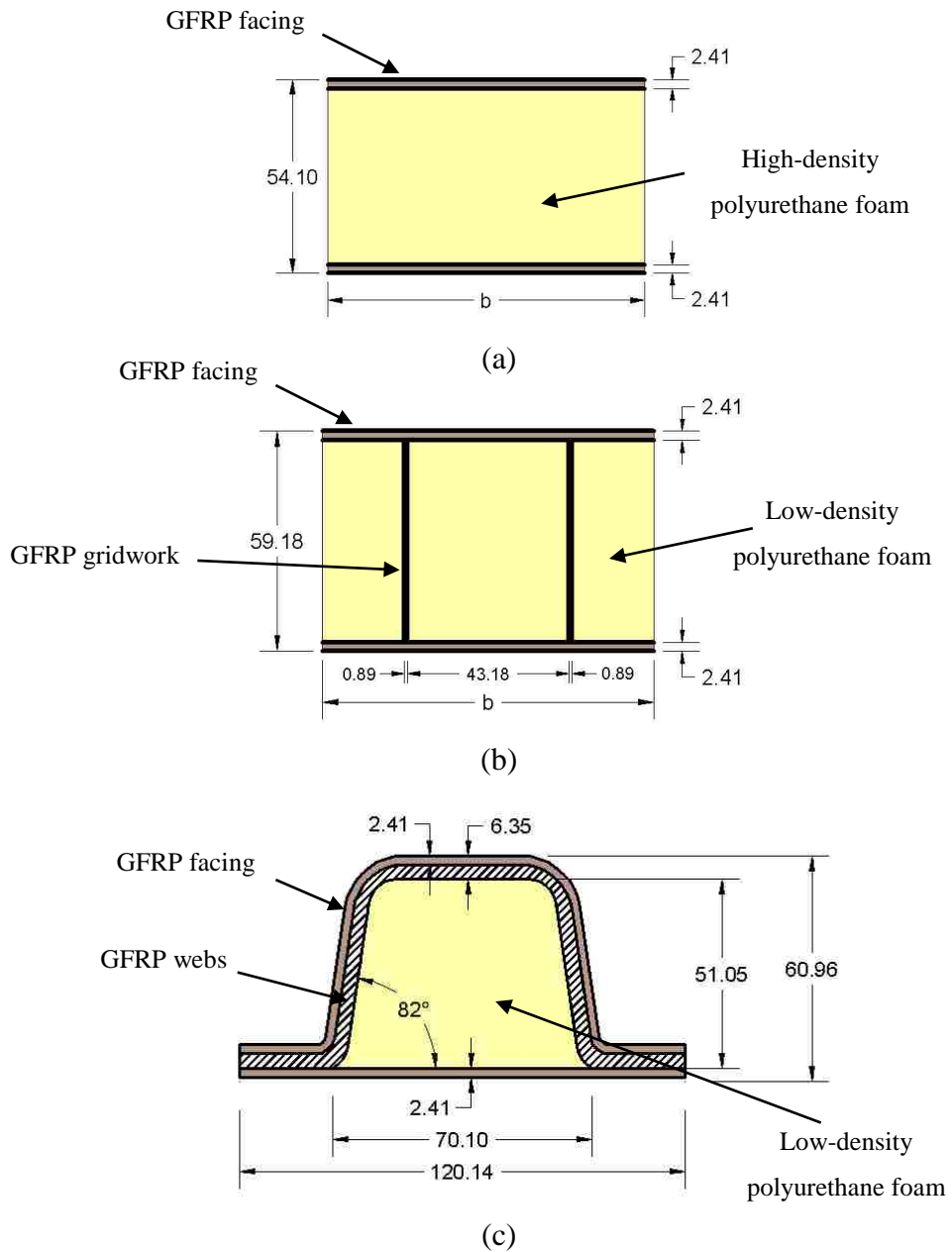| Panel Type	Width (mm)	Mass Density (kN/m3)	EI/width (kN.mm2/mm)	EI/mass-density (kN.mm2/(kN/mm3))
1	102.11	203.2	44,9412	24,886
2	105.66	208.4	59,691	31,429
3	83.06	484.4	106,740	18,302

Figure 1. Sandwich panel configurations: (a) Type 1, (b) Type 2, and (3) Type 3. (all dimensions in mm, 1 in. = 25.4 mm)

(a)   (b)   (c)
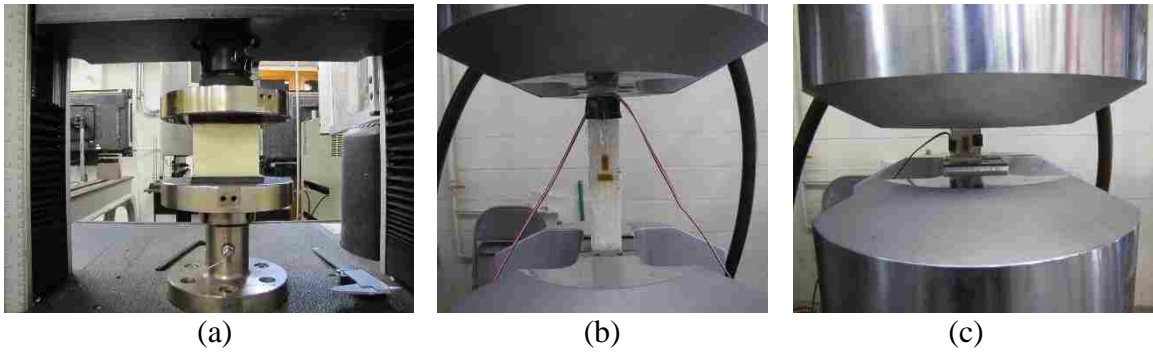
Figure 2. Test setups: (a) flatwise compressive test, (b) tensile coupon test, and (c) compressive coupon test

(a) (b)

Figure 3. Test setup for flatwise sandwich: (a) compressive test and (b) tensile test for Type 1
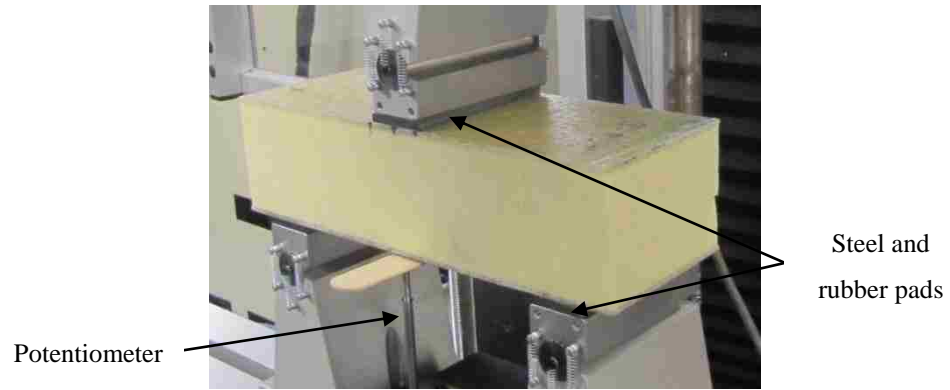
(a)
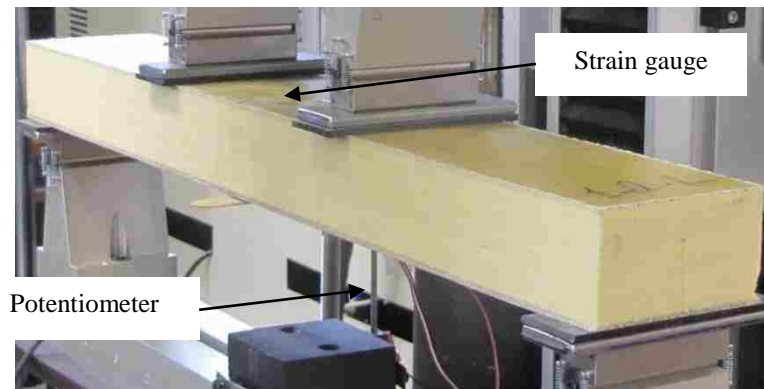
(b)

Figure 4. Test setups: (a) three-point and (b) four-point bending tests for Type 1
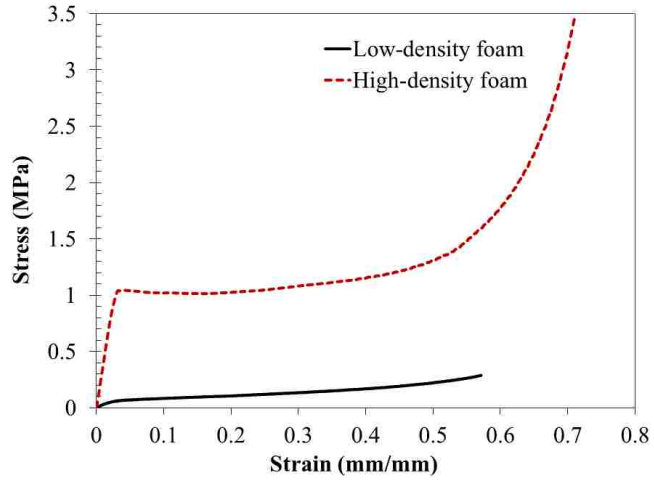
(a)   (b)

Figure 5. Flatwise foam compressive test: (a) stress-strain curves and (b) specimen during testing
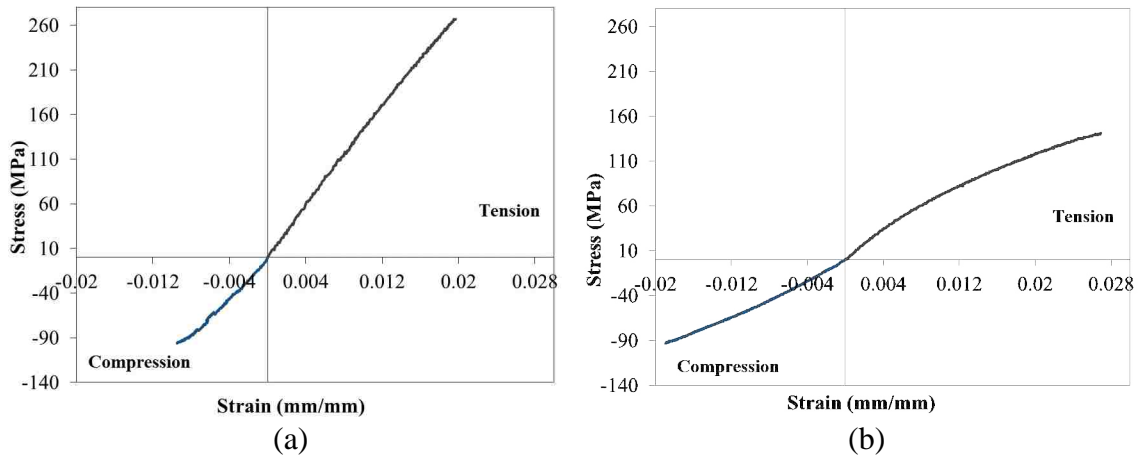
Figure 6. Stress-strain curves: (a) GFRP facing and (b) web layers
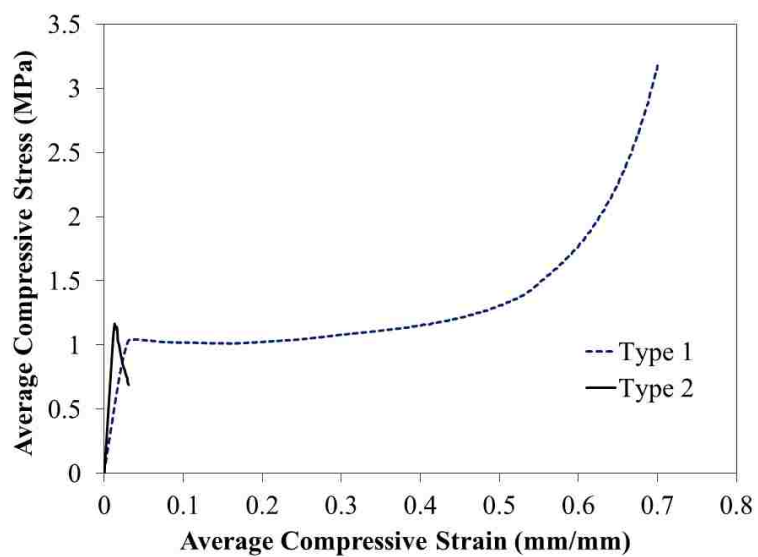
Figure 7. Flatwise sandwich compressive tests: (a) stress-strain curves, (b) failure mode of Types 1, and (c) failure mode of Types 2

(b)

(c)

(a)
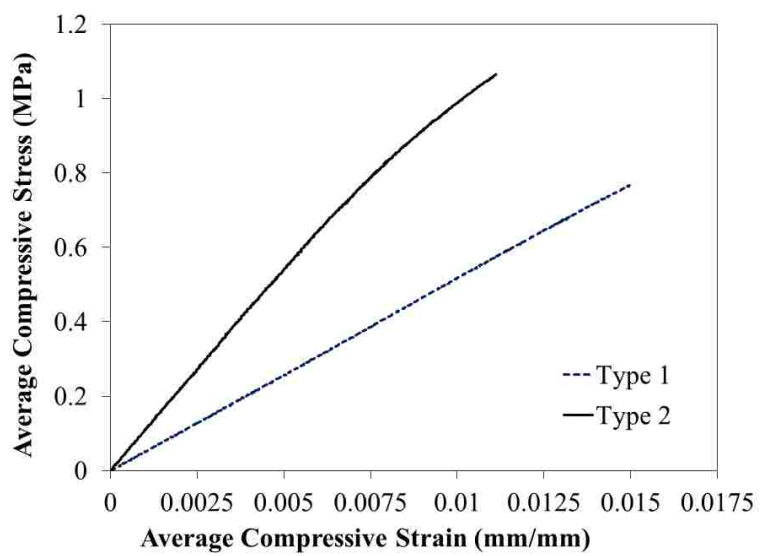
Figure 8. Flatwise sandwich tensile tests: (a) stress-strain curves, (b) failure mode of
Types 1, and (c) failure mode of Types 2
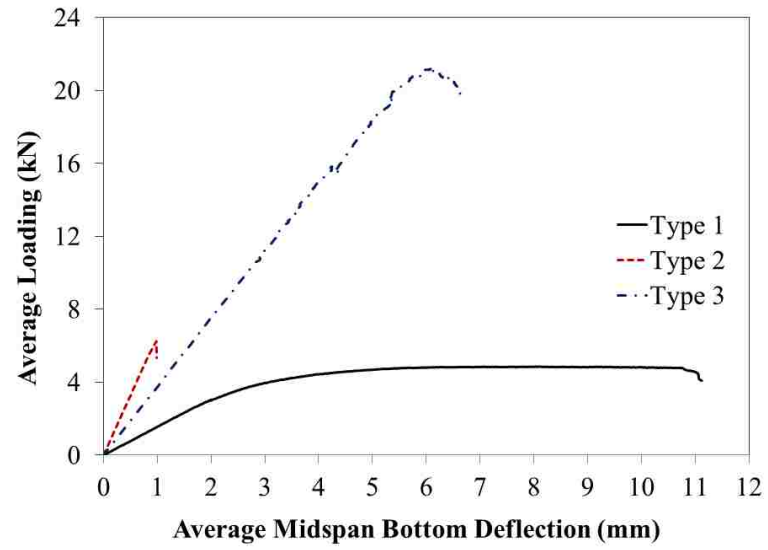
(a)
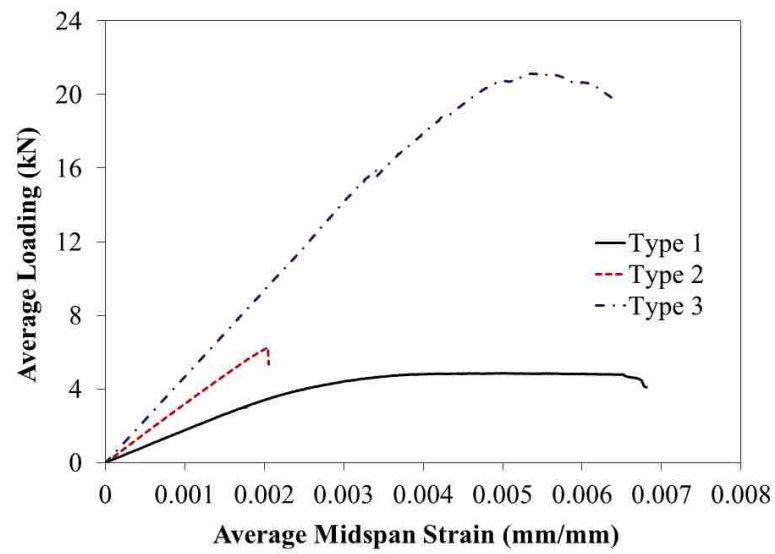
(b)

Figure 9. Three-point bending tests: (a) load vs. mid-span deflection and (b) load vs. mid-span bottom strains

(a)

(b)

\\

(c)

(d)

Figure 10. Failure modes: (a) local buckling, (b) crushing of the top facing and foam in Type 1, (c) buckling of the webs and compressive failure in the foam in Type 2, and (d) wrinkling of the top facing and crushing of the webs in Type 3
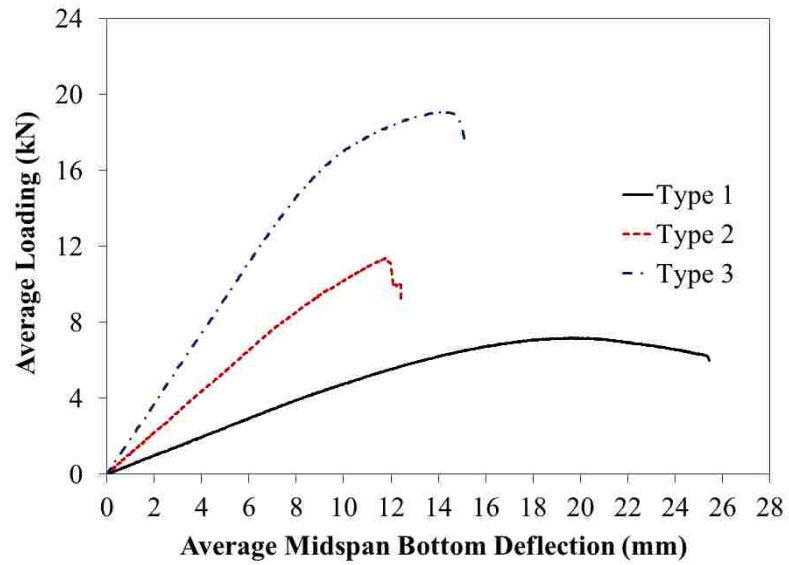
(a)
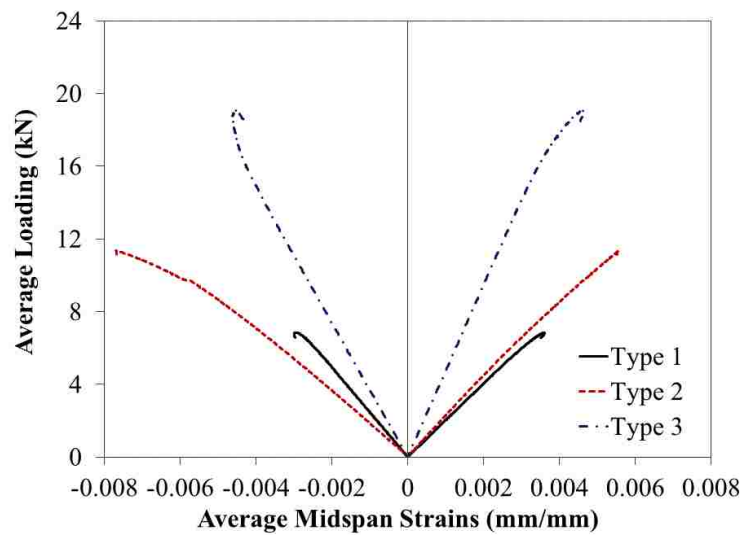
(b)

Figure 11. Four-point bending tests: (a) load vs. mid-span deflection, and (b) load vs. mid-span top and bottom strains
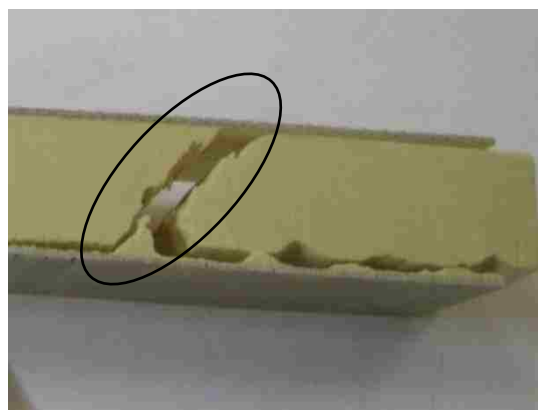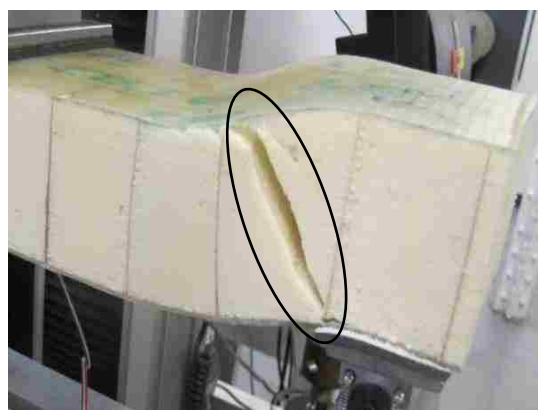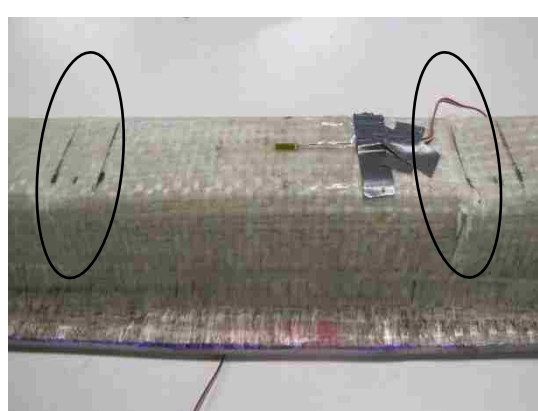
Figure 12. Failure modes: (a) bending fracture, (b) shear failure in Type 1, (c) intercellular buckling, (d) shear failure in Type 2, (e) deformed shape during testing, and (f) compression failure under loading points in Type 3
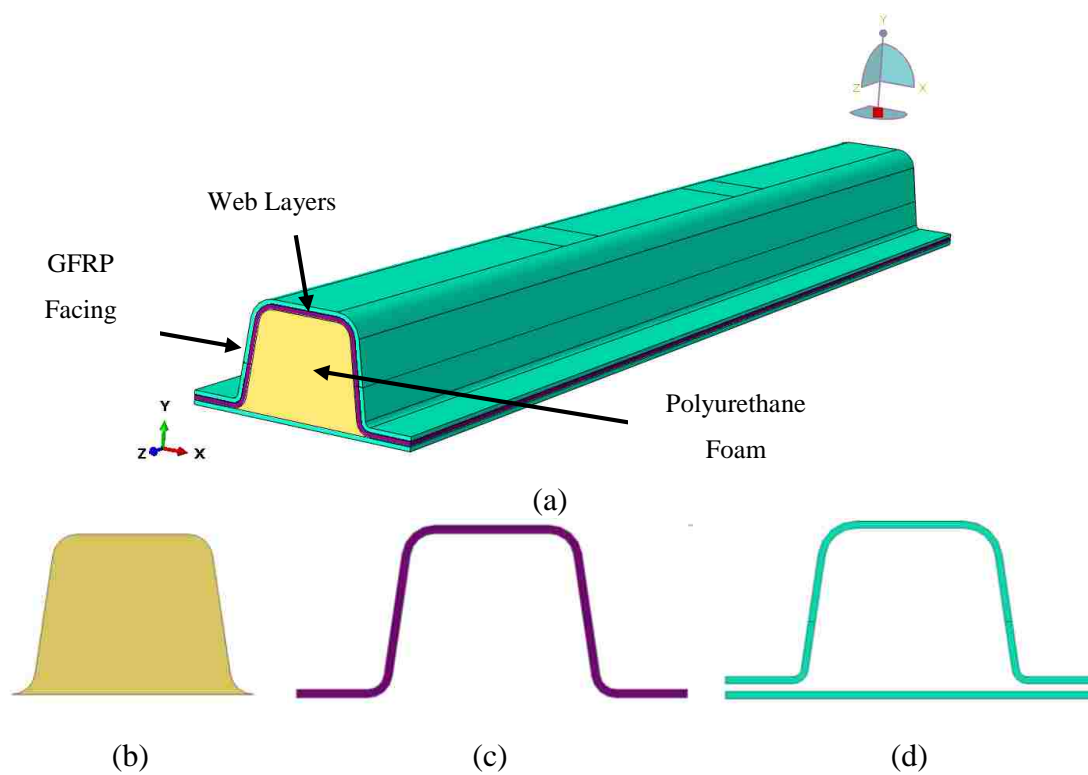
Figure 13. FE model: (a) overall FE model perspective of the tested panel, (b) polyurethane foam, (c) web layers, and (d) GFRP facings

(a)   (b)
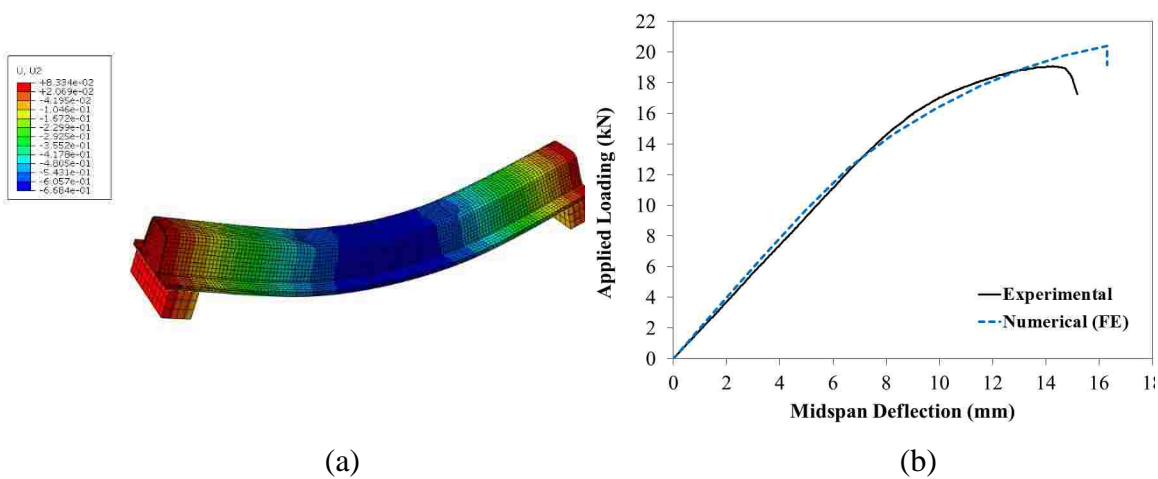
Figure 14. Results of FEM for Type 3: (a) deflection contour and (b) comparison of
experimental and numerical results

Compression failure (Experimental)   Compression failure (FEM)

Compression Failure
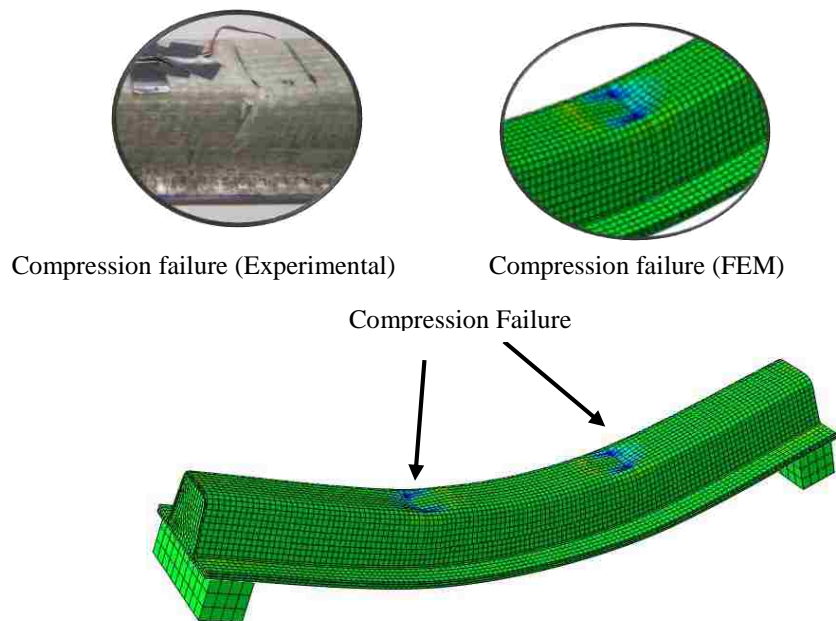
Figure 15. Failure modes and contours of longitudinal principal stresses. The compressive stresses concentrations at the loading points are observed both in experiments and in FEM

II. TESTING AND EVALUATION OF POLYURETHANE-BASED GFRP SANDWICH BRIDGE DECK PANELS WITH POLYURETHANE FOAM CORE

Hesham Tuwair[1]; Jeffery Volz[2]; Mohamed ElGawady[3]; Mohaned Mohamed[4];

K.Chandrashekhara[5]; V. Birman[6]

Abstract

This paper presents the evaluation of an innovative, low-cost, small-scale prototype deck panel under monotonic and fatigue bending. This new system introduces a trapezoidal-shaped, polyurethane foam core with a thermoset polyurethane resin that has a longer pot life to facilitate the infusion process. The proposed panel exhibited a higher structural performance in terms of flexural stiffness, strength, and shear stiffness. The panels consist of two glass fiber reinforced polymer (GFRP) facings with webs of bidirectional E-glass woven fabric that are separated by a trapezoidal-shaped, low-density polyurethane foam. The GFRP panels were manufactured using a one-step, vacuum-assisted, resin transfer molding (VARTM) process. The specimens studied were constructed in the Composite Manufacturing Laboratory in the Mechanical and Aerospace Engineering Department at Missouri University of Science and Technology. Small-scale

[1] Graduate research assistant, Department of Civil, Architectural, and Environmental Engineering, Missouri University of Science and Technology, USA E-mail: hrthw2@mst.edu

[2] Associate professor, School of Civil Engineering and Environmental Science, The University of Oklahoma, USA E-mail: volz@ou.edu

[3] Associate professor, Department of Civil, Architectural, and Environmental Engineering, Missouri University of Science and Technology, USA E-mail: elgawadym@mst.edu

[4] Graduate research assistant, Department of Mechanical and Aerospace Engineering, Missouri University of Science and Technology, USA E-mail: mmm7vc@mst.edu

[5] Curators' professor, Department of Mechanical and Aerospace Engineering, Missouri University of Science and Technology, USA E-mail: chandra@mst.edu

[6] Professor, Engineering Education Center, Missouri University of Science and Technology, USA E-mail: vbirman@mst.edu

prototype deck panels were tested both statically and dynamically in four-point bending to investigate their flexural behavior. The ultimate bearing capacity of the proposed sandwich panels were determined from compression crushing tests. In addition, the load-deflection behavior of the proposed panel was investigated under three loading conditions compression, static flexure, and dynamic flexure. The initial failure mode for all panels was localized outward compression skin wrinkling of the top facing. The ultimate failure was caused by local crushing of the top facing under the loading point due to excessive compressive stresses. First order shear deformation theory (FSDT) was used to predict the panel deformation in the service limit state. In general, the analytical results were found in good agreement with the experimental findings.

Keywords: FRP bridge deck, sandwich panels, GFRP, polyurethane foam

Introduction

According to a study conducted by the Federal Highway Administration (FHWA), 152,000 out of 607,000 bridges (25%) in the United States are in need of either repair or replacement due to corrosion of concrete steel reinforcement (Kirk and Mallett 2013). Replacement of deficient bridges at low costs represents an important challenge. Fiber reinforced polymer (FRP) composites have shown great promise as a potential bridge construction material, eliminating corrosion issues and meeting the goal of a 100-year life span. Although FRP bridges are cost effective over their life cycle, high initial costs hamper their use. Currently more than 50 FRP bridges are in service in the United States. In particular, the No-Name Creek Bridge, built in Kansas in 1996, was the first FRP

honeycomb sandwich bridge (Ji et al. 2010). However, honeycomb sandwich construction requires a labor-intensive manufacturing process that increases the cost of FRP panels and lengthens the lead time. As a result, honeycomb systems that have primarily been employed in the aerospace industry represent a rather questionable value in bridge applications.

FRP sandwich structures offer a number of advantages including: high strength, high flexural stiffness, reduced weight, environmental resistance, rapid construction, and ease of installation compared to conventional bridge materials such as steel or concrete. FRP bridge decks weigh approximately one-fifth of an equivalent reinforced concrete deck (Murton 1999). However, low strength of the core is among the challenges faced by sandwich structures, including those employed in bridge decks. Delamination of layers of the facings and debonding of the facings from the core present additional challenges. For example, the study conducted by Camata and Shing (2010) on structural and fatigue response of sandwich bridge decks revealed that delamination failure between the facings and the honeycomb core was the principle mode of failure. A number of studies have been conducted to develop better and more reliable FRP bridge decks. For example, Hassan et al. (2003) proposed an alternative system for FRP bridge decks using three-dimensional fibers (known also as through thickness-fiber), manufactured using either weaving or injection technology. These fibers are used to connect the top and bottom GFRP facings and thus overcome delamination in the facings and debonding between the facings and core. The proposed design also enhanced strength and stiffness over traditional sandwich composites. A somewhat similar approach was considered by Potluri et al. (2003) who found that the mechanical, structural, and fatigue properties of FRP panels improved significantly when stitches were added to connect the top and bottom skins. Rocca and

Nanni (2005) investigated the flexural and fatigue behavior of GFRP sandwich panels that contained a fiber reinforced foam (FRF) core and found that the residual compressive strength was not significantly reduced after two million fatigue cycles. They also observed that the deflection associated with the shear contribution (in the total deflection) can be ignored due to the shear strength provided by the core. Zi et al. (2008) proposed a new type of GFRP bridge deck consisting of GFRP with rectangular holes filled with polyurethane foam. Their study found that, when the rectangular holes were filled with polyurethane foam, the structural response and strength in the transverse direction were significantly improved. However, the elastic modulus (i.e. stiffness) did not increase.

Recently, a comprehensive research program was conducted at Missouri University of Science and Technology to evaluate the static and fatigue behavior of an innovative sandwich panel system consisting of GFRP facings separated by a trapezoidal-shaped, polyurethane foam core (Fig. 1) where the top and bottom facings were connected with corrugated shear layers. This present study investigated the monotonic and fatigue flexural strength of the proposed prototype panels. Material characterization through tensile and compressive coupon tests was also completed. The ultimate bearing capacity, local buckling, and crushing load were estimated through flatwise compressive tests of small-scale, prototype panels. Finally, the analytical beam theory was used to predict the deflection of the tested specimens. The overall flexural strength and stiffness were determined by testing two GFRP sandwich panels in a four-bending load test, which was subsequently compared to an analytical prediction using the first order shear deformation theory within the elastic region.

Panel Description and Manufacturing

The cross-sectional dimensions of the panels considered in the study are shown in Fig. 2. The top and bottom facings of the panel are constructed with three layers of plain-weave woven E-glass fabric (WR18/20) laid up in 0/90° fiber orientation. The fibers were purchased from Owens Corning (Toledo, Ohio) and infused with a new type of longer pot life, thermoset polyurethane resin that was developed by Bayer MaterialScience. The webs of the panels consist of corrugated shear layers (E-BXM1715), purchased from Vectorply (Phenix City, Alabama) and formed by three layers of +/-45° double bias, and the foam was matted with a combination of two plies and knitted E-glass laid up in +/-45° to produce better bond. The mass density of closed-cell polyurethane foam used in the core was 2 lb/ft^3 (32 kg/m^3), purchased from Structural Composites (Melbourne, Florida). The sandwich panels were fabricated using a one-step, vacuum-assisted, resin transfer molding (VARTM) process, which has lower production costs compared to other manufacturing methods. The polyurethane foam was selected to be compatible with the polyurethane resin systems as well as to further reduce the manufacturing costs and panel weight. The new thermoset polyurethane resin that was used in this study has improved properties compared to commonly used polyester and vinyl ester resin systems (Connolly et al. 2006).

Material Characterization

GFRP Facing and Web Characterization

To specify mechanical properties of the sandwich panels, three GFRP coupons were cut from the facings and another three were cut from the web. All coupons were tested under tension, as shown in Fig. 3, according to the ASTM D3039/D3039M-08 standard

(ASTM D3039 2008). All specimens were 10 in. (254 mm) long, 1 in. (25.40 mm) wide, and had the thickness of the corresponding element of the sandwich panel. End tabs were 2.5 in. (63.50 mm) long. The tension test was conducted with an MTS-880 universal testing machine at a loading rate of 0.05 in./min (1.27 mm/min), as recommended by the ASTM standard. Both longitudinal and transverse strains were recorded at the middle of the coupons using 350 ohm strain gauges produced by Micro Measurements Group. Additionally, three facings and three web coupons were tested in compression according to the ASTM D3410/D3410M-03 standard (ASTM D3410 2008). Each coupon was 5.8 in. (147.32 mm) long and 1 in. (25.40 mm) wide with a gauge length of 0.8 in. (20.32 mm). The crosshead speed of the compression test was set at 0.005 in./min (0.127 mm/min) per the recommendation of the ASTM D3410/D3410M-03 (ASTM D3410 2008). Two strain gauges were attached to the coupons to measure the longitudinal and transverse strains within the gauge length.

Tables 1 and 2 summarize the coupon test results. The longitudinal tensile average stress-strain curves of the facings and web coupons are shown in Figs. 4a and 4b, respectively. The failure mode for all facing coupons was a sudden kink rupture, as shown in Fig. 3a, while the failure mode for all web core coupons was shear rupture, away from the gripping region, as observed in Fig. 3b. The facings exhibited a linear elastic response up to an ultimate stress of approximately 38.4 ksi (264.7 MPa) corresponding to an ultimate strain of 0.019 in./in. (mm/mm). The web coupons displayed a slight softening nonlinearity that may be due to the orientation angle of the fiber (i.e. 45/-45 double bias), as the fibers will attempt to align with the direction of the applied load. The ultimate strain was approximately 0.027 in./in. (mm/mm) at an ultimate stress of 25.5 ksi (175.8 MPa). These

properties are also valid in the transverse direction for both the facings and web core because of the symmetric architecture of the reinforcing fibers.

The axial compressive average stress-strain curves for the facings and web core are shown in Figs. 5a and 5b, respectively. All compressed coupons failed when the fibers buckled and kinked. The ultimate compressive strengths of the facings and web were approximately 39% and 73% of their ultimate tensile strength, respectively.

Foam Core Characterization

Three cubes of polyurethane foam were tested according to the ASTM C365/C365-11a standard (ASTM C365 2011) to determine their compressive properties. Both the coupon dimensions and the mechanical properties of the tested specimens are listed in Table 3. Because the foam is very sensitive to small displacements, the testing was conducted with an Instron 4469 testing machine, which can provide very accurate measurements. All specimens were loaded using displacement control at a loading rate of 0.15 in./min (3.81 mm/min). This displacement rate was chosen to produce failure within 3 to 6 minuets per the recommendations of the ASTM C365/C365-11a standard (ASTM C365 2011). The compressive stress-strain curves displayed in Fig. 6a demonstrate that the foam behaved linearly up to an average stress of 8.1 psi (0.056 MPa). The onset of nonlinear behavior occurred when the internal walls and struts of the foam architecture started collapsing. No visible signs of failure were observed until densification of the foam occurred (see Fig. 6b). However, a visual inspection of the collapsed foam showed high residual displacements after unloading.

Small-Scale Panel Tests

Crushing Test Setup

The objective of this test was to determine the ultimate bearing capacity of the sandwich panel, the local buckling load, and the failure modes. The tests were conducted on an MTS-880 testing machine, with a load rate of 0.1 in/min (2.54 mm/min) (Fig. 7). Two specimens, had the same cross section shown in Fig. 2, with a length of 12.5 in. (317.50 mm) were cut from the panels and tested in flatwise compression up to failure. High resistance rubber pads with a shore A hardness of 60 and thick steel plates were placed between the specimen and the contact surfaces to uniformly distribute the load. The applied load and the displacement of the crosshead of the testing machine were recorded during testing.

Flexural Test Setup

The objective of the flexural testing was to record the flexural behavior of the sandwich panel. The sandwich panels were tested under four-point loading according to the ASTM C393-11e1 standard (ASTM C393 2011). Two sandwich specimens, subsequently referred to as 1-CP and 2-CP were tested in one-way bending under two equal point loads as shown in Figs. 8 and 9. The span length for the panel measured 43 in. (1092.20 mm) with the point loads applied at a distance of 15.5 in. (393.70 mm) from each support. Each specimen was loaded up to failure, at a loading rate of 0.05 in./min (1.27 mm/min), in a MTS880 universal testing machine.

A steel beam fixture was constructed and attached to the testing machine as shown in Fig. 8. The beam base consisted of two HSS hollow steel sections welded laterally to

provide the required width and capacity. Two cylindrical steel supports with diameters of 1.0 in. (25.40 mm) were welded to the base and spaced 43 in. (1092.20 mm) apart. For the loading beam, two HSS hollow steel sections were welded laterally and gripped to the movable loading head of the MTS-880 machine. Load distribution was accomplished with 2.0 in. (50.80 mm) steel plates that rotated freely around the 1.0 in. (25.40 mm) steel rods. Rubber pads with a shore A hardness of 60 were placed between the specimen and the contact points to avoid stress concentrations.

Axial strains were measured using high precision strain gauges that had a gauge length of 0.125 in. (3.18 mm) and a resistance of 350 ohm, produced by Micro Measurements Group. Eight strain gauges monitored the strain in the top and bottom facings and throughout the specimen depth. In addition, the displacements at ten locations were monitored by eight direct current variable transformers (DCVTs) and two linear variable differential transformer (LVDTs) transducers. The locations of the DCVTs, LVDTs, and the strain gauges are shown in Fig. 10.

Fatigue Test Setup

The fatigue test was conducted on three sandwich panels to assess the service life of the bridge deck under a repeated load. Shenoi et al. (1997) studied the fatigue behavior of FRP composite sandwich beams with a foam core. They concluded that loading configuration, load frequency, and waveform type did not significantly affect the fatigue results. In the current study, three specimens were fatigued at two different load levels. The panel designation included a combination of letters and numbers: FP for fatigued panels; 1, 2, and 3 for the three individual specimens (written on the left side of the letters); 1, 1.2,

2 indicate the number of cycles in millions (written on the right side of the letters), and 20 and 45 are the peak loads as a percentage of the ultimate load (i.e., 20 represent a peak cyclic load of 20% of the panel ultimate strength). Specimens 1-FP-20-1 and 2-FP-20-2 were subjected to 1.0 and 2.0 million loading cycles, respectively, under 20 percent of the ultimate load capacity as suggested in the ACI 440-2R-08 standard (ACI 440 2008). Specimen 3-FP-45-1.2 was loaded similar to the other specimens, but the amplitude of the load was equal to 45 percent of the ultimate load under 1.2 million cycles. The 2 million cycles fatigue value was based on the suggestion of AASHTO for steel bridge components (AASHTO 2007). A five percent threshold of the ultimate load was chosen as the minimum load for all of the specimens to ensure that the specimens remained in place during the fatigue cycling. The loading regime is summarized in Table 4. The specimen was loaded manually up to the minimum load of 0.89 kips (3.96 kN) and then the fatigue cyclic test started with a sinusoidal wave (with frequency of 4.0 Hz) ranging from the minimum load to maximum load of 3.56 kips (15.83 kN) and 8.01 kips (35.63 kN) for the 20% and 45% fatigue loading protocol, respectively.

The fatigue test was conducted on the MTS880 Universal Testing Machine using the same test setup and fixture as those utilized in the static flexural test with only minor adjustments. Steel bars with an L-shape were placed at the four corners of the beam fixture to restrain any lateral movements during testing, as shown in Fig. 11. A gap of approximately 0.5 in. (12.70 mm) was allowed between the L-shape steel bars and the specimen so that the boundary conditions of the test would not be violated.

The DCVTs, LVDTs, and strain gauges were attached in the same manner as in the static flexural test. Upon the completion of the fatigue test, each sandwich panel was

statically tested up to failure under a displacement control of 0.05 in./min (1.27 mm/min). Both the residual ultimate strength and the stiffness degradation were compared to the control results.

Panel Stiffness Calculations

The classical Euler-Bernoulli beam theory provides reasonable results for sandwich beams with a large span-to-depth ratio. However, it under-estimates the deflection when the span-to-depth ratio is relatively small since it ignores transverse shear deformations. The first order shear deformation theory (FSDT) that is applicable to shear deformable structures predicts results that are in closer agreement with experiments (Carlsson and Kardomateas 2011). Accordingly, this theory was adopted in the analysis to evaluate the test results. Besides standard assumptions of the FSDT, the following additional assumptions were adopted in the analysis:

1) Perfect bond exists between different panel components. This assumption is acceptable for design purposes under service loads.

2) FRP material is homogeneous, isotropic, and linearly elastic up to failure.

Both of these assumptions have been confirmed in the current experimental work.

The beam stiffness was determined according to the transformed area method, which converts the nonhomogeneous panel components into an equivalent homogeneous section (ETAB, CSI 2001). Because the foam elastic compressive modulus was only approximately 0.02% of the compressive modulus of the GFRP facing and webs, the foam

contribution to the stiffness was ignored in the calculations. The stiffness was calculated

by first computing the transformation factor and modular ratio n, as illustrated in equation

(1):

$$n_i = \frac{E_i}{E_{sw}} \qquad (1)$$

Where E_{sw} is the GFRP web's modulus of elasticity and E_i is the i-th constituent

modulus of elasticity. The material properties used in these calculations were based on the

coupon tests, as presented in Tables 1 through 3. The transformed section's moment of

inertia, I_{tr}, was determined according to the elastic neutral axis, as illustrated in equations

2 through 4. Equation 4 represents the overall effective bending stiffness, which can be

obtained by summing the contributions for each part of the construction:

$$A_{tr,i} = n_i \times A_i \qquad (2)$$

$$\bar{y} = \frac{\sum_i^n A_{tr,i} \cdot y_i}{\sum_{i=1}^n A_{tr,i}} \qquad (3)$$

$$E_e I_{tr} = \sum_{i=1}^n E_i(I_{tr,i} + A_{tr,i} (y_i - \bar{y})^2) \qquad (4)$$

Where, for component i, A_i is the cross-sectional area, $A_{tr,i}$ is the transformed area,

y_i is the distance from the center of gravity of the component to the extreme lower fiber, E_i

is the modulus of elasticity, $I_{tr,i}$ is the moment of inertia of the transformed section, E_e and

I_{tr} are the effective modulus of elasticity and the effective moment of inertia, respectively,

for the entire section, and $\bar{y}$ is the distance from the neutral axis of the transformed cross-

section to the extreme lower fiber. After determining the location of the neutral axis of the

transformed section using equation (3), section elements were divided into compression

and tension regions so that they corresponded to their material properties. The transformed

moment of inertia for each component was then determined, and the overall bending stiffness of the sandwich panel was calculated with equation (4).

Once this step was complete, the FSDT could be implemented by using the homogenized bending stiffness calculated from equation (4). Both the loading configuration and the panel dimensions are given in Fig. 10. The expressions for the bending and shear force are presented as follows, respectively:

$$M_{xx} = -E_e I_{tr} \frac{\partial \varphi}{dx} \tag{5}$$

$$Q_x = k\,AG(-\varphi + \frac{\partial w}{\partial x}) \tag{6}$$

Equations (5) and (6) can be integrated, accounting for the boundary conditions corresponding to simple support. Deflection along the panel could then be computed using equations (7) and (8):

$$w(x) = \frac{Px^3}{12E_e I_{tr}} + \frac{Pa^2 x}{4E_e I_{tr}} - \frac{PaLx}{4E_e I_{tr}} - \frac{Px}{2kGA} \qquad for\ 0 \leq x \leq a \tag{7}$$

$$w(x) = \frac{Pa^3}{12E_e I_{tr}} + \frac{Pax^2}{4E_e I_{tr}} - \frac{PaLx}{4E_e I_{tr}} - \frac{Pa}{2kGA} \qquad for\ a \leq x \leq L - a \tag{8}$$

Where M_{xx} is the bending moment along the x axis, Q_x is the transverse shear force, and φ is the angle of rotation of the normal to mid-surface of the beam. $w(x)$ is displacement along the x axis, P is the applied load, L is the span length, and a is the distance between the support and the loading point (see Fig. 9), k is the shear correction factor (it is assumed equal to 5/6), and AG is the effective shear stiffness of the core, which includes the foam and web layer.

The bending stiffness of the tested sandwich panels was also determined by fitting the experimental results to those generated by the FSDT. The polyurethane foam, the web,

and the facings were modeled as isotropic materials. According to the theory of shear deformable beams, the bending stiffness of the sandwich panels was computed accounting for deformations due to bending and transverse shear. The bending stiffness can be determined using the experimental values of deflections at loading point and mid-span locations and solving equations (9) and (10) (Carlsson and Kardomateas 2011). A summary of the corresponding results is given in Table 6.

$$\Delta_{midspan} = \frac{Pa^3}{3EI} - \frac{Pa^2L}{4EI} - \frac{Pa}{2kAG} \qquad \text{for } 0 \le x \le a \qquad (9)$$

$$\Delta_{loading-point} = \frac{Pa^3}{12EI} - \frac{PaL^2}{16EI} - \frac{Pa}{2kAG} \qquad \text{for } a \le x \le \text{L-a} \qquad (10)$$

Where EI is the bending stiffness of the panel using the experimental values.

Results and Discussions

Crushing Behavior

Fig. 12 illustrates the average load-deflection curve for the flatwise crushing tests. The initial nonlinear portion of the curve occurred due to small gaps in the system and can therefore be ignored. The curve exhibited a linear response up to the point at which the foam started to crack at an average load of 17.5 kips (77.84 kN). A noise was heard during the test, which revealed that the webs began to buckle at a load of approximately 22.3 kips (99.2 kN) corresponding to an average compressive stress of 127 psi (0.88 MPa). Since the width of the panel varies throughout the cross-section, an effective surface area of the panel was difficult to define. Thus, the average compressive stress was calculated by dividing the buckling load by the surface area at the neutral axis. All of the specimens failed in the same

manner as illustrated in Fig. 13. The results, however, exhibited a large scatter in the ultimate compressive stress as shown by the high standard deviations and coefficients of variation in table 5. This high variability occurred because each panel was cut from different larger panels, each of them having slightly different manufacturing defects. These manufacturing defects, although relatively minor, resulted in significant variation across the different specimen samples. It is worth noting that the quality of manufacturing the panels improved as the specimens size increased. Moreover, improvements in the manufacturing occurred due to the learning curve associated with constructing the specimens in the Missouri S&T Composites Lab. Finally, a composite manufacturer was able to produce full-scale deck panels using the concept presented in this manuscript with consistent characteristics and without significant defects.

Static Flexural Behavior

Fig. 14 illustrates the load-deflection curves for the two sandwich panels that were subjected to four-point loading tests. The deflection was measured with the DCVTs placed along the two edges at mid-span. All specimens were loaded to failure. The behavior of each specimen was nearly linear up to failure; a slight reduction was observed in stiffness prior to failure. The linear response was expected considering the behavior of the individual materials used to manufacture the panels, which are brittle in nature and typically respond in a linear-elastic fashion up to failure. Fig. 15 illustrates the deflection profile for the two specimens. The maximum vertical deflection for panels 1-CP and 2-CP at mid-span measured 1.04 in. (26.42 mm) and 0.98 in. (24.89 mm) at failure loads of 18.26 kips (81.22 kN) and 17.40 kips (77.39 kN), respectively. Table 6 summarizes the results of the static

flexural test for each specimen. A "popping" noise was heard for both panels at the load of approximately 12.8 kips (56.94 kN) and the deflection of 0.75 in. (19.05 mm), as some of the fibers at the top surface of the middle cell (Fig. 16a) debonded from the core. This debonding occurred at the section between the loading points and was accompanied with the loud "popping' noise. At the load of 17.83 kips (79.31 kN), a louder noise was heard, which was associated with local crushing of the facing under one of the loading points, as illustrated in Figs. 16b and 16c. Then the test was stopped since the load dropped significantly reflecting failure of the specimen.

It is worth noting that bridge deck elements have deflection limits that are intend to ensure the element functions properly and does not cause discomfort to individuals using the structure. Based on AASHTO and FHWA guidelines, the deflection of bridge deck need to be smaller than 1/800 of the supporting span length. If this limit is applied using the span length of 43 in., the deflection limit state for the investigated FRP panel is 0.054 in. which is significantly smaller than the deflection of the investigated panel at its peak flexural strength indicating that the design of these panels will likely be controlled by flexural stiffness and serviceability rather than strength. This result was also expected considering the results of testing other types of GFRP bridge decks available in literature.

The maximum tensile strain recorded at the bottom facing was 0.00907 in./in. (mm/mm) at a load of 17.83 kips (79.31 kN), which represents 53% of the ultimate tensile strain obtained from the tensile coupon tests of the GFRP facing (0.019 in./in. (mm/mm)). This is consistent with visual inspection, where no cracks were observed at the bottom facing. Rather, failure initiated due to debonding that started at the top compression surface. As a result, the top face began to wrinkle outward. This phenomenon is also visible

in the strain gauge readings at the top face (Fig. 17). These readings exhibited nonlinearity, reversing their direction at approximately -0.00365 in./in. (mm/mm). After the onset of wrinkling, the sandwich panel continued to carry the applied load with a reduced stiffness until failure. The final failure was caused by local crushing of the compressed facing under one of the loading points due to excessive compressive strains.

Four strain gauges (S4, S5, S6, and S7) were glued along the specimen's thickness to monitor the longitudinal strain variation. These measurements validated the assumption that plane sections remained plane during loading. The longitudinal strains were linear up to failure, regardless of their location along the thickness, as shown in Fig. 18. When the strains for different load ranges were plotted, as illustrated in Fig. 19, the neutral axis for the panel section was found to be 2.49 in. (63.25 mm) from the bottom face of the panel. Using the elastic beam theory and transformed section (without considering the foam) resulted in the position of the neutral axis at 2.4 in. (60.96 mm) from the bottom facing, representing 96% of the measured value.

Fatigue Behavior

The residual stresses, stiffness degradation, and failure mode of the tested fatigue specimens were also investigated. After the predetermined number of cycles was reached, each panel was statically tested in the same loading configuration as that used for the control sandwich panels. The stiffness degradation due to fatigue was calculated as the ratio of the stiffness of the fatigued specimen to that of the control specimen that was tested statically.

For all panels, no signs of surface cracks or collapse occurred during the fatigue test. Table 7 summarizes the results of the fatigue flexural loading test for each specimen. Fig. 20 illustrates the load vs. mid-span deflection curves for both fatigued and control specimens. The behavior of the fatigued panels is identical to those tested monotonically (control panels). The maximum deflection for panels 1-FP-20-1 and 2-FP-20-2 was 1.25 in. (31.75 mm) and 0.95 in. (24.13 mm), respectively, and for panel 3-FP-45-1.2, the value was 1.2 in. (30.48 mm), while the maximum average deflection for the control panels was 1.01 in. (25.65 mm) However, the ultimate load capacities increased by 31.5%, 14.6%, and 34%, respectively, compared to the control panels. Note that the fatigue test was stopped at 1.2 million cycles for panel 3-FP-45-1.2 due to mechanical difficulties with the MTS test machine.

In general, no stiffness reduction was detected in all the three specimens. Each specimen failed in a manner similar to the control panels. However, a delamination failure occurred prior to the ultimate failure (Fig. 21a) between the foam and the GFRP facing at the four corners after the outward facing wrinkled, as illustrated in Figs. 21b and 21c. Delamination started at the outer corners of the webs only where shear layers were not provided. This failure mode that was not observed in statically loaded panels was introduced only under fatigue loading. Fig. 22 illustrates both the residual bending rigidities and the residual ultimate load for all tested panels. The results indicate that the panels that were conditionally fatigued the most, exhibited a higher bending stiffness. The increase in stiffness and strength can be explained by the enhancement of polymer linkages in the FRP material. This enhancement is due to the process where the fatigue loading

aligns or reorganizes the polymer-linkages so that minor defects in the material are eluded, as has been reported by Rocca and Nanni (2005).

Comparison of FSDT and Experimental Results

Fig. 23 compares the force-deformation curves calculated using first order shear deformation theory (FSDT) and those obtained from the experimental results. In general, the FSDT slightly overestimated the bending stiffness and underestimated the expected deflection. The predicted stiffness and deflection using FSDT represents 106.7% and 85% of those measured using the experimental work, respectively. This variation likely occurred for two reasons. First, although the panel section's thickness varied with a coefficient of variation of 7.2%, only one nominal thickness for each component (see Fig. 2) was used in the theoretical calculation. Second, FSDT assumes perfect bond between the facings, web, and foam. However, debonding at the top facing occurred during the experimental, resulting in stiffness degradation.

The bending stiffness of each investigated panel was computed using equation 9 and 10 of FSDT through the recorded deflections at mid-span and at loading points from the experimental work. Results are presented in Tables 6 and 7. It was found that the shear deformation is minimal. This occurred because the core webs significantly increased the shear stiffness and therefore decreased the shear deformation.

Conclusions

This study investigated the structural behavior of a new type of sandwich panels with a polyurethane-filled web core. The investigation focused on the new prototype system utilizing a new thermoset polyurethane resin as well as supplemental web shear layers of GFRP. The new resin system that has a longer pot life was successfully implemented in the VARTM process to fabricate the panels. The test results demonstrated that the polyurethane resin exhibited superior performance in both static and dynamic tests. The shear layers contributed significantly to enhancing the structural response and shear stiffness; they also delayed delamination of the facings from the core. Excellent bond between different components of the panel was observed. A local outward wrinkling phenomenon, however, was observed between the core and the top facing of the middle cell. This wrinkling could be avoided by increasing the number of plies of the top facing. This prototype system, in general, reduced both the construction time and the initial cost compared with conventional honeycomb sandwich panels. The accuracy of existing analytical models predicting the sandwich panel deflection was also examined. The following conclusions can be drawn:

1. The behavior of the plain-weave facings under tension exhibited a linear elastic response, while the web layers where the fibers were oriented at $+/-45^{\circ}$ behaved nonlinearly. Both the facing and web layers behaved almost linearly under compression.

2. The crushing test provided the ultimate bearing capacity, which occurred due to buckling of the web. The failure load during the four-point loading test was

lower than the ultimate bearing capacity. Hence, the buckling in the web core did not occur in the four-point loading test.

3. All panels tested in four-point bending exhibited a linear-elastic behavior up to failure. A slight reduction in stiffness due to minor outward skin wrinkling was observed prior to failure. Failure occurred due to local crushing under the applied load.

4. Introducing corrugated webs (shear layers) is an effective way to increase both the core shear stiffness and the global flexural stiffness in the longitudinal direction.

5. In the static flexural test, the maximum strain readings from the bottom gages of the tested panel indicated that the panel was stressed at 47% of its ultimate capacity as determined from the coupon tests, which is consistent with the outward skin wrinkling failure mode of the top facing. In other words, the skin wrinkling failure mode occurs at a lower stress level than the ultimate capacity.

6. The accuracy of the first order shear deformation theory (FSDT) to predict the deflection of the panels was examined leading to the follow conclusions:

   a. The FSDT over-estimated stiffness and under-estimated deflection.

   b. The average difference between the measured deflections and the FSDT results ranged from 6 to 13%.

7. After conditioning the sandwich panels to the predetermined fatigue cycles at the stress levels representing 20% and 45% of their ultimate load, it was

observed that no degradation occurred in either bending stiffness or strength. However, delamination failure was observed as an additional failure mode in panels experiencing fatigue loading that was not present in the control panels.

8. The proposed sandwich panel prevented or reduced the facing-core debonding trend observed in conventional sandwich panel construction.

Acknowledgments

References

AASHTO. (2007). "AASHTO LRFD Bridge Design Specifications," SI Units, 4th Ed., Washington, DC.

Abdelkarim, O., and ElGawady, M. A. (2014). "Analysis And Finite Element Modeling of FRP-Concrete-Steel Double-Skin Tubular Columns." J. Bridge Eng., 10.1061/(ASCE)BE.1943-5592.0000700, B4014005.

ACI. (2008). "Guide for the Design and Construction of Externally Bonded FRP Systems for Strengthening Concrete Structures," (440. 2R–08). Farmington Hills, MI: American Concrete Institute.

American Society of Testing and Materials. (2008). "ASTM Standard Test Method for Tensile Properties of Polymer Matrix Composite Materials (ASTM D3039/D3039M-08)," West Conshohocken, Pennsylvania: ASTM International.

American Society of Testing and Materials. (2008). "ASTM Standard Test Method for Compressive Properties of Polymer Matrix Composite Materials with Unsupported Gage Section by Shear Loading (D3410 / D3410M – 03)," West Conshohocken, Pennsylvania: ASTM International.

American Society of Testing and Materials. (2011). "ASTM Standard Test Method for flatwise Compressive Properties of Sandwich Cores (C365/C365M-11a)," West Conshohocken, Pennsylvania: ASTM International.

American Society of Testing and Materials. (2011). "ASTM Standard Test Method for Flexural Properties of Sandwich Constructions (C393/C393M-11e1)," West Conshohocken, Pennsylvania: ASTM International.

Camata, G. and Shing, P.B. (2010). "Static and Fatigue Load Performance of a GFRP Bridge Deck," Composites Part B: Engineering. Vol. 41, issue 4, pp. 299–307.

Connolly, M., King, J., Shidaker, T., and Duncan, A. (2006). "Processing and Characterization of Pultruded Polyurethane Composites," Huntsman Enriching lives through innovation.

Carlsson, L.A. and Kardomateas, G.A. (2011). "Structural and Failure Mechanics of Sandwich Composites," Springer.

ETAB, CSI. (2001). "Technical Note Transformed Section Moment of Inertia." Composite Beam Design AISC-ASD89," ©Computers and Structures, INC., Berkeley, California.

Hassan, T., Reis, E.M., and Rizkalla, S.H. (2003). "Innovative 3-D FRP Sandwich Panels for Bridge Decks," Proceedings of the Fifth Alexandria International Conference on Structural and Geotechnical Engineering. Alexandria, Egypt.

Ji, H.S., Song, W., and Ma, Z.J. (2010). "Design, test and field application of a GFRP corrugated-core sandwich bridge," Engineering Structures. Vol. 32, pp. 2814-2824.

Kirk, R.S., and Mallett, W.J. (2013). "Highway Bridge Conditions: Issues for Congress," Congressional Research Service, Report to congress. Contract No. R43103.

Murton, M. C. (1999). "Commercialization of FRP Bridge Decks: Lessons and Challenges for Ohio's Project 100," International SAMPE Symposium and Exhibition: [Proceedings]. Vol.46 I, pp 943-951.

Potluri, P., Kusak, E. and Reddy, T.Y. (2003). "Novel stitch-bonded Sandwich Composite Structures,' Composite Structures Vol. 59 No. 2, pp. 251-9.

Rocca, S.V. and Nanni, A. "Mechanical Characterization of Sandwich Structure Comprised of Glass Fiber Reinforced Core," Part 1, Composite in Construction, Third International Conference. Lyon, France.

Shenoi, R. A., Allen, H. G., and Clark, S. D. (1997). "Cyclic Creep and Creep-fatigue Interaction in Sandwich Beams," Journal of Strain Analysis. Vol. 32, No. 1, pp. 1-18.

Zi, G., Kim, B.M., Hwang, Y.K., and Lee, Y.H. (2008). "An experimental study on static behavior of a GFRP bridge deck filled with a polyurethane foam," Composite Structures. Vol. 82, pp. 257-268

Table 1. Material Properties from Tensile Coupon Tests

Coupon Type	Width, in. (mm)	Thick., in. (mm)	Tensile Modulus, ksi (MPa)			Ultimate Strength, ksi (MPa)			Ultimate Strain, in./in., mm/mm		
			Mean	S.D*	C.V*	Mean	S.D	C.V	Mean	S.D	C.V
Facing	1 (25.40)	0.09 (2.89)	2027.2 (13,977)	19.1 (131.7)	0.94	38.4 (264.8)	2.3 (15.9)	6.1	0.019	0.001	5.88
Web core	1 (25.40)	0.19 (4.83)	1711.9 (11,803.1)	136.1 (938.4)	7.95	25.6 (176.5)	1.4 (9.7)	5.5	0.03	0.004	14.06

*S.D: Standard Deviation
*C.V: Coefficient of Variation (%)

Table 2. Material Properties from Compressive Coupon Tests

Coupon Type	Width, in. (mm)	Thick., in. (mm)	Compressive Modulus, ksi (MPa)			Ultimate Strength, ksi (MPa)			Ultimate Strain, in./in., mm/mm		
			Mean	S.D	C.V	Mean	S.D	C.V	Mean	S.D	C.V
Facing	1 (25.40)	0.09 (2.89)	1919.3 (13,233)	248.2 (1,711.3)	12.9	14.9 (102.7)	2.36 (16.27)	15.8	0.011	0.004	34.66
Web core	1 (25.40)	0.19 (4.83)	1053 (7,260.2)	157.9 (1,088.7)	15	18.6 (128.7)	1.38 (9.5)	7.41	0.024	0.005	22.90

Table 3. Material Properties from Compressive Tests

Width, in. (mm)	Length, in. (mm)	Thick., in. (mm)	Elastic Modulus, psi (MPa)			Compressive Strength, psi (MPa)			Compressive Strain, in./in. mm/mm		
			Mean	S.D	C.V	Mean	S.D	C.V	Mean	S.D	C.V
2.53 (64.26)	2.59 (65.79)	2.73 (69.34)	301.8 (2.1)	21.5 (0.15)	7.1	8.1 (0.056)	0.5 (0.0034)	6.9	0.025	0.005	21.45

Table 4. Loading Regime

Load Percentage	Pu = 17.80 (79.3) kips (kN)
5% (minimum load)	0.89 (3.96)
20% for specimens 1-FP-20-1 and 2-FP-20-2	3.56 (15.83)
45% for specimen 3-FP-45-1.2	8.01 (35.63)

Table 5. Summary of Crushing Test Results

Specimen No.	Failure Load, kips (kN)	Compressive Stress, psi (MPa)	Compressive Strain, in./in., mm/mm
1	29.7 (132.1)	169.7 (1.17)	0.054
2	20.0 (88.9)	114.3 (0.78)	0.065
Mean	24.8 (110.3)	142.0 (0.98)	0.059
S.D	6.8 (30.2)	39.2 (0.27)	0.0075
C.V	27.6	27.6	12.5

Table 6. Summary of Static Flexure Test Results

Specimen No.	Pu, kips (kN)	Δmidspan, in. (mm)	Δloading-point, in. (mm)	EI, kip.in2 (kN.m2)	GA, kips (kN)	σskin-bot, ksi (MPa)	τ, ksi (MPa)
1-CP	18.26 (81.2)	1.04 (26.42)	0.94 (23.87)	25,472.7 (7,310)	~ ∞	15.28 (105.35)	0.185 (1.28)
2-CP	17.40 (77.4)	0.98 (24.89)	0.89 (22.61)	26,970.0 (7,739.8)	~ ∞	14.56 (100.39)	0.175 (1.21)
Mean	17.83 (79.3)	1.01 (25.65)	0.915 (23.24)	26,221.4 (7,525)	~ ∞	14.92 (102.87)	0.18 (1.24)
S.D	0.43 (1.9)	0.03 (0.76)	0.025 (0.64)	748.65 (214.8)	-	0.36 (2.48)	0.005 (0.034)
C.V	2.41	2.97	2.73	2.86	-	2.4	2.7

Table 7. Summary of Fatigue Flexure Test Results

Specimen Series	Number of Load Cycles (millions)	Ultimate Load, ksi (MPa)	Mid-span Deflection, in. (mm)	Flexural Stiffness, $kip.in^2$ ($kN.m^2$)
1-FP-20-1	1	23.4 (161.3)	1.25 (31.75)	27,532.4 (7,886.7)
2-FP-20-2	2	20.4 (140.7)	0.95 (24.13)	30,154.6 (8,637.8)
3-FP-45-1.2	1.2	24.0 (165.5)	1.20 (30.48)	29.892.3 (8,562.7)
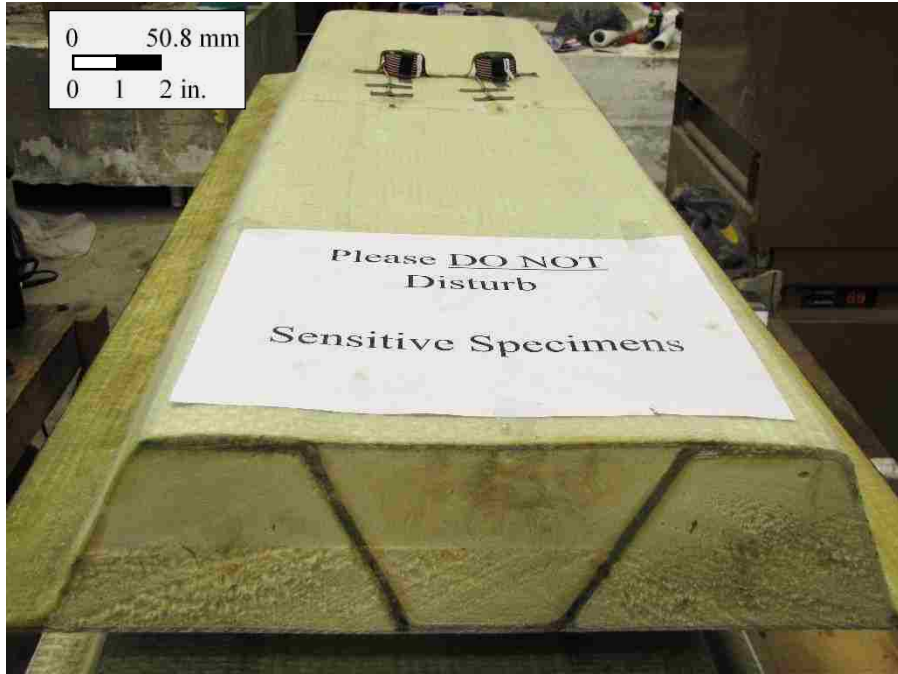
Figure 1. Sandwich panel system used in experiments
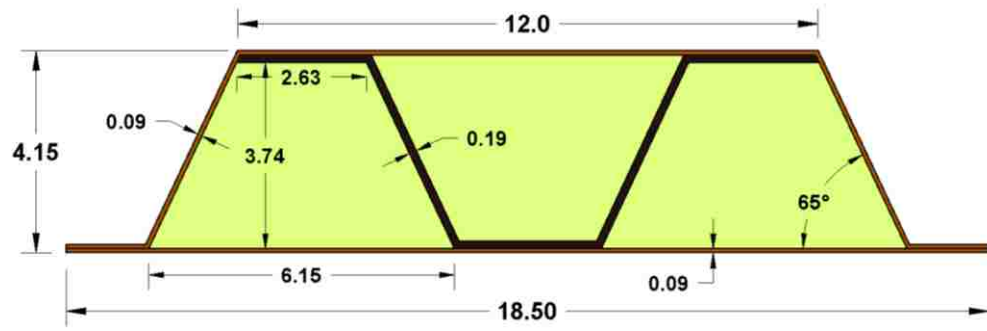
Figure 2. Schematic of cross-section (all dimensions in inches, 1 in. = 25.4 mm)
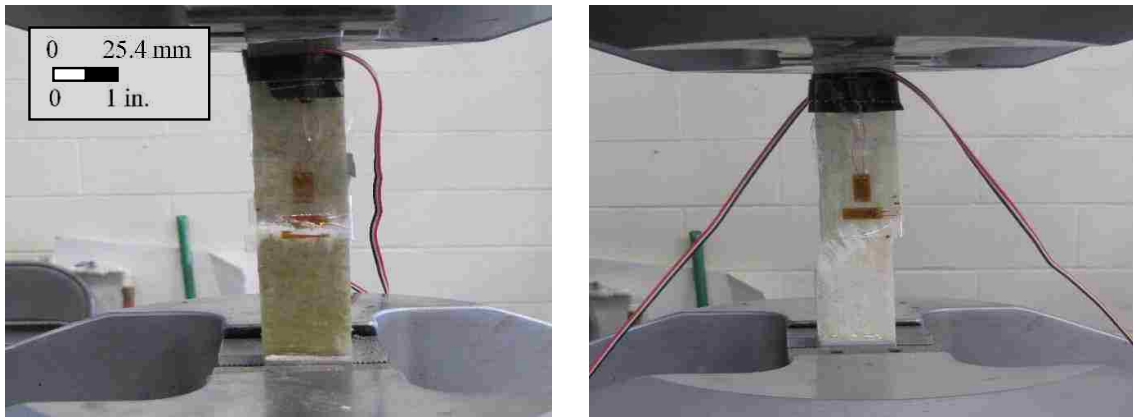
(a)   (b)

Figure 3. Failure modes: (a) GFRP facings and (b) web layers

(a) (b)
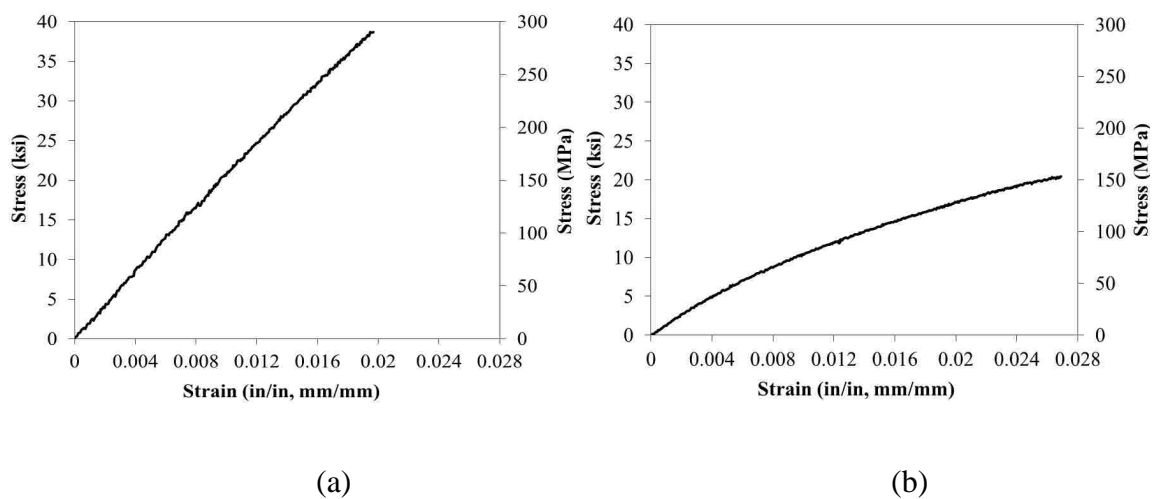
Figure 4. Average tensile stress-strain curves: (a) GFRP facings and (b) web layers

(a)   (b)
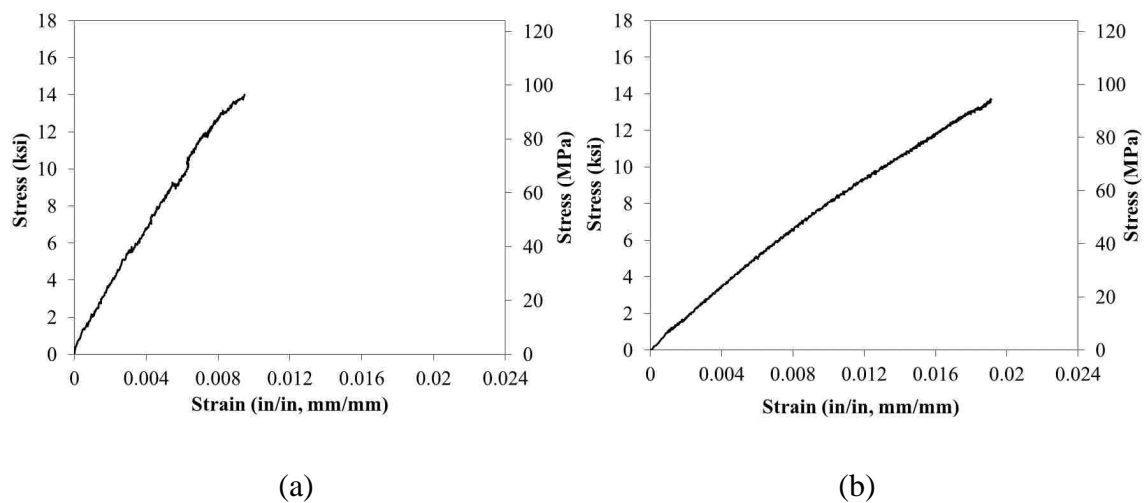
Figure 5. Average compressive stress-strain curves: (a) GFRP facings and (b) web
layers
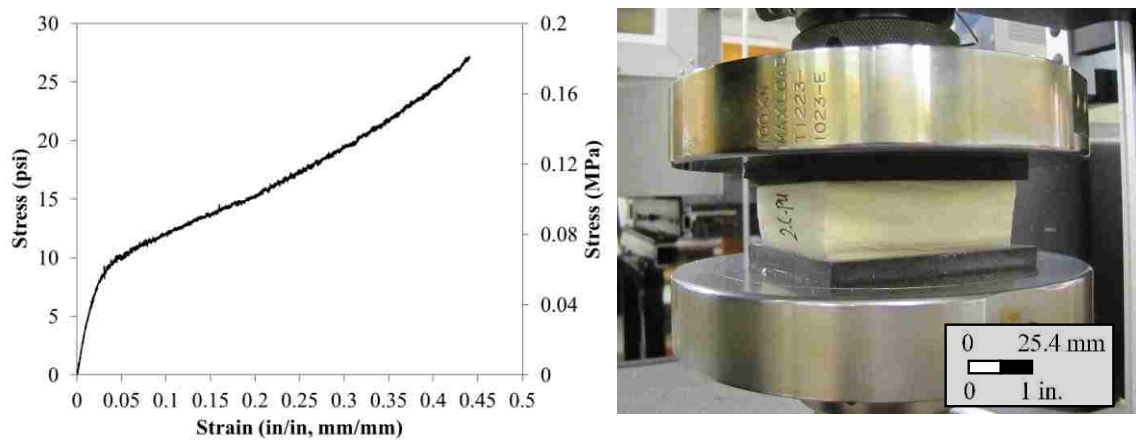
(a) (b)

Figure 6. Flatwise compressive test: (a) average compressive stress-strain curves and

(b) test setup

Figure 7. Crushing test setup
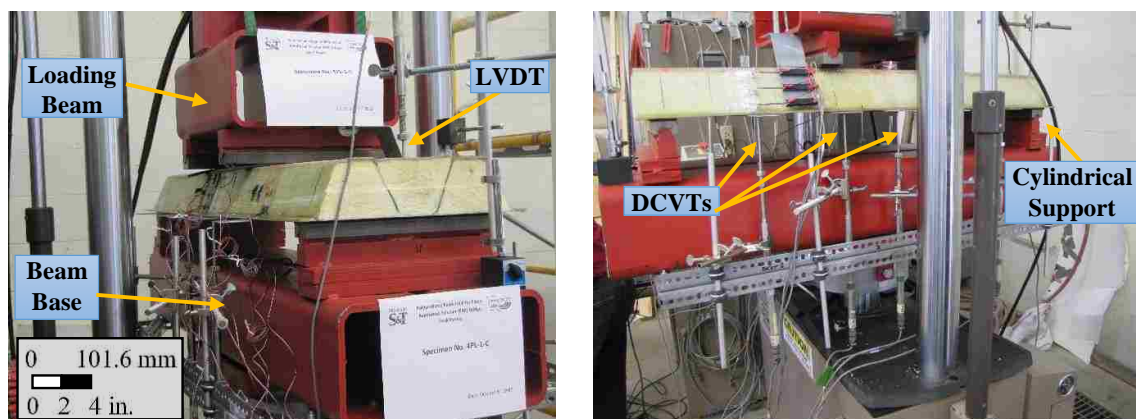
Figure 8. Four-point bending test setup for the flexural test
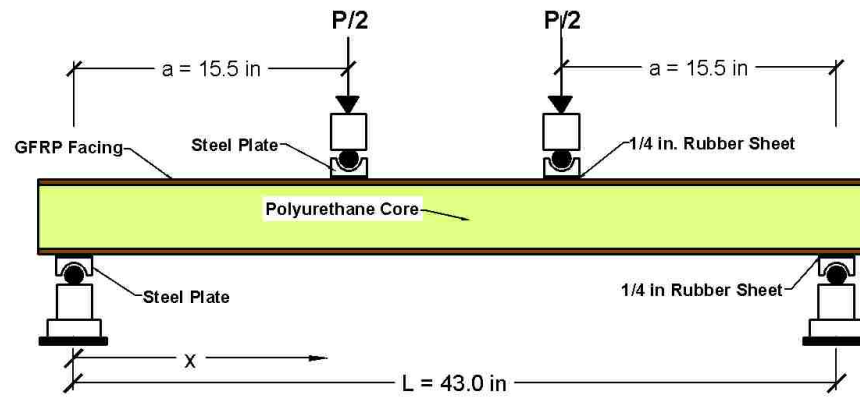
Figure 9. Schematic of four point bending test setup. Web core perpendicular to the plane of drawing is not shown. (all dimensions in inches, 1 in. = 25.4 mm)
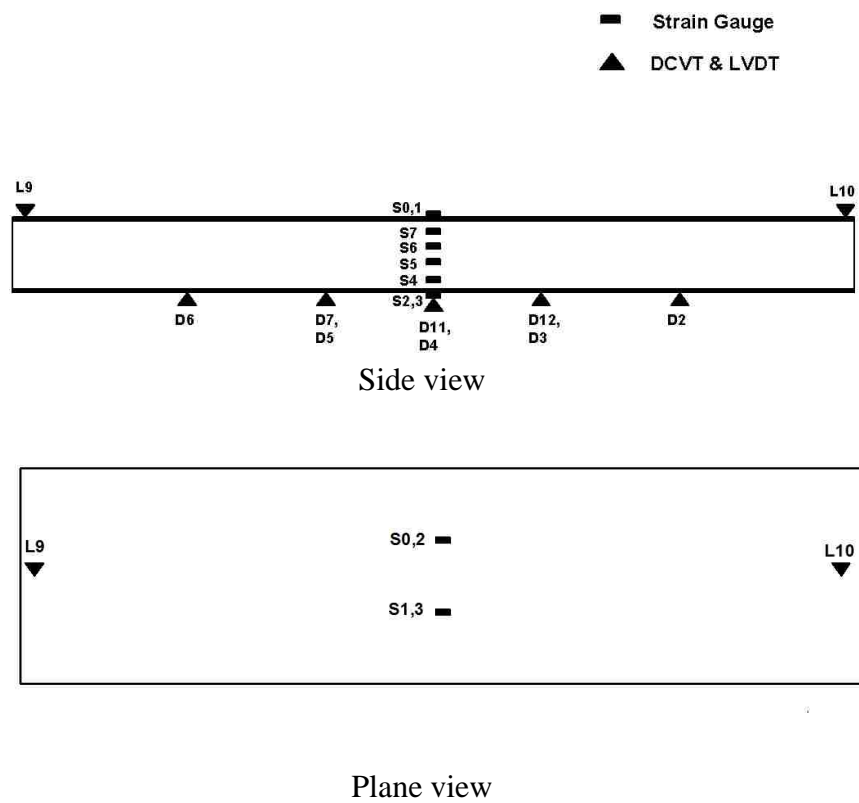
Figure 10. Schematic of instrumentation locations
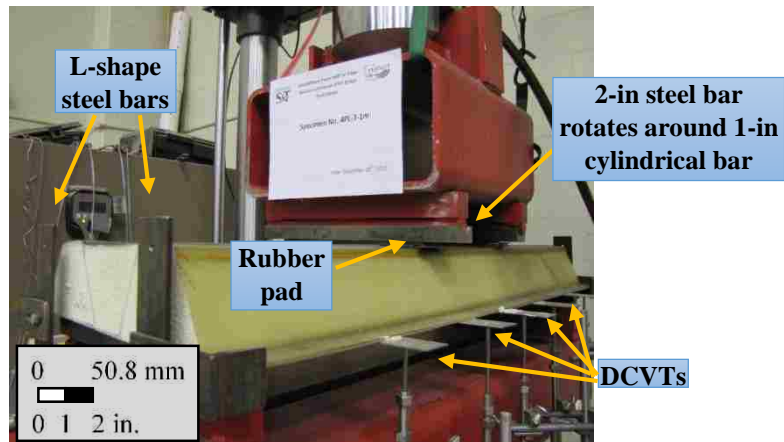
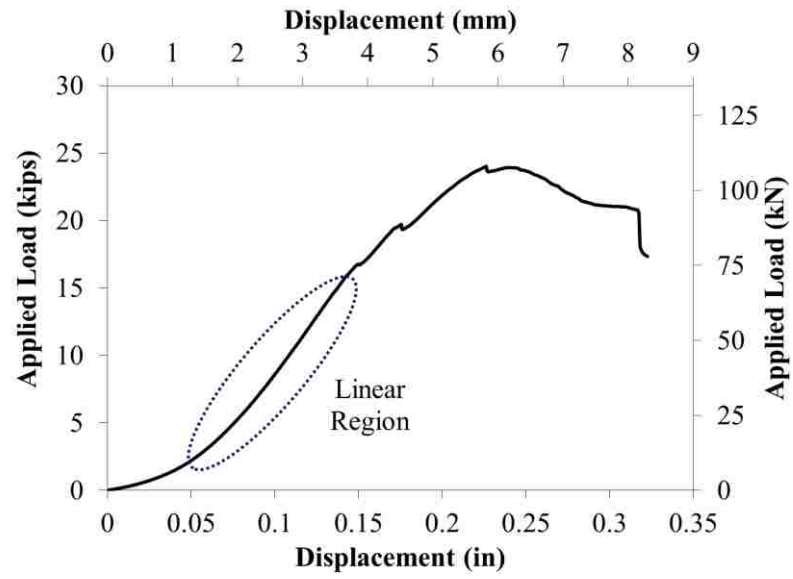Figure 11. Four-point bending test setup for the fatigue test

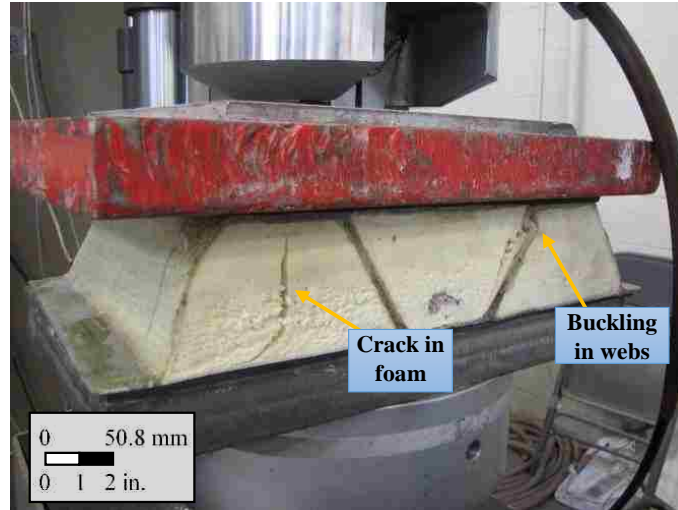Figure 12. Average load-displacement curve for crushing test

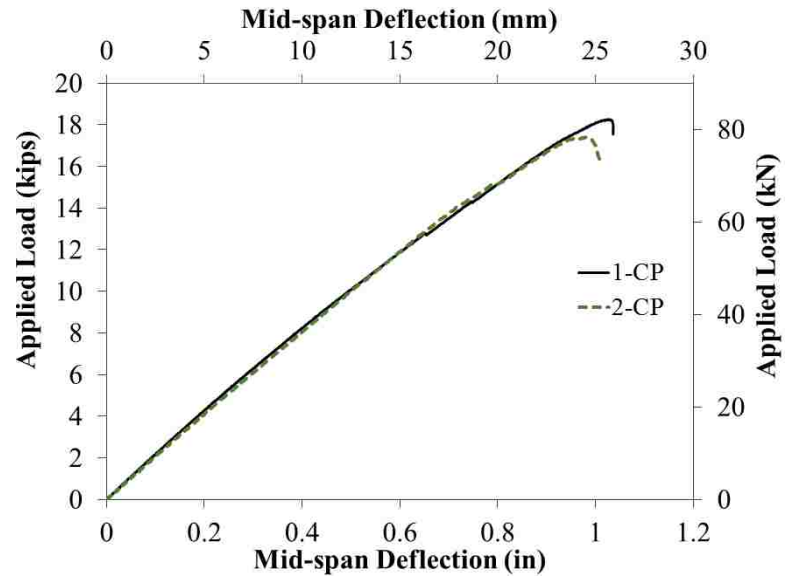Figure 13. Failure of specimen subjected to crushing test

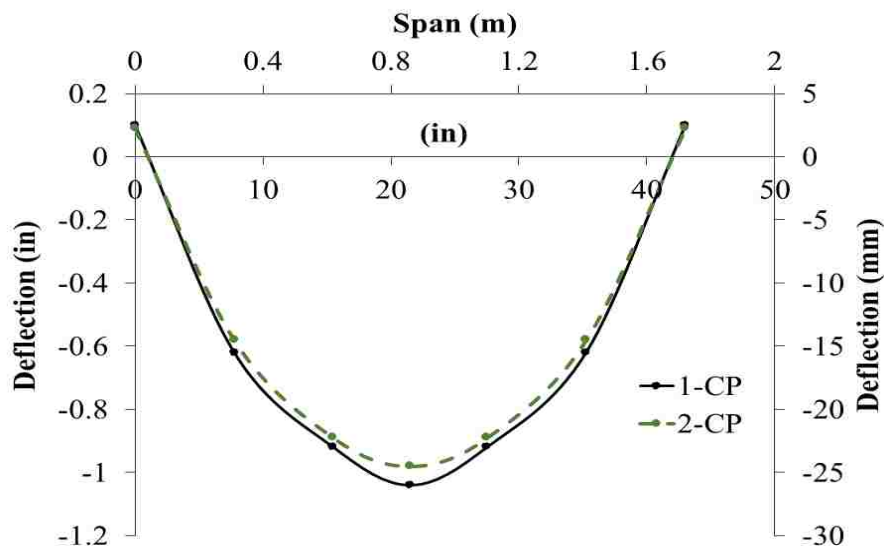Figure 14. Load vs. mid-span deflection for flexure test

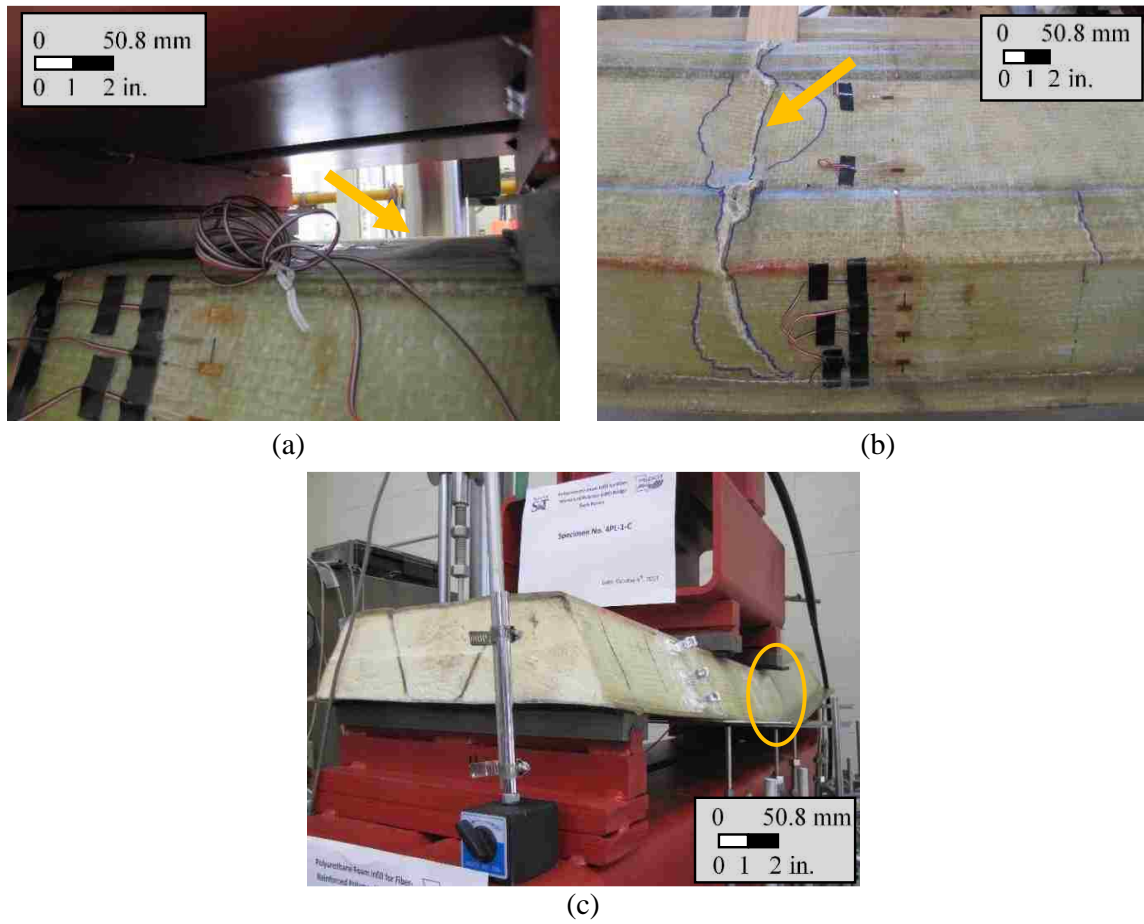Figure 15. Deflection profile along span length during flexure test

Figure 16. Failure modes: (a) initial failure due to outward compression facing wrinkling, (b) ultimate failure due to compression failure of the facing under loading point, and (c) final failure mode trigged by crushing
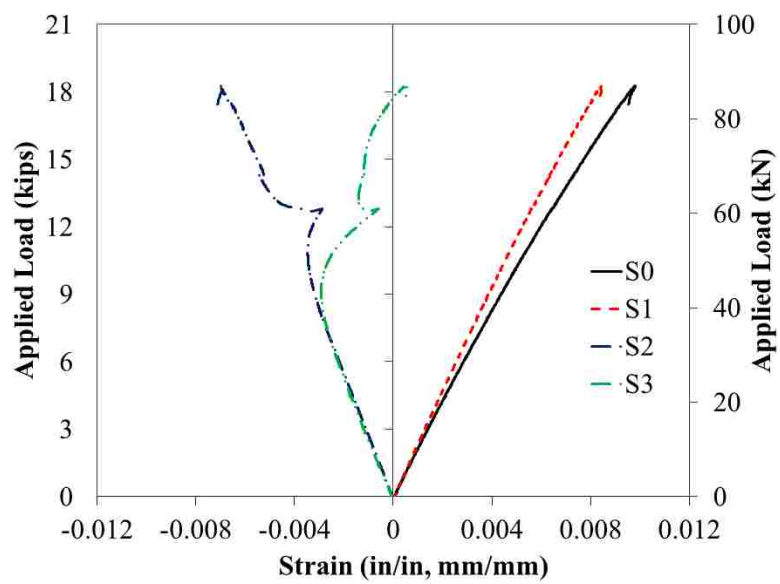
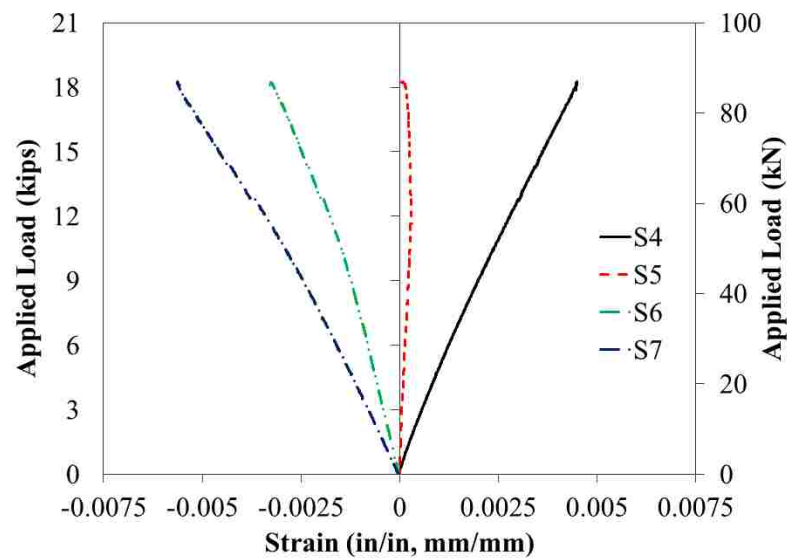Figure 17. Load-strain curves for the top and bottom facings
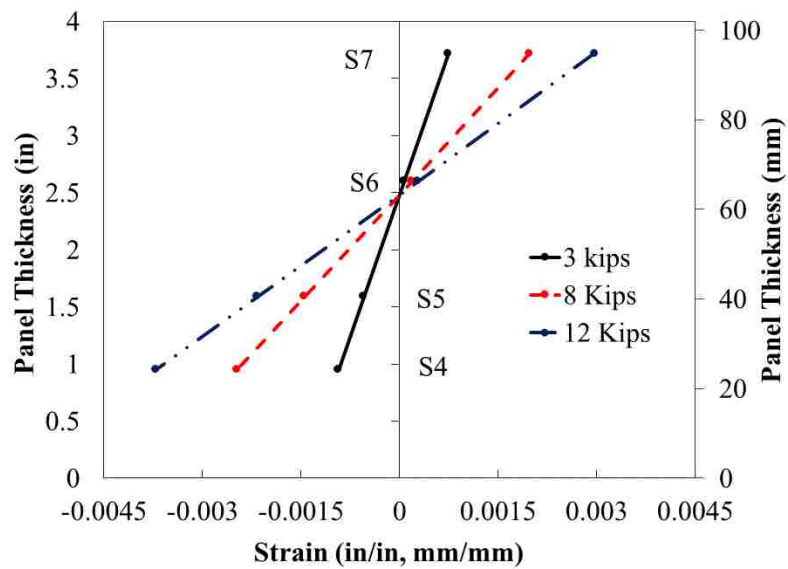
Figure 18. Load-strain behavior of sandwich panel

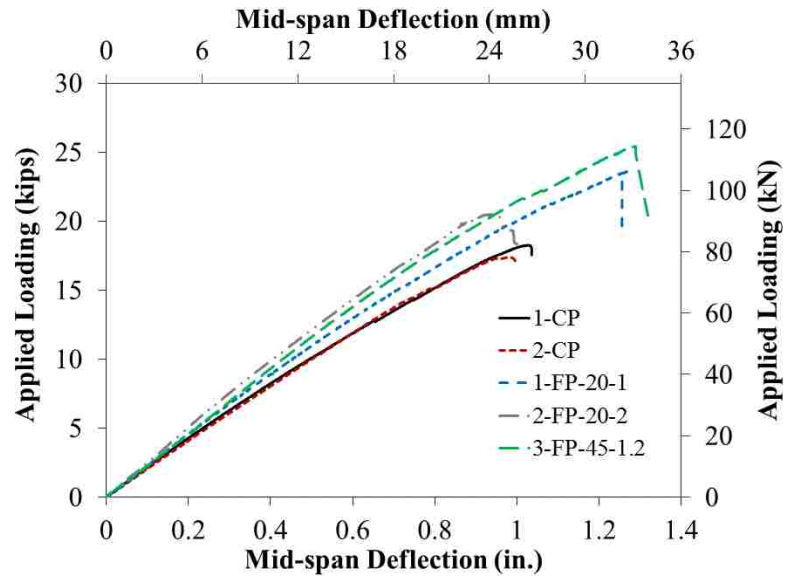Figure 19. Strains distribution through the thickness for strain gauges S4, 5, 6, and 7

Figure 20. Load vs. mid-span deflection for control and fatigued panels
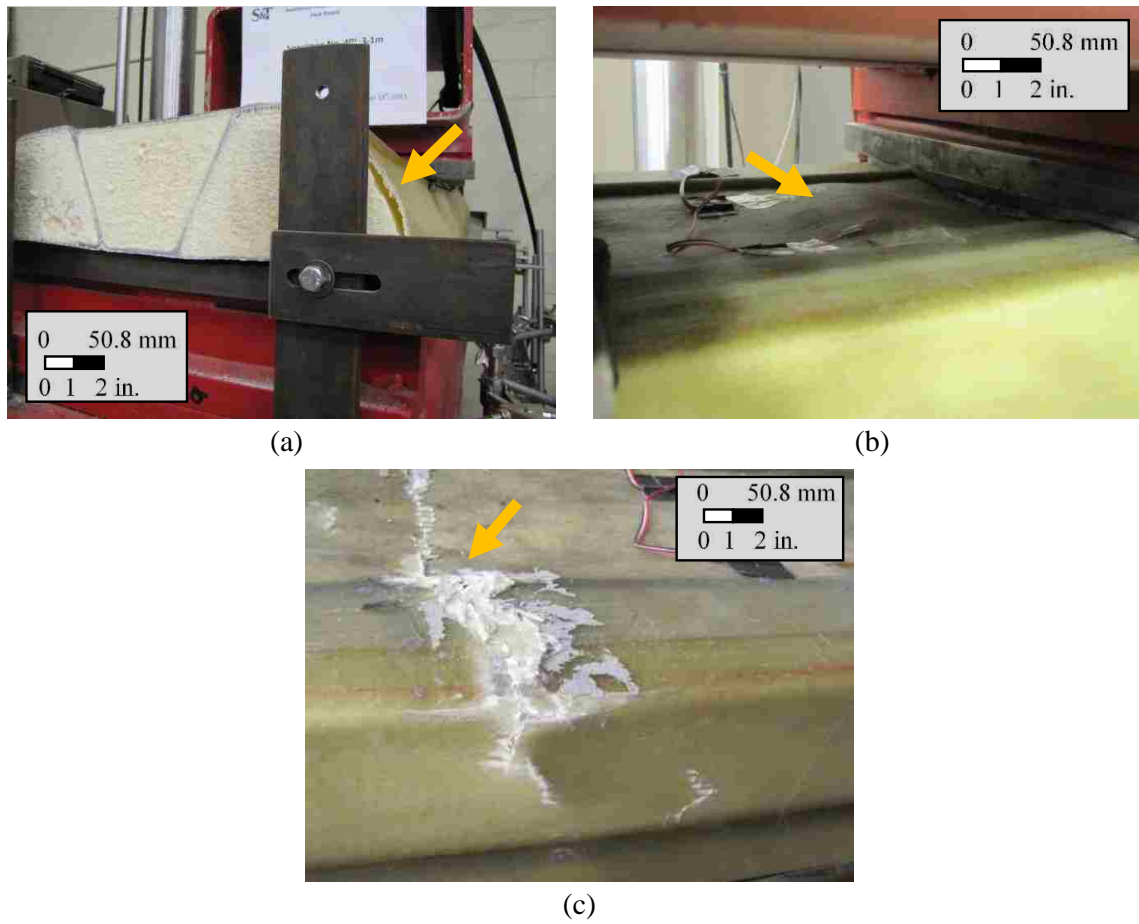
(a)

(b)

(c)

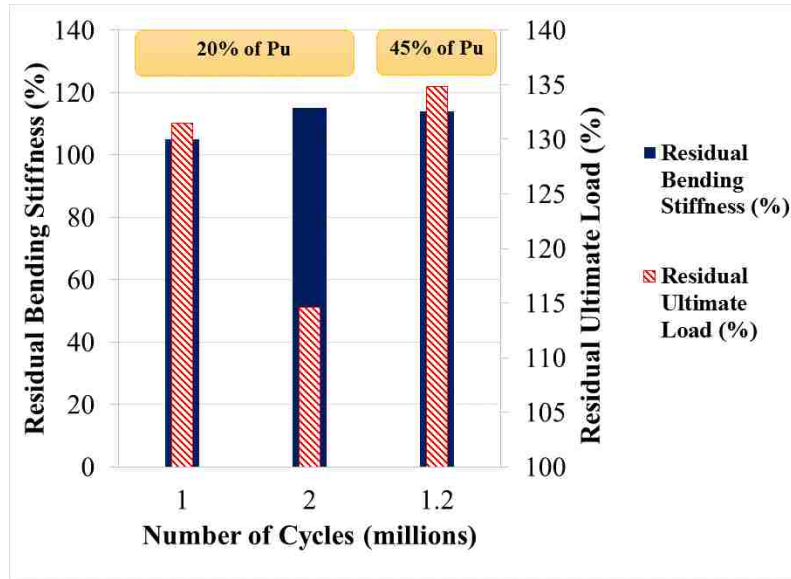Figure 21. Failure modes: (a) delamination, (b) outward facing wrinkling, and (c) compression failure

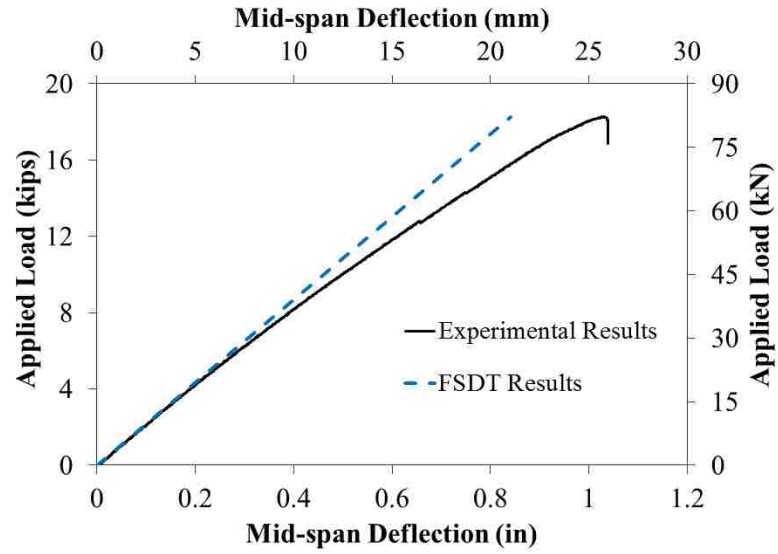Figure 22. Residual stiffness and strength over fatigue life

Figure 23. Comparison between experimental results and theoretical predictions
by the FSDT theory

III. MODELING AND ANALYSIS OF GFRP BRIDGE DECK PANELS FILLED WITH POLYURETHANE FOAM

Hesham Tuwair[1]; Jeffery Volz[2]; Mohamed ElGawady[3]; K. Chandrashekhara[4]; Victor.

Birman[5]

Abstract

This paper presents finite element analyses and analytical models of innovative, small-scale, prototype deck panels examined under monotonic bending. The deck panels consisted of two glass fiber reinforced polymer (GFRP) facesheets separated by webs formed from E-glass woven fabric placed around trapezoidal-shaped, low-density, polyurethane foam segments. The proposed panel exhibited a higher structural performance in terms of flexural stiffness, strength, and shear stiffness compared to conventional sandwich panels. Analytical models were used to predict critical facesheet wrinkling in the sandwich panel. Furthermore, a three-dimensional model using ABAQUS was developed for analysis of the proposed panel system under monotonic four-point loading. The finite element results in terms of strength, stiffness, and deflection were found to be in good agreement with those from the experimental results. A parametric study was also conducted to further evaluate the effects of the stiffness of the top facesheet fiber

---

[1] Graduate research assistant, Department of Civil, Architectural, and Environmental Engineering, Missouri University of Science and Technology, USA E-mail: hrthw2@mst.edu

[2] Associate professor, School of Civil Engineering and Environmental Science, The University of Oklahoma, USA E-mail: volz@ou.edu

[3] Associate professor, Department of Civil, Architectural, and Environmental Engineering, Missouri University of Science and Technology, USA E-mail: elgawadym@mst.edu

[4] Curators' professor, Department of Mechanical and Aerospace Engineering, Missouri University of Science and Technology, USA E-mail: chandra@mst.edu

[5] Professor, Engineering Education Center, Missouri University of Science and Technology, USA E-mail: vbirman@mst.edu

layers, the mass density of the polyurethane foam, the existence of web layers, and the introduction of an overlay above the top facesheet. A flexural beam theory approach was used to predict the sandwich panel's flexural strength.

Key words: Sandwich panels, GFRP, polyurethane foam, wrinkling, finite element analysis.

Introduction

Fiber reinforced polymer (FRP) composites have become a popular construction material for infrastructures such as columns and bridge decks (Dawood and ElGawady 2013, Abdelkarim and ElGawady 2015). FRP sandwich panels are typically used for bridge decks. These panels are typically comprised of two stiff FRP facesheets separated by a core material. The cores can be either solid, flexible, or cellular, including honeycombs, corrugated structures, truss webs, C-shaped cores, I-shaped cores, and Z-shaped cores. Balsa was the first core material considered for use in applications in which the weight was not critical (Stanley and Adams 2001). Honeycomb cores represent one of the best options available for providing high shear strength and transverse stiffness to weight ratios. Unfortunately, they also require special care to guarantee sufficient bonding, which increases the first production costs. Facesheets typically provide the bending strength while the core provides the shear strength (Allen 1969). The core delays local buckling of the compressed facesheets.

FRP sandwich bridge decks represent an alternative to conventional concrete bridge decks. These panels offer a number of additional benefits, including high corrosion

resistance, environmental resistance, higher strength to weight ratio. They can also be used to accelerate bridge construction while incurring minimum traffic interruptions. Using lightweight FRP decks significantly reduces the seismic demand on bridges (Russo and Zuccarello 2007, Alagusundaramoorthy and Reddy 2008).

Skin wrinkling may be a critical mode of failure to sandwich panels because the facesheets have a relatively small thickness. Wrinkling is defined as a form of local instability in a compression facesheet, where the wavelength of the wrinkled part is of the same order as the thickness of the core (Carlsson and Kardomateas 2011). It can also be produced by nonlinear displacement patterns within the soft core (Sokolinsky and Frostig 1999). Wrinkling leads to stiffness losses and may control the sandwich panel's ultimate strength.

Wrinkling forms can be classified into three types: single-sided, symmetrical, and anti-symmetrical. Single-sided wrinkling typically occurs in the sandwich panel's compression facesheet during bending. Both symmetrical and anti-symmetrical wrinkling generally occurs in sandwich elements which have the faces that are subjected to concentric axial compressive loads (Allen 1969). Wrinkling may occur either toward the core or outward, depending on the core's compression stiffness and adhesive strength. Wrinkling, however, is a local phenomenon that is affected by the material properties of the facesheet and core.

The critical wrinkling load is a function of the core's stiffness, the facesheet's stiffness, the loading configurations, and the system's geometry. Gdoutos et al. (2003) studied facesheet wrinkling in both sandwich columns and beams containing foam cores and honeycomb cores. They found that wrinkling occurred in sandwich panels that had

foam cores. However, it did not occur in those with honeycomb cores. Birman and Bert (2004) analytically examined the wrinkling of composite-facesheet sandwich panels that were tested under biaxial loading, where different models were employed. The authors concluded that the models used are appropriate for the wrinkling analysis depending on the size of the buckling, the effect of the core stiffness, and the shearing stresses in the core.

Using analytical approaches to find an exact solution for wrinkling problems may be limited by assumptions adopted in these methods. Thus, in the last two decades researchers began to implement finite element analysis to investigate wrinkling behavior (e.g., Aref and Sreenivas 2001). Wan et al. (2004) used ANSYS to develop a 3D model that could be used to investigate the structural behavior of a GFRP bridge deck system. They also conducted a parametric study and found that a good balance is required between the rigidity of the supporting girders and the GFRP deck to meet the design strength and serviceability demands.

Many approaches, were used to model the sandwich panels, replacing the sandwich structure with an equivalent plate or shell element that had approximately the same properties. Another approach is called discrete layer model, where the sandwich panel is divided into discrete layers, and each layer is defined separately (Noor et al. 1996). Morcous et al. (2010) used four finite element modeling approaches, including one-layer modeling, three-layer modeling, actual configuration modeling, and simplified I-beam modeling, to assess the structural behavior of honeycomb sandwich panels. They found that the simplified I-beam modeling approach was the most computationally efficient method to study the overall performance of honeycomb sandwich panels.

Tuwair et al. (2014) recently developed a new multi-cellular FRP bridge panel (Fig. 1) where initial production costs and the manufacturing difficulties were reduced while improving the system performance. This proposed system was designed so that the panel would behave as a flexural system in the perpendicular direction to traffic and as a truss system in the parallel direction. The panel consisted of GFRP facesheets that were separated by a trapezoidal-shaped, polyurethane foam core. Since the most common problem in sandwich panels arises when the facesheets debond from the core, the web layers were introduced in this system to further connect the top and bottom facesheets. In addition, these web layers increased both the core's shear stiffness and the panel flexural stiffness. The corrugated shape was chosen to reduce the span length within a compressed facesheet so that the effects of localized deformations could be mitigated. To take the research out of the lab, a full-scale deck panel was recently manufactured by Structural Composites, Inc. to serve as a proof-of-concept (Volz et al. 2014). Based on the manufacturing findings, the costs of this panel system was less than the costs of comparable honeycomb FRP decks and this system could compete with initial costs of reinforced concrete decks.

In this study, classical mechanics-based models including Heath, Allen, the Winkler Elastic Foundation, and Hoff and Mautner's models were used to predict critical facesheet wrinkling in the developed sandwich panel. In addition, ABAQUS finite element code (ver. 6.11) was used to conduct numerical simulations of the developed panels. The results were verified and compared with the experimental results gathered from four-point bending tests conducted on the sandwich panels (Tuwair et al. 2014 and 2015). The verified finite element model was then used to conduct a parametric study to investigate the effects

of the stiffness of the top facesheet fiber layers, the mass density of the polyurethane foam, and the existence of an overlay on top of the deck on the deflection, initial stiffness, and strength of the GFRP panels. Additionally, a simple theoretical approach based on load equilibrium and strain compatibility was developed to predict the flexural strength of the sandwich panel.

Calculating the Critical Wrinkling Stress

Several approaches were used in this study to predict the critical wrinkling stress in the sandwich panel's facesheet (σ_{cr}). Heath (1960) developed a model that takes into consideration the thickness of the facesheet and core in addition to the material properties to calculate the wrinkling load of a sandwich panel. The model assumes that both the facesheets and the core are isotropic materials. The wrinkling stress, according to Heath's model, can be calculated as

$$\sigma_{cr,Heath} = \left[\frac{2\,h_f\,E_c\,E_f}{3\,h_c\,(1-v_f^2)} \right]^{\frac{1}{2}} \tag{1}$$

where E_c and E_f are the Young's modulus of the foam and facesheet material, respectively, h_f and h_c are the facesheet and core thicknesses, respectively, and v_f is the Poisson's ratio of the facesheet material.

Allen (1969) modeled the facesheet as an infinitely long plate on an elastic core of infinite thickness. The wrinkling stress of the top facesheet was derived by assuming that the facesheet is attached to the core's surface and allowed to deform in an out-of-plane direction only. Thus, no axial strains occur at the facesheet-core interface in the course of wrinkling. Following Allen,

$$\sigma_{cr,Allen} = 3[12(3 - v_c)^2(1 + v_c)^2]^{-1/3} E_f^{1/3} E_c^{2/3} \tag{2}$$

where v_c is the Poisson's ratio of the core.

The Winkler Elastic Foundation model (WEF) (Carlsson and Kardomateas 2011) was used to predict critical wrinkling stress. This approach assumes that the core consists of linear elastic springs acting as an elastic foundation that supports the facesheet; the core shear modulus is neglected. The WEF becomes more realistic in the case of the symmetry as the mode of deformation in the core is both tension/compression. The wrinkling stress by the WEF model is given by

$$\sigma_{cr,WEF} = 2\sqrt{\frac{E_f E_c h_f}{6h_c}} \tag{3}$$

All three approaches ignore the effect of the shear modulus of the core. Thus, they provide reasonable results for sandwich panels that have either a very low shear modulus or a relatively long wrinkling wavelength.

Hoff and Mautner (1945) considered an energy approach to predict the critical wrinkling stress under the following two assumptions: 1) the facesheet undergoes a symmetrical sinusoidal displacement, and 2) the wave damps out linearly through the thickness. The following equation was developed to calculate the critical compressive stress:

$$\sigma_{cr,Hoff\&Mautner} = 0.91\sqrt[3]{E_f E_c G_c} \tag{4}$$

where G_c is the transverse shear modulus of the core. It should be noted that the web layers in the core were not included in these equations since the wrinkling is a local phenomenon that occurs at the midspan's top facesheet between the web layers.

Experimental Work

Panel Description

The sandwich panels developed for this study were comprised of GFRP/polyurethane facesheets separated by a low-density, trapezoidal-shaped, polyurethane foam. The top and bottom facesheets were connected by corrugated web layers (Fig. 1). Each of the top and bottom facesheets were constructed out of three layers of 0/90°, woven E-glass roving fabric (WR18/3010, Owens Corning, Toledo, Ohio). Three plies of ±45° double bias of E-glass fabric (E-BXM1715, Vectorply, Phenix City, Alabama) were oriented relative to the longitudinal axis of the panel. There plies were used to form each of the corrugated webs that were integrated into the facesheets. Each of the facesheet and web layers contained 9.73 oz/sq.yd (330 g/m^2) and 8.96 oz/sq.yd (304 g/m^2) of E-glass fibers in their longitudinal and transverse directions, respectively. The fabric was infused with a new thermoset polyurethane resin system. This resin was recently modified by Bayer MaterialScience company and features a longer pot life which enabled it to be used with the VARTM process. The average thickness of the different laminates (after resin infusion) are shown in Fig. 1a. More detailed information on this new panel system can be found in Tuwair et al. (2014 and 2015). In the case of a full-scale panel, which will be presented in a different study, vertical web layers may be added at the ends of the panel so that the extended bottom flange would not exist as seen in these tested small-scale panels (Fig. 1a).

Test Setup for Four-Point Loading

Each specimen was tested under four-point loading. Each panel had a span length of 43.0 in. (1092.20 mm) and total depth of 4.15 in. (105.41 mm). This represent approximately 1/2 scale. However, it should be noted that the thickness and characteristics of the different layers need to be tailored for the full-scale panel based on the required design loads. Each panel was tested under two equal point loads that were applied at 15.5 in. (393.70 mm) from each support. This setup provided a section of constant moment within the panel as well as a shear span to depth ratio of 3.74 (considering shear span of 15.5 in. and depth of 4.15 in.).

The specimen was simply supported using two steel plates, each with a width of 2.0 in. (50.80 mm), that could freely rotate around a 1.0 in. (25.40 mm) diameter steel rod, as illustrated in Fig. 1b. The loading was applied through 2.0 in. (50.80 mm) steel plates. Rubber pads with a shore A hardness of 60 were placed between the specimen and the contact points to avoid potential local crushing. Each specimen was loaded in a displacement control at a loading rate of 0.05 in./min (1.27 mm/min), in an MTS880 Universal Testing Machine, until failure occurred.

Finite Element Analysis of the Sandwich Panel

A finite element (FE) commercial code ABAQUS (release 6.11) was used to construct the prototype deck panel that is discussed in the experimental work section. The FE model (depicted in Fig. 2) was used to better understand the behavior of the proposed configuration and to verify the model against the experimental results under monotonic

loading. Once the model was validated, it was also used to manufacture a full-scale panel that will be presented in a different study.

The 3-D FE modeling can be approached using either detailed or reduced models. In both models the core is modeled using solid elements. However, in the detailed models, the facesheets are modeled by solid elements; whereas in the reduced models, the facesheets are modeled by shell elements. A 3-D fully detailed model is computationally expensive as the facesheets are typically much thinner than the core, dictating a very refined mesh in the fully detailed model. However, 3-D fully detailed model typically yield more accurate results. A 3-D fully detailed approach was utilized in this study.

Element Type and Assumptions

The elements of the core, the facesheets, and the web layers (Fig. 3) were defined by solid 3-D continuum elements that had eight-node, integration-reduced, linear brick elements (C3D8R, hourglass control). These elements had three translational degrees of freedom at each node. The use of these elements helped in avoiding mesh instability, commonly referred to as "hourglassing," that may occur in reduced-integration elements (ABAQUS 2013).

A perfect bond was assumed to exist between the sandwich panel components used in the model as delamination did not occur during the experimental tests. After each experimental test, the panels were carefully examined for delamination. Furthermore, several cross sections were taken from each tested panel and no delamination was observed. The different panel components were meshed so that the interface between any two panel components shared the same nodes.

Loading and Boundary Conditions

The sandwich panel was modeled as a simply supported beam. Similar to the experimental work, the applied loads were simulated in the model as line loads applied by steel plates that were 2 in. (50.80 mm) wide. Three-dimensional, rigid elements were used to model the steel plates. Rigid steel plates were placed at the support location. The boundary conditions for the pin supports (Fig. 2b) were defined at the rigid steel plate's centerline where the vertical and horizontal displacements were restrained while the rotations were allowed. A perfect contact was assumed to exist between the loading steel plates and the sandwich panel's surface. The panel was monotonically loaded at the loading pads in a displacement control mode until failure occurred. The ABAQUS implicit solver was used to analyze the sandwich panels.

Material Properties

FRP Composites

The FRP materials were assumed as linear elastic isotropic materials on the macro-scale level since the interwoven fibers were orthogonal to each other and the glass fiber content in the longitudinal (wrap) and transverse (fill) directions are approximately the same. Moreover, the thickness of these layers is small compared to other dimensions.

Based on material characterization tests (Tuwair et al. 2015), the facesheet's elastic moduli in tension ($E_{f,+}$) and compression ($E_{f,-}$) were 2,027 ksi (13.97 GPa) and 1,919 ksi (13.23 GPa), respectively. The web layers' elastic moduli were 1,712 ksi (11.80 GPa) and 1,053 ksi (7.26 GPa) in tension and compression, respectively. The ultimate tensile stress (σ_{f+}) of the facesheet and the web layers was 38.4 ksi (264.80 MPa) and 25.6 ksi (176.50

MPa), respectively, while the ultimate compressive stress ($\sigma_{f\text{-}}$) of the facesheet and the web layers were 14.9 ksi (102.70 MPa) and 18.6 ksi (128.7 MPa). The Poisson's ratio (υ) was 0.27 and 0.30 for the facesheets and the shear layers, respectively. The FE model is assumed to fail when the stresses in FRP materials reach the ultimate tensile or compressive stress value.

Polyurethane Foam

A low-density, closed-cell, polyurethane foam with trapezoidal-shaped segments was used as the core material. The material properties were determined experimentally. The foam had a mass density of 2.0 lb/ft^3 (32 kg/m^3) (low-density foam) and was 48 in. (1219.20 mm) long. A crushable foam model (available in the ABAQUS library) was used to model the foam material. An elastic modulus of 301.8 psi (2.1 MPa) and a yield stress of 8.1 psi (0.056 MPa) (Fig. 4) used to model the low-density foam were determined from earlier experimental work. A high-density polyurethane foam of 6.0 lb/ft^3 (96 kg/m^3) was also used for the parametric study.

Results and Discussions

Experimental Results

The average load-deflection curve measured at the mid-span for two panels, is illustrated in Fig. 5. Both panels exhibited, essentially, a linear response throughout the ascending loading-deflection response. A slight reduction in the stiffness was observed just prior to the panel failure. This reduction resulted from outward skin wrinkling that occurred at the top facesheet between the loading points. This observation was also verified by strain

gauge readings. The average maximum deflection recorded at the mid-span was 1.01 in. (25.65 mm) at an average failure load of 17.83 kips (79.31 kN).

Both specimens produced a loud "popping" sound at the load of approximately 12.80 kips (56.94 kN) and the deflection of 0.75 in. (19.05 mm). Closer examination revealed that a portion of the top facesheet (at the mid-span) suffered outward wrinkling (Fig. 6a). Figure 6b reflects a sudden softening that occurred in the compression facesheet as a result of wrinkling. Both specimens produced a second loud "popping" sound at failure. This sound was accompanied by compression failure of the top facesheet beneath one of the loading points.

Bridge deck elements are stiffness-driven and are typically controlled by deflection to ensure the element functions properly and does not cause discomfort to individuals using the structure. In addition, limiting the deflection is made in an attempt to minimize cracking of the wearing surface. Unfortunately, there is no deflection limits suggested for FRP decks, but a limit ranging from L/300-L/800 is adopted in the design of various FRP bridge decks (King et al. 2012, Alampalli and Kunin 2002; Alampalli et al. 2002). The limit state is typically kept at L/800 as proposed in the AASHTO code and is also proposed in the current practices in FRP composites technology by FHWA (Federal Highway Administration). If a typical range of L/300-L/800 is applied to the 43 in. (1092.20 mm) tested panel span results in a deflection limit range of 0.05 in. − 0.14 in. (1.27 mm − 3.56 mm). The investigated panel reached its initial failure mode, in the form of wrinkling, at a deflection of about 0.40 in. (10.16 mm) or 2.9 times the upper serviceability deflection limit. As expected, serviceability is the controlling limit state in these sandwich panels. This result indicates that the design of these panels will likely always be controlled by

flexural stiffness and serviceability rather than strength. This result is also expected, considering that the fiber reinforced polymer panels that were explored in previous research were almost always controlled by serviceability in experiments and design. Thus, a larger cross-section, with reasonable facesheet and web layers thicknesses is needed to achieve the serviceability limit state.

Analytical Results

The measured applied load from the experimental work was used to calculate the stress at both the top and the bottom facesheets. The calculations predicted the maximum compressive bending stresses of 11.24 ksi (77.50 MPa) and the wrinkling stress of 5.05 ksi (34.82 MPa), corresponding to the load of 8.0 kips (35.58 kN) (Fig. 6b). Technical beam theory (Allen 1969) was used to estimate the global stresses.

Equations 1- 4 were employed to predict the critical wrinkling stresses of the top facesheet. Both the polyurethane foam and the facesheets were modeled as isotropic materials. The data used for the calculations is summarized in Table 1. Heath, Allen, WEF, and Hoff and Mautner's models yielded the values 3.07 ksi (21.17 MPa), 3.17 ksi (21.86 MPa), 2.96 ksi (20.41 MPa), and 3.70 ksi (25.51 MPa), respectively. A comparison between these analytical formulas as well as the experimental results is presented in Fig. 7. As seen in the figure, all models except for Hoff and Mautner model underestimated the facesheet wrinkling by approximately 39%. The Hoff and Mautner model also underestimated the facing wrinkling by 270% being the most accurate model because it accounts for the influence of the transverse shear modulus of the core. It was also noted that the wrinkling wavelength was relatively short (Fig. 6a), representing the situation

where the Hoff and Mautner model accounting for the shear stiffness of the core is quite reasonable.

The two strain gauges used in the experimental work were mounted to the facesheet's middle top surface. Each one was attached on a distance 2 in. (50.80 mm) far from the longitudinal centerline of the panel. As it will explained in the subsequent section of the finite element results, an asymmetry issue was observed during the experimental work, causing the recorded wrinkling observed in the experimental work to be relatively higher than the value at which the actual wrinkling began. Consequently, the values predicted by the these models will always provide more conservative (lower) results than those recorded through the experimental work.

Finite Element Results

The deformed shapes of both the experimental test panel and the FE model are illustrated in Fig. 8. It should be noted that since the experimental results of the two specimens were almost identical, one FE model was discussed in this section to avoid potential confusion. The deflection measured at the panel's mid-span in the experiment is compared to that obtained from the FE model in Fig. 9. The FE model was, in general, able to capture the tested sandwich panel behavior. The average maximum deflection recorded at mid-span in the test was 1.01 in. (25.65 mm), at the average failure load of 17.83 kips (79.31 kN). The FE model predicted an ultimate load of 21.3 kips (94.75 kN), 19.4% higher than that measured during the experiment. The FE models also predicted deflection of 1.28 in. (32.51 mm) at the peak load, that was 26.7% higher than that measured during the experiment (Fig. 9). The flexural rigidity predicted by FE model was 6.6% lower than that

exhibited by the panel during the test. The maximum tensile strain at the mid-span's bottom facesheet recorded during the experiment was 0.0091 in./in. (mm/mm), while the value obtained for the FE model was 0.0097 in./in. (mm/mm). Thus, the difference between the two strain values was 6.2 %.

The FE model tended to overestimate the predicted deflection at mid-span and strength. The difference in the deflection between the FE model and the experiment was attributed to several reasons. One reason was the asymmetry that appeared during the experiment. Although every effort was applied to ensure symmetrical loading, the wrinkling at the top facesheet that occurred during the test was closer to one of the loading points, not exactly in the middle of the specimen, indicating slight asymmetry in either the test fixture or test specimen. The area underneath the loading points was not perfectly leveled, producing asymmetrical loading conditions during the experiment. These conditions caused one of the 2-in. (50.80 mm) loading steel plates to apply more load than the other, which resulted in an earlier compression failure than that observed in the FE model. This explanation was verified by running two FE models where the loading was asymmetric. One loading point was assumed to be subjected to higher loads than the other by 5% and 10% for the first and second models, respectively. The results collected from this portion of the study are illustrated in Fig. 9. Including the asymmetry reduced both the panel's ultimate strength and its maximum deflection.

Another potential reason for the difference in the results obtained from the experiment and the FE model is the manufacturing process, which produces some variability in the different layers. This slight variability affected the FE model predictions as well. Finally, inherent and simplified assumptions used in the FE model, such as

assuming the FRP material is isotropic, resulted in additional differences between the experimental and analytical results.

The FE model correctly predicted the deformed shape and mode of failure (Figs. 8 and 10, respectively). The contours of the total equivalent plastic strain (which is a scalar quantity) are illustrated in Fig. 10c; a value greater than zero indicates that plastic deformation occurred. The top FRP facesheet exhibited outward wrinkling between the two applied loads during the experiment, subsequently displaying local compression failure at the loading line. This failure was induced by a high stress concentration (Fig. 10a). The FE model exhibited a similar behavior (Fig. 10b and 10c); it predicted a high stress concentration at the top facesheet between the two loading points, indicating outward wrinkling. Ultimate failure occurred due to high stress concentration at the contact surface under the loading pads that led to crushing of the top facesheet. Overall, these results validated the modeling assumptions and simplifications that were used in the analysis to predict the sandwich panel behavior. Accordingly, this model can reasonably predict the behavior of such sandwich panels under monotonic loading.

Parametric Study

The benefit of finite element modeling is the ability to alter a wide variety of parameters to investigate a range of behavior of the prototype panel. As a result, the FE model that was previously experimentally verified was used for the parametric study to better understand the behavior and potential of the panels. The parameters investigated included the following:

- The effect of the stiffness of the FRP layers in the top facesheet.

- The effect of the mass density of the polyurethane foam.

- The effect of web layers.

- The effect of an overlay.

The FE model of the actual panel that was validated in the preceding section was used as the sandwich panel-reference model (SP-R) in the following simulation studies.

Effects of Stiffness of the Top FRP Facesheet

This section of the study was conducted to investigate the effect of the top facesheet stiffness on outward skin wrinkling and overall performance. The top facesheet stiffness was increased by adding GFRP layers. The modified cross section was identical to the reference model, SP-R, except for the number of layers in the top facesheet, which were increased to 5, 7, and 9 layers for models SP-5L, SP-7L, and SP-9L, respectively. The load versus the mid-span deflection responses for these panels are illustrated in Fig. 11a. Figure 11b is a plot of the top facesheet longitudinal strain distributions between the two loading points normalized by the maximum longitudinal strain of the reference panel (SP-R). The relative out-of-plane deflection that occurred along the clear distance between the loading points is illustrated in Fig. 11c.

As shown in Fig. 11 (a), increasing the top facesheet stiffness increased the ultimate load and initial stiffness as well as slightly increased the mid-span deflection at peak loads. The increased stiffness compensated for the increased strength and limited the increase in the deflection. Increasing the number of layers of the top facesheet resulted in an increase in the moment of inertia for models SP-5L, SP-7L, and SP-9L by 15.4%, 28.9%, and 41%, respectively. In addition, increasing the number of top facesheet layers increased the panel

initial stiffness by 17.3%, 31.5%, and 43.2% for models SP-5L, SP-7L, and SP-9L, respectively. Generally, the strength was increased from 21.3 kips (94.75 kN) at a deflection of 1.28 in. (32.51 mm) for panel SP-R to 34.4 kips (153.02 kN) at deflection of a 1.59 in. (40.39 mm) for panel SP-9L. This corresponds to an increase of 61% and 24% in strength and deflection at peak load, respectively.

Increasing the FRP top facesheet stiffness also changed the mode of failure. Panels with fewer FRP layers (SP-R and SP-5L) experienced outward skin wrinkling at mid-span as shown in Fig. 11b, while panels with a large number of FRP layers (SP-7L and SP-9L) had smaller local compressive strains and did not display wrinkling deformation (Fig. 11b and 11c). Note that the change from 7 to 9 layers resulted in very little change in the normalized compressive strain and outward deflection in the top facesheet. SP-R model displayed the largest variation in compression strain distribution with a ratio of 10 between a maximum and a minimum strain. The SP-5L, SP-7L, and SP-9L models displayed ratios of variations of 2.5, 1.0, and 1.0, respectively. Local crushing under loading points caused ultimate failure in all panels.

Effects of Polyurethane Foam

The influence of density of polyurethane foam on the sandwich panel structural performance was also investigated. Three panel models, namely, SP-1F, SP-R, and SP-2F were examined, which corresponds to panels with no foam, a low-density foam (2 lb/ft^3, 32 kg/m^3), and a high-density foam (6 lb/ft^3, 96 kg/m^3), respectively. The compressive stress-strain behavior of both types of foam is illustrated in Fig. 4.

The load versus the mid-span deflection response of the three panels is compared in Fig. 12a. As shown in the figure, the existence and absence of the foam core did not affect the panel's stiffness, which confirms Allen's (1969) findings that low-density cores do not noticeably contribute to the overall bending stiffness of sandwich panels. In contrast, the ultimate strength increased by 7.5% when the high density foam was used in the case of SP-2F panel. It should be noted also that the top facesheet compressive strain value was approximately 0.003 (Fig. 6b), which corresponds to compressive stresses of approximately 10 and 60 psi for the low and high density foams (Fig. 4), respectively. These low values also supported the previous finding that the foam did not noticeably contribute to the overall bending stiffness.

Unexpectedly, the local compressive strain concentration was reduced by 40% in the SP-1F panel compared to the SP-R panel (Fig. 12b). This reduction was explained by the absence of foam, which triggered the external webs to buckle outward (Fig. 13). As a result, the interior webs moved apart from each other, bringing the top facesheet downward, i.e., outward wrinkling was reduced as a result of the buckling of the external webs.

Local compressive strains at the top facesheet were reduced by 72% when the low-density foam was replaced with a high-density foam in the SP-2F panel (Figs. 12b and 12c). This reduction was due to the high transverse shear modulus of the high-density foam, which significantly increased the stress at wrinkling from 3.70 ksi (25.51 MPa) in panel SP-R to 25.3 ksi (174.44 MPa) in panel SP-2F. As a result, SP-2F failed due to the compressive stresses under the loading pads at stresses lower than the wrinkling stresses.

Thus, if it is required to prevent wrinkling, high-density foam should be used. Considering the downside of this foam that is its weight, resulting in a heavier deck panel, the optimal sandwich panel could be using a low-density polyurethane foam, combined with additional layers of FRP in the top facesheet, to prevent wrinkling.

Effects of Web Layers

The core of a sandwich panel has to be stiff and rigid enough to resist the shear forces and prevent sliding of the facesheets relative to each other. The rigidity of the core also alleviates local stress concentration and wrinkling.

Three panel models were investigated to better understand the effects of the web layers on the response of the FRP panels. One model (SP-R) represented the reference panel. Panel SP-1W had no web layers (i.e., the top and bottom facesheets were connected only by the low-density polyurethane foam). Panel SP-2W had two external webs only, without foam. The external webs were used to maintain a composite action between the facesheets and the foam core.

All panels were loaded in the same manner as that used for the experimental specimens. The load versus mid-span deflection of the three sandwich models is illustrated in Fig. 14a. Removing the web layers significantly changed the specimen's response. The SP-1W curve had an initially linear region, followed by a nonlinear region. The panel behavior was affected by the polyurethane foam core behavior, i.e., the panel supported higher load without significant damage. The top and bottom facesheets did not reach their ultimate stresses as they behaved as two independent plates due to the very low stiffness (301.8 psi, 2.1 MPa) of the polyurethane foam core. Both the ultimate strength and initial

stiffness were significantly reduced by 96% and 95%, respectively. As illustrated in Figs 14b and 14c, local wrinkling did not occur in the SP-1W panel. However, local indentation was the major concern as a result of the flexible foam, as clearly demonstrated in Fig. 14c, causing the facesheet to buckle on the compression side.

For the SP-2W panel model, both the ultimate strength and initial stiffness were reduced by 56.6% and 27.0%, respectively (Fig. 14a). The SP-2W panel behaved linearly until it failed due to excessive local compression failure at the loading points. Wrinkling did not occur (Figs. 14b and 14c) as the external webs failed due to buckling prior to the top facesheet reaching a critical wrinkling.

Effects of an Overlay Applied Over the Top Facesheet

Bridge decks require a surface texture to provide skid resistance and wear-resistance to traffic. In addition, the overlay helps distribute the applied load on the bridge deck and hence avoid highly localized concentrated forces on the FRP panels. Many different wearing surfaces such as steel, asphalt, polymer concrete, etc. have been used on bridge decks (Aboutaha 2001). Polymer concrete overlays were not considered in this study as several studies conducted for Departments of Transportation showed that polymer concrete will likely crack due to differential movement between the deck panels (Robert et al. 2002).

Three panels, SP-R, SP-C, and SP-A were used to investigate the effects of no overlay, a concrete overlay, and an asphalt overlay, respectively, on the performance of the panels. The SP-R panel was used as the reference model. A half-inch concrete layer was used in panel SP-C as the overlay on the top of the sandwich panel (Fig. 15). It should be

noted that the overlay thickness of full-scale bridge deck would be higher than what's used in this analysis. However, the goal here is to understand the effect of the overlay on the system. Three-dimensional brick, solid elements (C3D8R) were used to model the concrete layer. The concrete damage plasticity model was employed to model overlay with a concrete compressive strength of 7.25 ksi (49.98 MPa). The material properties used for the concrete and model parameters were obtained from Tyau (2009) and Dawood et al. (2012). The tension and compression stress-strain curves, and their corresponding damage curves, were defined in the ABAQUS software. The general parameters of the concrete damage plasticity were as follows:

- Dilation angle (ψ) = 31

- Flow potential eccentric (m) = 0.1

- Initial biaxial/uniaxial ratio (σ_{c0}/σ_{b0}) = 1.16

- Ratio of the second stress invariant on the tensile meridian (k_c) = 0.666

- Viscosity parameter (μ) = 0

Full composite action was assumed between the FRP sandwich panel and the overlay. The full composite action can practically be achieved by either adhesives and/or mechanical connectors (Deskovic et al. 1995, Jain and Lee 2012).

In panel SP-A, a half-inch asphalt overlay (Fig. 15) was used over the sandwich panel. The asphalt is expected to perform better than the concrete in terms of durability and constructability. Asphalt is a flexible material so that any differential movements between the FRP panels would not significantly affect it compared to concrete. Another advantage of using asphalt is a much shorter installation time, i.e. it does not require long cure time compared to both regular concrete and polymer concrete. Three-dimensional brick, solid

elements (C3D8R) were used to model the asphalt layer. The asphalt material was modeled in ABAQUS using the Prony series to model viscoelasticity of the asphalt material. The asphalt has a Young's modulus of 507.63 ksi (3500 MPa) and a Poisson ration of 0.35 (Koohmishi 2013).

The explicit solver was used to analyze the SP-C model because the implicit solver (used for all other models) was not able to solve this problem due to convergence problems. The explicit analysis using the Newton-Raphson iteration to enforce the equilibrium condition at each step can be employed to solve highly nonlinear systems.

The concrete layer weighed approximately 24.5 lb. (109 N) (assuming a normal-weight concrete with a mass density of 150 lb/ft^3, 23.6 kN/m^3), while the sandwich panel itself weighed 23.6 lb. (105 N) with a mass density of approximately of 15 lb/ft^3 (2.36 kN/m^3). The flexural moment demand due to the self-weight of the concrete layer was 144 lb.in. (16.3 N.m) being only around 0.1% of the flexural moment capacity of the reference panel SP-R.

The load versus mid-span deflection responses for the three panels are shown in Fig. 16a. The SP-C panel with concrete overlay behaved linearly until it reached the load of approximately 23.4 kips (104.09 kN) at a mid-span deflection of 0.59 in. (14.98 mm). A sudden drop then occurred in the load, produced by compression failure in the concrete layer, close to the loading points. This failure can be explained by the recorded von Mises stresses at the concrete and the FRP surfaces. The recorded von Mises stresses in the middle span top facesheet are shown in Fig. 17. The stresses in the concrete layer displayed a linear behavior until concrete reached its ultimate compressive stress of 7.25 ksi (49.98 MPa). The FRP panel contribution to the composite panel strength was quite small until this stage.

High compressive stress concentrations at the loading points led to sudden failure. The load was then carried by the FRP panel itself (Fig. 17). The SP-C panel, however, displayed initial stiffness 124% higher than that of the reference FRP panel SP-R. This is attributed to the beneficial contribution of the concrete overlay, which delayed local FRP rupture under the loading points. High stress concentration under the loading points led to failure of the FRP after the top facesheet reached its ultimate strength (14.15 ksi, 97.56 MPa).

The normalized longitudinal strain distributions and the relative out-of-plane deflection that occurred along the clear distance between the top facesheet loading points are illustrated in Figs. 16b and 16c. As shown in Fig. 16b, the SP-C panel experienced a small, nearly uniform compressive strain compared to the highly concentrated strains in the case of SP-R panel. The peak compressive strain in the top facesheet of SP-C was only approximately 4% of that in the SP-R panel. Wrinkling was, however, recorded for the SP-C panel at the maximum load just before the first failure occurred in the concrete layer.

The SP-A panel behaved linearly until it reached a load of approximately 42.2 kips (187.71 MPa) at a mid-span deflection of 1.23 in (Fig. 16a). Then, the panel started to fail due to buckling in the webs. The SP-A panel displayed initial stiffness of approximately 94% higher than that of the reference FRP panel SP-R due to the beneficial contribution of the asphalt overlay. It should be noted that the viscoelasticity of the asphalt prevented failure in the facesheet until the stresses reached 86% of its ultimate tensile strength whereas failure occurred in the SP-R panels when the stress reached only 53% of its ultimate tensile strength.

Figures 16b and 16c illustrate the normalized longitudinal strain distribution and the relative out-of-plane deflection between the top facesheet loading points. SP-C and SP-

A panels did not experience excessive compressive strain concentrations. Therefore, it can be observed that both overlays significantly decreased the compression strains preventing wrinkling.

Simplified Flexural Analysis Method

This section discusses a simplified analysis method that may be applied to the prototype panel analyzed in this study. The sandwich panel (Fig. 1) was analyzed by assuming one-way bending. The analysis is based on the principles of strain compatibility and force equilibrium. The main assumptions used in the analysis were as follows: a) the plane section remains plane; b) perfect bond exists between the panel components; and c) the materials are linear elastic. The analysis based on these assumptions provides design engineers with the tool to calculate the nominal flexural strength of the proposed sandwich panel.

The sandwich panel compressed facesheet experiences local instability (wrinkling), if the compressive stress induced in the top facesheet exceeds the wrinkling stress. The panel strength will, therefore, be limited by the strains that cause wrinkling.

Since the wrinkling stress (σ_{wr}) estimated using the Hoff and Mautner model was the closest to the experimental result, it is used in this calculation as the limiting stress for the top facesheet. The wrinkling strain (0.0027 in./in., mm/mm) was found by dividing the wrinkling stress by the facesheet compressive modulus of elasticity. The wrinkling strain was assumed uniform along the top facesheet. Due to the change in strain through the thickness (in addition to the trapezoidal geometry of the panel), the section properties were calculated in small segments at 1/20th along the cross-section height (Fig. 18). Using strain

compatibility for the studied section, the strains in each segment were estimated by using similar triangles (see Equation 5 below). Consequently, Equation 6 shown below was used to calculate the forces in each segment level. Here, the strain was multiplied by both its modulus of elasticity (whether in tension or in compression) and the area of the segment. The foam was neglected in the strength calculations because it has a low modulus of elasticity. Then, the neutral axis location (c) was calculated using an iterative procedure using Equations (7) and (8) and superimposing the requirement of equilibrium between tensile and compressive forces in the cross section. The section capacity was then computed using Equation 9.

$$\varepsilon_i = \left(\frac{d_i}{c}\right) \varepsilon_{wr} \tag{5}$$

$$F_i = E_i \, \varepsilon_i \, A_i \tag{6}$$

$$F_{t,total} = \sum_{i=1}^{n=(d-c)/20} F_i \tag{7}$$

$$F_{c,total} = \sum_{i=1}^{n=c/20} F_i \tag{8}$$

$$M_{cap} = \sum_{i=1}^{n=d/20} F_i \, d_i \tag{9}$$

where ε_i is the strain in segment i, d_i is the distance from the center of segment i to the neutral axis, c is the distance from the extreme upper fiber of the panel to the neutral axis, d is the panel thickness, ε_{wr} is the wrinkling strain for the compressed facesheet, F_i is the compressive or tensile force, E_i is the modulus of elasticity (either of the facesheet or of the web layer) when the segment i is in either compression or tension, A_i is the cross-

sectional area of segment i, $F_{t,total}$ is the total of all of the tensile forces in the tension side, $F_{c,total}$ is the total of all of the compressive forces in the compression side, and M_{cap} is the capacity flexural moment for the sandwich panel.

The analytical results indicate that reasonable accuracy can be achieved with the assumptions used in this approach. The analytical procedure underestimated the flexural capacity by 16.2% (as compared to the experimental results). This difference could be due to the assumptions used in estimating the wrinkling strain as well as in the flexural analysis. Furthermore, the experimental panel section thickness varied with a coefficient of variation of 7.2%, while the analytical model used only one thickness value. Another reason for the difference between the experimental and analytical results could be due to the variability (12.9% coefficient of variation) in the results obtained from the experimental calculations for the compressive modulus of elasticity of the top facesheet, which directly affects the wrinkling stress.

Summary and Conclusions

Two specimens were tested in one-way bending under four-point bending. Both FE model and analytical methods were used to analyze each panel behavior. A parametric study was conducted using FE model by considering the effect of the number of FRP layers in the top facesheet, the mass density of the polyurethane foam, the effect of web layers, and the effect of an overlay of concrete or asphalt above the top facesheet. The analytical model based on flexural beam theory was used to estimate the sandwich panel flexural capacity. The following conclusions were drawn from this study:

- The behavior of the developed sandwich panel can be treated as a linear-elastic up to failure.

- The proposed FE model can reasonably predict the bending behavior of sandwich panel under monotonic loading.

- The ultimate strength obtained from the FE model was 19.4% higher than that obtained from the experiment. This difference was due to the asymmetry encountered in the experimental setup. However, the flexural rigidity predicted by modeling was 6.6% lower than that obtained in the experiment.

- Different analytical models were used to estimate the outward skin wrinkling, which triggered failure in the experiment. All the models underestimated the facesheet wrinkling stress by 26.7% to 39%. The Hoff and Mautner model was the most accurate one as it accounts for the influence of the transverse shear modulus of the core.

- The following can be concluded from the results of the FE parametric study:

  a. Outward skin wrinkling tendency decreased as the number of layers in the top facesheet increased.

  b. The foam core characteristics affect the local stress concentration in the compression facesheet. However, the occurrence of wrinkling was local and did not affect the bending stiffness of the different specimens. Finally, since all panels displayed an ultimate limit state of local FRP rupture at the applied load, the existence of the core-foam had insignificant effect on strength.

c. The panel behavior significantly dependent on the properties of the web layers. Using a low-density polyurethane foam as a core without webs proved to be insufficient to provide the necessary rigidity, leading to local indentation phenomenon under loading points. Both the ultimate strength and the flexural rigidity were reduced by approximately 95%. However, adding the external webs to the core, in addition to foam, significantly improved the panel behavior.

d. The concrete and asphalt overlay significantly improved the behavior of the panels. The flexural stiffness increased by 125% and 94% for concrete and asphalt, respectively. The overlay layers significantly reduced outward wrinkling of the top facesheet.

- The simplified flexural analysis method reasonably predicted the panel flexural capacity with an error of approximately 16%. Therefore, this method can be used for estimating the proposed panel capacity at preliminary design stage.

Acknowledgments

References

Allen, H. G. (1969). "Analysis and design of structural sandwich panels", Pergamon Press, London.

Alagusundaramoorthy, P. and Reddy, R.V. (2008). "Testing and evaluation of GFRP composite deck panels", Ocean Engineering 35, 287–293

Alampalli, S. and Kunin, J. (2002). "Rehabilitation and field testing of an FRP bridge deck on a truss bridge." Composite Structures 57 (1-4):373-5.

Alampalli, S., O'Connor, J., and Yannotti, A. (2002). "Fiber reinforced polymer composites for the superstructure of a short-span rural bridge." Composite Structures 58 (1):21-7.

Aref, A.J., Sreenivas, Alampalli, (2001). "Vibration characteristics of a fiber reinforced polymer bridge superstructure", Composite Structures 52, 467–474.

ABAQUS Software and Documentation, version 6.11-1 (2013). ©Dassault Systèmes, SIMULIA.

Aboutaha, R. (2001). "Investigation of durability of wearing surfaces for FRP bridge decks", Report prepared for Transportation Infrastructure Research Consortium New York State Department of Transportation (TIRC/NYSDOT). Project # C-01-50.

Birman, V. and Bert, C.W. (2004). "Wrinkling of Composite-facesheet Sandwich Panels Under Biaxial Loading", Journal of Sandwich Structures and Materials 2004; 6; 217.

Carlsson, L.A. and Kardomateas, G.A. (2011). "Structural and Failure Mechanics of Sandwich Composites", Springer.

Deskovic, N., Meier, U. and Triantafillou, T.C. (1995). "Innovative Design of FRP Combined with Concrete: short term behavior", Journal of Structural Engineering, 121, 7, pp 1069-1078.

Gdoutos, E.E., Daniel, I.M., and Wang, K.A. (2003). "Compression facing wrinkling of composite sandwich structures", Mechanics of Materials 35 (2003) 511–522.

Heath, W.G. (1960). "Sandwich construction, Part 2: The optimum design of flat sandwich panels", Aircraft Eng. 32, 230–235.

Hoff, N.J. and Mautner, S.F., (1945). "The Buckling of Sandwich-Type Panels", J. Aeron. Sci., 12, pp. 285-297.

Jain, R. and Lee, L. (2012). "Fiber Reinforced Polymer (FRP) Composites for Infrastructure Applications: Focusing Innovation, Technology Implementation and Sustainability." Springer

Koohmishi, M., (2013). " Comparison of Pavement Layers Responses with Considering Different Models for Asphalt Concrete Viscoelastic Properties", Slovak Journal of Civil Engineering, Vol. XXI, No. 2, pp 15-20.

King, L., Toutanji, H., and Vuddandam, R. (2012). "Load and resistance factor design of fiber reinforced polymer composite bridge deck." Composites: Part B 43:673-680

Morcous, G., Cho, Y., El-Safty, A., and Chen, G. (2010). "Structural Behavior of FRP Sandwich Panels for Bridge Decks", KSCE Journal of Civil Engineering 14(6):879-888.

Noor A.K., Burton W.S., and Bert C.W. (1996). " Computational models for sandwich panels and shells", Appl Mech Rev; 49(3):155–99.

Russo, A, Zuccarello, B. (2007). "Experimental and numerical evaluation of the mechanical behavior of GFRP sandwich panels", Composite Structures; 81, pp 575-586.

Robert, J., Chung, C., and Alayed, H. (2002). "Deck Replacement for the Skewed Truss Bridge on MD 24 Over Deer Creek in Harford County, Maryland Utilizing a Fiber-Reinforced Polymer (FRP) Bridge Deck", The Bridge Engineering Software and Technology (BEST) Center, University of Maryland, College Park, Marylan, Report No. IBC-02-56.

Sokolinsky, V., and Frostig, Y. (1999). "Boundary conditions effects in buckling of ''soft'' core sandwich panels", Journal of Engineering Mechanics, Vol. 125, No. 8, pp 865-874.
Stanley, L.E., Adams, D.O. (2001). "Development and Evaluation of Stitched Sandwich Panels", Technical Report, University of Utah, Salt Lake City, Utah.

Tuwair, H., Volz, J., ElGawady, M., Mohamed, M., Chandrashekhara, K., and Birman, V. (2014). "Testing and Evaluation of GFRP Sandwich Bridge Deck Panels Filled with Polyurethane Foam," American Society for Composites 29th Technical Conference and 16th US-Japan Conference and ASTM D30 Meeting, Sand Diego, California.

Tuwair, H. (2015). " Development, Testing, and Analytical Modeling of Fiber-Reinforced Polymer Bridge Deck Panels." PhD Dissertation, Missouri University of Science and Technology. Rolla, MO.

Tyau, J.S. (2009). "Finite Element Modeling of Reinforced Concrete using 3-Dimensional Solid Elements with Discrete Rebar". Thesis, Brigham Young University. Provo, Utah.

Volz, J., Chandrashekhara, K., Birman, V., Hawkins, S., Huo, Z., Mohamed, M., Tuwair, H. (2014).''Polyurethane foam infill for fiber-reinforced polymer (FRP) bridge deck panels.'' Final Report Prepared for Missouri Department of Transportation. Project TRyy1203.

Wan, B., Rizos, D.C., Petrou, M.F., and Harries, K.A. (2004). "Computer simulations and parametric studies of GFRP bridge deck systems", Composite Structures 69 (2005) 103–115.

Table 1. Summary of the Data used for the Wrinkling Calculations

Parameters	value
h_f [facesheet thickness, in. (mm)]	0.09 (2.29)
h_c [core thickness, in. (mm)]	3.97 (100.84)
E_c [compressive modulus of low-density foam, psi (MPa)]	301.8 (2.1)
E_{ct} [compressive modulus of high-density foam , psi (MPa)]	5,380 (37.1)
E_f [compressive modulus of facesheet, ksi (GPa)]	1,919 (13.23)
υ_f [Poisson's ratios of the facesheet material]	0.27
υ_c [Poisson's ratio of the foam]	0.3
G_c [transverse shear modulus of low-density foam, psi (MPa)]	116.1 (0.8)
G_c [transverse shear modulus of high-density foam, psi (MPa)]	2,069 (14.3)

(a)

(b)
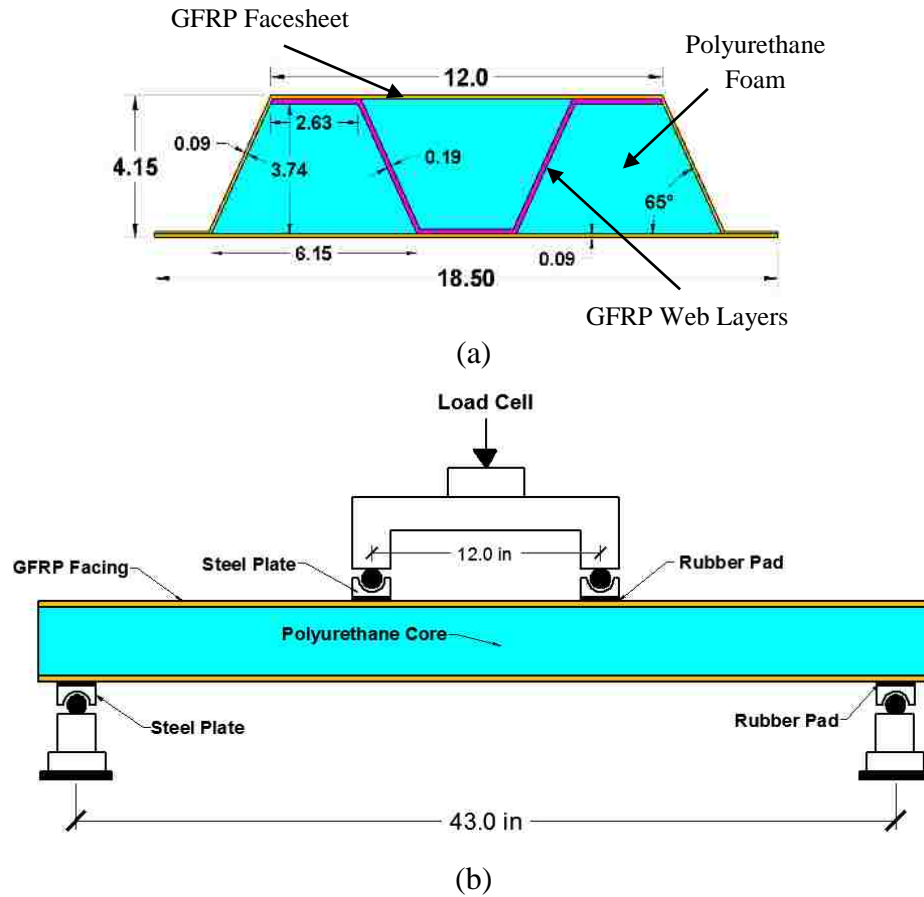
Figure 1. Test setup: (a) cross-section of the developed panel (all dimensions in inches, 1 in. = 25.4 mm) and (b) schematic of static flexural test setup

Supporting

steel pad
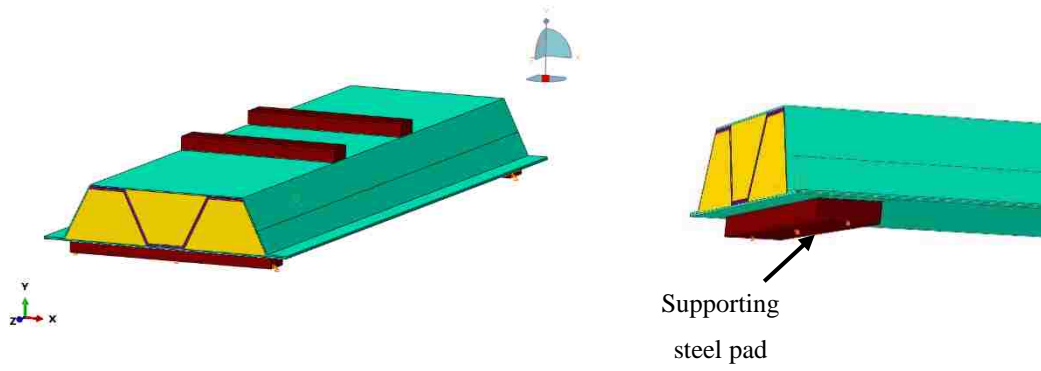
(a)   (b)

Figure 2. FE model: (a) 3D view of simulated FE model and (b) a centerline
boundary condition of the support

(a)

(b)

(c)
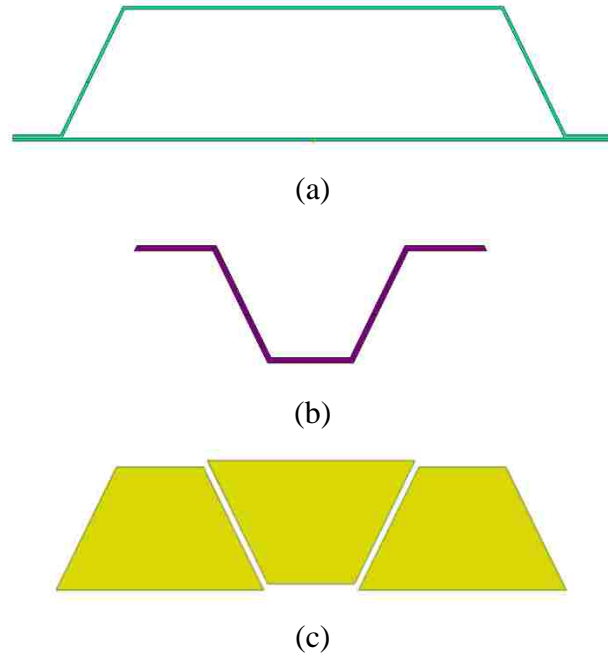
Figure 3. FE model components: (a) GFRP facesheets, (b) GFRP web layers, and (c) Low-density polyurethane foam
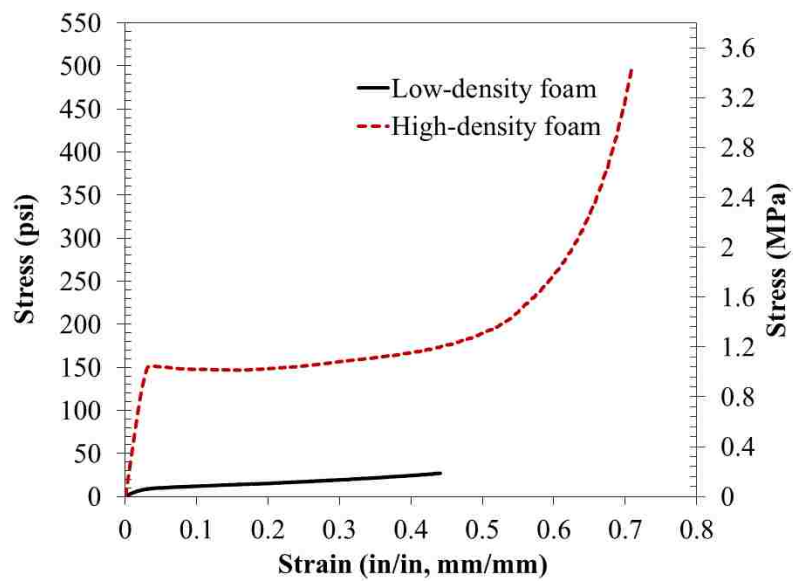
Figure 4. Compression stress vs. strain curves of low and high-density polyurethane foam
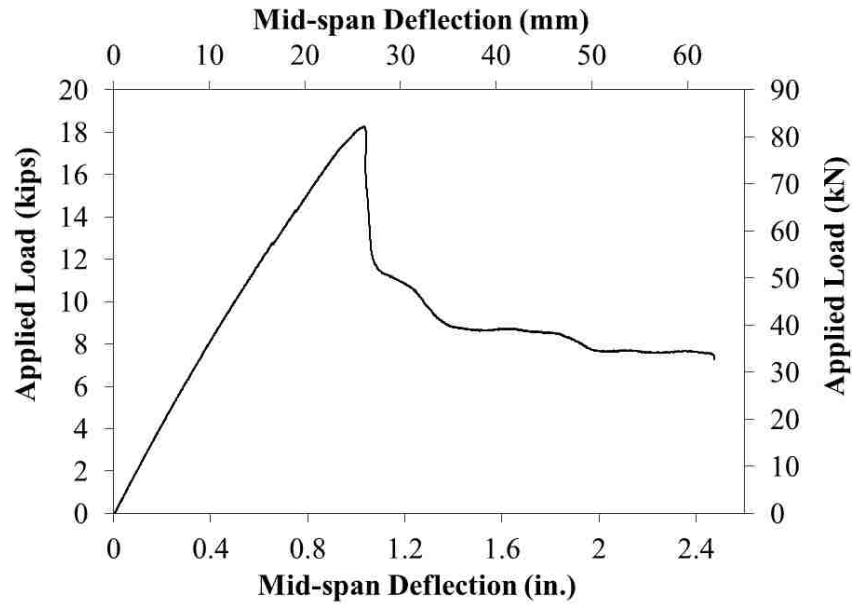
Figure 5. Experimental load-deflection results
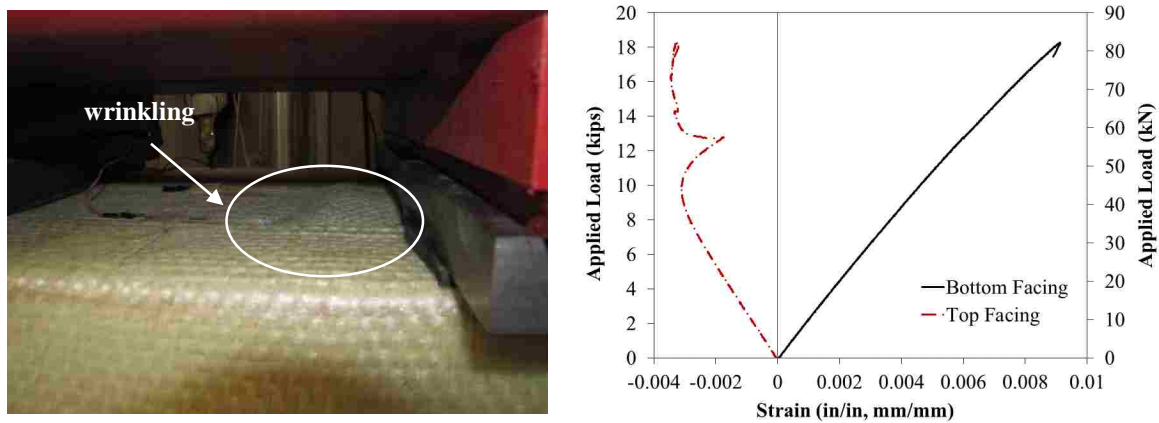
<table>
<tr><td align="center">(a)</td><td align="center">(b)</td></tr>
</table>

Figure 6. Experimental test results: (a) Outward facesheet wrinkling failure and (b) load vs. strain at mid-span
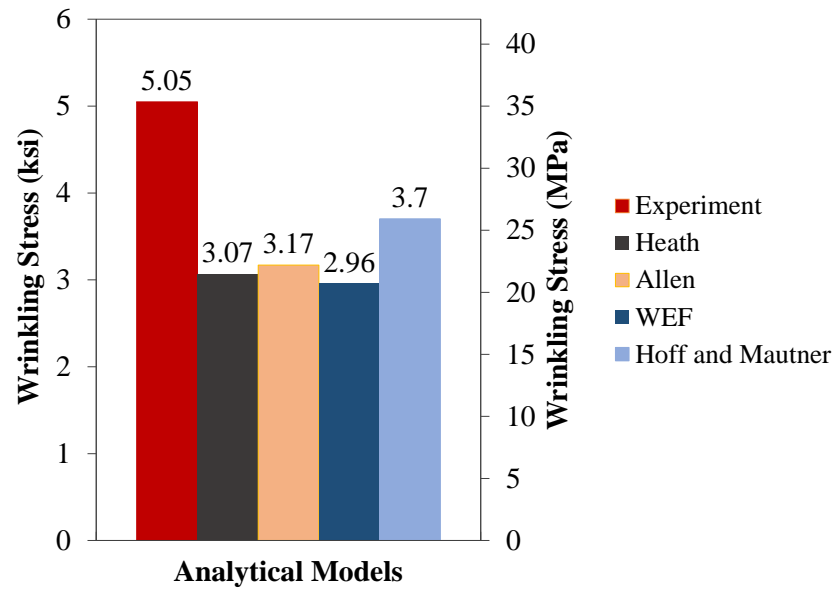
Figure 7. Comparisons of different analytical formulas with the experimental
result
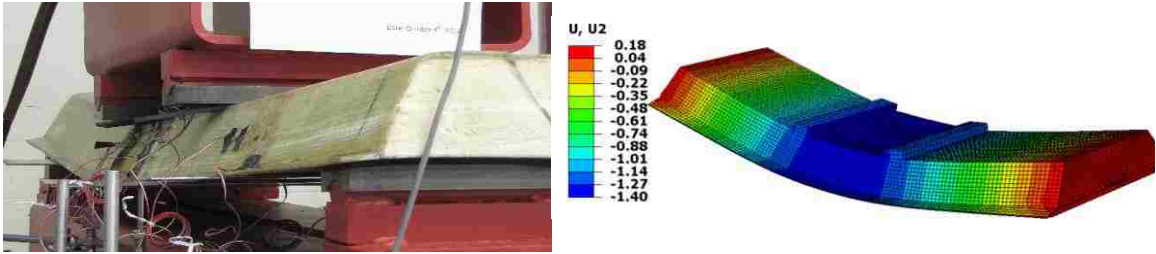
Figure 8. Deformed shape for experimental and FE results
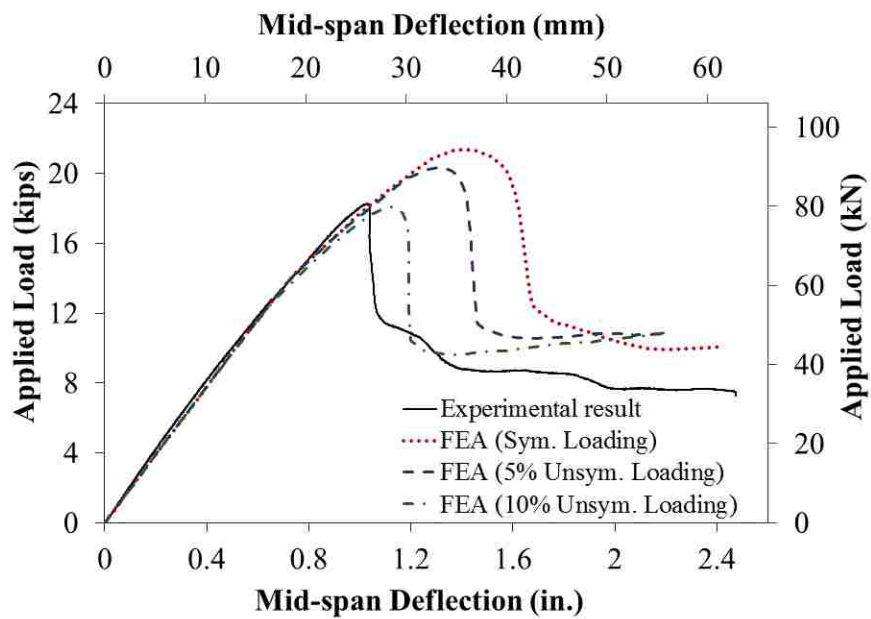
Figure 9. Comparison of experimental results versus numerical results

Max. compressive stresses

(a)   (b)

(c)
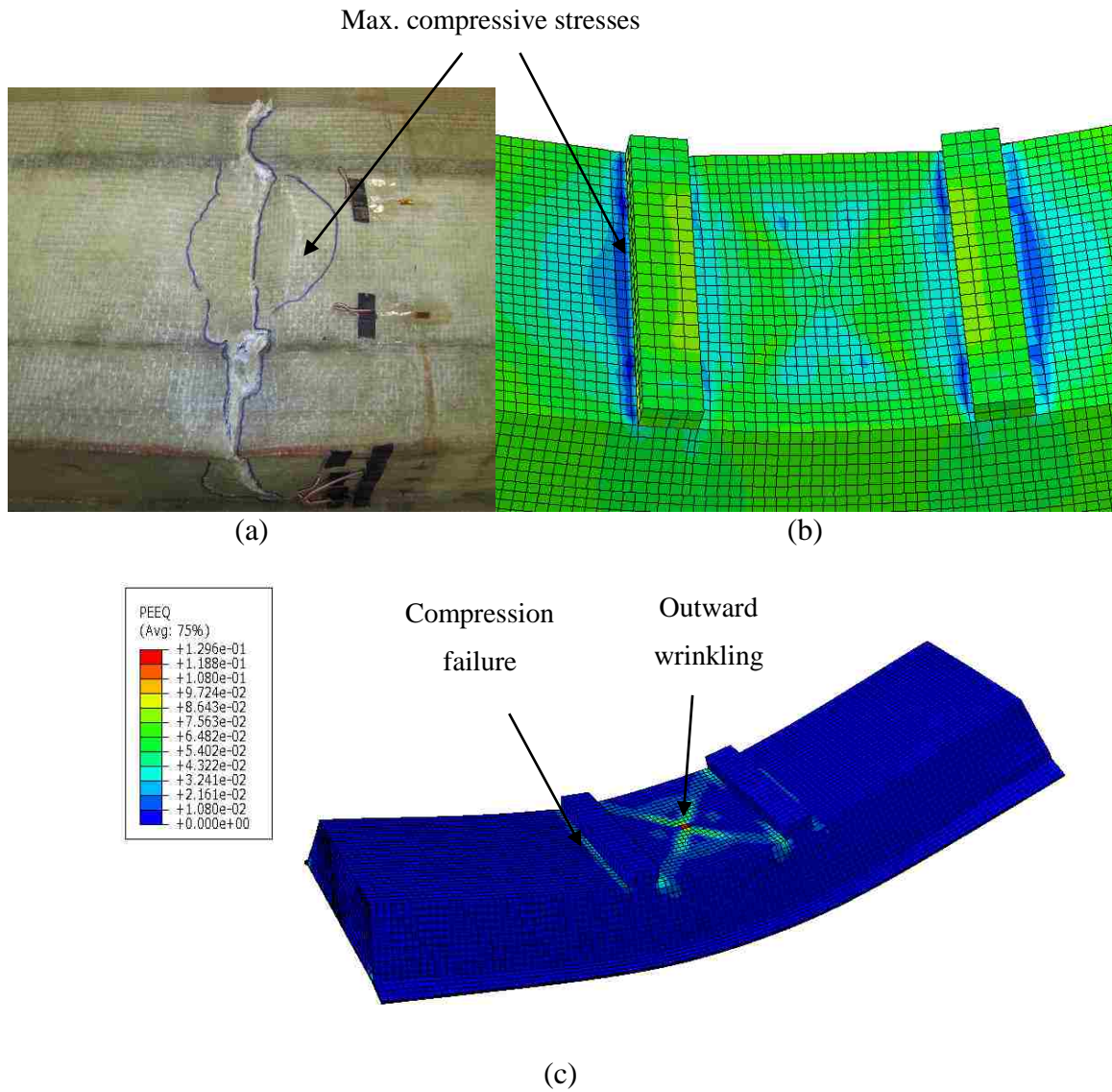
Figure 10. Compressive failure under the loading pads: (a) for the experimented specimen, (b) for the FE model, and (c) contours of plastic strains shows initial failure at the top facesheet caused by wrinkling and ultimate failure caused by excessive compressive stresses at the loading points
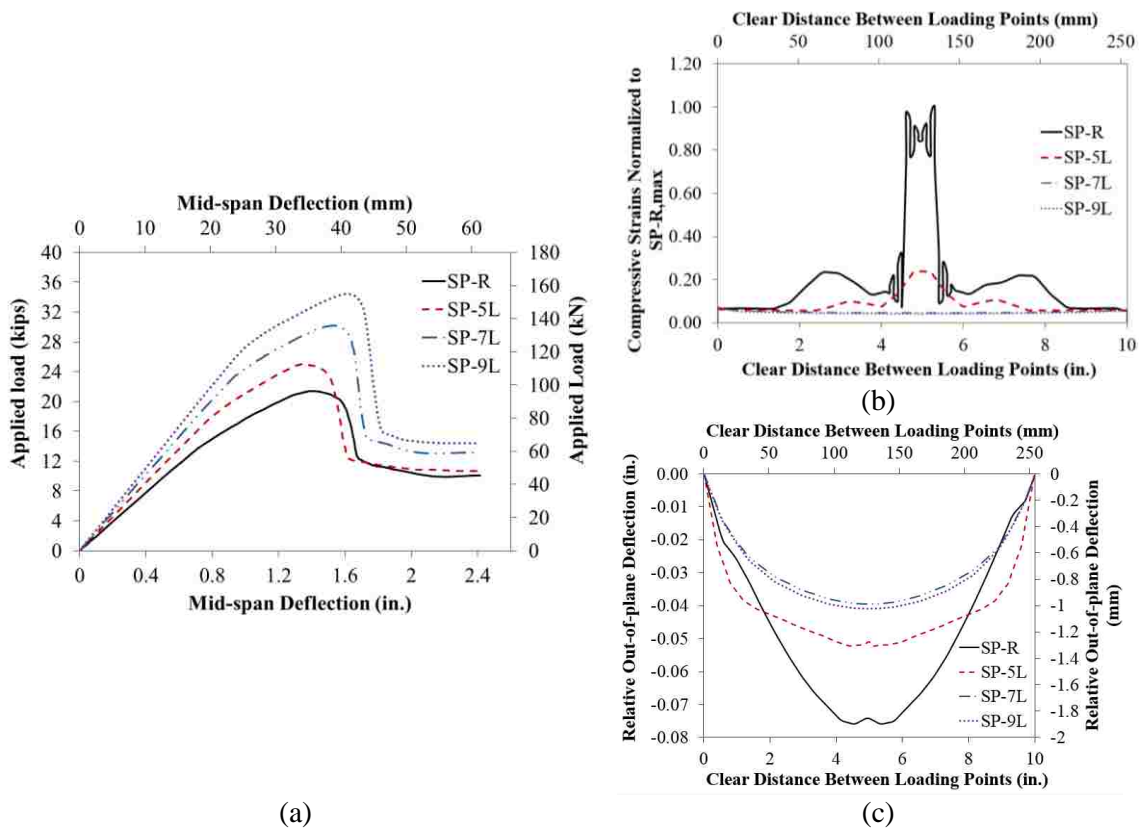
Figure 11. Effects of FRP in the top facesheet: (a) applied load vs. mid-span deflection, (b) and (c) longitudinal compressive strains and relative out-of-plane deflection in top facesheet between the loading points, respectively
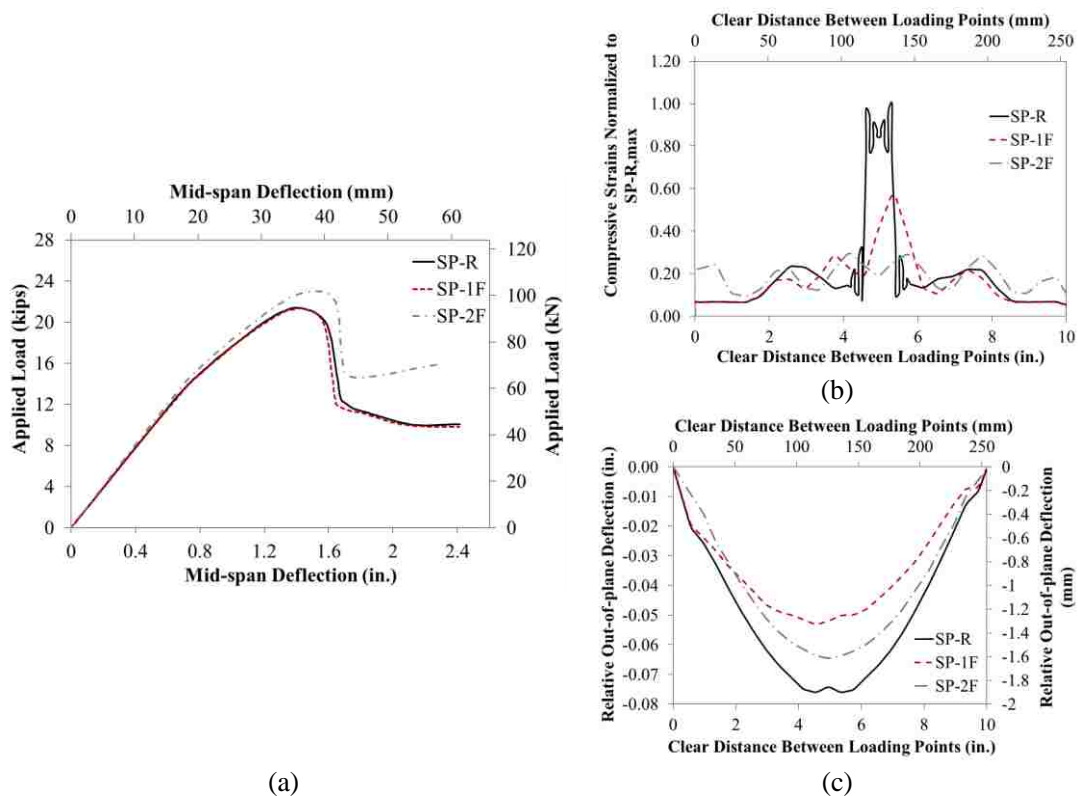
Figure 12. Effects of polyurethane foam: (a) applied load vs. mid-span deflection, (b) and (c) longitudinal compressive strains and relative out-of-plane deflection in top facesheet between the loading points, respectively.
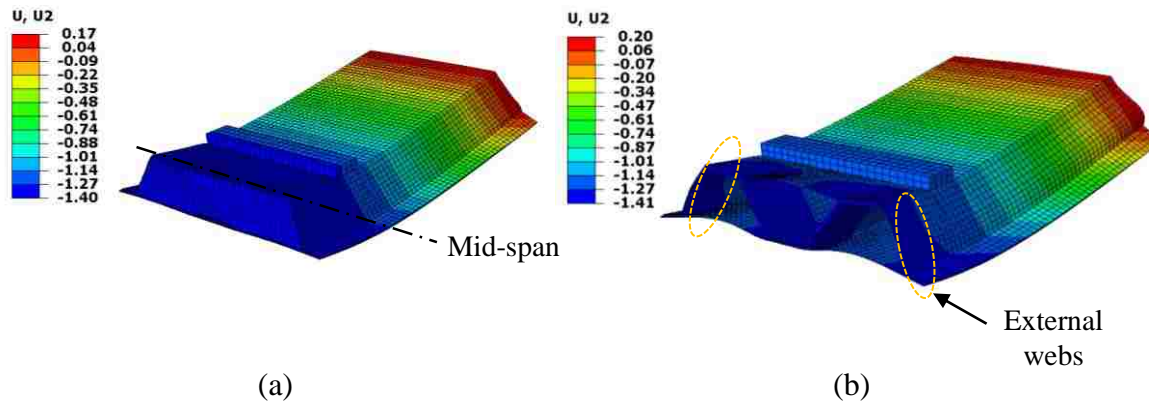
Figure 13. Deformed shape for (a) SP-R panel and (b) SP-1F panel.

(a)

(b)

(c)
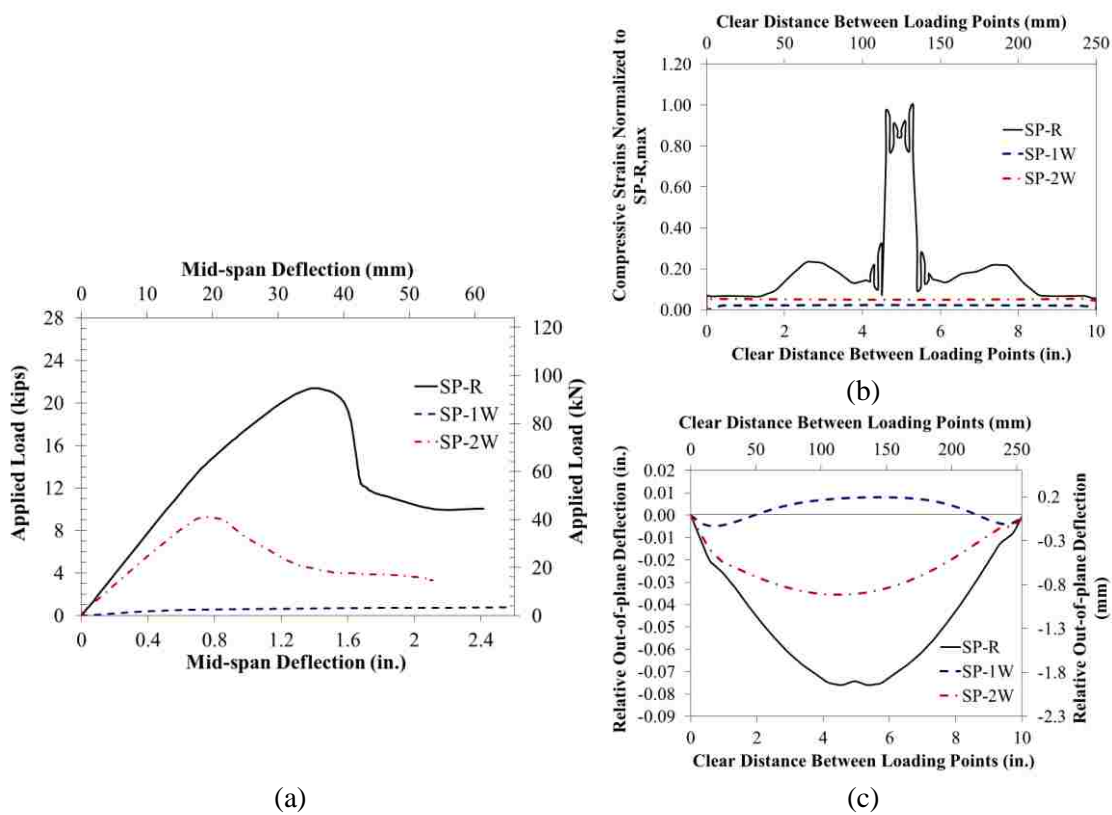
Figure 14. Effects of web layers: (a) applied load vs. mid-span deflection, (b) and (c) longitudinal compressive strains and relative out-of-plane deflection in top facesheet between the loading points, respectively.

Concrete or Asphalt
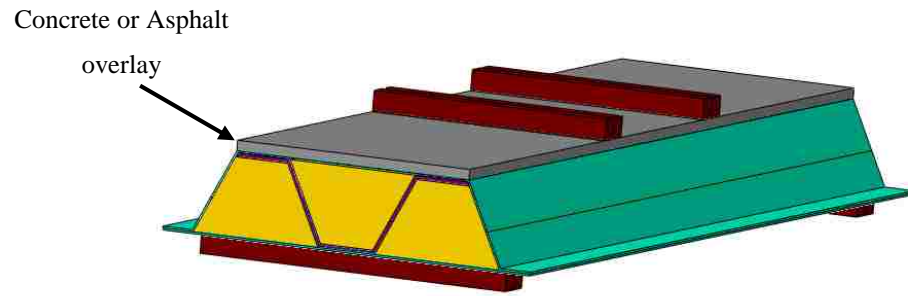
overlay

Figure 15. 3D view of simulated FE model with an overlay

(a)

(b)

(c)
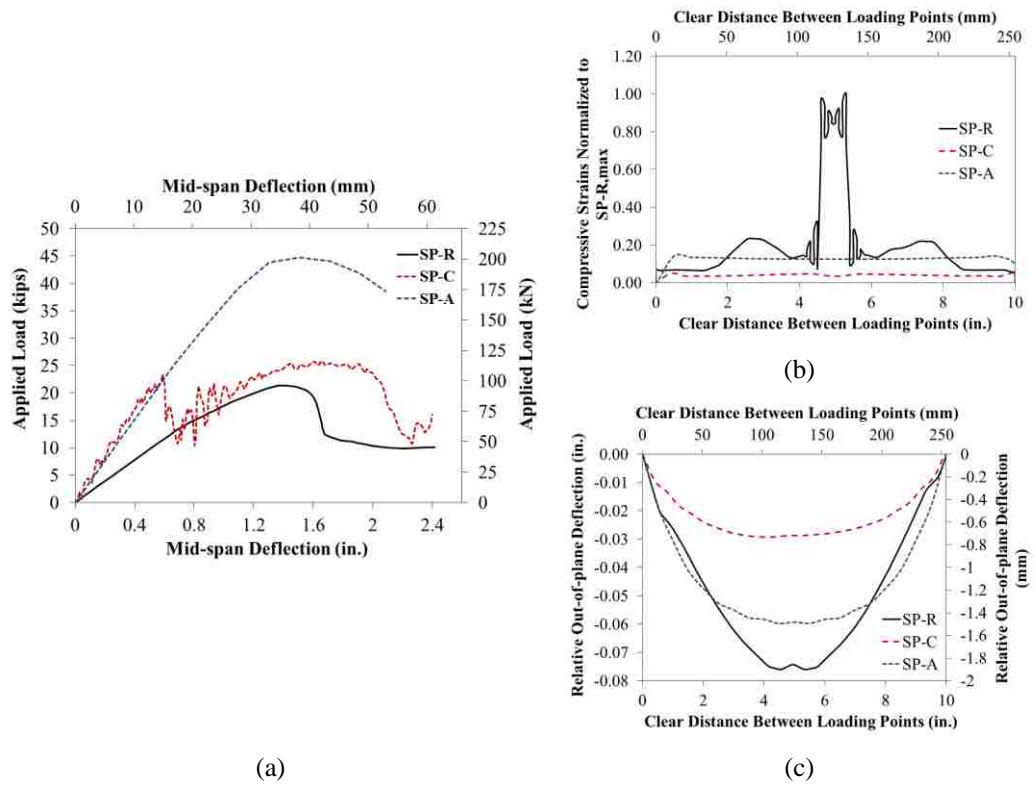
Figure 16. Effects of an overlay: (a) applied load vs. mid-span deflection, (b) and (c) longitudinal compressive strains and relative out-of-plane deflection in top facesheet between the loading points, respectively
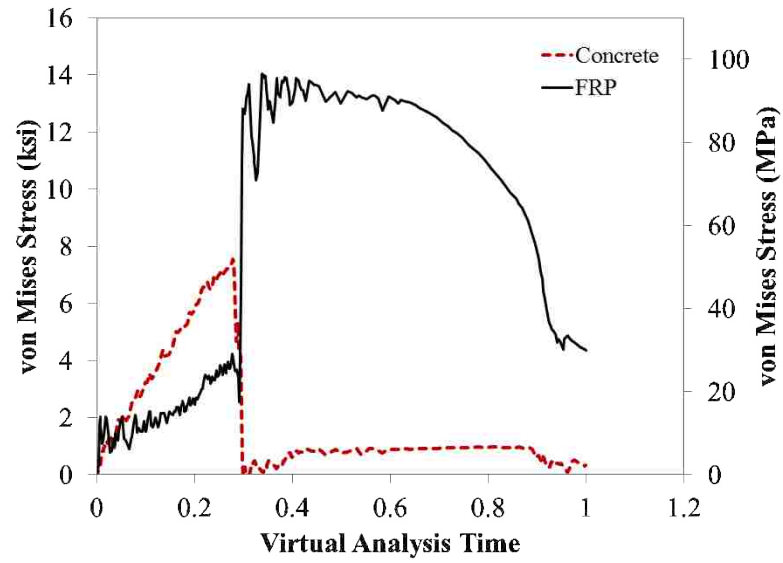
Figure 17. Longitudinal stresses at the mid-span's top facesheet for the concrete and FRP surfaces
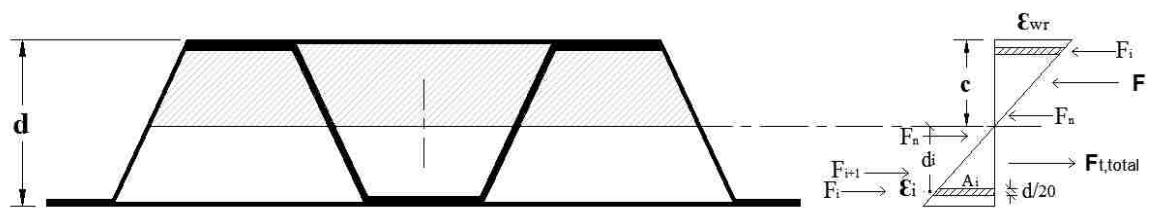
Figure 18. Compression and tension couple at nominal moment

IV. DURABILITY OF POLYURETHANE FOAM INFILL FOR GFRP BRIDGE DECK PANELS SUBJECTED TO VARIOUS ENVIROMENTAL EXPOSURE

Hesham Tuwair[1]; Jeffery Volz[2]; Mohamed ElGawady[3]; Mohaned Mohamed[4];

K.Chandrashekhara[5]; Victor Birman[6]

ABSTRACT

This paper investigates the performance of polyurethane foam-infill bridge deck panels (PU sandwich panels) after being exposed to various environmental conditions. These panels were constructed with woven E-glass fiber/polyurethane facesheets that were separated by a trapezoidal-shaped, low-density, polyurethane foam. Corrugated web layers were introduced into the core to enhance the panel's structural characteristics. The PU panels were manufactured through a one-step vacuum assisted resin transfer molding (VARTM) process. An experimental program was designed to simulate their in-situ environments. The environmental conditions used included different conditioning regimens to examine the behavior of both GFRP laminates and PU sandwich panels. The GFRP laminates, which were made from the same materials as the PU sandwich panels, were exposed to ultraviolet radiation, a deicing solution at both room temperature and

[1] Graduate research assistant, Department of Civil, Architectural, and Environmental Engineering, Missouri University of Science and Technology, USA E-mail: hrthw2@mst.edu

[2] Associate professor, School of Civil Engineering and Environmental Science, The University of Oklahoma, USA E-mail: volz@ou.edu

[3] Associate professor, Department of Civil, Architectural, and Environmental Engineering, Missouri University of Science and Technology, USA E-mail: elgawadym@mst.edu

[4] Graduate research assistant, Department of Mechanical and Aerospace Engineering, Missouri University of Science and Technology, USA E-mail: mmm7vc@mst.edu

[5] Curators' professor, Department of Mechanical and Aerospace Engineering, Missouri University of Science and Technology, USA E-mail: chandra@mst.edu

[6] Professor, Engineering Education Center, Missouri University of Science and Technology, USA E-mail: vbirman@mst.edu

elevated temperature, and thermal cycling. The PU sandwich panels were exposed to thermal cycling (a series of freeze-thaw, mid-high temperatures, and mid-high relative humidity cycles). The thermal cycling exposure was conducted in a computer-controlled environmental chamber to duplicate seasonal effects in Midwestern states. Following the exposure regimens, tensile strength tests and four-point loading tests were performed on the GFRP laminates and the PU sandwich panels, respectively. The evaluation was based on visual inspection, strength, stiffness, and failure modes, as compared to those that were not conditioned (the control). The results of this study revealed that degradation in strength and stiffness does exist, to a certain extent, in some of these conditioning regimens. These results will be used to determine design factors in using polyurethane-based GFRP materials in bridge construction in the United States Midwest.

Key words: FRP Bridge Deck, Durability, Environmental degradation, Sandwich Panel, GFRP, Polyurethane Foam, Polyurethane Resin.

1. Introduction

With the continuous deterioration of the nation's infrastructure, it was found that over half of the nation's 607,000 bridges were built before 1940 [1]. These bridges have reached the end of their useful service lives. In study recently conducted by Ellis [2] for the Federal Highway Administration (FHWA) estimated the annual direct cost of repairing corrosion on highway bridges to be between $6.43 and $10.15 billion. This estimate includes $1.07 to $2.93 billion needed each year to maintain the concrete bridge decks. In an effort to address these sobering statistics, transportation agencies have been trying to

identify new, cost-effective, and reliable construction materials that can be used to not only fabricate but also rehabilitee bridge decks. Advanced composites made of fibers embedded in a polymeric resin, also known as fiber-reinforced polymer (FRP) materials, have received considerable attention as a strong candidate to replace deteriorating concrete and steel structures. These composites, commonly used for civil engineering applications, are reinforced with an inexpensive fiberglass. The advantages of FRP composites have been widely recognized and include their low weight, ease of installation (reducing traffic delay), resistance to both environmental and chemical attacks, and resistance to fatigue loads.

Extensive durability studies have been conducted on FRP composites for aerospace and marine applications. Autoclave-based fabrication was, however, used to manufacture each of these applications under strict specifications. Cheaper manufacturing processes have been used in the civil market (e.g., wet layup, vacuum assisted resin transfer molding [VARTM], and pultrusion), resulting in lower temperature cure epoxies. The FRP composites used in the field for rehabilitation purposes are cured under ambient temperatures. Thus, these composites are more vulnerable to moisture damage and plasticization than those used for aerospace and marine applications. Accordingly, it is impossible to interpret the results of those studies established by the Department of Defense for civil engineering applications [3].

Since FRP composites are made through the combination of micron-sized fibers and polymer matrices, the polymer matrix of the FRP composite is considered the weak link as it may experience change in its physical properties and chemical degradation during environmental exposure. Polymer composites are vulnerable to ultraviolet radiation, both

freeze-thaw and high temperature cycles, moisture, deicing chemicals, and alkali attacks, leading to degradation in strength and stiffness [4-11].

A number of studies have been conducted on the effects on the durability of FRP composites. Among those, Karbhari and Pope [9] and GangaRao et al. [10] investigated the impact of freeze-thaw cycles on these composites. They found that such exposure can negatively change the thermo-mechanical response of the resin. Another study conducted by Verghese, et al. [12], found that degradation is primarily associated with the micro-cracking that occurs when the volume of absorbed water changes. Jamond et al. [13] and Malvar et al. [14] investigated several commercial composites under environmental exposure. They found that seawater immersion and salt-fog exposure caused the greatest degradation in mechanical properties. Lopez-Anido et al. [11] investigated the performance of the adhesive bonds of the FRP composite under freeze-thaw cycles. They noted that the bond was reduced significantly and the failure mode was changed. Connolly et al. [15] reported changes in the physical properties of the followings: the pultruded polyurethane, the vinyl ester, the unsaturated polyester, and the unsaturated polyester-urethane hybrid composites under ultraviolet radiation, salt water, hydrocarbon fluids and strong acid solutions. They found that the polyurethane pultruded composites exhibited superior strength and toughness under environmental exposure, when compared to the other examined composites.

Polyurethane resin has better properties than traditional resin systems (e.g., polyester and vinyl ester resin systems) [15]. Additionally, the polyurethane composites' profiles have exhibited promising preliminary results in environmental exposure tests. Glass-fiber-reinforced polyurethane composites are conventionally manufactured using a

pultrusion process. However, pultrusion is limited to the manufacture of constant cross-section profile composite parts. The VARTM process is a low-cost composite manufacturing process that is widely used throughout the composite industry. This process has been developed over the last two decades for applications in commercial, military, and marine composite structures [16]. However, viscosity and pot-life limitations of polyurethane resins have prevented its use with the VARTM process until recently where a major development in novel catalysis chemistry was developed by Bayer MaterialScience. This dual catalyst system extended the pot life of mixed resins at room temperature [17]. The resin itself was developed quite recently. Thus, the durability studies of glass-fiber-reinforced polyurethane composites manufactured as part of the VARTM process, under harsh environmental conditions, for infrastructure applications, has not been reported in the literature.

This study presents an experimental work that investigates the effects of environmental exposure on the behavior of both GFRP laminates and PU sandwich panels. The panel was previously proposed by Tuwair et al. [18]. The prototype PU sandwich panels, comprised of two woven E-glass fibers/polyurethane facesheets that were separated by a trapezoidal-shaped, low-density, polyurethane foam (see Fig. 1). The foam core was comprised of a stiff web layers that served as a truss structure between the facesheets. The VARTM process was used to manufacture these PU sandwich panels.

2.   Experimental program

Testing the entire sandwich panel under different environmental conditions is essential to determine the full stiffness and strength degradation, and mode of failure of the

panel. This type of test, however, cannot provide the degradation data of each constituent material of the PU sandwich panels. Thus, testing of small coupon specimens of the GFRP material, in addition to PU sandwich panels was conducted. The conditioning regimens conducted in this study consisted of exposure to ultraviolet radiation, a deicing solution at both a room temperature and an elevated temperature, and thermal cycling (a series of freeze-thaw, mid-high temperatures, and mid-high relative humidity cycles). Each test was conducted in a computer-controlled environmental chamber.

2.1. *GFRP laminate characterization*

The GFRP laminates examined in this study were manufactured in the Composite Manufacturing Laboratory of the Mechanical and Aerospace Engineering Department at Missouri University of Science and Technology. These laminates were made to represent the facesheet and web core of the PU sandwich panels. The facesheet laminate was comprised of three plies of plain-weave woven E-glass fabric (WR18/20) laid up equally in a $0/90^o$ fiber orientation. The web core laminate was formed from three plies of $+/-45^o$ laid up equally in a double bias of E-glass woven fabric (E-BXM1715). Both the facesheet and the web core laminates were infused with a new type of longer pot-life, a thermoset polyurethane resin developed by Bayer MaterialScience.

The facesheet and web core laminates were cut into 50 coupon specimens (see Fig. 2) so that their in-plane tensile properties, before and after the environmental conditioning, could be examined. ASTM D3039/D3039M standard [19] recommends that the minimum length of the specimen be taken as the gripping length at both ends, plus two times the coupon width, plus a gage length. The width should also be taken as needed. As such, the

coupon dimensions were 10 in. (254.00 mm) long and 1 in. (2.54 mm) wide. Aluminum end tabs of a length of 2.5 in. (63.50 mm) were placed one day before the testing. Between four and five coupon specimens were typically considered for the control specimens and for every conditioning regimen specimens.

An MTS880 universal testing machine with wedge-type mechanical grips was used to conduct tensile strength tests on the control and the conditioned specimens. The speed of the test was set to provide a constant strain rate within a gage length of 0.01 min-1, as recommended by the standard, which is 0.05 in/min (1.27 mm/min). One electric resistance strain gauge 0.236 in. (6.00 mm) long, with a resistance of 350 ± 0.2 Ω, was used to measure the longitudinal strains. A Data Acquisition System (DAS) was used to record the test data, including load and stroke of the MTS machine.

The mechanical properties of GFRP coupons, namely the young's modulus and the tensile strength, were used to assess the stiffness and strength. The modulus of elasticity was taken as the highest slope of a straight line from the initial portion of the stress-strain curve. The tensile strength of the material was calculated by dividing the maximum applied load by the initial undeformed cross-sectional area of the coupon.

2.2.   *Conditioning regimens*

2.2.1.   *Ultraviolet radiation*

Glass fiber-reinforced polymer (GFRP) composites are used for long periods of time in outdoor applications (e.g., bridges). As such, these composites are exposed to large amounts of ultraviolet (UV) radiation, which can have a degrading effect. In general, the influence of UV radiation on total solar global radiation is 5-6% (depending on both the

location and the time). The UV spectral range observed on the Earth's surface varies from approximately 295 to 400 nm [3]. This UV light can alter the molecular chain of polymers, creating microcracks that deteriorate GFRP's durability.

A UV chamber constructed specifically for this study was used to perform this test. This chamber was made to meet the requirements defined in ASTM G151 [20] and ASTM G154 [21]. Not all of the requirements were strictly followed. The chamber (depicted in Fig. 3) was built from a wooden box and had the following dimensions: 27.5 in. (698.50 mm) long, 19.5 in. (495.30 mm) wide, and 20 in. (508.00 mm) high. These dimensions were used to accommodate the coupon specimens. The desired wattage intensity recommended by the standard was used to determine the box's length. The standard suggested the intensity should be 0.89 W/(m2·nm) at the specimen's surface. The actual wattage intensity recorded at the specimen's surface, however, was between 0.77 and 0.95 W/(m2·nm). A wattage meter (Fig. 3a) was used to check the wattage's uniformity. Aluminum foil was used to cover the interior surface of the chamber so that the UV light would be reflected onto the specimens. The ASTM G154 standard [21] suggested that a spectral UV distribution of UVA 340 lamp be used. A spectral UVA 365 lamp employed in this study due to its market availability. These lamps were purchased from the Worldwide Specialty Lamp (located in Austell, Georgia). Only three UV lamps (see Fig. 3b) placed on each side of the chamber, could provide a reasonable, uniform UV spectrum. These lamps generated a temperature of approximately 167°F (75°C). Therefore, 8 fans (2 on the top and 2 on the bottom of each longitudinal side), each with a diameter of 1.5 in. (38.10 mm), were created to reduce the temperature to 125°F (51.6°C) (see Fig. 3a). A light

timer was used to cycle the UV light so that each cycle consisted of four hours of UV exposure and four hours of condensation (dark period).

A total of 10 coupon specimens (5 representing the facesheets and 5 for the diagonal web core) were used for the aging regimen. The coupons were hung in the middle of the chamber (as illustrated in Fig. 3b) so that they were equally exposed to the UV light from both sides. An ultraviolet test was conducted in accordance with the ASTM G154 standard [21] to simulate the solar radiation effect created by sunlight. The testing cycles were in accordance with the ASTM D2508 standard [22]. Each coupon was run through a tension test in accordance with the ASTM D3039/D3039 standard [19] after the predetermined conditioning time was reached. The results were then compared to those taken from the control specimens to evaluate whether or not exposure to the UV environment would reduce the effectiveness of the conditioned specimens.

2.2.2. Deicing solution

Deicing salts are used on bridges during the winter months to reduce traffic accidents, injuries, and fatalities. The deicing chemicals may have adverse effects on the fibers (e.g., a degradation of stiffness and strength). Therefore, the influence of sodium chloride (NaCl) on the behavior of GFRP/PU materials was investigated. This investigation was conducted on two solutions. One tank contained a solution that was maintained at room temperature, and another one contained a solution that was kept at 122°F (50°C)to accelerate the absorption (see Figs. 4a and 4b). This temperature was below the glass transition temperature (Tg) of the polyurethane resin to avoid any degradation mechanism that may occur at that point. Each tank accommodated 8 coupon specimens (4 for the

facesheet and 4 for the diagonal web core) that were immersed in a sodium chloride solution. The deicer solution was comprised of 3% by weight sodium chloride. Conditioning was maintained for 90 days. The coupons were then subjected to tensile tests. These results were compared to those taken from the control specimens to evaluate whether or not the deicing solution reduced the effectiveness of the conditioned specimens.

2.2.3. Thermal cycling

The thermal cycling conditioning, in terms of a series of freeze-thaw, mid-high temperatures, and mid-high relative humidity cycles, was designed to simulate in-situ environments. ASTM C666 standard [23] was followed for the conditioning cycling test. This standard was originally designed for testing the durability of concrete; it was used here as a guide for measuring the durability of composite structures. The computer-controlled environmental chamber used in this study (Model WR-1750) was manufactured by B-M-A, Inc. It is pictured in Fig. 5. It had a temperature range of between 180°F (82.2°C) and -30°F (-34.4°C) and an extensive range of cycling capabilities. The environmental cycle regimen that was used to cycle both temperature and humidity is illustrated in Table 1. This regimen was based on weather data accumulated in the Midwest United States over the previous 30 years [24].

The conditioning procedure used was comprised of three main phases (see Table 1):

1. 50-cycle freeze-thaw phase
2. 50-cycle mid-high temperature phase
3. 150-cycle mid-high relative humidity phase

These phases were used to simulate the effects of the winter and summer seasons. The minimum temperature reached in the freeze-thaw cycles was -4°F (-20°C) while the maximum temperature reached in the high temperature cycles was 122°F (50°C). The maximum relative humidity was 95%. Approximately 5 cycles per day were accomplished with 30 minutes of ramp time and 2 hours of hold time for each temperature ring, totaling 73 days required to complete the test exposure. Once all of the phases had been run, the specimens were evaluated based on visual inspection, flexural stiffness, strength, and failure modes, compared to the unconditioned specimens.

2.3.   *PU sandwich panel characterization*

The PU sandwich panels investigated in this study were also manufactured in the Composite Manufacturing Laboratory of the Mechanical and Aerospace Engineering Department at Missouri University of Science and Technology. A schematic of the PU mid-scale sandwich panel cross section is given in Fig. 6. Both the top and the bottom facesheets were constructed with three plies of 0°/90°, biaxial, E-glass, plain weave, woven fabric (WR18/3010); they were manufactured by Owens Corning. The diagonal webs, manufactured by VectorPly, consisted of three plies of +45°/-45°, double-bias, E-glass, stitch-bonded fabric (EBXM1715) that was integrated with the facesheets. The foam was matted with two plies of +45°/-45°, E-glass, knitted fabric to enhance bonding between the foam core and the plies.

The VARTM process was used to manufacture the PU sandwich panels. The mid-scale panels used a two-part, thermoset polyurethane resin system that was manufactured by Bayer MaterialScience. A photograph of one of the panels undergoing the VARTM

manufacturing process is given in Fig. 7. The specimens were post-cured for 1 hour at

160ºF (71.1ºC) and for 4 hours at 180ºF (82.2ºC) in a walk-in oven. A total of four mid-

scale panels were manufactured with the cross-section (see Fig. 6). Each had an overall

length of 47 in. (1193.80 mm). Two of the panels were subjected to a predetermined

sequence of thermal cycling conditioning while the remaining panels was designated as the

control panels. A photograph of the four mid-scale PU sandwich panels is given in Fig. 1.

2.3.1. *Test procedure and conditioning regimen*

Prior to the conditioning of the PU sandwich panel specimens in the environmental

chamber, the specimens were prepared by protecting their ends with supplemental epoxy

coating and waterproof tape (see Fig. 8). This step was necessary because the actual bridge

deck panels would completely encapsulate the foam core. The actual weight and

dimensions of the specimens were taken before the environmental exposure was begun.

The panels were elevated within the environmental chamber to allow air circulation on all

sides (see Fig.8). The panels were removed, thoroughly inspected for signs of damage,

instrumented with strain gauges, and then placed into the static loading test setup after the

required number of days within the chamber was accomplished. The examination included

a comparison between the flexural strength, stiffness, and failure mode of the conditioned

specimens and the control specimens.

2.3.2. *Four-point bending flexural test*

Characterization of the durability behavior of the PU sandwich panels was

accomplished by testing the PU sandwich panels under the four-point bending tests. A

picture of the test-setup is illustrated in Figs. 9 and 10. This test was performed according

to the ASTM C393 standard [25]. The objective of this test was to determine the flexural stiffness and the strength of the panels. Each panel was tested in one-way bending with a span of 43 in. (1092.20 mm), under two equal point loads applied at 15.5 in. (393.70 mm) from each support, as depicted in Fig. 10. An MTS880 testing machine was used to load the specimen up to failure at a load rate of 0.05 in/min (1.27 mm/min).

Four strain gauges monitored the strain; two each were attached in the compression and tension areas at the specimen's mid-span. Eight direct current variable transformers (DCVTs), two at the mid-span, two at each loading point, and one at each end were used to monitor displacement at five locations.

3. Experimental results

3.1. Tensile testing results

Figures 11 and 12 compare the average ultimate tensile strength and tensile modulus of elasticity between the control facesheet specimens and the coupon specimens subjected to ultraviolet radiation, deicing solution at both room temperature and elevated temperature, and thermal cycling, while Figs. 13 and 14 compare the average ultimate tensile strength and tensile modulus of the specimens taken from web layers. The black bar shown in each figure represents the standard deviation of the results. These variations in results can be attributed to the quality of laminate manufacture (e.g., percentage of voids and resin-rich areas). A summary of the results is presented in Tables 2-5.

The average results of tensile strength of the control facesheet and web layer coupons were 37.1 ksi (255.8 MPa) and 25.8 ksi (177.9 MPa), respectively, as illustrated in Figs. 11 and 13, while the tensile modulus of elasticity of the control facesheet and web

layer coupons was 2,030 ksi (14.0 GPa) and 1,691 ksi (11.7 GPa), respectively (Figs. 12 and 14). All of the facesheet and web core coupons ruptured suddenly in the fiber direction (0° for the facesheet and 45° for the web core). (see Fig. 15). The failure pattern was consistent for all GFRP coupon specimens, both with and without environmental conditioning.

A set of coupon specimens was tested under tensile strength after they were conditioned in ultraviolet radiation for 2000 hours. The results gathered from this test are illustrated in Figs. 11-14. A visual inspection revealed that a surface gloss loss and a yellowing of the coupon specimens had occurred (see Fig. 16). Polymers that contain styrene crosslinks are particularly prone to the yellowing phenomena. The average weight of the conditioned facesheet and the web layer coupon specimens was reduced by 0.86% and 0.63%, respectively, due to the loss of resin from the outer surface. The fibers, however, were not visible. The average results of the facesheet coupons indicated that the tensile strength was 37.3 ksi (257.2 MPa), and the tensile modulus of elasticity was 2,261 ksi (15.6 GPa) (Figs. 11 and 12). The average results of the web core coupons showed that the tensile strength and tensile modulus of elasticity were 27.4 ksi (188.9 MPa) and 1,839.8 ksi (12.7 GPa), respectively, as illustrated in Figs. 13 and 14. The residual tensile strength and residual tensile modulus of elasticity, when compared to the results collected from the control facesheet coupon specimens, was approximately 100.5% and 111.4%, respectively, while the residual tensile strength and residual tensile modulus of elasticity of the web core coupons were approximately 106.2% and 108.8%, respectively.

Another set of coupon specimens was tested after they were conditioned in a deicing solution at room temperature. A visual inspection did not reveal any change in the

specimen's surface. The average weight of the conditioned facesheet and the web layer coupon specimens was increased by approximately 0.50% and 0.40%, respectively, due to solution absorption (also known as plasticization). The average results of the facesheet coupons showed that the tensile strength and tensile modulus of elasticity (Figs. 11 and 12) were 31.6 ksi (217.9 MPa) and 1,949.6 ksi (13.4 GPa), respectively, while the average results of the ultimate tensile strength and tensile modulus of elasticity of the web core coupons were 21.5 ksi (148.2 MPa) and 1,360.7 ksi (9.4 GPa), respectively (Figs. 13 and 14). The residual tensile strength, when compared with the facesheet coupon results, was approximately 85.2% while the residual tensile modulus was approximately 96%. The residual tensile strength and residual tensile modulus of elasticity of the web core coupons were approximately 83.3% and 80.5%.

A series of coupon specimens was also conditioned in a deicing solution at an elevated temperature of 122°F (50°C). They were then tested under tension. This regimen did not affect the specimens' appearance when compared to the control specimens. The average weight of the conditioned facesheet and web layer coupon specimens was increased by approximately 1.21% and 0.99%, respectively, due to solution absorption. It should be noted here that the elevated temperature helped accelerate absorption. The results of web core coupons were missed during the test due to a problem that occurred in the data acquisition. The average results taken from the facesheet coupons revealed that the tensile strength was 31.3 ksi (215.8 MPa) and the tensile modulus of elasticity was 1,738.6 ksi (11.9 GPa), as shown in Figs. 11 and 12, respectively. Comparison of the results with the control coupon specimens showed that the residual tensile strength was approximately 84.4%, while the residual tensile modulus was approximately 85.6%.

Finally, a set of coupons was conditioned under a series of freeze-thaw, mid-high temperatures, and mid-high relative humidity cycles in a computer-controlled environmental chamber for 350 cycles (1,752 hours). Unfortunately, the results for the web core coupons were lost during the test. The average results for the facesheet coupons indicated that the tensile strength of 34.9 ksi (240.6 MPa) and a tensile modulus of elasticity of 2,040 ksi (14.0 GPa) (see Figs. 11 and 12). Comparing the results with the control coupon specimens showed that the residual tensile strength was approximately 94%, while the residual tensile modulus was approximately 100.5%.

3.2.   *Four-point bending flexural testing results*

The PU sandwich panels were removed and thoroughly inspected for signs of damage after they had been in the chamber for the required number of days. A visual inspection revealed that the outer surface had lost some of its brightness. The sectional dimensions of each conditioned panel did not change when compared to their original dimensions. The weight, however, did increase by approximately 0.5%. The PU panels were then instrumented with strain gauges and placed into the static loading test setup (Figs. 9 and 10). The applied load versus the mid-span deflection of both the conditioned and the control PU sandwich panels is illustrated in Fig. 17. All of the panels exhibited nearly the same tendency; they behaved almost linearly up to failure. The control and the conditioned PU panels failed at an average load of approximately 17.8 kips (79.2 kN) and 13.5 kips (60.1 kN), at a mid-span deflection of approximately 1.01 in. (25.65 mm) and 0.69 in. (17.53 mm), respectively. Accordingly, the average ultimate load of the environmentally conditioned PU panels indicated a noticeable decrease in static flexural strength by approximately 24 % compared to the control PU panels. In addition, the

average stiffness exhibited by both of the conditioned PU panels was approximately 11%

higher than that exhibited by the control PU panels. These results are summarized in Table

6.

Failure of the two control panels occurred by two failure phases: an initial failure

mode that occurred by the outward skin wrinkling on the top facesheet (see Fig. 18a),

followed by an ultimate failure mode that occurred due to excessive compressive stresses

in the top facesheet under the loading points, as depicted in Fig. 18b. In the case of the

conditioned PU panels, they failed under excessive compressive stresses in the top

facesheet under the loading points, as depicted in Fig. 19. Outward skin wrinkling did not

occur compared to the control panels, as the static flexural load that causes wrinkling was

not reached due to the load reduction (see Fig. 20).

The strain gauges that were bonded to the bottom and top faces at the mid-span of

the panels were measured to test the curve's linearity. The load versus strain curves for

both the control and the conditioned PU sandwich panels are illustrated in Fig. 20. The

average maximum tensile strain recorded (bottom facesheet) for the control PU panels was

0.00907 in./in. (mm/mm) at an average load of approximately 17.8 kips (79.2 kN) and that

for the environmentally conditioned PU panels it was approximately 0.006782 in./in.

(mm/mm). Thus, the strain was reduced by nearly 25%. The wrinkling phenomena that

occurred in the control PU panels can be observed in the response of the top strain gauge's

curve (see Fig. 20). The reading exhibited both nonlinearity and a reversal of direction

before it reached the ultimate load. The top strain gauge readings in the environmentally

conditioned PU panels had a linear response up to failure, confirming the previous

observation that outward skin wrinkling did not occur.

4. Discussion and summary of results

4.1. GFRP laminates

Ultraviolet radiation increased both the ultimate tensile strength and the tensile modulus of elasticity for both the facesheet and the web core coupons by approximately 103% and 110%, respectively. This increase is assumed to be due to the post-curing of the resin when exposed to elevated temperatures. For example, exposure to an elevated temperature can facilitate the linking of these polymers, causing additional curing. Manufactured civil composites are seldom fully cured. Thus, thermal exposure does not always harm the FRP composites as long as the temperature is below the Tg of the matrix.

The deicing solution under a room temperature and under an elevated temperature adversely affected the ultimate tensile strength and tensile modulus of elasticity of both the facesheet and the web core coupons. The average degradation was approximately 16% in the tensile strength and 12% in the tensile modulus of elasticity for both the facesheet and web core coupons. This reduction can be attributed to the high percentage of voids, which can be easily seen by the naked eye. These voids increased the permeability and subsequent diffusion of light atomic weight free salt ions into the GFRP composite, causing differential swelling stresses and degradation to the physical properties of the fiber. This result suggests that quality control during the manufacturing process not only controls the strength of the composites, but also affects their resistance to environmental effects. Moisture has also been shown to act as a plasticizer in cured thermosets by causing the polymer to swell. This swelling can lead to increased internal stresses and micro-cracking in the composite. Moisture may also have deleterious effects to the matrix-fiber interface. Reduction under

an elevated temperature, in the deicing solution, was close to the aging regimen at room temperature (within the normal scatter). Although the purpose of using a higher temperature was to accelerate absorption, the high temperature seemed to post-cure the polymer, which downplayed the effect of the deicing solution on the exposed coupons.

The thermal cycling conditioning reduced the ultimate tensile strength and increased the tensile modulus of elasticity for the facesheet coupon specimens by approximately 6% and 0.5%, respectively. This increase was likely a result of post-curing of the resin during the high temperature cycles. The strength reduction could be related to the freeze-thaw cycles. Due to the mismatch of the coefficient of thermal expansion (CTE), microcracks and voids in the polymer matrix occurred, causing progressive damage within the fiber materials due to the expansion and contraction cycles (thermal fatigue) of the entrapped water.

4.2. *PU sandwich panels*

The stiffness of the thermal cycling conditioned PU sandwich panels was increased by between 8 and 14%. This increase is likely due to the extended curing of the polyurethane resin during high temperature sequences. It was assumed that the elevated temperatures could enhance the curing of the resin because it is common that the GFRP composites are not fully cured (due to insufficient time). Thus, exposure to elevated temperatures that is higher than the curing temperature can facilitate the linking of these polymers, causing additional curing. This additional curing will increase the stiffness of the GFRP material.

In contrast, the thermal cycling (freeze-thaw) conditioning regimen negatively affected the material property of the fibers in terms of its flexural strength. This loss of strength (24%) could be related to the freeze-thaw cycles. Due to the mismatch of the coefficient of thermal expansion (the polymeric resin coefficient is generally an order of magnitude higher than that of the fiber), microcraks and voids in the polymer matrix and in the matrix-fiber interface occurred, causing progressive damage within the fiber materials due to the expansion and contraction cycles (thermal fatigue) of the entrapped water. This reduction is consistent with the FHWA guidelines on composite deck designs. These guidelines recommend an environmental durability factor of 0.65 to account for the degradation of properties over time, and represents a 35% decrease in strength.

It should be noted that the same trends exhibited in testing the conditioned GFRP coupon specimens are reiterated by the results of the mid-scale PU panels testing, where the strength was reduced and stiffness was increased. It is expected that web core coupons would behave in the same manner, thereby bringing the total reduction to 24%. Yet again, the design of FRP bridge deck panels is often controlled by stiffness rather than strength. Therefore, such structures tend to be designed as small as 10-15% of their ultimate strength [26].

5. Conclusion

The effects of environmental conditioning on the behavior of both GFRP laminates and PU sandwich panels were investigated in this study. Different conditioning regimens were used to examine the behavior of each specimen. Tensile strength tests and four-point loading tests were then performed on the GFRP laminates and the PU sandwich panels,

respectively. The degradation was determined in terms of ultimate strength and stiffness. The following conclusions were drawn from this study:

- The PU sandwich panels displayed linear-elastic behavior throughout the majority of their response during the static flexural testing, with only a slight decrease in stiffness near failure.

- Neither the tensile strength nor the tensile modulus were adversely affected when the facesheet and web core coupons were exposed to ultraviolet radiation. Instead, each increased as a result of the post-curing of the resin system.

- The deicing solution, under both room temperature and elevated temperature, reduced the ultimate tensile strength and the tensile modulus of elasticity in both the facesheet and the web core coupons.

- Thermal cycling conditioning reduced the ultimate tensile strength and increased the tensile modulus of elasticity for the facesheet coupon specimens by approximately 6% and 0.5%, respectively.

- The flexural behavior of the PU sandwich panels exposed to thermal cycling in an environmental chamber resulted in a 24% degradation in the ultimate strength but a slight increase in stiffness. Failure of the conditioned panels under the subsequent static loading occurred in the same manner as the control panels.

- The strength reduction is consistent with the FHWA guidelines on composite deck design, which recommends an environmental durability factor of 0.65 to account for degradation of properties over time and represents a 35 percent decrease in strength.

This study demonstrated comprehensive durability testing for the new polyurethane foam-infill bridge deck panels (PU sandwich panels) under four environmental conditions. As with most FRP deck panels, stiffness is always control their design. This study showed that the only degradation that occurred for tensile modulus of elasticity of the GFRP coupons was due to the effects of the deicing solution. This reduction was mainly attributed due to the high percentage of voids. It is believed that this reduction would be overcome or reduced if the quality control during the manufacturing process is improved. Generally, the expected in-service stress levels in the PU panel maintain the potential for long-term durability.

Acknowledgments

References

[1]   Kirk RS, Mallett WJ. Highway bridge conditions: Issues for congress. Congressional Research Service, report to congress. Contract No. R43103, 2013.

[2]   Ellis Z. Corrosion cost and preventive strategies in the united states", FHWA-RD-01-156, 2011.

[3]   Karbhari VM. Durability of composites for civil structural applications. Woodhead Publishing Limited, Cambridge England, 2007.

[4]   Shen CH, Springer GS. Effects of moisture and temperature on the tensile strength of composite materials. Environmental Effects on Composite Materials, G.S. Springer, Ed., Technomic Publication Co. 1981, p. 79.

[5]   Halliwell SM. Weathering of polymers. RAPRA Review Reports. 1984. Vol. 53.

[6]   Giori C, Yamauchi, T. Effects of ultraviolet and electron radiations on graphite-reinforced polysulfone and epoxy resins." Journal of Applied Polymer Science. 1984. 29, p. 237.

[7]   Caceres A, et al. Salt-fog accelerated testing of glass fiber reinforced polymer composites." DTIC Document 2002.

[8]   Hollaway LC. A review of the present and future utilisation of FRP composites in the civil infrastructure with reference to their important in-service properties. Construction and Building Materials, 2010. Vol. 24, No. 12, pp. 2419-2445.

[9]   Karbhari VM, Pope G. effect of cold region type environment on impact and flexure properties of glass/vinyelester composites. ASCE Journal of Cold Regions Engineering, 1993. 8(1), 1-20.

[10]   GangaRao HVS, Vijay PV, Dutta PK). Durability of composites in infrastructure. Proceedings of Corrosion, 1995. Paper No. 550, pp. 1-8.

[11]   Lapoez-Anido R, Michael AP, Sandford TC. Freeze–thaw resistance of fiber-reinforced polymer composites adhesive bonds with underwater curing epoxy. Journal of Materials in civil engineering, 2004.

[12]   Verghese NE, Hayes M, Garcia K, Carrier C, Wood J, Lesko JJ. Effects of temperature sequencing during hygrothermal aging of polymers and polymer matrix composites: the reverse thermal effect. Fiber Composites in Infrastructure, Proceedings of the Second International Conference on Fiber Composites in Infrastructure ICCI'98. 1998, 2, 720-739.

[13]   Jamond RM, Hoffard TA, Novinson T, Malvar LJ. Composites in simulated marine environments. NFESC Special Publication, 2000. SP-2083-SHR.

[14]   Malvar LJ, Jamond RM, Hoffard TA, Novinson T. GFRP composites in simulated marine environments. 2nd International Conference on Durability of FRP Composites for Construction, CDCC'02, Montreal, Quebec, Canada, 2002. pp. 191-202.

[15]   Connolly M, King J, Shidaker T, Duncan A. Processing and characterization of pultruded polyurethane composites. Huntsman Enriching lives through innovation, 2006.

[16]   Karakuzu R, Erbil E, Aktas M. impact characterization of glass/epoxy composite plates: an experimental and numerical study. Composite Part-B, 2010. 41: 388-395.

[17]   Bareis D, Heberer D, Connolly M. Advances in urethane composites resins with tunable reaction times. American Composites Manufacturers Association Ft. Lauderdale, Florida. Huntsman Polyurethanes Auburn Hills, MI. 2011: 1-7.

[18]   Tuwair H, Volz J, ElGawady M, Mohamed M, Chandrashekhara K, Birman V. Testing and evaluation of GFRP sandwich bridge deck panels filled with polyurethane foam. American Society for Composites 29th Technical Conference and 16th US-Japan Conference and ASTM D30 Meeting, Sand Diego, California, Sept. 2014.

[19]   American Society of Testing and Materials. ASTM standard test method for tensile properties of polymer matrix composite materials (ASTM D3039/D3039M-08). West Conshohocken, Pennsylvania: ASTM International, 2008.

[20]   American Society of Testing and Materials. ASTM standard practice for exposing nonmetallic materials in accelerated test devices that use laboratory light sources (G151-10). West Conshohocken, Pennsylvania: ASTM International, 2010.

[21]   American Society of Testing and Materials. ASTM standard test method for standard practice for operating fluorescent light apparatus for UV exposure of nonmetallic materials (G154-00a). West Conshohocken, Pennsylvania: ASTM International, 2010.

[22]   American Society of Testing and Materials. ASTM standard test method for standard practice for fluorescent ultraviolet (UV) exposure of photodegradable plastics (D2508-14). West Conshohocken, Pennsylvania: ASTM International, 2014.

[23]   American Society of Testing and Materials. ASTM standard test method for resistance of concrete to rapid freezing and thawing (C666/C666M-08)." West Conshohocken, Pennsylvania: ASTM International, 2008.

[24]   Micelli F, Myers J. Durability of FRP-confined concrete." Proceedings of the institution of Civil Engineers. 2008: 161(4): 173-185.

[25]   American Society of Testing and Materials. ASTM standard test method for flexural properties of sandwich constructions (C393/C393M-11e1). West Conshohocken, Pennsylvania: ASTM International, 2011.

[26]   Karbhari VM, Seible F. Fiber-reinforced polymer composites for civil infrastructure in the USA." Structural Engineering International, 1999. Volume 4.

Table 1. Thermal cycling regimen

Cycles	Freeze-Thaw	Temperature	Relative Humidity (60-95%)		
Temperature Range, ºF (ºC)	-4 (-20) to 50 (10)	68 (20) to 122 (50)	68 (20)	77 (25)	104 (40)
Number of Cycles	50	150	50	50	50
Total Number of Cycles		350			

Table 2. Summary of facesheet coupons' tensile strength results

Tensile Strength	Control	Ultraviolet Effect	De-icing Effect	Heated Deicing Effect	Thermal Cycling Effect
Mean, ksi	37.1	37.3	31.6	31.3	34.9
(MPa)	(255.8)	(257.2)	(217.9)	(215.8)	(240.6)
S.D, ksi	0.89	0.84	2.21	1.32	1.28
(MPa)	(6.1)	(5.8)	(15.2)	(9.1)	(8.8)
C.V (%)	2.41	2.25	7.14	4.23	3.68

*S.D: Standard Deviation

*C.V: Coefficient of Variation

Table 3. Summary of facesheet coupons' modulus of elasticity results

Modulus of Elasticity	Control	Ultraviolet Effect	De-icing Effect	Heated Deicing Effect	Thermal Cycling Effect
Mean, ksi	2,030	2,261	1,950	1,739	2,040
(GPa)	(14.0)	(15.6)	(13.4)	(11.9)	(14.0)
S.D, ksi	15.63	120.30	158.50	120.48 (0.83)	97.51
(GPa)	(0.11)	(0.83)	(1.09)		(0.67)
C.V (%)	0.77	5.32	8.13	6.93	4.78

Table 4. Summary of web core coupons' tensile strength results

Tensile Strength	Control	Ultraviolet Effect	Deicing Effect
Mean, ksi	25.8	27.4	21.5
(MPa)	(177.9)	(188.9)	(148.2)
S.D, ksi	0.17	0.61	0.74
(MPa)	(1.2)	(4.2)	(5.1)
C.V (%)	0.65	2.24	3.45

Table 5. Summary of web core coupons' modulus of elasticity results

Modulus of Elasticity	Control	Ultraviolet Effect	Deicing Effect
Mean, ksi	1,691	1,840	1,361
(GPa)	(11.7)	(12.7)	(9.4)
S.D, ksi	121.74	38.13	87.52
(GPa)	(0.84)	(0.26)	(0.60)
C.V (%)	7.20	2.07	6.43

Table 6. Structural behaviors of four-point bending flexural results

Condition	Control Panels			Conditioned Panels		
	Ultimate Load Capacity, kips (kN)	Flexural Stiffness, kip.in^2 (kN.m^2)	Failure Mode	Ultimate Load Capacity, kips (kN)	Flexural Stiffness, kip.in^2 (kN.m^2)	Failure Mode
Mean	17.8 (79.2)	26,221.35 (7,525)	Wrinkling + compressive failure	13.5 (60.0)	29,105.70 (8,353)	Compressive failure
S.D	0.43 (1.91)	748.65 (214.8)		0.10 (0.44)	870.00 (249.6)	
C.V (%)	2.41	2.86		0.74	2.98	

Figure 1. Four prototype mid-scale panels
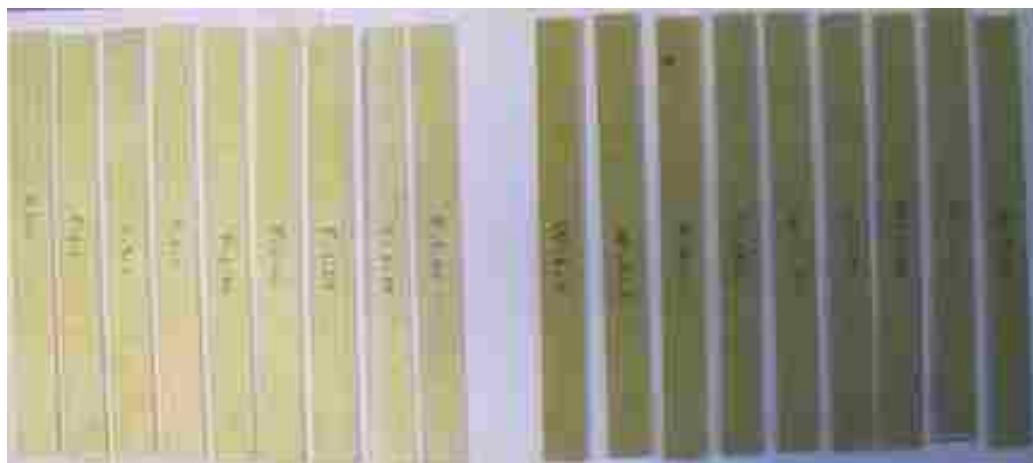
Figure 2. Coupon specimens of GFRP laminates

(a)   (b)
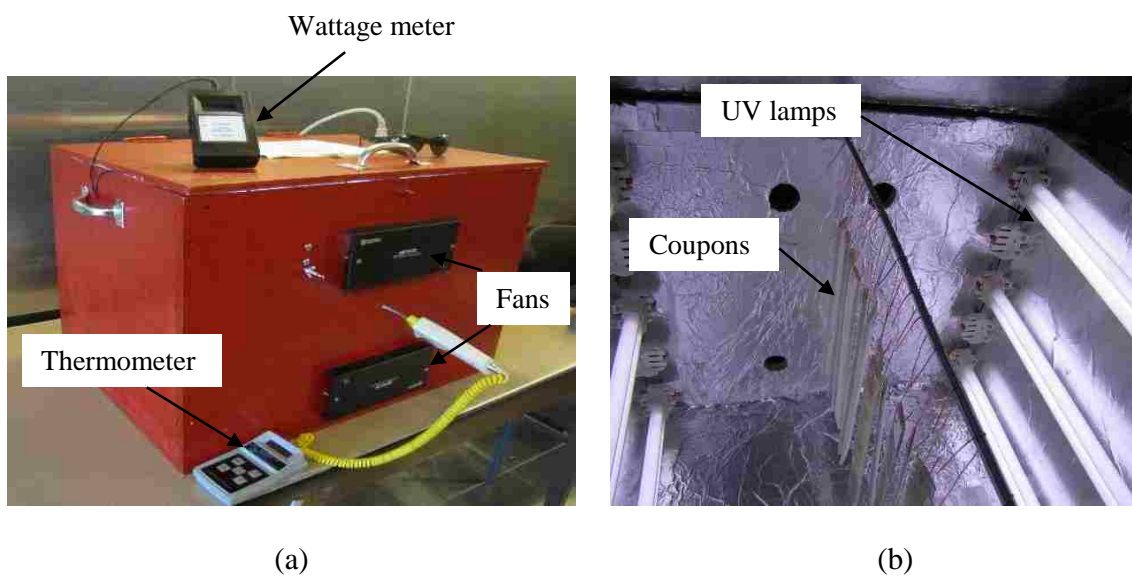
Figure 3. UV chamber: (a) outside view and (b) inside view

(a)   (b)

Figure 4. Deicing exposure: (a) coupon specimens at room temperature and (b) at elevated temperature

Figure 5. Environmental test chamber
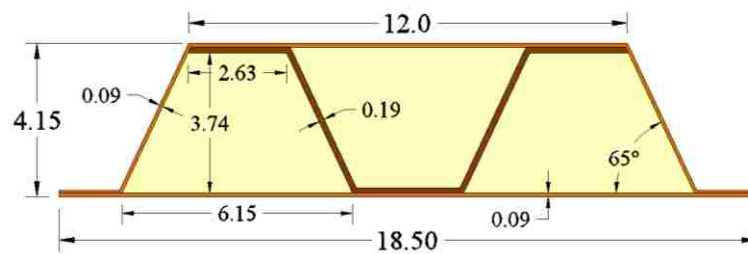
Figure 6. Schematic of mid-scale panel cross section (all dimensions in inches, 1 in. = 25.4 mm)

Figure 7. VARTM manufacturing process for mid-scale panels

Protecting panels' ends

Figure 8. PU sandwich panels within environmental test chamber
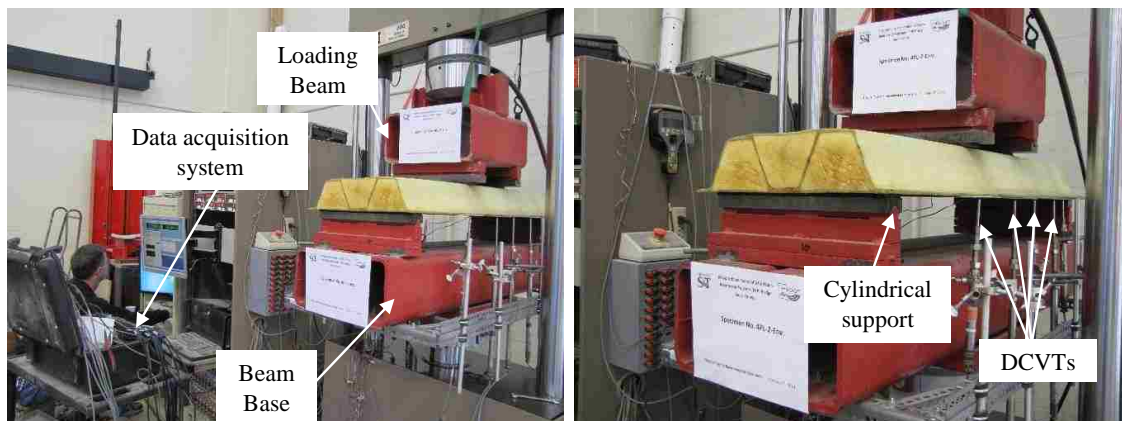
Figure 9. Four-point bending flexural test setup
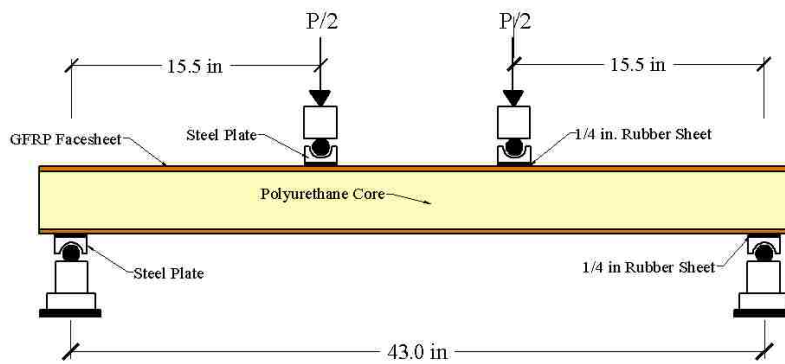
Figure 10. Schematic of four-point bending flexural test setup section (all dimensions in inches, 1 in. = 25.4 mm)
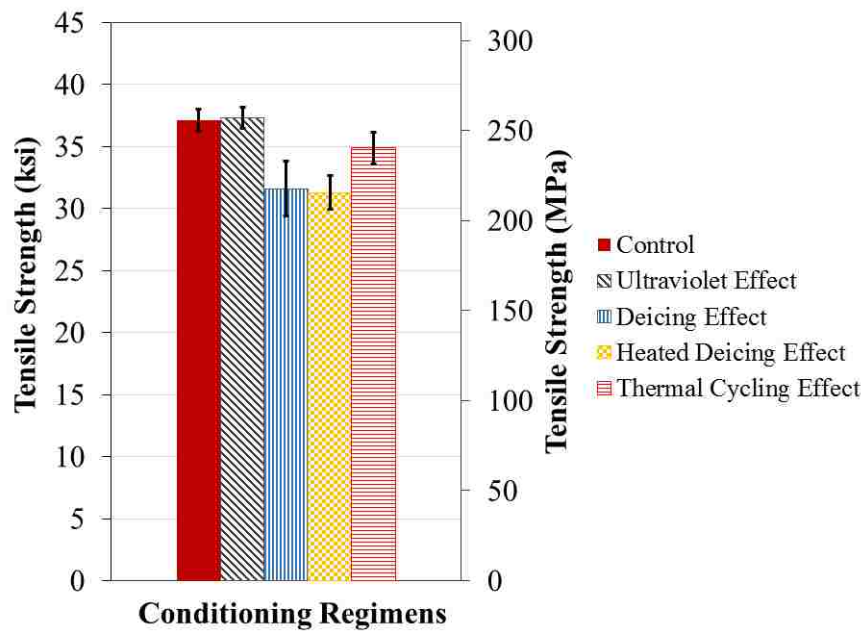
Figure 11. Tensile strength of facesheet coupons under different regimens
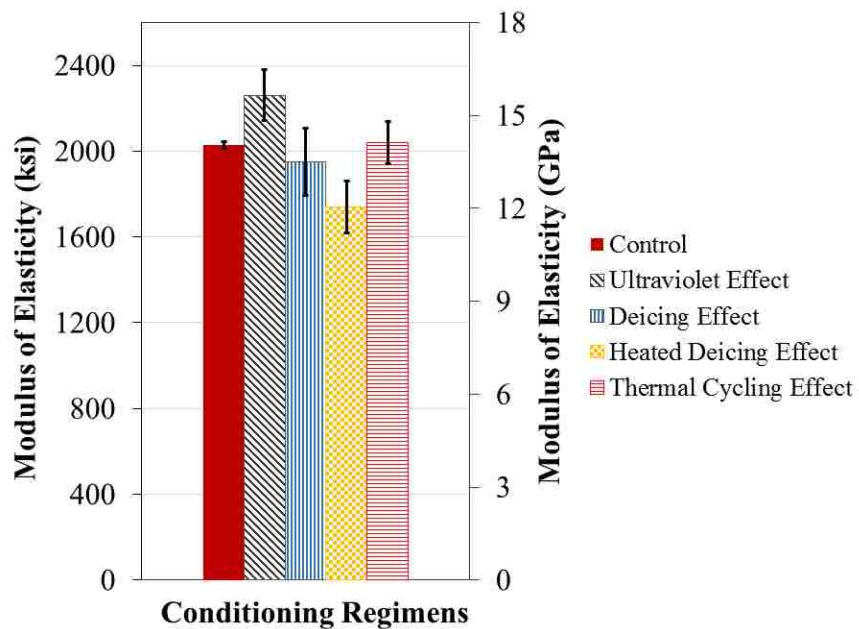
Figure 12. Tensile modulus of elasticity of facesheet coupons under different regimens
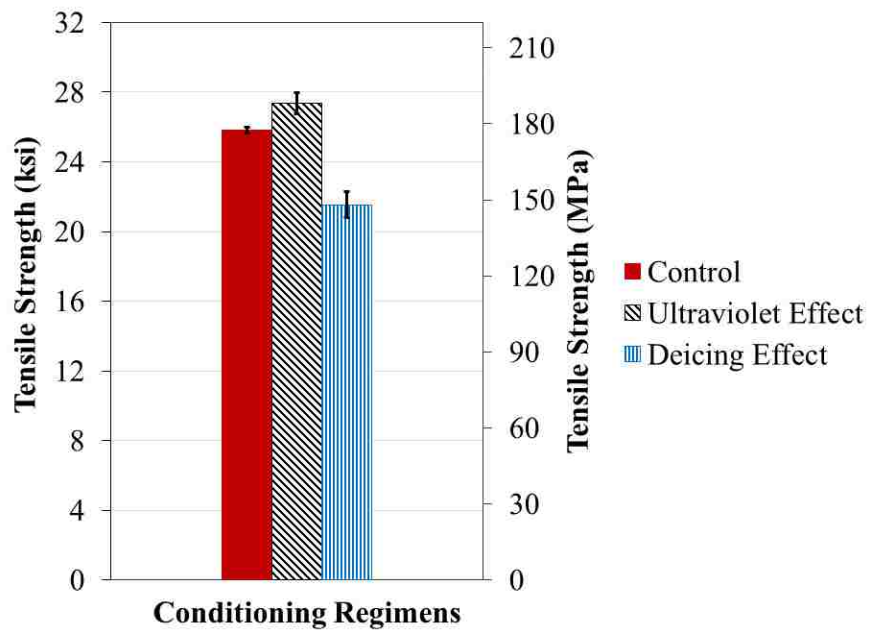
Figure 13. Tensile strength of web coupons under different regimens
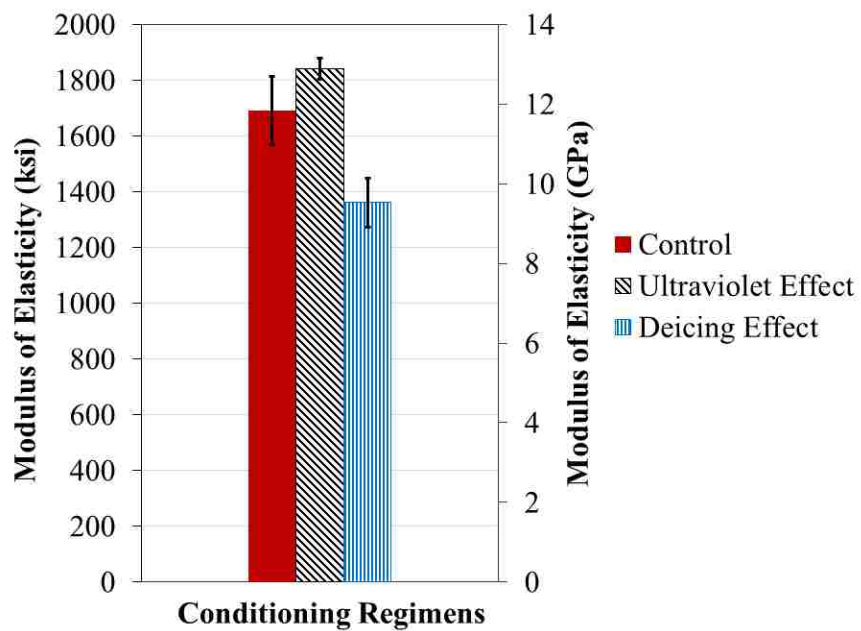
Figure 14. Tensile modulus of elasticity of web coupons under different regimens

(a)   (b)
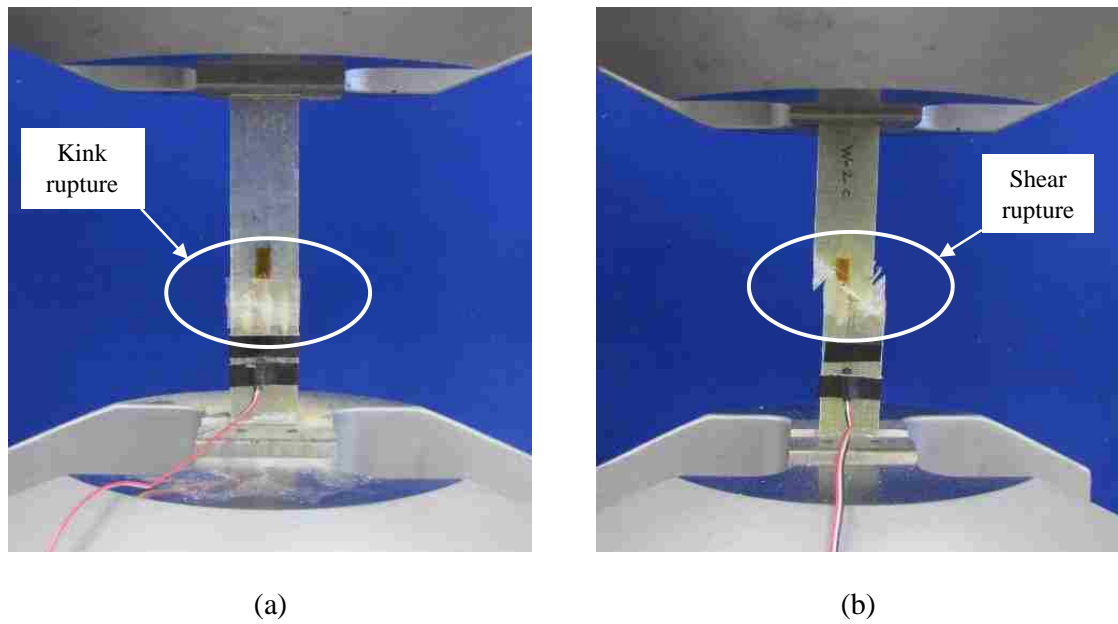
Figure 15. Failure modes: (a) facesheet coupon and (b) web core coupon

Figure 16. Color comparision between the control (left) and UV conditioned (right) specimens
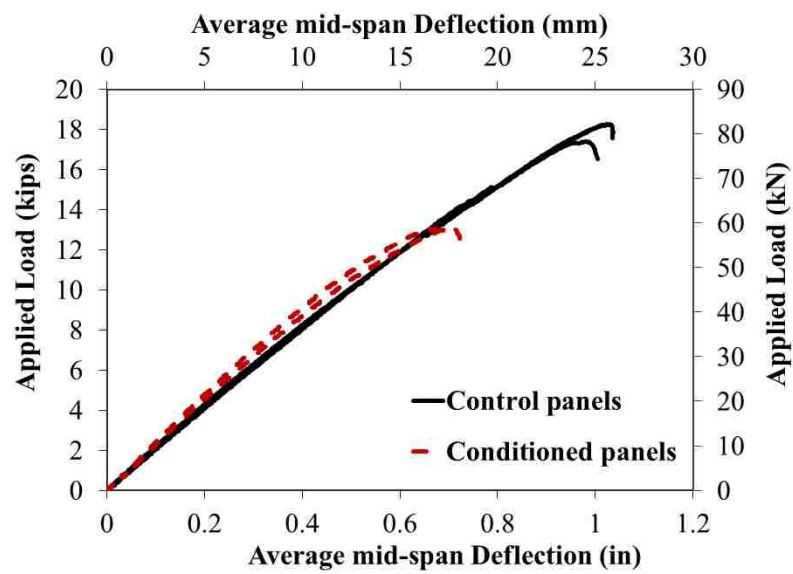
Figure 17. Applied load vs. mid-span deflection

<div style="text-align:center">(a)   (b)</div>

Figure 18. Failure modes: (a) initial failure due to outward compression facing wrinkling and (b) ultimate failure due to compression failure of the facesheet under loading points

Figure 19. Compressive failure of the facesheet under loading points
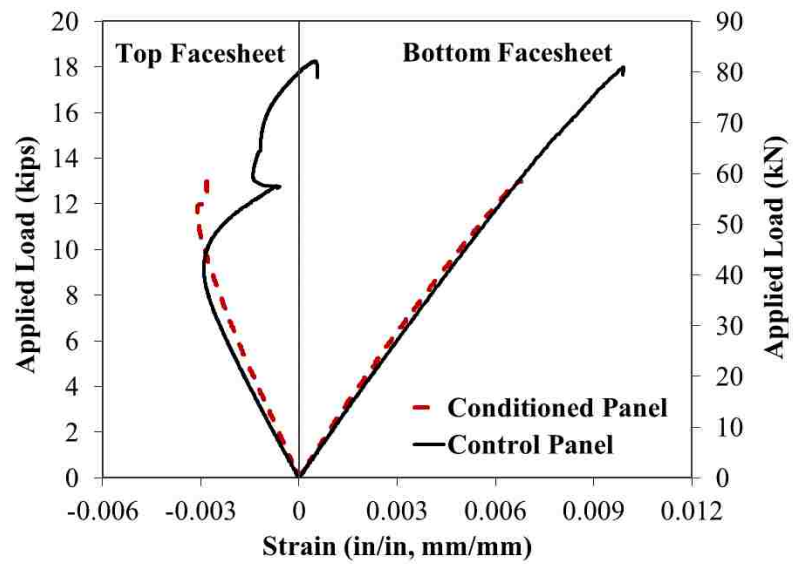
Figure 20. Applied load vs. mid-span strain

SECTION

3. SUMMARY, CONCLUSIONS AND RECOMMENDATIONS

3.1. SUMMARY OF RESEARCH WORK

The purpose of this research was to develop, test, and evaluate fiber-reinforced, polyurethane (PU) foam cores to replace the costly honeycomb construction currently used to manufacture FRP bridge deck panels. The research plan involved four phases.

Three different polyurethane foam configurations were used for the inner core during the study's first phase. These configurations consisted of a high-density polyurethane foam (Type 1), a gridwork of thin, interconnecting, glass fiber/resin webs that formed a bidirectional gridwork in-filled with a low-density polyurethane foam (Type 2), and a trapezoidal-shaped, low-density polyurethane foam that utilized E-glass web layers (Type 3). Several experimental investigations were conducted. Based on the results of this part of study, the Type 3 sandwich panel was recommended to move forward to the second phase of the study.

In the second phase, larger-scale versions of the Type 3, namely "mid-scale panels", were tested both statically and dynamically to verify performance. Analytical models and finite element analysis (FEA) were each conducted during a third phase. Analytical models were used to predict critical facesheet wrinkling that had been observed during phase two. A three-dimensional model using ABAQUS was developed to describe the behavior of Type 3 panels under the effect of the applied loads used in the experimental program. The finite element results were in good agreement when compared to the experimental results. A parametric study was also conducted to further evaluate the effects of the stiffness of the top facesheet fiber layers, the mass density of the polyurethane foam, the presence of web

layers, and the introduction of an overlay above the top facesheet. A flexural beam theory approach was also used to predict the sandwich panel's flexural strength.

The fourth phase of this research investigated the performance of Type 3 panels under exposure to various environmental conditions to duplicate seasonal effects in the Midwest United States. Conclusion and recommendations based on the results are presented in the following sections.

3.2. CONCLUSIONS

The following section summarizes the conclusions from the experimental, modeling, and analytical studies of the FRP/PU foam sandwich beams/panels.

3.2.1. Small-scale FRP/PU Beams. This phase of the study introduced three potential core alternatives for GFRP foam-infill sandwich beams/panels in an attempt to compete with the initial costs of reinforced concrete bridge decks. The structural behaviors of the three proposed types were investigated, and the following conclusions were drawn:

- The behavior of the plain-weave facings under tension exhibited a linear elastic response, while the web layers where the fibers were oriented at $+/-45^o$ behaved nonlinearly. Both the facing and web layers behaved almost linearly under compression.

- All sandwich beams tested in bending exhibited a linear-elastic behavior. This initial response was followed by a reduction in stiffness prior to failure.

- The Type 3 construction exhibited better strength as well as flexural and shear stiffness than either of the other types tested. This is due to the very positive

effect of introducing web layers. In comparison, Type 1 beams had significantly lower flexural and shear stiffness.

- Excellent bond was observed between the polyurethane foam core and the facings in the Type 3 beams.

- The Type 3 beams were less vulnerable to localized effects under a concentrated load compared to the other systems. On the other hand, Types 1 and 2 were quite susceptible to localized effects under concentrated loads, such as inward local bending and wrinkling of the compression facing under the concentrated loads, which resulted in a lower ultimate strength.

- Types 1 and 2 experienced very large deflections associated with significant shear deformation of the core. Type 2, however, was less affected by shear deformation than Type 1. The effect of shear deformation led to a highly nonlinear behavior.

- The ultimate strength of the Type 3 beams was governed by the compressive strength of the top facing under the loading points.

- The proposed Type 3 beam prevented or reduced the facing-core debonding trend that has been observed in conventional sandwich beam construction.

- The proposed FE model can reasonably predict the behavior of Type 3 beams in bending under monotonic loading.

3.2.2. Mid-scale FRP/PU Panels.

3.2.2.1. Experimental testing. This phase of the study included static and fatigue flexural testing in order to evaluate strength, stiffness, overall behavior, and modes of

failure of the mid-scale Type 3 sandwich construction that was selected from the small-scale testing and analysis phase. These mid-scale panels used standard foam segments, had a nominal thickness of 4.0 in., and were manufactured through the VARTM possess. The purpose of this phase of the research study was to verify the performance of the Type 3 sandwich construction in order to determine whether it truly represented a viable bridge deck alternative to reinforced concrete. Based on the results of this study, the following conclusions can be made:

- The behavior of the plain-weave facings under tension exhibited a linear elastic response, while the web layers where the fibers were oriented at $+/-45^{\circ}$ behaved nonlinearly. Both the facing and web layers behaved almost linearly under compression.

- The crushing test provided the ultimate bearing capacity, which occurred due to buckling of the web. The failure load during the four-point loading test was lower than the ultimate bearing capacity. Hence, the buckling in the web core did not occur in the four-point loading test.

- All panels tested in four-point bending exhibited a linear-elastic behavior up to failure. A slight reduction in stiffness due to minor outward skin wrinkling was observed prior to failure. Failure occurred due to local crushing under the applied load.

- Introducing corrugated webs (shear layers) is an effective way to increase both the core shear stiffness and the global flexural stiffness in the longitudinal direction.

- In the static flexural test, the maximum strain readings from the bottom gages of the tested panel indicated that the panel was stressed to 47% of its ultimate capacity as determined from the coupon tests, which is consistent with the outward skin wrinkling failure mode of the top facing. In other words, the skin wrinkling failure mode occurs at a lower stress level than the ultimate capacity.

- The accuracy of the first order shear deformation theory (FSDT) to predict the deflection of the panels was examined leading to the follow observations:

    o The FSDT over-estimated stiffness and under-estimated deflection.

    o The average difference between the measured deflections and the FSDT results ranged from 6 to 13%.

    o Results from the FSDT revealed that the transverse shear contribution to deflection is minimal. The core webs contributed significantly to a decrease in the shear-associated portion of the total deflection.

- After conditioning the sandwich panels to the predetermined fatigue cycles at the stress levels representing 20% and 45% of their ultimate load, it was observed that no degradation occurred in either bending stiffness or strength. However, delamination failure was observed as an additional failure mode in panels experiencing fatigue loading that was not present in the control panels.

- The proposed sandwich panel prevented or reduced the facing-core debonding trend observed in conventional sandwich panel construction.

3.2.2.2. Modeling and analysis. This phase of the study included finite element analysis (FEA) and analytical models of the mid-scale Type 3 sandwich construction. Analytical models were used to predict critical facesheet wrinkling. A 3-D finite element ABAQUS model was developed for the purpose of conducting a parametric study. Flexural beam theory was used to predict the sandwich panel's flexural strength. Based on the results of this study, the following conclusions can be drawn:

- The panel can be treated as a linear-elastic composite up to failure.

- The proposed FE model can reasonably predict the sandwich panel behavior in bending under monotonic loading.

- The ultimate strength obtained from the FEA was 19.4% higher than that obtained from the experimental testing. This difference was due to the asymmetry encountered in the experimental setup. However, the flexural rigidity predicted by modeling was 6.6% lower than that obtained in the experiment.

- Different analytical models were used to estimate outward skin wrinkling, which triggered failure in the experiment. All the models underestimated the facesheet wrinkling stress by 26.7% to 39%. The Hoff and Mautner model was the most accurate one as it accounts for the influence of the transverse shear modulus of the core.

- The following can be concluded from the results of the FE parametric study:

  o Outward skin wrinkling tendency decreased as the number of layers in the top facesheet increased.

- o The foam core characteristics affect the local stress concentration in the compression facesheet. However, the occurrence of wrinkling was local and did not affect the bending stiffness of the different specimens. Finally, since all panels displayed an ultimate limit state of local FRP rupture at the applied load, the existence of the core-foam had insignificant effect on strength.

- o The panel behavior significantly changed when the web layers were removed from the panel. Both the ultimate strength and the flexural rigidity were reduced by approximately 95%. Using a low-density polyurethane foam as a core without webs proved to be insufficient to provide the necessary rigidity, leading to local indentation phenomenon under the loading points. Both the ultimate strength and the flexural rigidity were reduced by approximately 95%. However, adding the external webs in the core, in addition to foam, significantly improved panel capacity.

- o The concrete and asphalt overlay significantly improved the behavior of the panels. The flexural stiffness increased by 125% and 94% for concrete and asphalt, respectively. The overlay layers also significantly reduced outward wrinkling of the top facesheet.

- It can be concluded that a simplified flexural analysis method, based on the principle of strain compatibility and force equilibrium, adequately predicted the panel flexural capacity.

3.2.3. Durability Study. This phase of the study investigated the effects of environmental conditioning on the behavior of both the GFRP laminates and PU sandwich panels. The environmental exposure included different conditioning regimens. The GFRP laminates were exposed to ultraviolet radiation, deicing solution at both room temperature and elevated temperature, and thermal cycling (a series of freeze-thaw, mid-high temperatures, and mid-high relative humidity cycles). The PU sandwich panels were conditioned to a series of freeze-thaw, mid-high temperatures, and mid-high relative humidity cycles in the environmental chamber. Following the exposure regimens, tensile strength tests and four-point loading tests were performed on the GFRP laminates and PU sandwich panels, respectively. The degradation was determined in terms of ultimate strength and stiffness. The following conclusions were drawn from this phase of the study:

- Neither the tensile strength nor the tensile modulus were adversely affected when the facesheet and web core coupons were exposed to ultraviolet radiation. Instead, each increased as a result of the post-curing of the resin system.

- The deicing solution at both room temperature and elevated temperature reduced the ultimate tensile strength and tensile modulus of elasticity of both the facesheet and web core coupons.

- Thermal cycling conditioning reduced the ultimate tensile strength and increased the tensile modulus of elasticity for the facesheet coupon specimens by approximately 6% and 0.5%, respectively.

- The flexural behavior of the PU sandwich panels exposed to thermal cycling in an environmental chamber resulted in a 24% degradation in the ultimate

strength but a slight increase in stiffness. Failure of the conditioned panels under the static loading occurred in the same manner as the control panels.

- The strength reduction is consistent with the FHWA guidelines on composite deck design, which recommends an environmental durability factor of 0.65 to account for degradation of properties over time and represents a 35 percent decrease in strength.

- The only reduction that occurred in the tensile modulus of elasticity of the GFRP coupons was due to the effects of the deicing solution. This reduction was mainly attributed due to the high percentage of specimen voids, which resulted in absorption of the deicing solution.

3.3. RECOMMENDATIONS

Based on the results of this study, the Type 3 panel is the most practical alternative to reinforced concrete bridge decks. Meeting the serviceability requirements of bridge decking will require a larger cross-section, but it will be achievable with reasonable facing and web layers thicknesses, as well as a smaller and more practical panel depth than the other two construction types. Despite the rapid development and achievements made in the course of this research project, a considerable amount of research needs to be undertaken prior to field application of this product.

Based on the conclusions stated in the previous section, future research should be considered as follows:

- Static and fatigue tests on full-scale panels needs to be conducted to simulate actual loading conditions on a bridge.

- The effect of an impact loading needs to be studied to investigate the foam effects on the proposed panel.

- If a concrete overlay is to be added on top of the proposed panels, the composite action either using mechanical connections or adhesive between the two surfaces needs to be investigated. In addition, the alkali effects must be examined.

- In future durability testing, a longer time of durability regimen maybe considered.

- Develop and test panel-to-panel and panel-to-girder connections.

- Issues such as bridge skew, roadway crown, bridge rail attachment, and deck drainage need to be addressed.

- To maintain quality control of the panels, the research team recommends that inspection methods be written into the specifications for FRP deck panels. Typical inspection methods already used in the composites industry include visual inspection, tapping, acoustic emission, thermography, ultrasound, and x-ray radiography.

APPENDIX A

A. PHOTOGRAPHS OF SMALL-SCALE SPECIMENS AND TESTS

This appendix includes different photographs of the small-scale specimens and their tests, including material characterizations, flatwise compressive tests, flatwise tensile tests, three-point flexural tests for short beams, and four-point flexural tests for long beams.

Figure A.1. Material characterization for polyurethane foams and GFRP composites

Figure A.2. Material characterization for GFRP composites under compression and tension tests
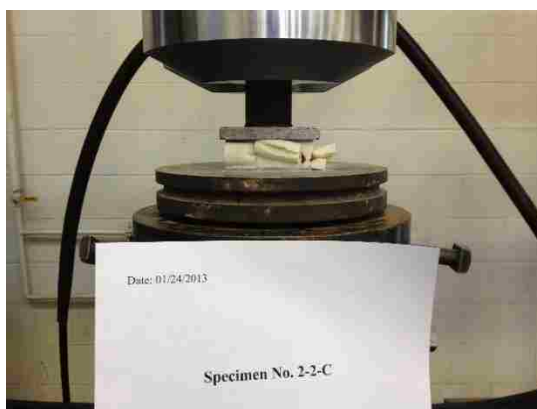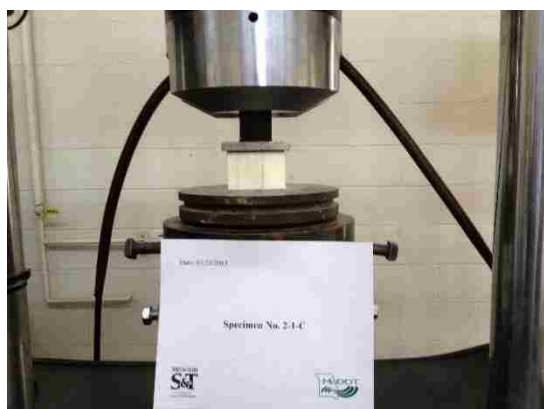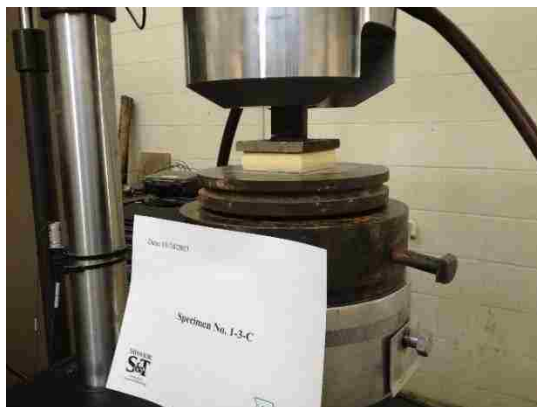
Figure A.3. Flatwise compressive tests for types 1 and 2
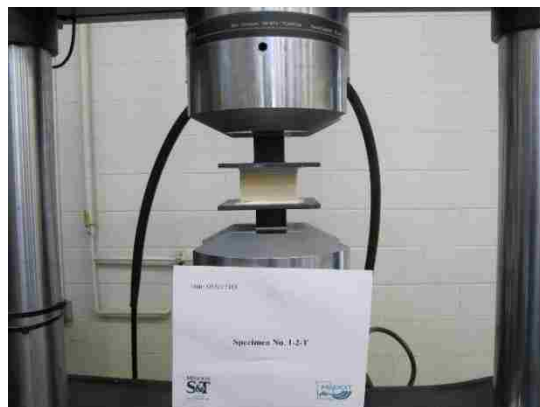
Figure A.4. Flatwise tensile tests for types 1 and 2

Figure A.5. Three-point flexural tests for Type 1 short beams
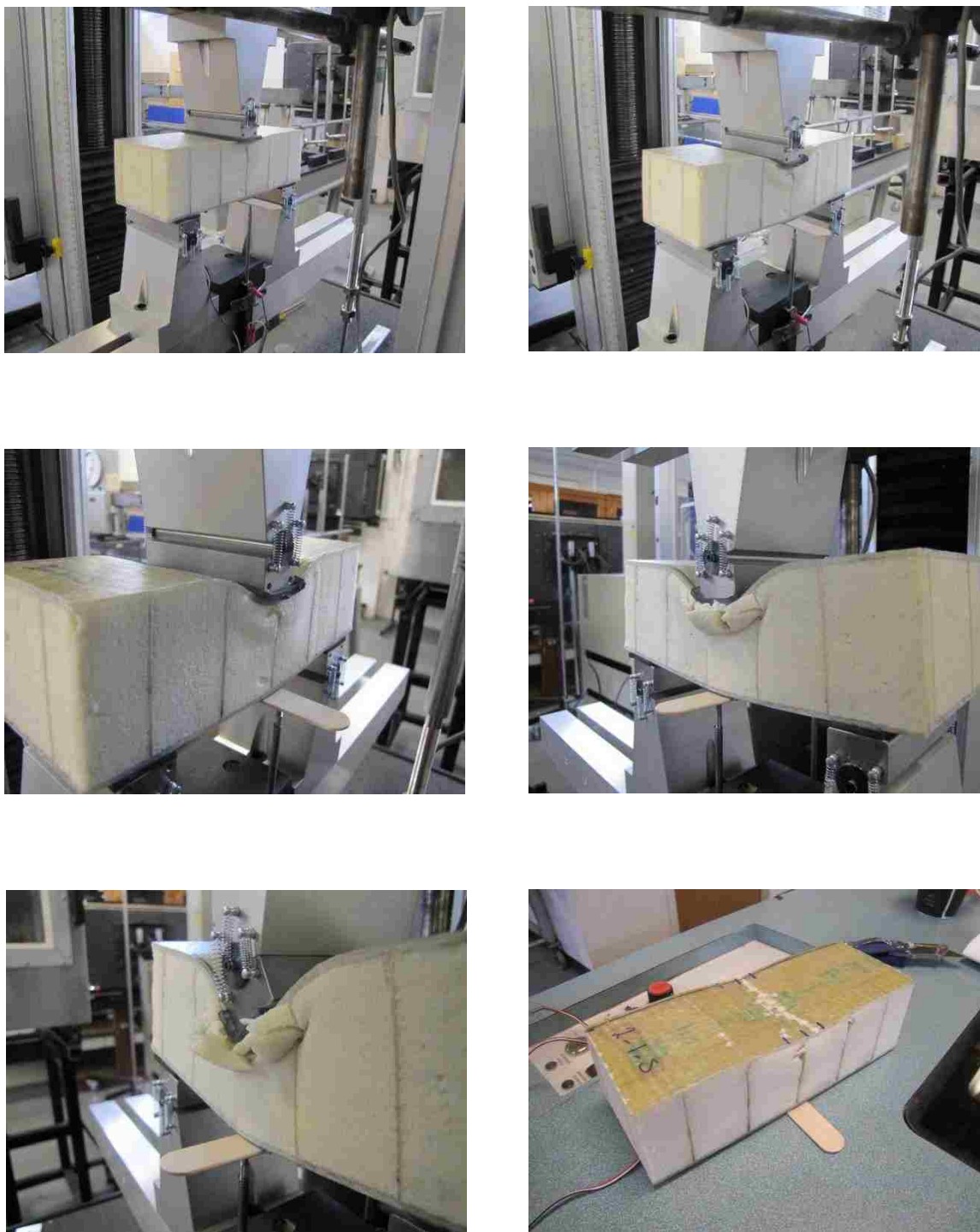
Figure A.6. Three-point flexural tests for Type 2 short beams
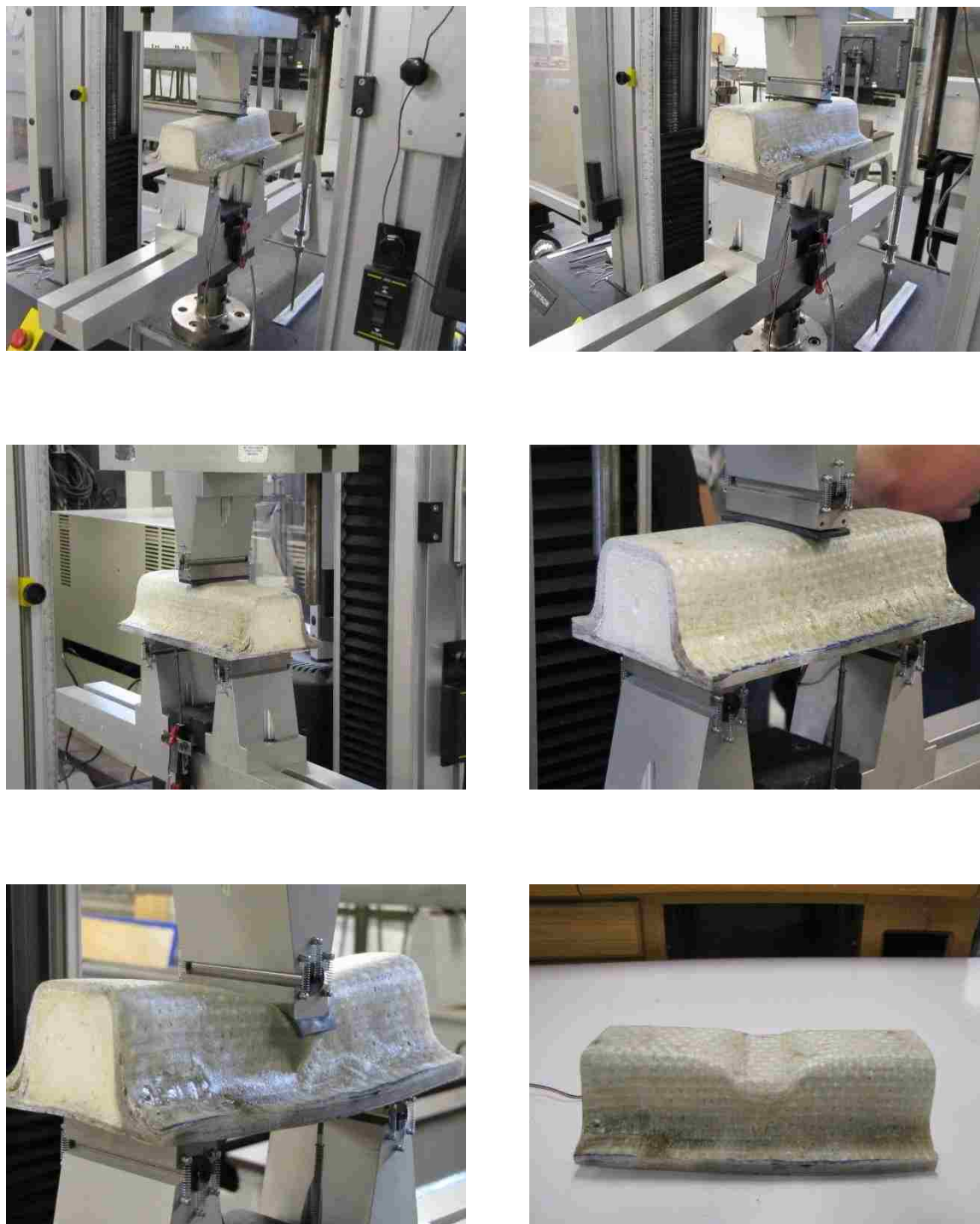
Figure A.7. Three-point flexural tests for Type 3 short beams

Figure A.8. Four-point flexural tests for Type 1 long beams
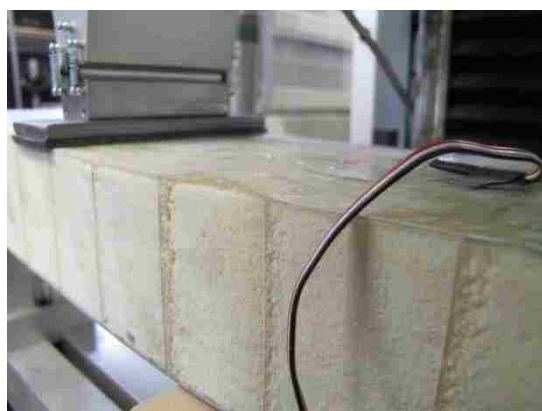
Figure A.9. Four-point flexural tests for Type 2 long beams

Figure A.10. Four-point flexural tests for Type 3 long beams

APPENDIX B

B. SMALL-SCALE TESTING RESULTS

This appendix includes the results of the small-scale tests, including flatwise compressive tests, flatwise tensile tests, three-point flexural tests for short beams, and four-point flexural tests for long beams.

FLATWISE COMPRESSIVE TEST RESULTS
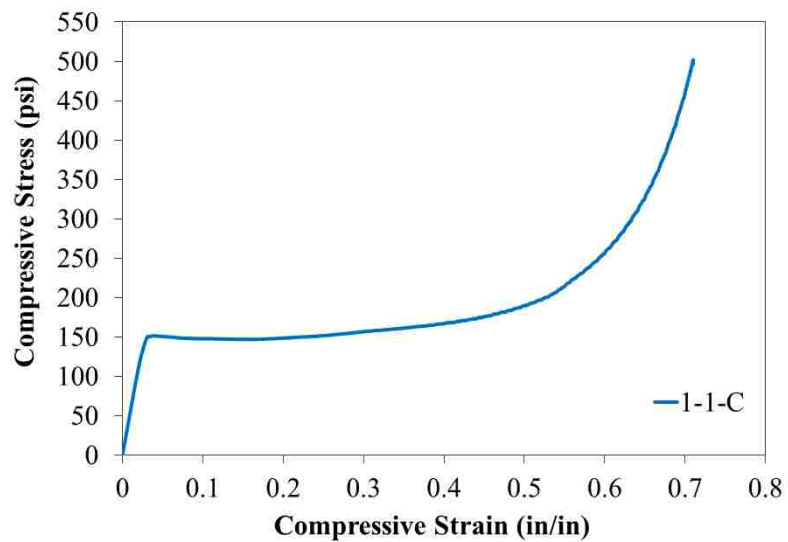
Figure B.1. Compressive stress vs. strain for Type 1 core
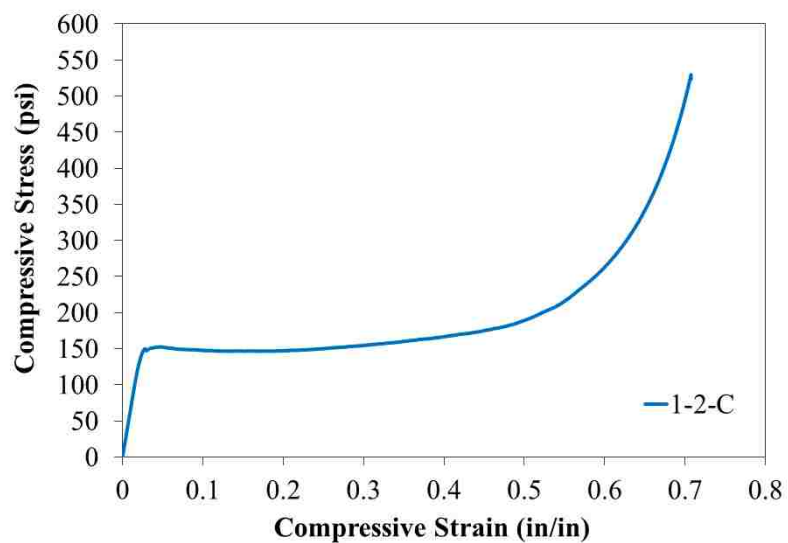
Figure B.2. Compressive stress vs. strain for Type 1 core
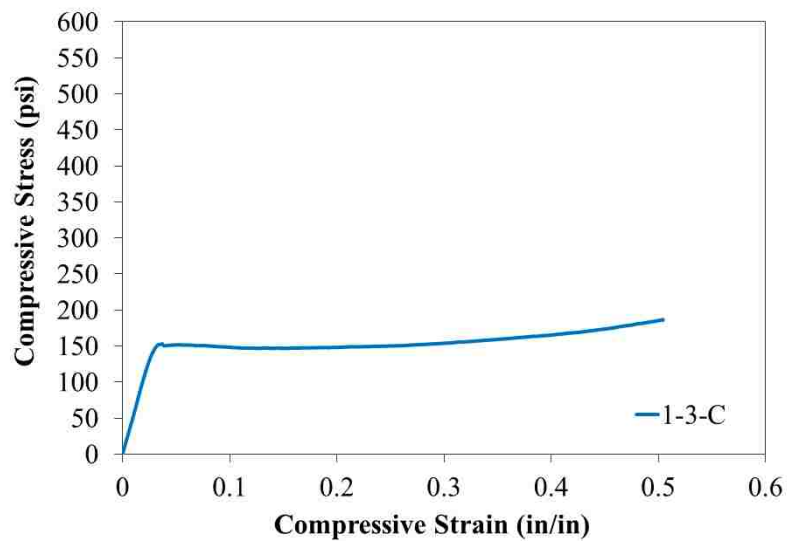
Figure B.3. Compressive stress vs. strain for Type 1 core

Table B.1: Summary of Flatwise Compression Tests of Type 1 construction

Specimen ID	Compressive Modulus (psi)	Compressive Strength (psi)	Compressive Strain (in./in.)
1-1-C	5,210	151	0.035
1-2-C	6,120	150	0.03
1-3-C	4,810	153	0.04
Displacement Rate is 0.10 in./ min			
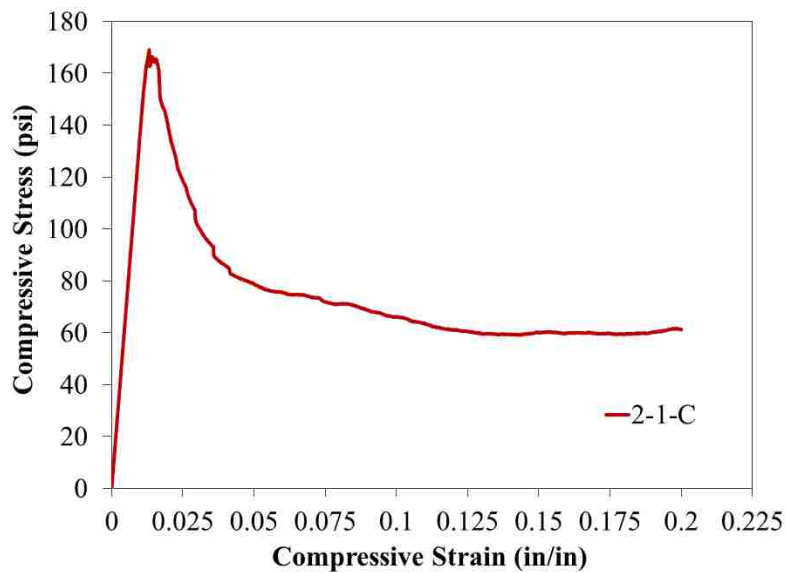
Figure B.4. Compressive stress vs. strain for Type 2 core
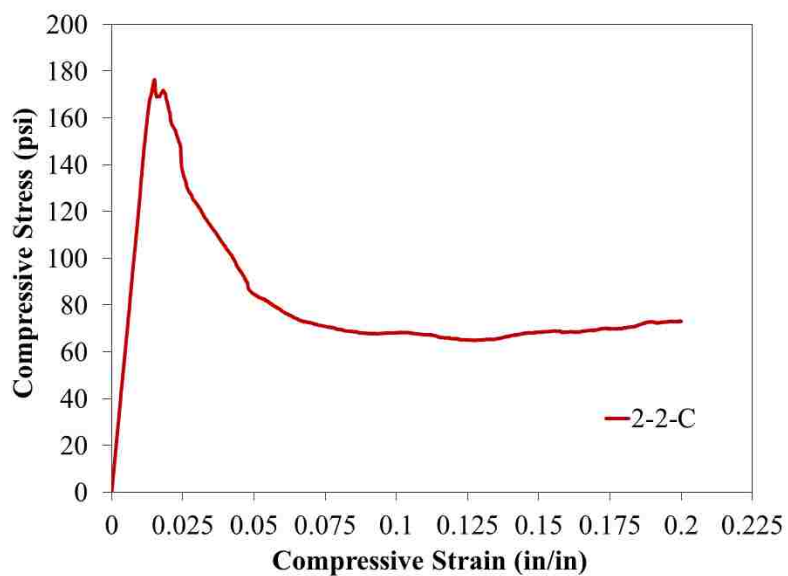
Figure B.5. Compressive stress vs. strain for Type 2 core
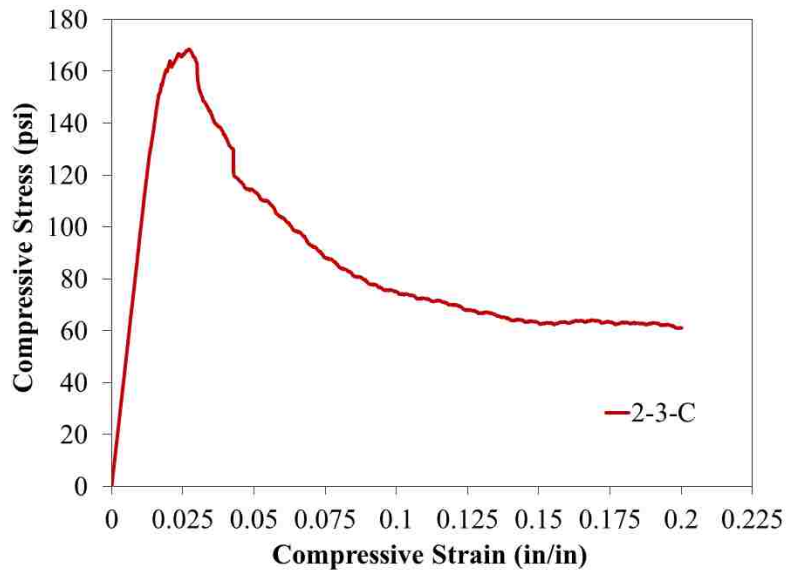
Figure B.6. Compressive stress vs. strain for Type 2 core

Table B.2: Summary of Flatwise Compression Tests of Type 2 construction

Specimen ID	Compressive Modulus (psi)	Compressive Strength (psi)	Compressive Strain (in./in.)
2-1-C	12,400	169	0.015
2-2-C	11,530	176	0.017
2-3-C	8,850	168	0.016
Displacement Rate is 0.10 in./ min			

FLATWISE TENSILE TEST RESULTS
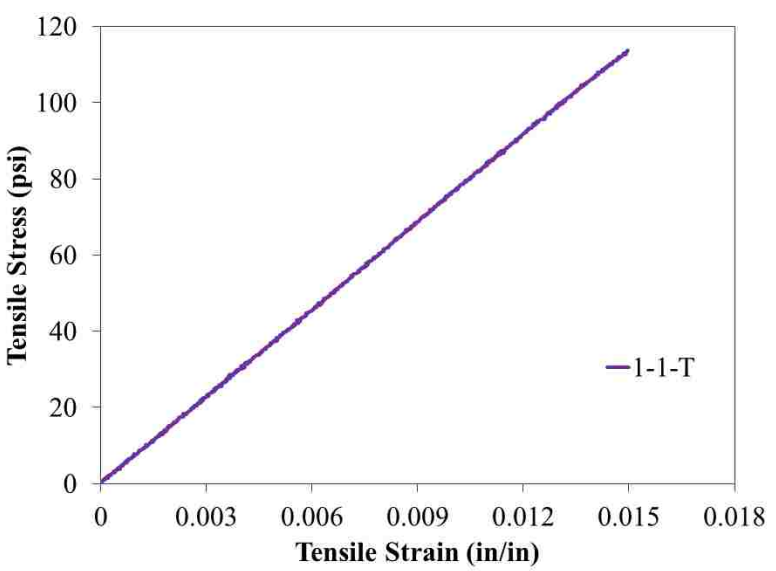
Figure B.7. Tensile stress vs. strain for Type 1 core
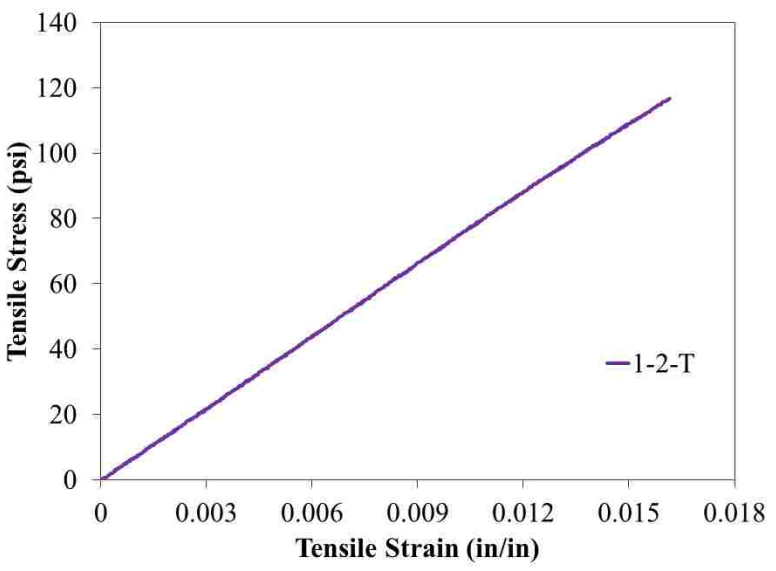
Figure B.8. Tensile stress vs. strain for Type 1 core

Table B.3: Summary of Flatwise Tension Tests of Type 1 construction

Specimen ID	Tensile Modulus (psi)	Tensile Strength (psi)	Tensile Strain (in./in.)
1-1-T	6,900	112	0.016
1-2-T	6,800	117	0.017
Displacement Rate is 0.01 in./ min			
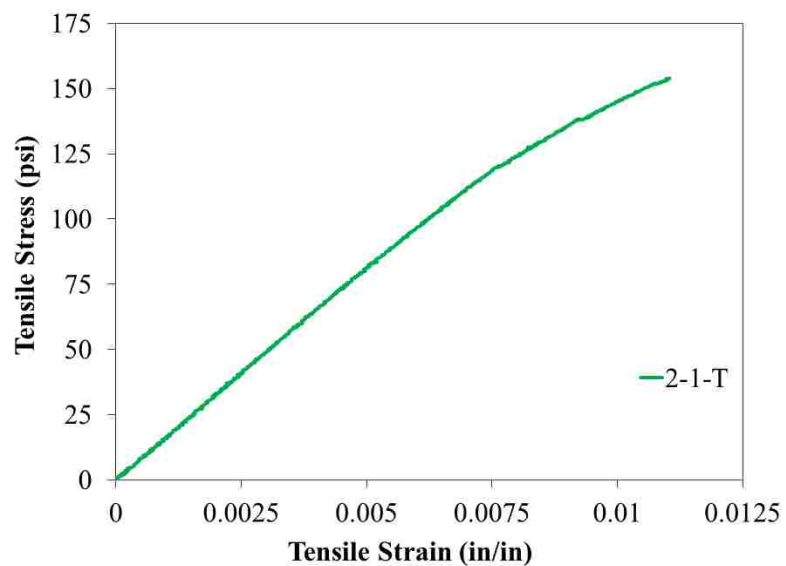
Figure B.9. Tensile stress vs. strain for Type 2 core
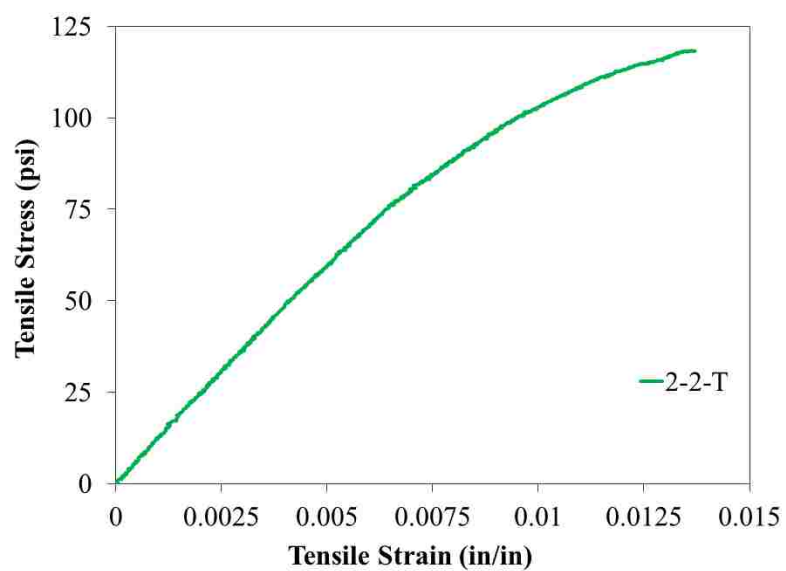
Figure B.10. Tensile stress vs. strain for Type 2 core
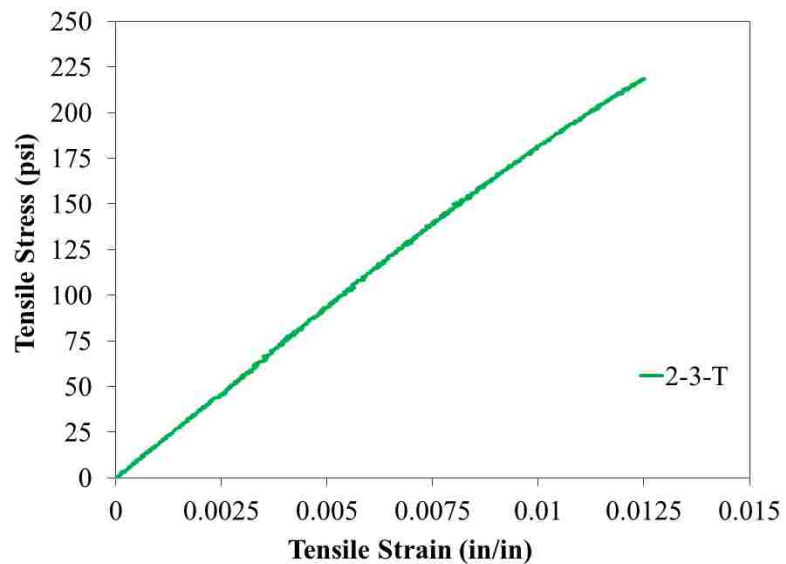
Figure B.11. Tensile stress vs. strain for Type 2 core

Table B.4: Summary of Flatwise Tension Tests of Type 1 construction

Specimen ID	Tensile Modulus (psi)	Tensile Strength (psi)	Tensile Strain (in./in.)
2-1-T	14,270	150	0.012
2-2-T	11,050	120	0.015
2-3-T	16,800	219	0.014
Displacement Rate is 0.01 in./ min			

FLEXURE BEHAVIOR (THREE-POINT TESTS) FOR SHORT BEAMS
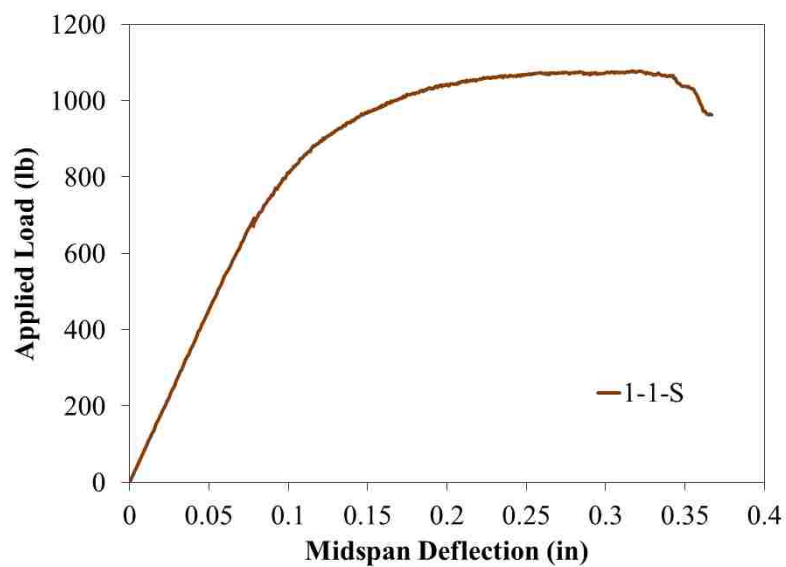
Figure B.12. Load vs. mid-span deflection for Type 1 beam
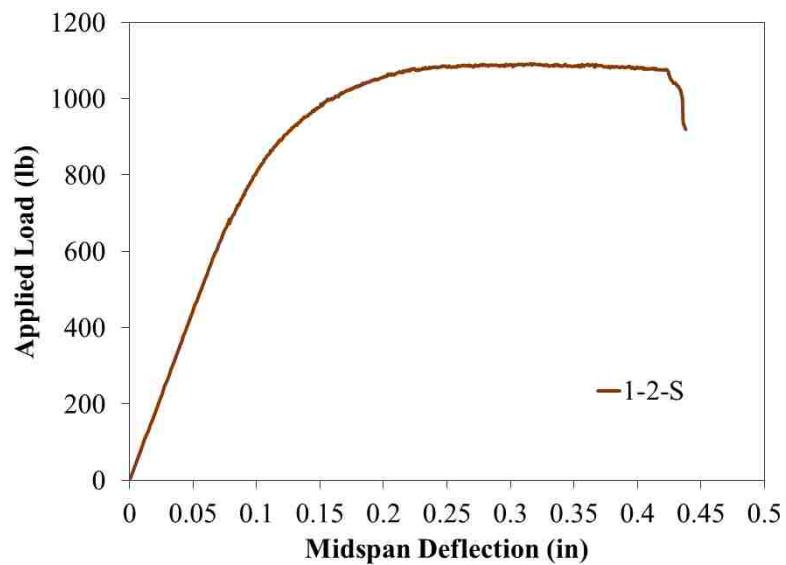
Figure B.13. Load vs. mid-span deflection for Type 1 beam
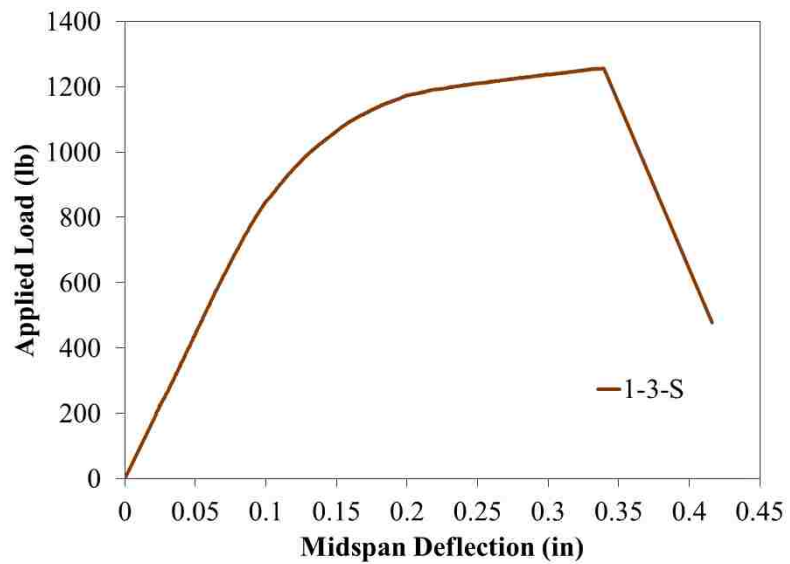
Figure B.14. Load vs. mid-span deflection for Type 1 beam
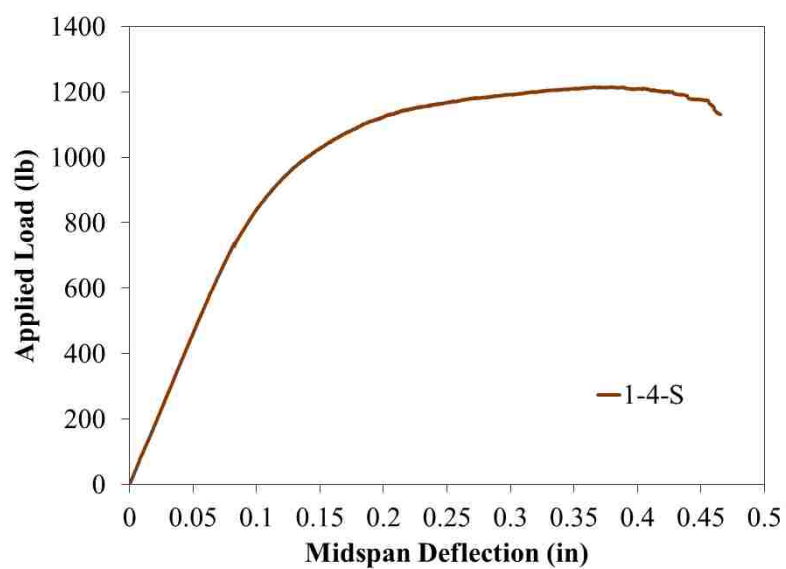
Figure B.15. Load vs. mid-span deflection for Type 1 beam

Table B.5: Summary of Three-point Flexural Tests of Type 1 Beams

Specimen ID	Ultimate Load (lb)	Ultimate Bending Stress (psi)
1-1-S	1,078	2,948
1-2-S	1,092	2,985
1-3-S	1,257	3,397
1-4-S	1,215	3,278
Displacement Rate is 0.1 in./ min		
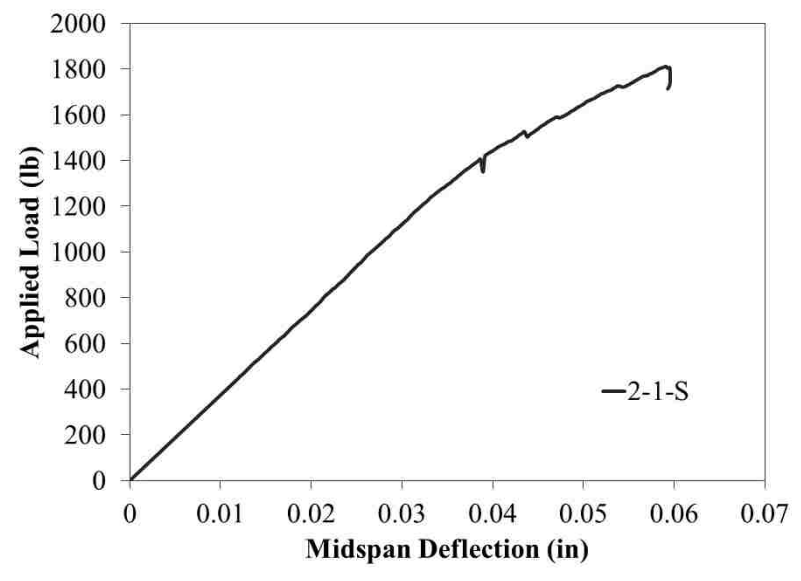
Figure B.16. Load vs. mid-span deflection for Type 2 beam
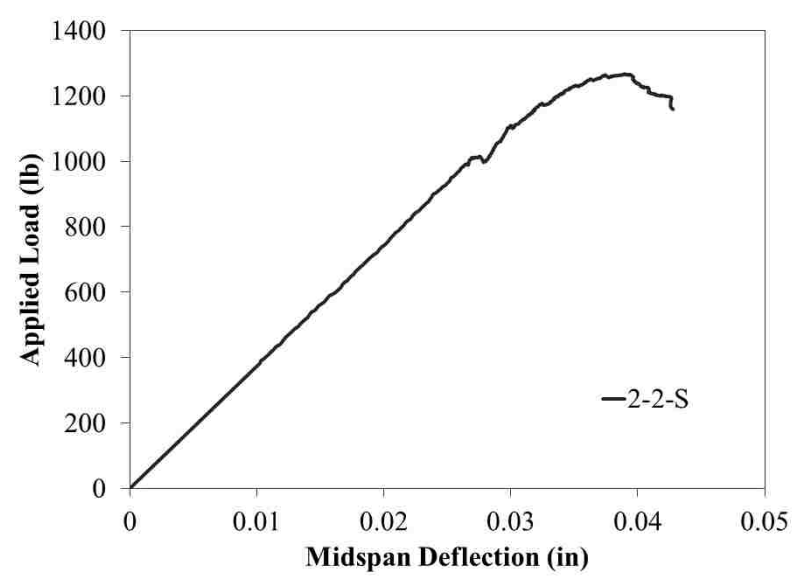
Figure B.17. Load vs. mid-span deflection for Type 2 beam
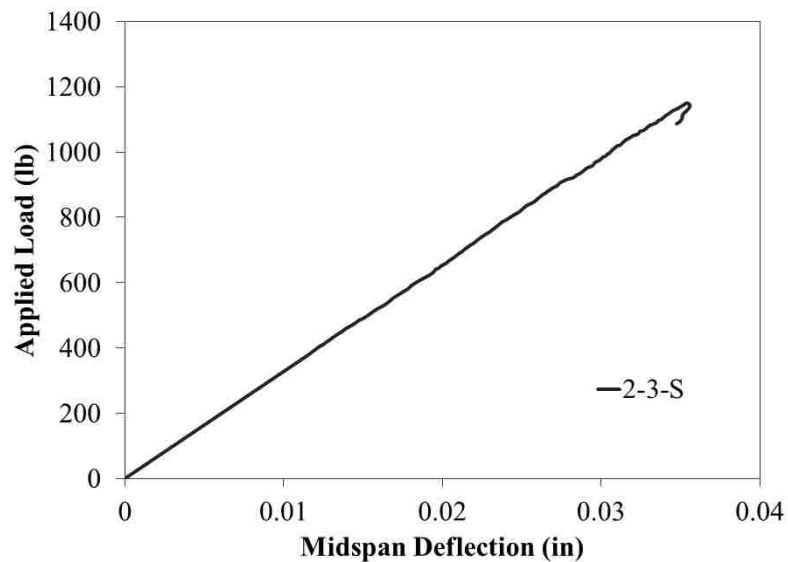
Figure B.18. Load vs. mid-span deflection for Type 2 beam

Table B.6: Summary of Three-point Flexural Tests of Type 2 Beams

Specimen ID	Ultimate Load (lb)	Ultimate Bending Stress at Bottom Facing (psi)
2-1-S	1,812	4,471
2-2-S	1,267	3,095
2-3-S	1,150	2,853
Displacement Rate is 0.1 in./ min		
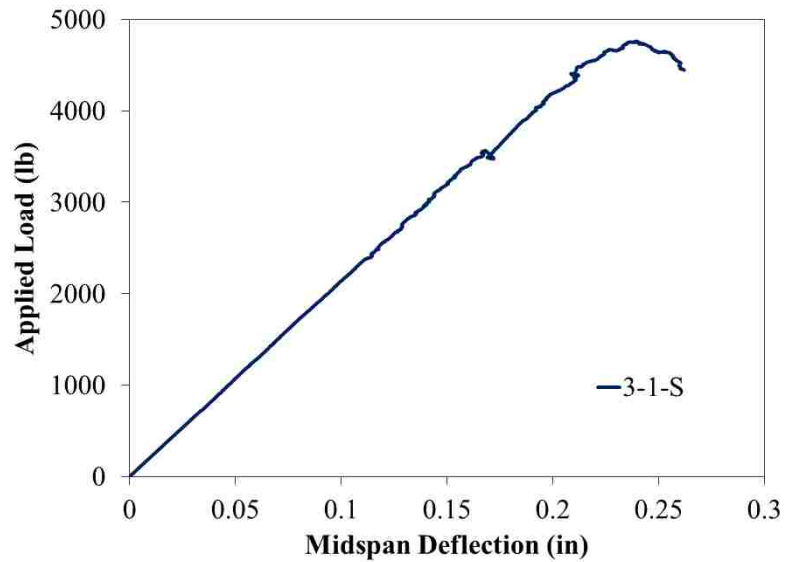
Figure B.19. Load vs. mid-span deflection for Type 3 beam

Table B.7: Summary of Three-point Flexural Tests of Type 3 Beams

Specimen ID	Ultimate Load (lb)	Ultimate Bending Stress at Bottom Facing (psi)
3-1-S	5,895	4,187
Displacement Rate is 0.1 in./ min		

FLEXURE BEHAVIOR (FOUR-POINT TESTS) FOR LONG BEAMS
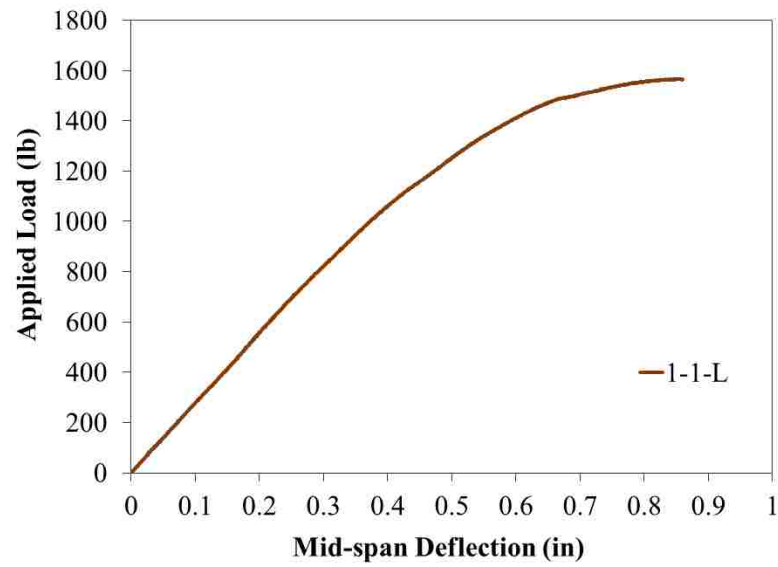
Figure B.20. Load vs. mid-span deflection for Type 1 beam
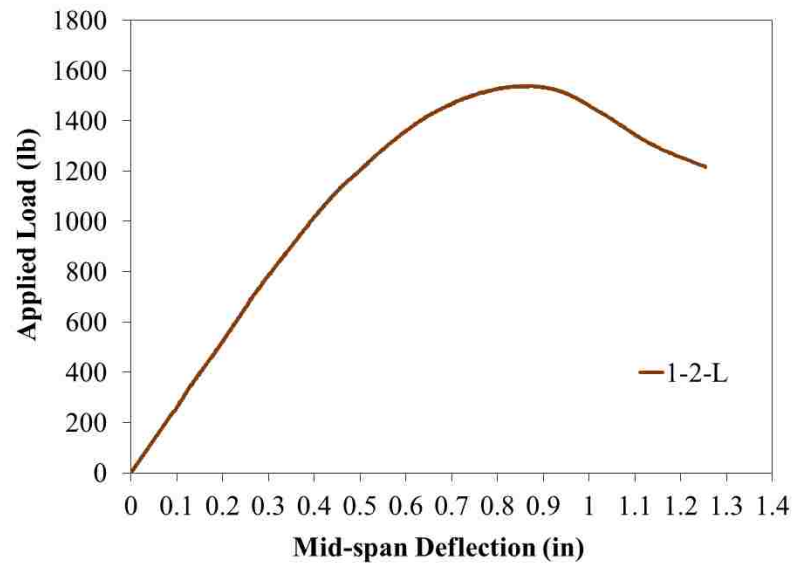
Figure B.21. Load vs. mid-span deflection for Type 1 beam
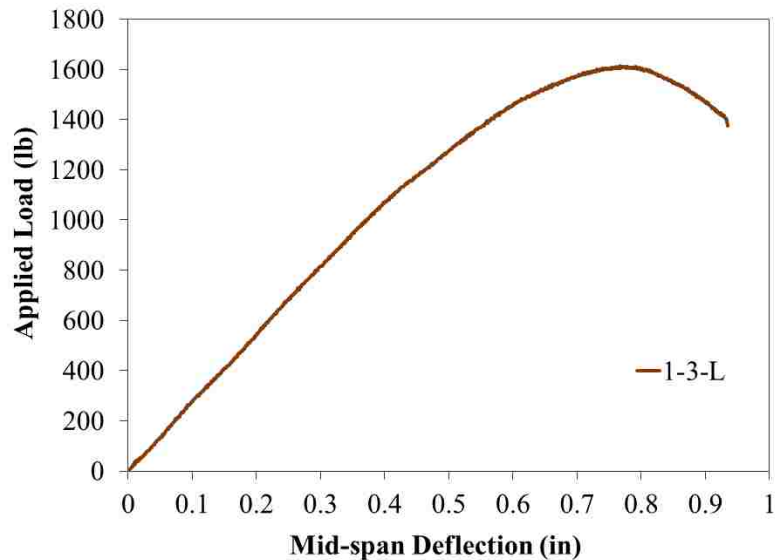
Figure B.22. Load vs. mid-span deflection for Type 1 beam

Table B.8: Summary of Four-point Flexural Tests of Type 1 Beams

Specimen ID	Ultimate Load (lb)	Ultimate Bending Stress at Bottom Facing (psi)
1-1-L	1,566	8,668
1-2-L	1,539	8,827
1-3-L	1,613	9,054
Displacement Rate is 0.1 in./ min		
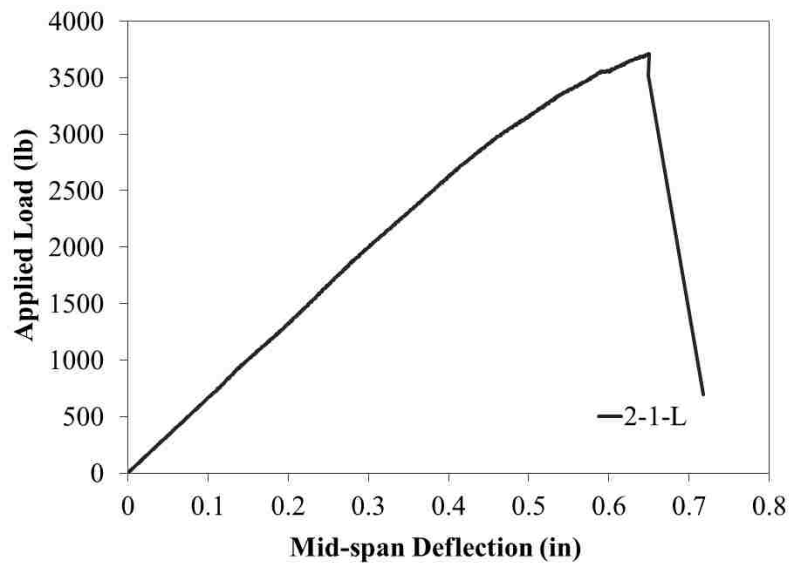
Figure B.23. Load vs. mid-span deflection for Type 2 beam
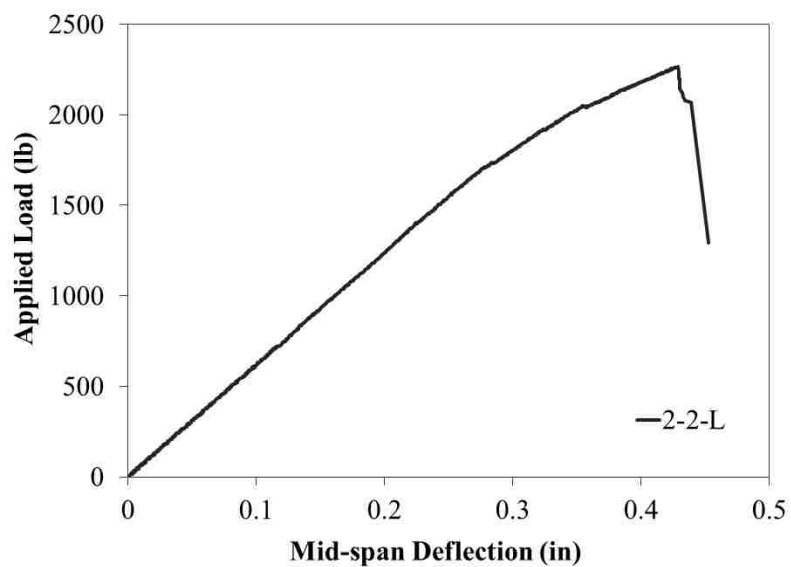
Figure B.24. Load vs. mid-span deflection for Type 2 beam
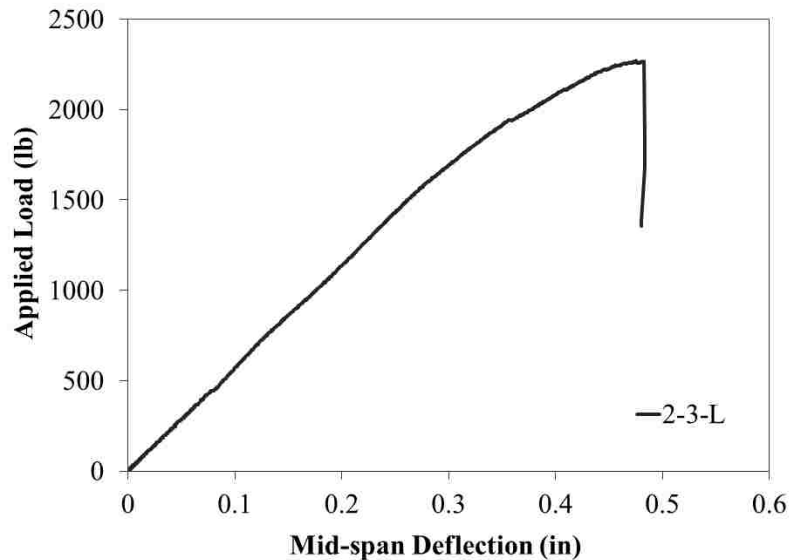
Figure B.25. Load vs. mid-span deflection for Type 2 beam

Table B.9: Summary of Four-point Flexural Tests of Type 2 Beams

Specimen ID	Ultimate Load (lb)	Ultimate Bending Stress at Bottom Facing (psi)
2-1-L	3,712	16,802
2-2-L	2,267	11,972
2-3-L	2,269	10,209
Displacement Rate is 0.05 in./ min		
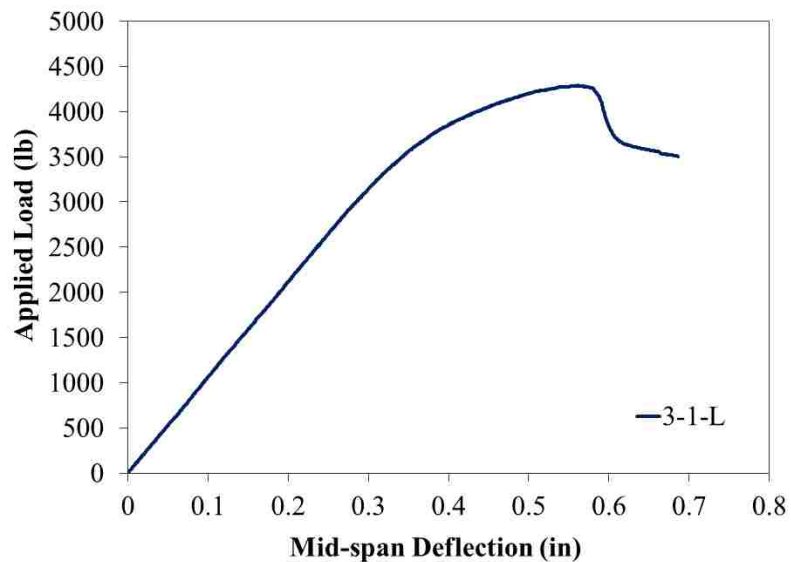
Figure B.26. Load vs. mid-span deflection for Type 3 beam

Table B.10: Summary of Three-point Flexural Tests of Type 3 Beams

Specimen ID	Ultimate Load (lb)	Ultimate Bending Stress at Bottom Facing (psi)
3-1-L	4,288	8,122
Displacement Rate is 0.1 in./ min		

APPENDIX C

C. PHOTOGRAPHS OF MID-SCALE SPECIMENS AND TESTS

This appendix includes different photographs of the mid-scale test fixture, mid-scale sandwich panels, and tests, including crushing tests, flexural tests, and fatigue tests.

Figure C.1. Fabricated steel test fixture for mid-scale panel testing

Figure C.2. Prototype mid-scale panels

Figure C.3. Crushing tests
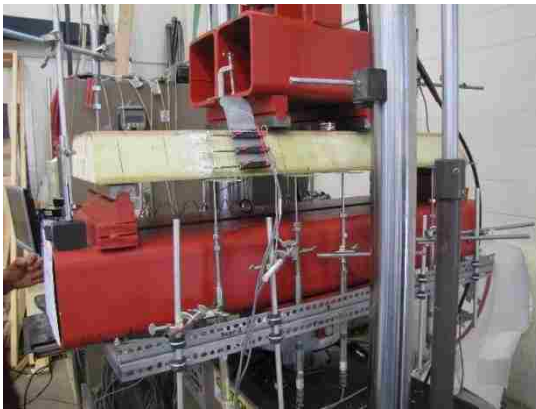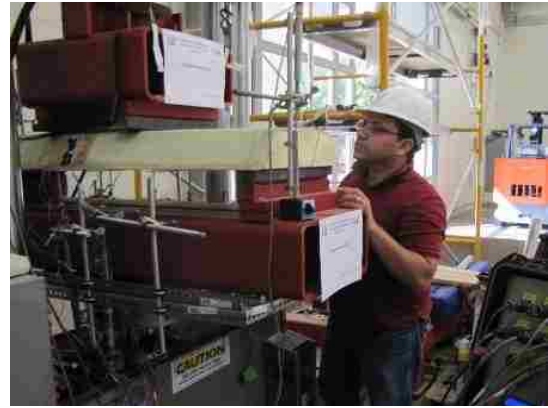
Figure C.4. Flexural Tests for mid-scale panels

Figure C.5. Fatigue Tests for mid-scale panels
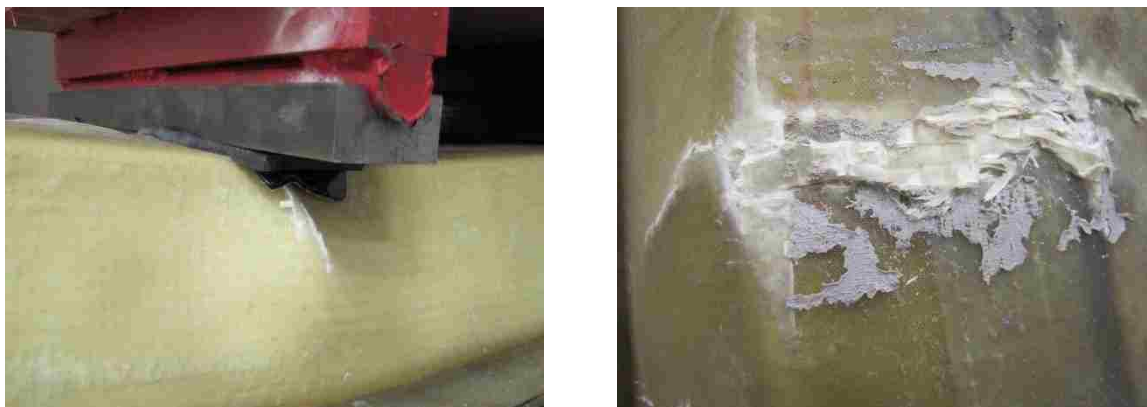
Figure C.6. Fatigue Tests for mid-scale panels

APPENDIX D

D. MID-SCALE TESTING RESULTS

This appendix includes the results of the mid-scale tests, including crushing tests, flexural tests, and fatigue tests.

CRUSHING TEST RESULTS
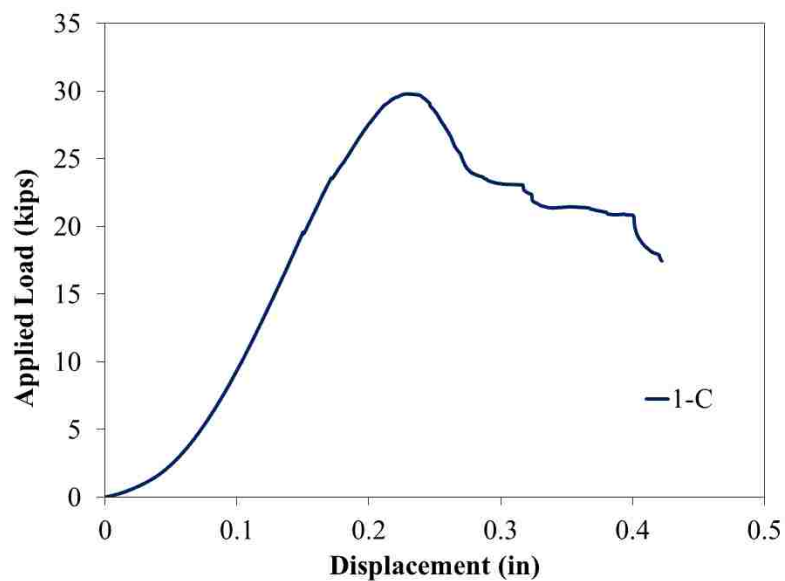
Figure D.1. Load vs. displacement for 12 in. x 12.5 in. panel
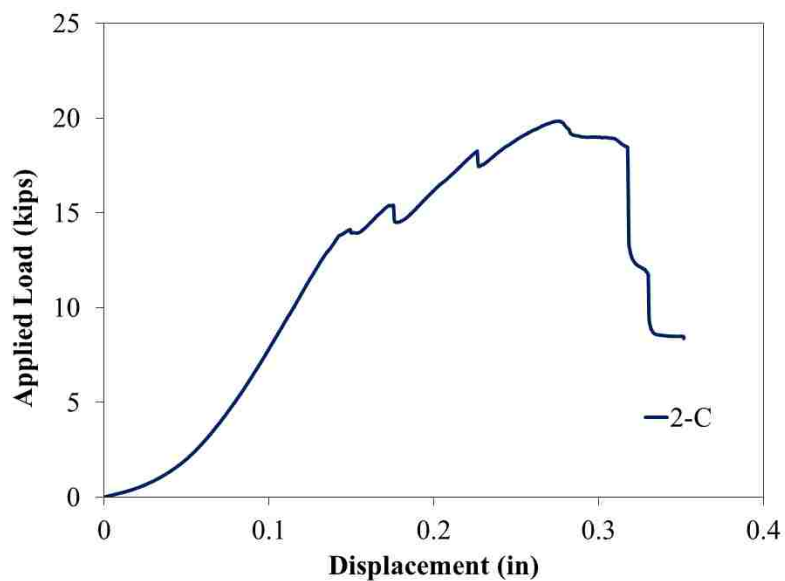
Figure D.2. Load vs. displacement for 12 in. x 12.5 in. panel

FLEXURAL TEST RESULTS
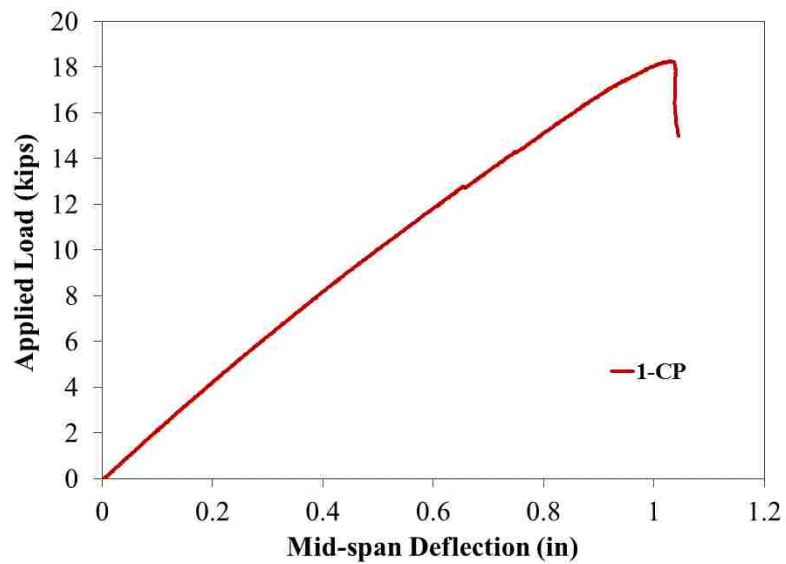
Figure D.3. Load vs. mid-span deflection
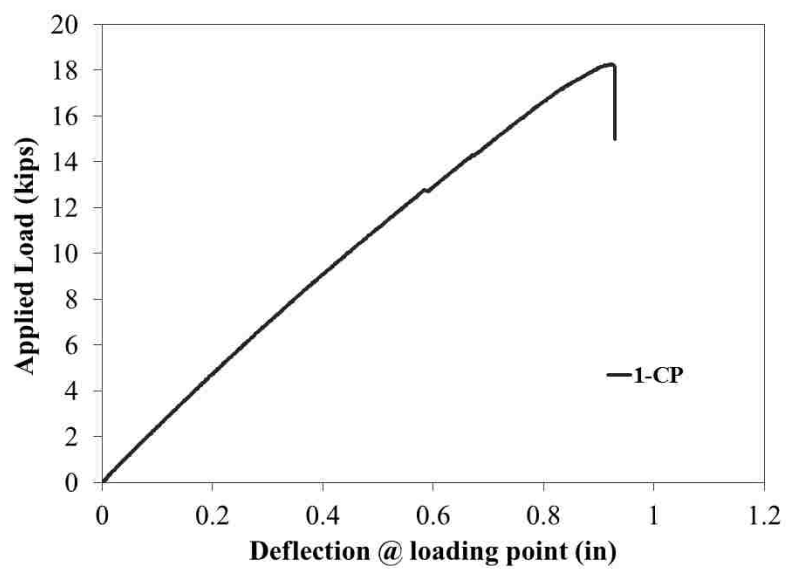
Figure D.4. Load vs. loading deflection
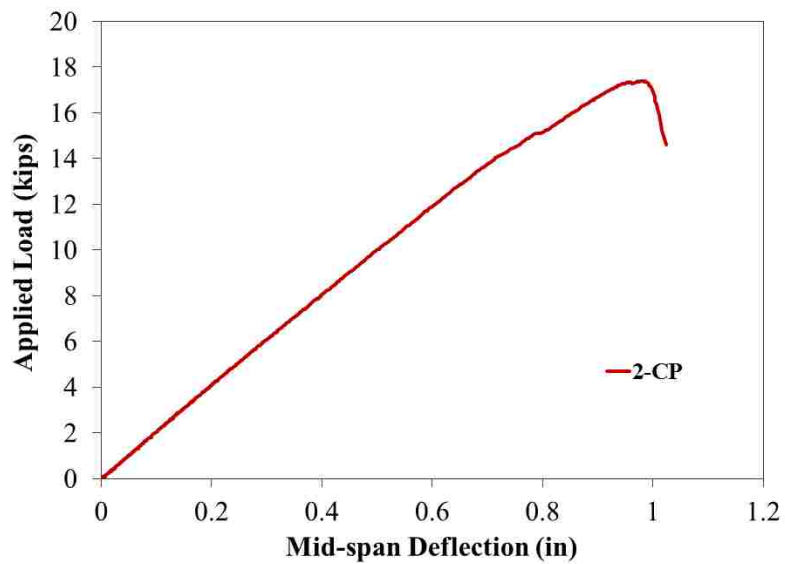
Figure D.5. Load vs. mid-span deflection
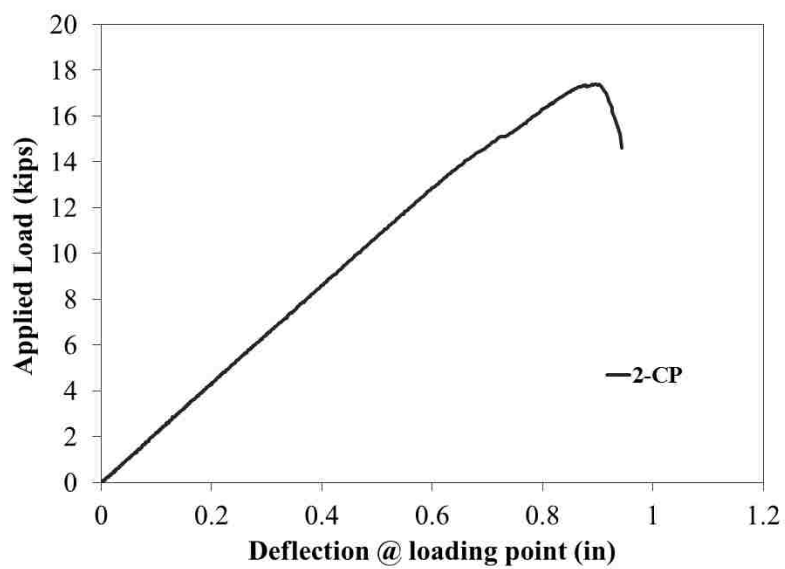
Figure D.6. Load vs. loading deflection
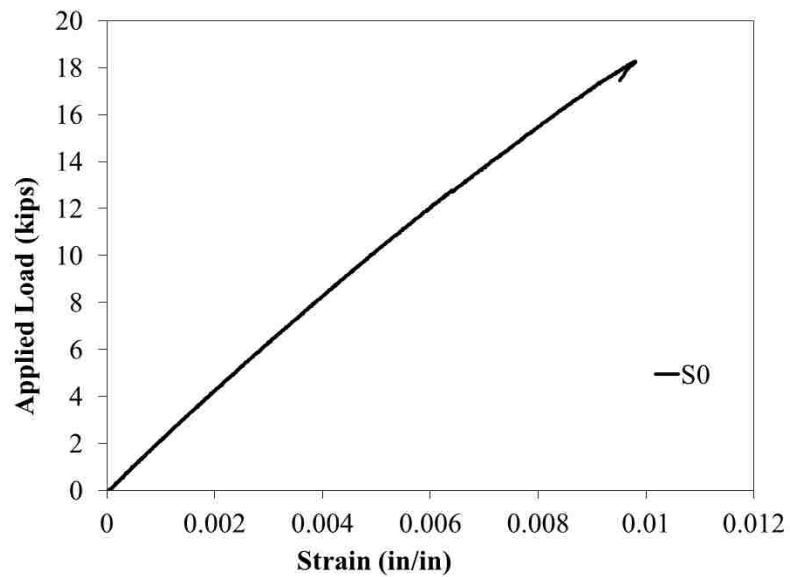
Figure D.7. Load vs. strain for 1-CP panel
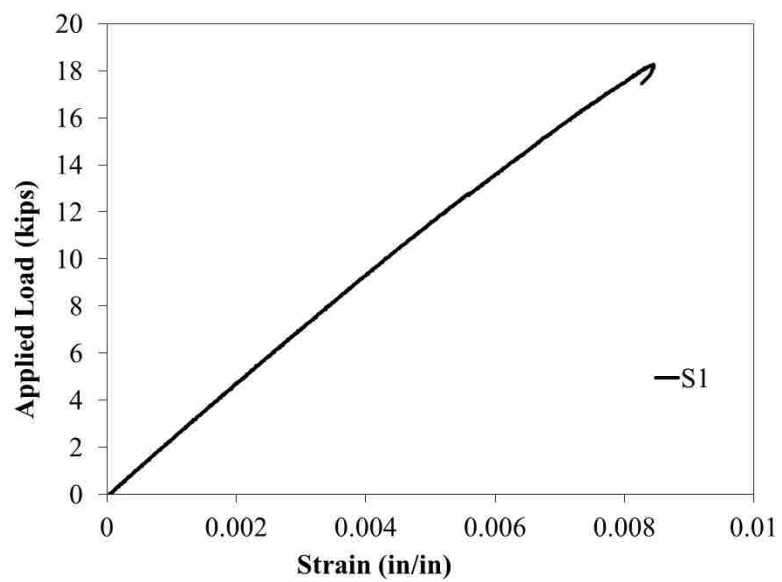
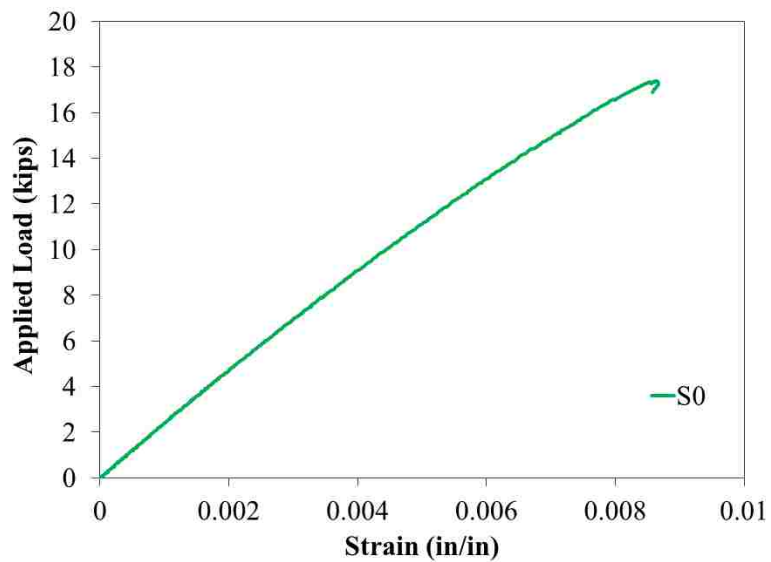Figure D.8. Load vs. strain for 1-CP panel
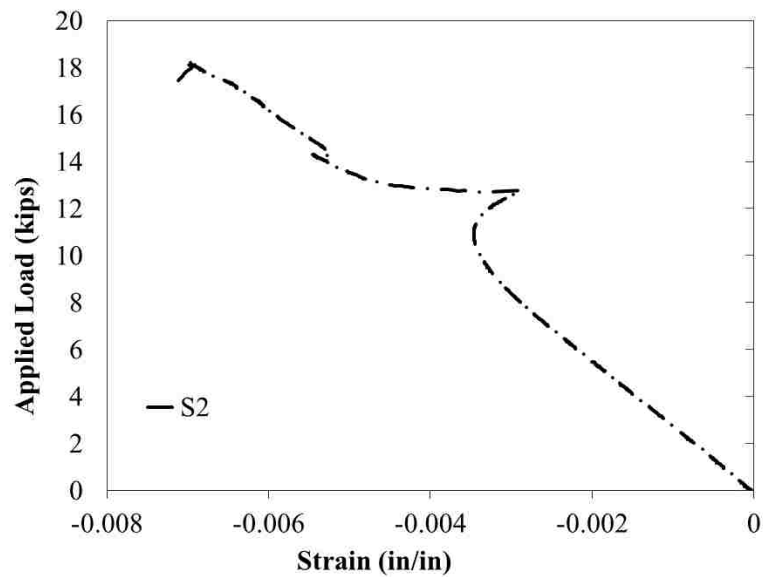
Figure D.9. Load vs. strain for 1-CP panel
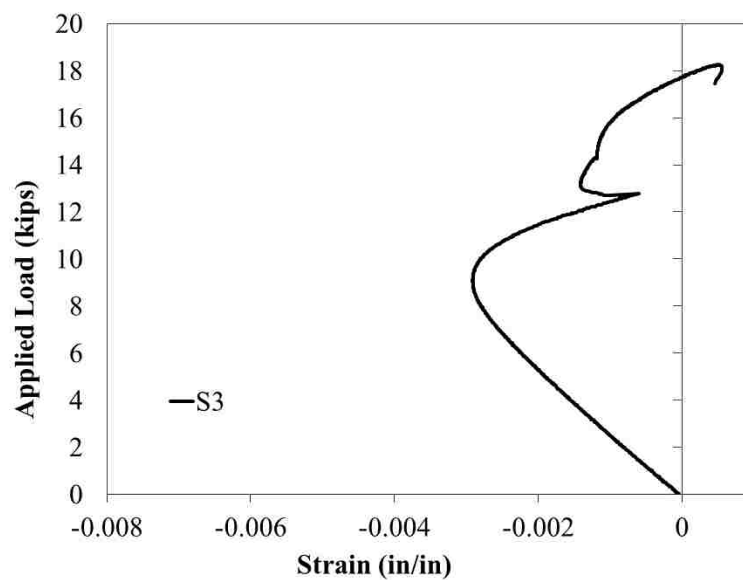
Figure D.10. Load vs. strain for 1-CP panel
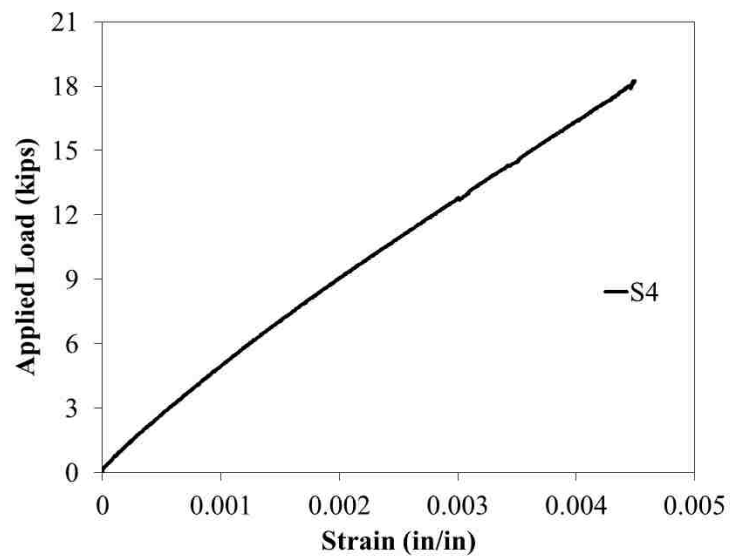
Figure D.11. Load vs. strain for 1-CP panel
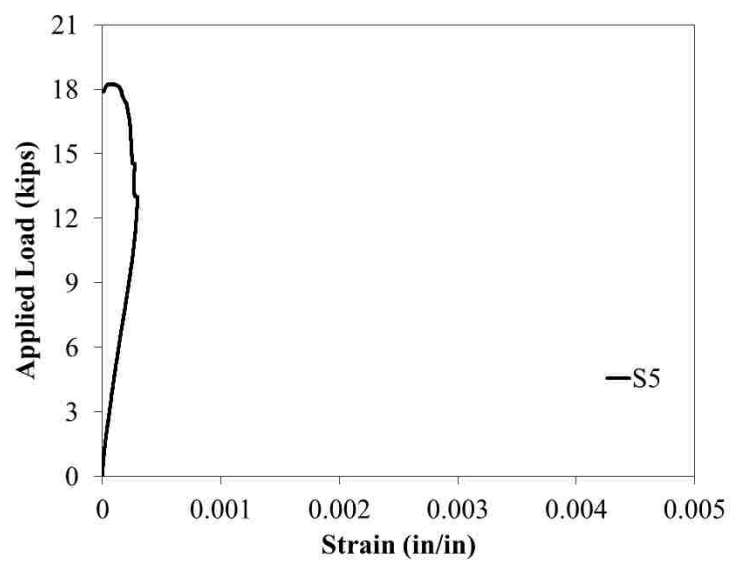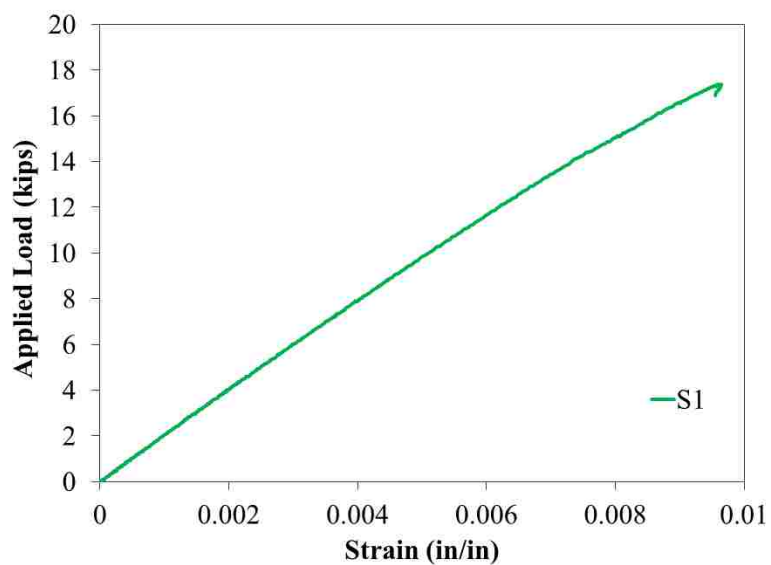

Figure D.12. Load vs. strain for 1-CP panel
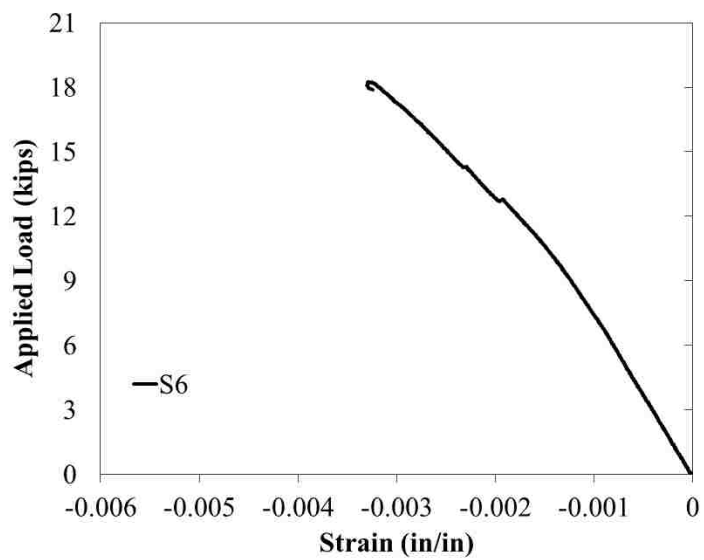
Figure D.13. Load vs. strain for 1-CP panel
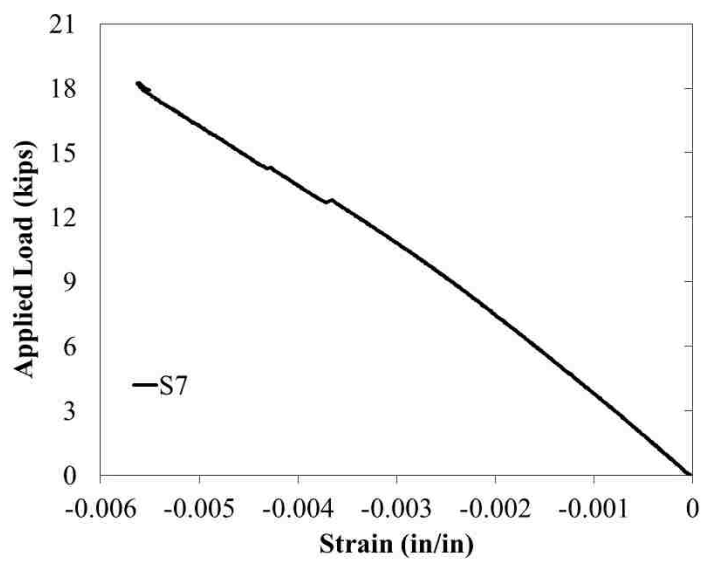
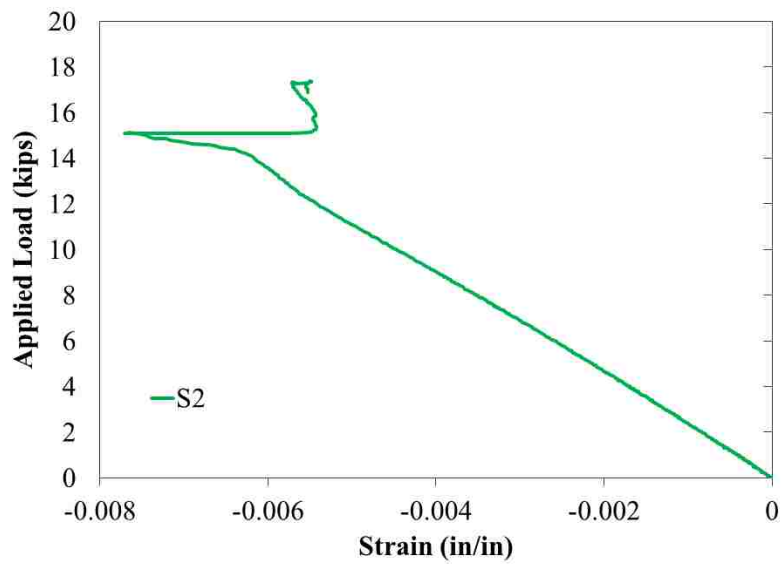Figure D.14. Load vs. strain for 1-CP panel

Figure D.15. Load vs. strain for 2-CP

Figure D.16. Load vs. strain for 2-CP
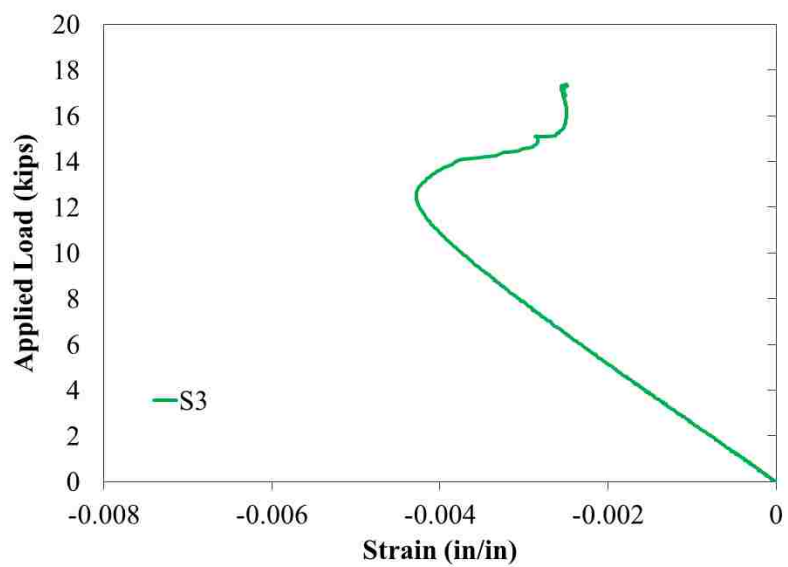
Figure D.17. Load vs. strain for 2-CP
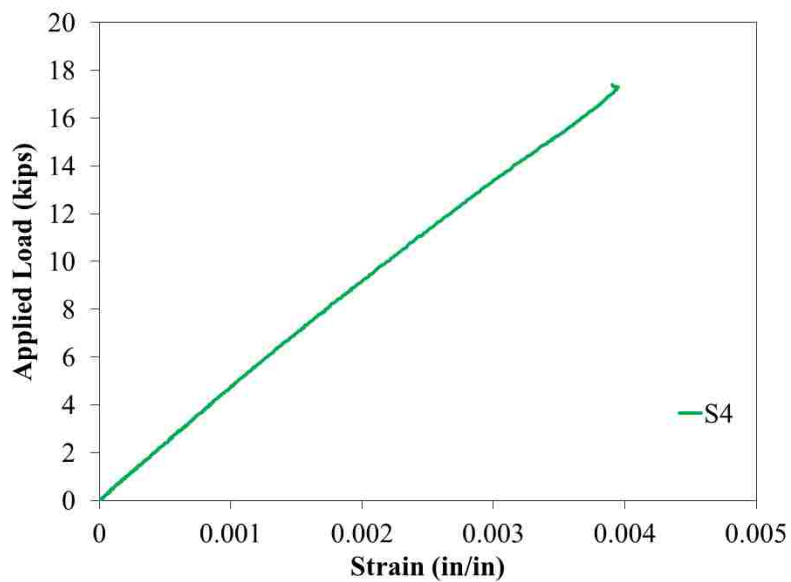

Figure D.18. Load vs. strain for 2-CP
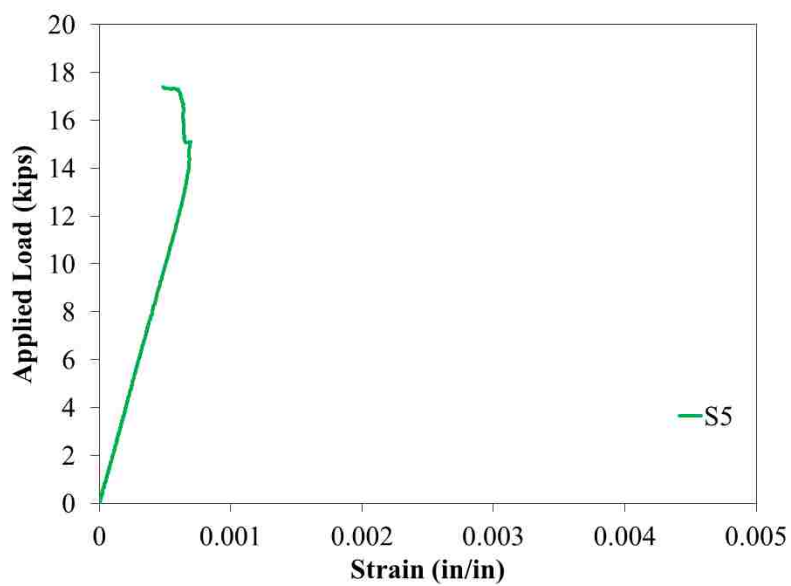
Figure D.19. Load vs. strain for 2-CP
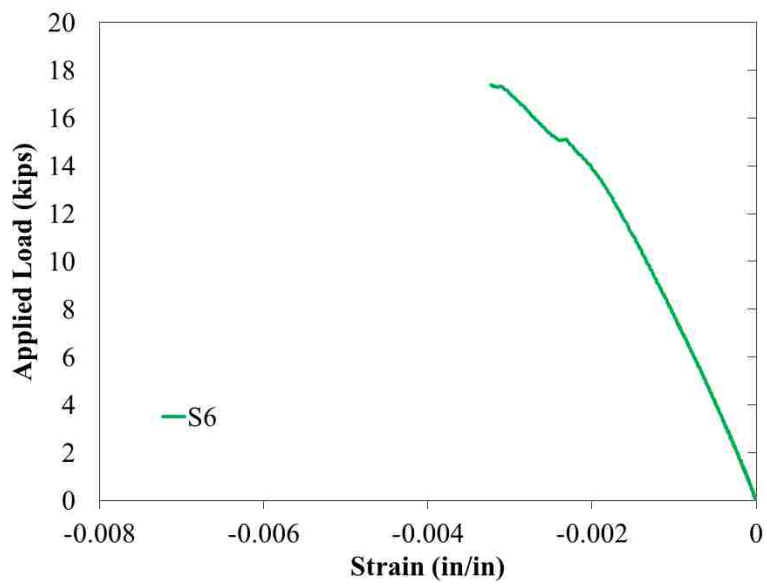

Figure D.20. Load vs. strain for 2-CP

Figure D.21. Load vs. strain for 2-CP

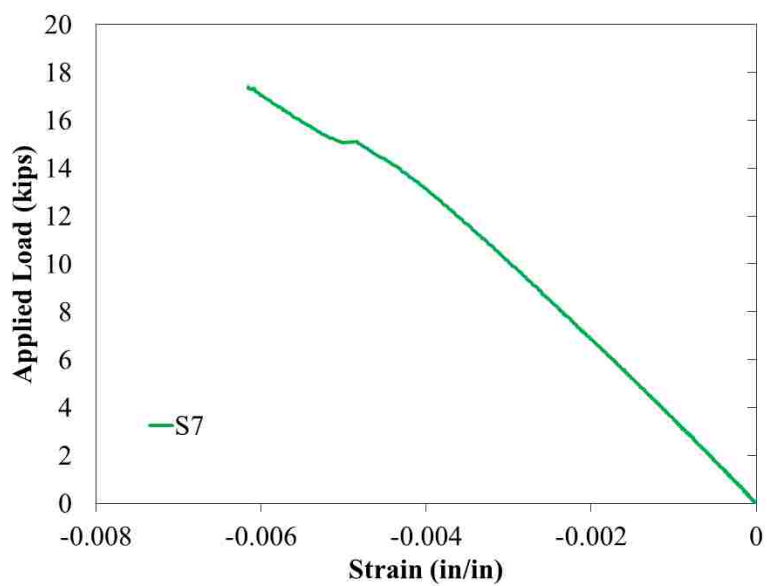

Figure D.22. Load vs. strain for 2-CP

FATIGUE TEST RESULTS
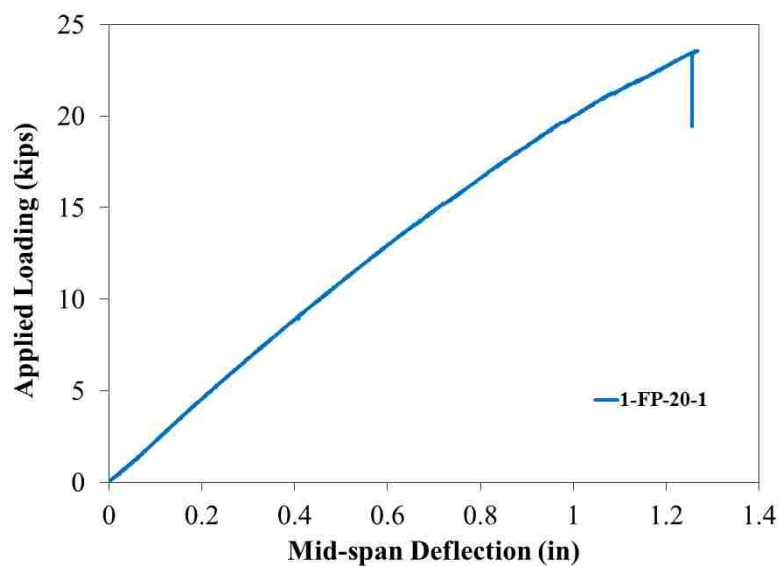
Figure D.23. Load vs. deflection

Figure D.24. Load vs. deflection
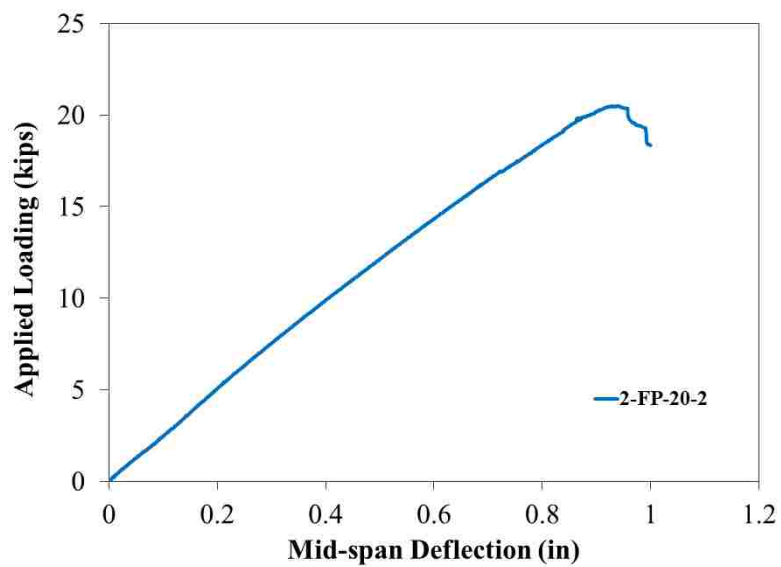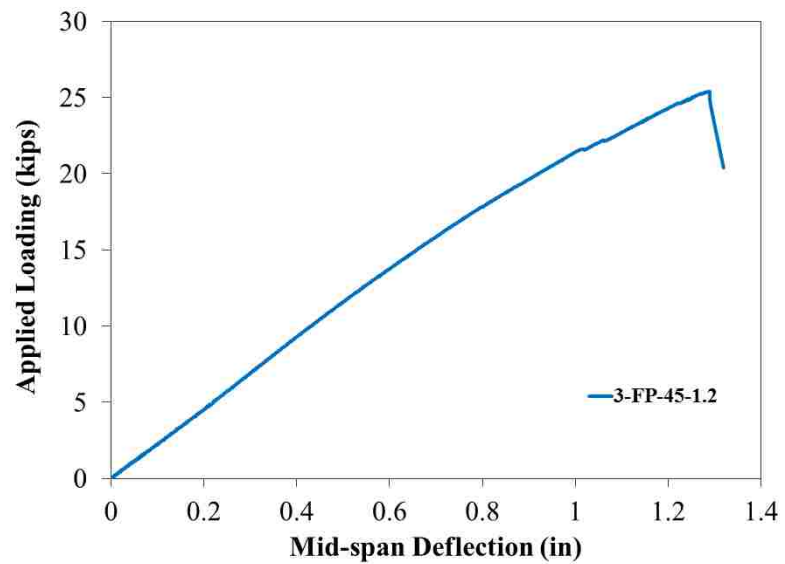
Figure D.25. Load vs. deflection

APPENDIX E

E. PHOTOGRAPHS OF DURABILITY TESTS

This appendix includes different photographs of the durability tests that conducted for the GFRP laminates, including ultraviolet radiation and deicing solution at both room and elevated temperatures.
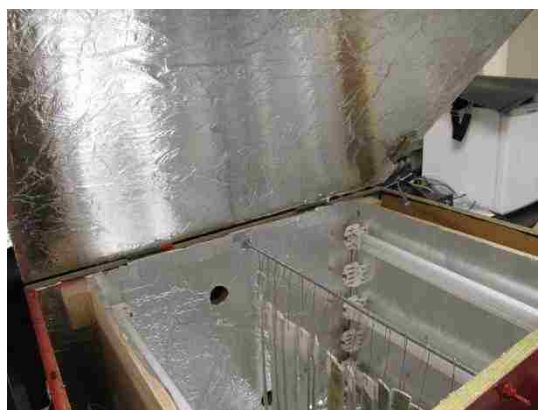
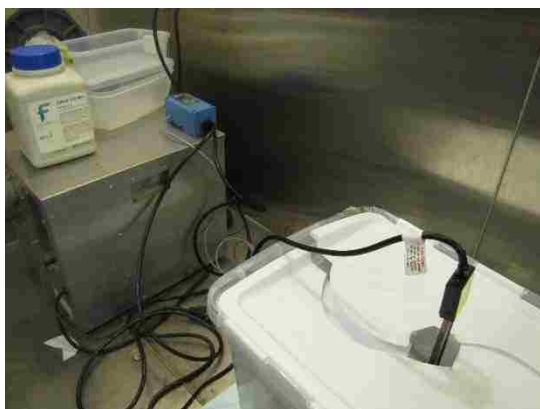Figure E.1. Ultraviolet radiation chamber

Figure E.2. Deicing solution at room and elevated temperatures

REFERENCES

Allen, H.G. (1969). "Analysis and Design of Structural Sandwich Panels," Oxford: Pergamon Press.

Allen, H. G., and Feng, Z. (1998). "Classification of Structural Sandwich Panel Behavior," Mechanics of Sandwich Structures. Kluwer Academic Publishers.

Alagusundaramoorthy, P. and Reddy, R.V. (2008). "Testing and Evaluation of GFRP Composite Deck Panels," Ocean Engineering 35, 287–293.

Anon (2001). "FRP Decks Help Control Corrosion." Better Roads 71(5): 46.

Aref, A.J., Sreenivas, Alampalli (2001). "Vibration Characteristics of a Fiber Reinforced Polymer Bridge Superstructure," Composite Structures 52, 467–474.

Ashby, M. (2005). "The Properties of Foams and Lattices," Philosophical Transactions of the Royal Society A Mathematical, Physical and Engineering Sciences 364 15-30.

Bruhn, E.F. (1973). "Analysis and Design of Flight Vehicle Structures," Purdue University, West Lafayette, IN: S.R. Jacobs and Associates, Inc. p. C12.1–C12.52.

Bitzer, T. (1997). "Honeycomb Technology," Chapman and Hall, London.

Bakis, C.E, Bank, L.C., Brown, V.L., Cosenza, E., Davalos, J.F., Lesko, J.J., Machida, A., Rizkalla, S.H., and Triantafillou, T.C. (2002). "Fiber-Reinforced Polymer Composites for Construction—State-of-the-Art Review," ASCE Journal Of Composites For Construction, 2: (73),1090-0268.

Bank, L. (2005). "Fiber-reinforced Grid System Provides Bridge with 75-year Life." Advanced Materials and Processes 163(8): 23-24.

Baba BO, Thoppul S, Gibson RF (2011). "Experimental and Numerical Investigation of Free Vibrations of Composite Sandwich Beams with Curvature and Debonds," Experimental Mechanics; 51 (6):857-868.

Bareis, D. Heberer, and Connolly, M. (2011). "Advances in Urethane Composites Resins with Tunable Reaction Times." American Composites Manufacturers Association Ft. Lauderdale, Florida. Huntsman Polyurethanes Auburn Hills, MI: 1-7.

Busel, J. P. and J. D. Lockwood (2000). "Engineered FRP Products in Civil Engineering." Boston, MA, Soc. for the Advancement of Material and Process Engineering.

Camata, G. and Shing, P.B. (2004). "Evaluation of GFRP Deck Panel for The O'fallon Park Bridge," Report No. CDOT-DTD-R-2004-2 Final Report to Colorado Department Of Transportation Research Branch.

Camata G, Shing PB. (2005). "Evaluation of GFRP Honeycomb Beams for the O'Fallon Park Bridge," J Compos Construct, ASCE; 8(6):545–55.

Camata, G. and Shing, P.B. (2010). "Static and Fatigue Load Performance of a GFRP Bridge Deck," Composites Part B: Engineering. Vol. 41, issue 4, pp. 299–307.

Connolly, M., King, J., Shidaker, T., and Duncan, A. (2006). "Processing and Characterization of Pultruded Polyurethane Composites," Huntsman Enriching lives through innovation.

Dawood, M., Taylor, E., Ballew, W., and Rizkalla, S. (2010). "Static and Fatigue Bending Behavior of Pultruded GFRP Sandwich Panels," Composites Part B: Engineering, Vol. 41, Issue 5, Pages 363–374.

Davalos, J.F., Qiao, P., Xu, X.F., Robinson, J., and Barth, K.E, (2001). "Modeling And Characterization of Fiber-reinforced Plastic Honeycomb Sandwich Panels For Highway Bridge Applications," Composite Structures 52: 441-452.

Davalos, J.F., Chen, A., and Zou, B. (2012). "Performance of a Scaled FRP Deck-on-Steel Girder Bridge Model with Partial Degree of Composite Action," Engineering Structures 40: 51–63.

Deshpande, V.S. and N.A. Fleck (2000). "Isotropic Constitutive Models for Metallic Foams," Journal of the Mechanics and Physics of Solids, 48(6-7): p. 1253-1283.

Doyoyo, M. and T. Wierzbicki (2003). "Experimental studies on the yield behavior of ductile and brittle aluminum foams," International Journal of Plasticity, 19(8): p. 1195-1214.

Ellis, Z. (2011). "Corrosion Cost and Preventive Strategies in the United States." FHWA-RD-01-156.

Fam, A. and Sharaf, T. (2010)."Flexural Performance of Sandwich Panels Comprising Polyurethane Core and GFRP Skins and Ribs of Various Configurations," Composite Structures 92 (12):2927- 2935.

Federal Highway Administration. (2013). "https://www.fhwa.dot.gov/bridge/frp/deckprac.cfm"

Gibson L.J. and Ashby M.F. (1988). "Cellular Solids: Structure and Properties." Oxford: Pergamon Press.

Gibson, L.J. and M.F. Ashby, (1997). "Cellular Solids: Structure and Properties," 2nd edition. Cambridge: Cambridge University Press.

Gdoutos, E.E., I.M. Daniel, and K.-A. Wang (2002). "Failure of Cellular Foams Under Multiaxial Loading," Composites Part A: Applied Science and Manufacturing. 33(2): p. 163-176.

Hayes, M. D., D. Ohanehi, et al. (2000). "Performance of Tube and Plate Fiberglass Composite Bridge Deck," Journal of Composites for Construction 4(2), 48-55.

Henderson, M. (2000). "Evaluation of Salem Avenue Bridge Deck Replacement: Issues Regarding the Composite Materials Systems Used," Final Report. Ohio Department of Transportation, December.

Hassan, T., Reis, E.M., and Rizkalla, S.H. (2003). "Innovative 3-D FRP Sandwich Panels for Bridge Decks," Proceedings of the Fifth Alexandria International Conference on Structural and Geotechnical Engineering. Alexandria, Egypt.

Hollaway, L. C. (2003). "The Evolution of and the Way Forward for Advanced Polymer Composites in the Civil Infrastructure." Construction and Building Materials 17(6-7): 365-378.

Harries, K. (2006). "FRP Bridge Decks-A Maturing Technology." Journal of Bridge Engineering 11(4): 382.

Hong, T. and M. Hastak (2007). "Simulation Study on Construction Process of FRP Bridge Deck Panels." Automation in Construction 16(5): 620-631.

Henao, A., Carrera, M., Miravete, A., Castejon, L. (2010). "Mechanical Performance of Through-thickness Tufted Sandwich Structures." Composite Structures 92 (9):2052-2059.

Joshi, R.R., Cheolas, E.H., Cassidy, E.F., Karoly, W.J., Coffee, H.D. (2001). "Polyurethane Based Pultruded Resins Improve the Environmental Image of Composite Materials," Proceedings of Composites 2001-CFA, (Composites Fabricators Association).

Ji, H.S., Song, W., and Ma, Z.J. (2010). "Design, Test and Field Application of a GFRP Corrugated-core Sandwich Bridge," Engineering Structures. Vol. 32, pp. 2814-2824.

Keller, T., and Gurtler, H. (2005). "Composite Action and Adhesive Bond Between Fiber-reinforced Polymer Bridge Decks and Main Girders." Journal of Composites for Construction, 9(4), 360-368.

Kim JH, Lee YS, Park BJ, Kim DH. (1999). "Evaluation of Durability and Strength of Stitched Foam-cored Sandwich Structures," Compos Struct; 47:543–50.

Kumar, P., Chandrashekhara, K., and Nanni, A. (2001). "Structural Performance of a FRP Bridge Deck," ASCE, Journal of Composites for Construction.

Karbhari, V. M. (2004). "Fiber Reinforced Composite Bridge Systems-transition from the Laboratory to the Field." Composite Structures 66(1-4): 5-16.

Kirk, R.S., and Mallett, W.J. (2013). "Highway Bridge Conditions: Issues for Congress," Congressional Research Service, Report to congress. Contract No. R43103.

Lopez-Anido, R., Troutman, R., and Busel, J. (1998). "Fabrication and Installation of Modular FRP Composite Bridge Deck," CI Composites Expo, Nashville, TN, Session 4-A/1-6.

Mamalis, A.G., Manolakos, D.E., Ioannidis, M.B. and D.P. Papapostolou. (2005). "On the crushing response of composite sandwich panels subjected to edgewise compression: experimental," Composite Structures. 71: 246–257.

Moon, F.L, Eckel, D.A., and Gillespie, J.W. (2002). "Shear Stud Connections for the Development of Composite Action Between Steel Girders and Fiber-reinforced Polymer Decks." Journals of Structural Engineering, 128(6), 762-770.

Morcous, G., Cho, Y., El-Safty, A., and Chen, G. (2010). "Structural Behavior of FRP Sandwich Panels for Bridge Decks," KSCE Journal of Civil Engineering 14(6): 879-888.

Norlin, P. and S. Reuterlöv. (2002). "The Role of Sandwich Composites in Turbine Blades," Reinforced Plastics. 3: 32-34.

Plantema F. (1966). "Sandwich construction," New York: John Wiley and Sons.

Plunkett, J.D., (1997). "Fiber-Reinforcement Polymer Honeycomb Short Span Bridge For Rapid Installation." IDEA project report.

Potluri, P., Kusak, E. and Reddy, T.Y. (2003). "Novel Stitch-bonded Sandwich Composite Structures." Composite Structures Vol. 59 No. 2, pp. 251-9.

Reising, R., Shahrooz, B., Hunt, V., Lenett, M., Christopher, S., Neumann, A., Helmicki, A., Miller, R., Konduri, S., and Morton, S. (2001). "Performance of a Five – Span Steel Bridge with Fiber Reinforced Polymer Composite Deck Panels," Transportation Research Board Annual Meeting, Washington, D.C.

Righman, J., Barth, K.E., and Davalos, J.F. (2004). "Development of an Efficient Connector System for Fiber Reinforced polymer Bridge Decks to Steel Girders." Journal of Composites for Construction, 8(4), 279-288.

Rocca, S.V. and Nanni, A. (2005). "Mechanical Characterization of Sandwich Structure Comprised of Glass Fiber Reinforced Core," Part 1, Composite in Construction, Third International Conference. Lyon, France.

Szycher, M. (1999). "Handbook of Polyurethanes," Boca Raton: CRC Press.

Stone, D., Nanni, A., and Myers, J. (2001). "Field and Laboratory Performance of FRP Bridge Panels," Composites in Construction, Porto, Portugal, J Figueiras, L. Juvandes and R. Furia, Eds, pp. 701-706.

Shen, H., Sokolinsky, V. S. , and Nutt, S. R. (2004). "Accurate Predictions of Bending Deflections for Soft-core Sandwich Beams Subject to Concentrated Loads." J. Composite structures 64, 115-122.

Sumerak, J.E. (2004). "Pultrusion Gets Tough: Polyurethane Resin Offers New Growth," Composites Fabrication, (American Composites Manufactures Association).

Triantafillou TC, Gibson LJ. (1987). "Failure Mode Maps for Foam Core Sandwich Beams," Materials Science and Engineering 95 (C):37-53.

Taylor, E.M. (2009). "Two-way Behavior and Fatigue Performance of 3-D GFRP Sandwich Panels," Master's Thesis, NCSU.

Wan, B., Rizos, D.C., Petrou, M.F., and Harries, K.A. (2005). "Computer Simulations and Parametric Studies of GFRP Bridge Deck Systems," Composite Structures; 69: 103–115.

Vinson, J. R. (1999). "The Behavior of Sandwich Structures of Isotropic and Composite Materials," Technomic Pub. Co., Lancaster, PA.

Vaughn, J.G., Lackey, E., Coffee, H.D., Barksby, N., Lambach, J.L. (2003). "Pultrusion of Fast-Gel Thermoset Polyurethanes: Processing Considerations and Mechanical Properties," Proceedings of Composites 2003-CFA, (Composites Fabricators Association).

Zenkert, D. (1997). "The Handbook of Sandwich Construction," Emas Publishing, UK.

Zhu HX, Mills NJ, Knott JF. (1997). "Analysis of the High Strain Compression of Open-cell Foams," Journal of the Mechanics and Physics of Solids 45 (11-12):1875-1904.

Zureick, A. (1997). "Fiber-reinforced Polymeric Bridge Decks," Proceedings of the National Seminar on Advanced Composite Material Bridges, FHWA.

Zhou, A., J. T. Coleman, et al. (2005). "Laboratory and Field Performance of Cellular Fiberreinforced Polymer Composite Bridge Deck Systems," Journal of Composites for Construction 9(5), 458-467.

Zou, B. (2008). "Design Guidelines for FRP Honeycomb Sandwich Bridge Decks," Doctoral Dissertation, West Virginia University. (UMI Number: 3376458).

Zi, G., Kim, B.M., Hwang, Y.K., and Lee, Y.H. (2008). "An Experimental Study on Static Behavior of a GFRP Bridge Deck Filled with a Polyurethane Foam," Composite Structures. Vol. 82, pp. 257-268.

Zhao, G., Wang, T., and Wang, Q. (2011). "Fiber-reinforced Polyurethane Composites," Society of Plastic Engineers (SPE).

VITA

Hesham Tuwair was born in Tripoli, Libya in 1979. He received his Bachelor of Civil Engineering degree in 2003 from University of Tripoli and his Master of Science in Civil Engineering degree in 2010 from University of Colorado at Boulder. He began his Ph.D. at Missouri University of Science and Technology in August 2011.

After graduation with a Bachelor's degree, he worked for two consultant engineering companies (DAMA and ACESCo) for five years. He was involved in reviewing civil engineering drawings submitted by contractors for large civil engineering projects. He also participated in technical meetings with clients and contractors to resolve technical debates and individual site problems. Mr. Tuwair worked as a designer as well as a site engineer for a couple of years. After he obtained his master's degree, he worked as a lecturer assistant in the civil engineering department at the University of Tripoli. In August 2015, he received his Ph.D. in Civil Engineering from Missouri University of Science and Technology.